To the Graduate Council:

I am submitting herewith a dissertation written by Kenneth Eduardo Fricke entitled "The Behavior of Large Shear Inserts in Concrete." I have examined the final copy of this dissertation for form and content and recommend that it be accepted in partial fulfillment of the requirements for the degree of Doctor of Philosophy, with a major in Civil Engineering.

Edwin G. Burdette

Edwin G. Burdette, Major Professor

We have read this dissertation
and recommend its acceptance:

Raymond A. King

W. Gordon

Eric C. Dam

Accepted for the Council:

Lew Minkel

Associate Vice Chancellor
and Dean of The Graduate School

THE BEHAVIOR

OF

LARGE SHEAR INSERTS IN CONCRETE

A Dissertation

Presented for the

Doctor of Philosophy

Degree

The University of Tennessee, Knoxville

Kenneth Eduardo Fricke

December 1992

DEDICATION

This dissertation is dedicated to the memory of my father

Mr. Kenneth S. Fricke

and my maternal grandmother

Sra. Rosalia Manrique de Planchart.

ACKNOWLEDGEMENTS

This work was performed at the Oak Ridge K-25 Site, Oak Ridge, Tennessee, operated by Martin Marietta Energy Systems, Inc. for the U.S. Department of Energy under contract DE-AC05-840R21400. The author would like to thank his major advisor, Dr. Edwin G. Burdette, for his support and advice during many years, and also for his consultation work during the GCEP concrete testing program. I would also like to thank each of the other members of my committee, Dr. David Goodpasture for his help during the GCEP mount hardware testing phase, and Drs. Ray Krieg and Eric Drumm for their advice during the finite element analysis part of this study. There are a lot of people at Martin Marietta that need to be thanked: Lanny Frazier, Don Kelley, Ron Adamski, and Parker O'Shell of the Stress Analysis Group of the Technical Services Division who coordinated the instrumentation, testing, and data acquisition; Dr. Dan Naus and the Prestressed Concrete Reactor Vessel Research and Development Group at the Oak Ridge Y-12 Plant who performed the concrete cylinder testing; Walt McClanahan, A. B. Reid, and Paul Williams for their help with some of the figures; Dale Jones, my immediate supervisor for most of this work, who was involved with the testing, and Dr. James Beavers and Charles McLoughlin, my Department Heads during this time, all of whom provided much encouragement. I appreciate ADINA R&D's permission to use figures from their documentation for the program. I would like to thank my mother, Solita Planchart de Fricke, and my brother Stuart for their support, and my Uncle Dr. Alfredo Planchart for always reminding me that this should be a goal to pursue. Finally, I would like to thank all my friends in Oak Ridge who have helped in many little and big ways, especially, my best friend Maureen.

ABSTRACT

One of the engineering problems encountered in the design of the Department of Energy Gas Centrifuge Enrichment Plant (GCEP) in Piketon, Ohio was the design of the mount system supporting the machines. A major factor in this design was the determination of the concrete bearing capacity around steel inserts having an embedment length/diameter ratio approaching unity. Tests were performed on eight inserts that were cast into a prototype reinforced concrete slab similar to the concrete floor slab designed for the GCEP facility. An eccentric shear load was applied to each insert and the bearing capacity of the concrete was determined. The results indicated that the ratio of the bearing capacity to the concrete compressive strength, f_b/f'_c, averaged about 3.8, or about 4.5 times greater than allowed by the ACI Concrete Code. The results were compared with various methods commonly used to determine bearing capacity of shear inserts and found to differ widely. A closer agreement was found with the bearing capacity determined for brackets embedded in concrete columns. The first part of the dissertation discusses the concrete insert tests in detail, and the second part discusses a nonlinear finite element analysis (FEA) that was performed to model the insert tests and try to reproduce the behavior obtained in the field tests. The computer code ADINA, which has a nonlinear concrete material model in its library, was used for this study. The results of this study were inconclusive. The FEA was only able to reproduce about half of the load-displacement curves obtained during the tests, stopping well short of ultimate failure as observed during the tests. Many problems with equilibrium were encountered after one or more elements were totally crushed in the FEA. Various parameters were modified during the study, with little success.

TABLE OF CONTENTS

Chapter		Page
I.	INTRODUCTION	1
	Inserts in Concrete	1
	The GCEP Problem	2
	Objective	6
	Overview	7
II.	REVIEW OF CURRENT PRACTICE IN THE ANALYSIS OF STEEL EMBEDMENTS IN CONCRETE	8
	Introduction	8
	Tensile Capacity of Single Embedments	9
	Shear Capacity of Single Embedments	11
	Embedment of Steel Sections in Concrete	13
III.	ANALYSIS OF THE GCEP CENTRIFUGE FLOOR MODULE	15
	Introduction	15
	Transmission of Loads from Machine to Floor Module	15
	Transmission of Loads from Floor Module to Concrete Slab	17
	Determination of Concrete Bearing Capacity	17
IV.	FULL-SCALE SOCKET TESTING PROGRAM	21
	Review of the GCEP Testing Program	21
	Description of the Socket Test Setup	25
	Summary of the Socket Tests	34
V.	FINITE ELEMENT ANALYSIS OF CONCRETE - A DISCUSSION	40
	Introduction	40
	Constitutive Modeling of Concrete	41
	Finite Element Modeling of Concrete Structures	45
	General Description of ADINA	47
	ADINA-84 Concrete Model	51
	ADINA 5.0 Concrete Model	60
VI.	FINITE ELEMENT ANALYSES	66
	Introduction	66
	Concrete Cylinder Model Analysis	68
	Cerruti's Problem Analysis	71
	Concrete-Socket Test Model	73
	Concrete-Socket Model Analyses	82
	Discussion of the Computer Analyses	101

VII. SUMMARY AND CONCLUSIONS 111
Summary 111
Conclusions 113

LIST OF REFERENCES 115

APPENDICES 123

APPENDIX A - TABLES 124

APPENDIX B - FIGURES 136

APPENDIX C - DERIVATION OF EQUATION (3-1) 200

VITA 204

LIST OF TABLES

Table		Page
1.	Summary Results of the Floor Module Tests	125
2.	Summary of Cylinder Break Tests	126
3.	Parameters and Results of Socket Tests	128
4.	ADINA Element and Material Model Summary	129
5.	Cerruti Problem Summary	130
6.	Summary of the Finite Element Model Configuration	131
7.	Boundary Condition Sets Used in Analyses	131
8.	Nonlinear Concrete Triaxial Data Curves Used in Analyses	132
9.	Summary of ADINA Linear Runs	133
10.	Summary of ADINA Nonlinear Runs	134
11.	Summary of ADINA Runs Modeling Concrete as an Elastic-Plastic Material	135

LIST OF FIGURES

Figure		Page
1.	GCEP Floor Module with Mount Lugs	137
2.	Detail of a Corner Socket with Mount Lug	138
3.	Typical Loading Pattern Analysis	139
4.	Floor Module Details	140
5.	Free Body Diagram of Socket Test	141
6.	Bushing and Mount Lug Installation	142
7.	Typical Arrangement for a Socket Test	142
8.	GCEP Full-Scale Floor Module Test Arrangement	143
9.	Socket Test Slab Details	144
10.	Socket Test Slab During Construction	145
11.	Pocked Area of Test Slab	146
12.	View of Thrust Bracket Assembly with Hydraulic Rams	147
13.	Cylinder Break Test 2-17 Load-Displacement Curves	148
14.	Condition of Concrete after Test No. 2	149
15.	Test No. 4 Load-Displacement Curve at Top-of-Socket	150
16.	Test No. 8 Load-Displacement Curve at Top-of-Socket	151
17.	Test No. 8 Load-Displacement Curve at Top-of-Mount Lug	152
18.	Load-Displacement Curves for Socket Tests	153
19.	ADINA Uniaxial Stress-Strain Curve in Concrete Model	154
20.	ADINA-84 Three-Dimensional Tensile Failure Envelope	155

Figure Page

21. ADINA Triaxial Compressive Failure Envelope 156

22. ADINA Uniaxial Stress-Strain Curve Modified for Multiaxial Stress Conditions 157

23. Comparison of ADINA Concrete Cylinder Model Results vs. Cylinder Test No. 2-17 158

24. Cracking and Crushing Pattern for Run CYLIN2DR 159

25. Model Used for Cerruti's Problem 160

26. Portion of Socket Test in Finite Element Model 161

27. View of Model 162

28. View of Socket Area of Model 163

29. Plan of Model at Layer Z = 0.0 164

30. Plan of Model Socket Area at Layer Z = 0.0 165

31. Plan of Model at Layer Z = 5.0 166

32. Plan of Model Socket Area at Layer Z = 5.0 167

33. Plan of Model at Layer Z = 10.5 168

34. Plan of Model Socket Area at Layer Z = 10.5 169

35. Plan of Model at Layer Z = 16.0 170

36. Plan of Model Socket Area at Layer Z = 16.0 171

37. Plan of Model at Layer Z = 17.5 172

38. Plan of Model Socket Area at Layer Z = 17.5 173

39. Plan of Model at Layer Z = 19.0 174

40. Plan of Model Socket Area at Layer Z = 19.0 175

41. Plan of Model at Layer Z = 21.5 176

Figure Page

42. Plan of Model Socket Area at Layer Z = 21.5 177

43. Plan of Model at Layer Z = 23.0 178

44. Plan of Model Socket Area at Layer Z = 23.0 179

45. Plan of Model at Top of Mount Lug, Z = 25.7 180

46. Reinforcing Bar Layout in Model at Elevation Z = 16.0 181

47. Reinforcing Bar Layout in Model at Elevation Z = 21.5 181

48. Load-Displacement Curves for Socket Tests, to 100 kips 182

49. Effect of Loading Plates on Initial Stiffness 183

50. Effect of Gap Elements on Initial Stiffness 184

51. Effect of Anchor Bar Element Type on Initial Stiffness 185

52. Load-Displacement Curve for Run nlin03 186

53. Crushed Elements, Run nlin03, at P=90 kips 187

54. Load-Displacement Curves for Runs nlin04 and nlin05 Compared to Test 8, Showing the Effect of Gap Elements in Nonlinear Analysis .. 188

55. Load-Displacement Curves for Runs nlin07 and nlin08 Compared to Test 8, Showing the Effect of Boundary Condition Set 1 vs. Set 2 ... 189

56. Load-Displacement Curves for Runs nlin08 and nlin09 Compared to Test 8, Showing the Effect of Load Step Increment 190

57. Load-Displacement Curve for Run nlin10 191

58. Comparison of Load-Displacement Curves for Runs nlin10, nlin12, and nlin14 192

59. Cracked Elements at Load P = 20 kips 193

60. Cracked Elements at Load P = 40 kips 193

61. Cracked Elements at Load P = 60 kips 194

Figure Page

62. Cracked Elements at Load P = 80 kips 195

63. Cracked Elements at Load P = 84 kips 195

64. Location of Crushed Elements at Z = 23.0 196

65. Comparison of Load-Displacement Curves for Run nlin16 and Test 8 .. 197

66. Load-Displacement Curves for Elastic-Plastic Runs nlinep01 and nlinep02 198

67. Load-Displacement Curves for Elastic-Plastic Runs nlinep02, nlinep03, nlinep06, and nlinep07, Compared with Test 8 199

NOTATION

Arabic letters

A,B,C = constants in the calculation of Young's modulus

A_1 = loaded area in a concrete bearing calculation

A_2 = area of the bearing surface, equal to the maximum area of the portion of the supporting surface that is geometrically similar to and concentric with the loaded area

A_s = area of steel embedment

b = width of the embedded section for section embedded in column

C_1,C_2,C_3 = unknowns in the free-body of the socket

C_1,C_2 = input variables used to determine γ in ADINA 5.0

$\hat{C}$ = stiffness matrix, used in $\sigma = \hat{C}e$

d = diameter of embedment

d_e = edge distance in shear failure calculations

d_h = diameter of embedment head

$\tilde{\varepsilon}_c$ = uniaxial strain corresponding to that the maximum stress

${}^t\tilde{\varepsilon}_{pi}$ = strain in the principal stress direction corresponding to ${}^t\sigma_{pi}$

$\tilde{\varepsilon}_u$ = uniaxial ultimate strain

${}^t\tilde{\varepsilon}$ = uniaxial strain at time (or load step) t

$\tilde{\varepsilon}'$ = uniaxial strain modified for multiaxial conditions

$E_{elastic}$ = elastic modulus used in bilinear model

E_{hard} = modulus used in the hardening region in the bilinear model

$\tilde{E}_o$ = initial tangent modulus in the uniaxial stress-strain curve

$\tilde{E}_{pi}$ = tangent modulus corresponding to the principal stress ${}^t\sigma_{pi}$ with strain ${}^t\tilde{\varepsilon}_{pi}$

$\tilde{E}_s$ = secant modulus corresponding to maximum stress = $\tilde{\sigma}_c/\tilde{e}_c$

$\tilde{E}_u$ = secant modulus corresponding to ultimate stress = $\tilde{\sigma}_u/\tilde{e}_u$

${}^t\tilde{E}$ = Young's modulus at time t

${}^tf$ = loading function used by ADINA

f_{max} = maximum value the loading function has reached by analysis to time t

f_1, f_2 = unknowns in equation

f_b = bearing capacity of concrete

f'_c = concrete compressive strength, based on 6-in. by 12-in. cylinder breaks

f_{ut} = ultimate strength of steel

f_y = yield point of steel

G^f_{ij} = shear modulus in the tensile softening region

K = ratio of bearing capacity of concrete to the concrete compressive strength, given by f_b/f'_c

l/d = ratio of length to diameter for embedment

l_e = embedment length

m = minimum side cover distance from the edge of the concrete to the center of an anchor

p = ratio of ultimate strain to strain at maximum stress = $\tilde{e}_u/\tilde{e}_c$

P_c = concrete tensile strength

P'_c = pullout strength reduced due to edge distance critical

P_s = tensile capacity of embedded steel element

P_t = minimum tensile strength of steel

P_u = factored tension load

R = friction factor

${}^t\hat{s}$ = square root of the second invariant of the deviatoric stress tensor at time t = $[\frac{1}{2}{}^ts_{ij}{}^ts_{ij}]^{1/2}$

$^{t}s_{ij}$ = deviatoric stress tensor at time t = $^{t}\sigma_{ij}$ - $\delta_{ij}{}^{t}\sigma_{m}$

spi(I) = ADINA input principal stress ratio curves for the triaxial failure envelopes, i=1,2,3 and I=1 to 6; spi = $\sigma_{pi}/\tilde{\sigma}_{c}$

t = time t, or load step number

t = column width for section embedded in columns

V_c = concrete strength against pullout

V_s = minimum ultimate tensile strength of steel

V_u = factored shear load

X,Y,Z = coordinate system used to define the finite element model

X1,X2,X3 = coordinate system used to define the displacements for Cerruti's problem

Greek letters

α = factor used in the loading function in ADINA-84

β = lateral force coefficient

β = principal stress ratio = σ_{p2}/σ_{p3}, usually set at 0.75

γ = constant input parameter used in ADINA-84

γ = variable parameter in ADINA 5.0 = $C_1\gamma_1 + C_2$

γ_1 = ratio of the multiaxial to the uniaxial strength = $\tilde{\sigma}'_c/\tilde{\sigma}_c$

δ_{ij} = Kronecker delta (=1 when i=j and 0 when i≠j)

η_s = shear stiffness reduction factor

η_n = normal stiffness reduction factor

κ = control parameter for changing material law (ADINA-84)

λ = center of rotation of the socket

μ = coefficient of friction

ν = Poisson's ratio

ξ = tensile strength softening region factor, where after reaching σ_t at a strain e_t, the tensile Young's modulus varies linearly to zero between e_t and λe_t

$\tilde{\sigma}_c$ = uniaxial maximum stress

${}^t\sigma_{ii}$ = first invariant of the stress tensor at time t = $\sigma_{11} + \sigma_{22} + \sigma_{33}$

$3{}^t\sigma_m$ = first invariant of the stress tensor at time t = ${}^t\sigma_{ii}$

${}^t\sigma_{pi}$ = principal stresses at time t, i = 1,2,3

$\tilde{\sigma}_u$ = uniaxial ultimate stress

${}^t\tilde{\sigma}$ = uniaxial stress at time (or load step) t

$\tilde{\sigma}'$ = multiaxial stress and strain

ϕ = ACI strength reduction factor

CHAPTER I

INTRODUCTION

I. INSERTS IN CONCRETE

The embedment of steel members in concrete is a common occurrence in the civil engineering field. By far the most common concrete embedment is the anchor bolt, stud, or similar type anchorage. Anchor bolts may be attached to floors, walls, or ceilings, and are liable to be subjected to tension, shear, and bearing loads, and to combinations of those loads. The behavior of an embedment is dependent on many factors including the strength of the encasing concrete, the strength and ductility of the steel material, the dimensions of the embedment such as diameter and the depth of the anchorage, the distance between the anchorage and the edge of the concrete, and the degree of confinement around the embedment (edge distance is part of this). Typically, anchor bolts loaded in tension require an embedment length of 8 to 12 bolt diameters in order to ensure a ductile failure mode (failure of the bolt) and not a brittle failure mode of the concrete. Embedment lengths for anchorages loaded in shear are generally designed to be about the same. There exists a considerable amount of literature on the design and behavior of anchor bolts, with some testing data available supporting the different methods that are commonly in use. However, none of the literature, even that reviewing short anchor bolts, ever discusses the behavior of embedments having an embedment length/diameter (l_e/d) ratio approaching unity. The obvious conclusion from the literature is that the capacity of such a system will be controlled by the concrete and that the failure should be expected to be sudden. The problem involved

in the work described herein concerns the analysis of the behavior of large diameter, very shallow ($l_e/d = 1.167$) embedment inserts in concrete, loaded by an eccentric load parallel to the surface of the concrete.

II. THE GCEP PROBLEM

Introduction

The gas centrifuge process for enriching uranium had been under development for almost two decades prior to the decision in 1977 to build the Gas Centrifuge Enrichment Plant (GCEP) near Portsmouth, Ohio. In the gas centrifuge process, a mixture of gases of different molecular weights is separated through the action of a centrifugal force field produced by the spinning rotor. The first successful use of a centrifuge to separate gaseous isotopes was performed in 1934 by Dr. Jesse Beams at the University of Virginia. During World War II the centrifuge method was considered for the purpose of separating uranium into its two isotopes, U-235 and U-238. The method was successfully demonstrated, but was still not practical at the time, primarily due to the lack of availability of adequate strength materials. After the war, research continued and eventually demonstrated the feasibility of the centrifuge process for the separation of uranium isotopes in the 1960's. During the next two decades the U.S. Department of Energy (DOE) further continued the development, manufacture, and testing of gas centrifuge enrichment machines and also built small scale pilot plants, leading up to the GCEP Plant project. Various designs for the centrifuge mounts were used throughout the history of the project. The centrifuge machines were initially rigidly supported, using a very large steel framework to hold the machine at the top and the bottom. However, for seismic and other vibration considerations the rigid attachments

presented problems and eventually the support mechanism evolved into a vibration isolation mount system.

Since only a very small percentage of the uranium is separated in a single machine, the complete process requires a very large number of machines. As a consequence of the quantity of machines required, and the need to put them into a specified area, the machines are placed in a closely packed (about four feet center-to-center) rectangular arrangement. A centrifuge machine is attached to the floor through a structural steel frame called a floor module which is embedded in a reinforced concrete floor slab. Figure 1[1] shows a photograph of a typical floor module in place in the GCEP facility being prepared for load testing; visible in the photograph are the attaching steel frame, the four corner sockets, and two mount lugs already in place. The floor module is supported in the concrete by a second steel framework whose main purpose is to provide alignment during the installation and placement of the concrete. This secondary supporting framework does not actively participate in resisting the loads. The centrifuges are supported at a bottom center support pivot point (allowing rotation) and four socket/mount lugs placed at the corners of the floor module. The detail of a socket with a mount lug is shown in Figure 2. The socket is a hollow cylinder welded to the floor module, and the mount lug is a solid cylinder held in place with a capture nut and retaining ring arrangement at the bottom of the socket and a tapered lock bushing which attaches to the upper end of the socket. The center pivot support provides vertical support (upward motion is not prevented) and resists some horizontal forces; the stability of the machine is provided by isolators which attach to both the machine flange and the floor mounts through the mount lugs. If the machine begins to tilt, some of the isolators go into compression and some into tension, and the restoring forces right the machine.

---

[1] All figures and tables are presented in the Appendices

The Analysis Problem

In the event that a machine crashes, the energy transferred to the machine casing due to the disintegration of the rotor produces extremely large, roughly tangential forces at each of the four corner support locations of the floor module. In addition an overturning moment is created by the rocking action of the machine being resisted by the rubber isolators. Shear loads are transmitted to the concrete floor slab primarily through the bearing action of the sockets against the concrete. It is required that the floor modules and foundation be designed to protect adjacent machines from being impacted and possibly initiating a domino effect of machine failures. The design goals of the embedded floor module were that the centrifuge machine remain standing after a machine wrecks, and that the floor module remain reusable.

The determination of the structural capacity of the floor module and the surrounding reinforced concrete proved to be a rather challenging problem. It was determined very early in the design process that the use of standard guidelines such as codes and specifications were going to be of little help - these provided so much conservatism to the design that the foundation, floor module, machine bottom flange, and mount lugs would become excessively large, impacting the overall cost of the project in an unacceptable fashion. It was felt that the strength of the entire system was considerably greater than would be indicated by normal design methods. Some aspects of the design problem called for some serious consideration:

1. What safety factor should be applied to the loads? The scientists involved with the physics of the centrifuge machine defined the "design loads" such that the probability of exceedance was less than 0.005, resulting in a considerably greater increase factor to the nominal loads than the load factors defined by the ACI 318 Concrete Specifications (2). While the wreck loads are definitely considered

live loads for the concrete floor slab, do the loads merit being further increased by the ACI load factors? Should the ACI strength reduction factor, ϕ, be included? It was decided that the two factors should not be included in the design since the given design loads more than accounted for both factors.

2. It was highly unlikely that the four mount lugs would be simultaneously and uniformly loaded during the initial phase of a machine failure due to the stack-up of machining tolerances of the various components. It was expected that two of the lugs would initially be subjected to the horizontal wreck forces. This imbalance might continue throughout the entire event, though once these two lugs start to yield then the increasing distortions would probably be sufficient to allow contact of the remaining lugs. Though it was felt that this scenario was quite probable, it was decided to proceed with the assumption of simultaneous load application at each of the four corner locations. It would have been very complicated to consider the case where only some of the lugs are resisting the load.

3. What degree of confinement existed given the configuration of the floor module and the concrete? How could the benefits of confinement in concrete be applied in the design process when considering the bearing of the socket on the concrete?

4. What stress distribution should be assumed for the mount lug in the socket and for the socket in the concrete?

The design phase was accomplished in two parts. The first step was devoted to developing a mathematical theory and a practical design for the machine/floor interface, floor

module, and associated hardware. The second phase was a comprehensive testing program intended to actually verify the design. During the testing phase, hardware components (mount lugs, bushings, retaining rings), major sub-assemblies (sockets with mount lugs embedded in both a steel block and a concrete slab), and full-size assemblies (floor modules in the actual floor slab) were load tested.

III. OBJECTIVE

The objective of this dissertation was to obtain an understanding of the behavior of large ($l/d \approx 1$) inserts embedded in concrete and loaded in eccentric shear. This was accomplished as follows:

1. A simplified analytical theory was developed.
2. A small concrete slab reinforced similar to the GCEP floor slab was built in the laboratory and eight sockets embedded in it. Load tests were performed on each of the eight positions, recording steel and concrete stresses and strains, and obtaining load-displacement data.
3. A nonlinear finite element model was developed in an attempt to reproduce the load-displacement test curve.
4. The simplified theory, the test results, and the analytical finite element modeling results are compared, discussed, and conclusions and recommendations provided.

A secondary reason for performing a finite element analysis is to determine the practicality of using finite element models in the design process for problems of this nature - specifically those where a fairly complex and nonuniform state of stress exists.

IV. OVERVIEW

A number of tests were conducted to develop and ensure the adequacy of the centrifuge machine mounts and foundation design. Tests were performed on the mount lugs, vibration isolators, the embedded sockets, and the full-size floor modules; then a finite element analysis of the embedded socket tests was performed. The work in the present dissertation covers the entire spectrum and is roughly divided into two parts: the first part, Chapters II through IV, presents the preliminary work used in the development of the final GCEP mount design, and includes the testing program; the second part presents the finite element analysis of the embedded socket tests.

Chapter II reviews the current practices in the design of concrete inserts, focusing primarily on the behavior and analysis of anchor bolts subjected to tension and/or shear forces. Chapter III briefly describes the analysis that was performed prior to the laboratory testing. The complete GCEP machine mount testing program is covered in Chapter IV, with the emphasis on the socket testing program. Chapter V reviews the current state-of-the-art of finite element analysis of concrete as well as constitutive modeling of concrete, and also describes the program ADINA (**A**utomatic **D**ynamic **I**ncremental **N**onlinear **A**nalysis), with a section devoted to the ADINA concrete model. The finite element model descriptions of the test slab and embedded socket and analyses are presented in Chapter VI. Chapter VII summarizes the work and presents conclusions and recommendations.

CHAPTER II

REVIEW OF CURRENT PRACTICE IN THE ANALYSIS OF STEEL EMBEDMENTS IN CONCRETE

I. INTRODUCTION

As mentioned in the Introduction, the most common embedment in concrete is the anchor bolt, stud, or similar type anchorage. Embedments are commonly loaded in tension and shear and with combinations of those loads. The pullout strength of a single embedment is dependent on the strength of the surrounding concrete, the strength and ductility of the steel material, the geometry of the embedment, and the edge distance to a free surface (the degree of confinement around the embedment). In the case of multiple embedments, additional factors affecting the anchorage strength include the spacing between adjacent embedments and the thickness of the concrete.

The current literature contains a number of documents that provide methods for predicting the tensile and shear capacities of concrete embedments. The testing reported by Cannon et al. (33), Bailey and Burdette (10), and McMackin et al. (62) was instrumental in the development of the original Appendix B addition to the ACI 349-85 Code (3) on steel embedments. In addition, published procedures exist by the Prestressed Concrete Institute (PCI) (73), the Tennessee Valley Authority (TVA) (47), and the TRW Nelson Division (43). Cannon, Godfrey, and Moreadith (34) basically reiterate the ACI 349-85 Appendix B procedures, with minor differences for non-Nuclear facilities. Shipp and Haninger's (79)

paper on the design of headed anchor bolts also suggests an approach compatible with ACI 349-85.

The following sections provide a very brief summary of the procedures available for the prediction of the pullout strength of anchor embedments in concrete. Since this work is interested in the actual capacity of the embedment, and not in the design, the use of the ϕ factors and other code related safety factors are not included in this discussion. Only the basic strength of single embedments is discussed since in the GCEP floor module the corner sockets are not spaced closely enough (7 in. deep, 29 in. apart) that multiple embedments need be considered.

II. TENSILE CAPACITY OF SINGLE EMBEDMENTS

The capacity of steel embedments loaded in pure tension is governed by either failure of the steel member, or by a complete or partial failure of the concrete. Steel strength controls when the pullout strength of the concrete exceeds the minimum tensile strength of the steel based on f_{ut} and full load transfer between the steel and the concrete can occur (3,34). Concrete strength controls when the anchor embedment length is short or a small edge distance (lack of proper confinement) exists, in which case the pullout strength of the concrete is less than the steel anchor strength. If edge distance is not a factor, then the concrete failure surface takes on a roughly 45° conical shape. In the case where the edge distance is less than the depth of the embedment, only a partial cone failure surface can develop. If the edge distance is too small, regardless of whether there is sufficient embedment length, the concrete fails by local bursting around the head of the anchor.

For steel failure controlling, three references (3,47,73) calculate the tensile capacity as $P_s = A_s f_y$, while two references (43,79) compute the capacity as $P_s = A_s f_{ut}$. Cannon (34) uses

the smaller of f_y or $0.8f_{ut}$. Note that in the ACI 349-85 Code (3), though the embedment length requirement is based on f_{ut}, the actual steel capacity is based on f_y.

In the case of failure of the concrete, when edge effect is not a factor, the basic procedure used to predict the tensile capacity of the embedment is to use the resultant of tensile stresses equal to the maximum concrete tensile strength, directed parallel to the applied load and acting on the projected area of the stress cone, either including (47) or excluding (3,34) the area of the anchor head. In the former case the formula for the concrete tensile capacity becomes

$$P_c = \frac{\pi}{4}(2l_e + d_h)^2(4\sqrt{f_c'}) \tag{2-1}$$

while in the latter it is given by

$$\begin{aligned} P_c &= \frac{\pi}{4}[(2l_e + d_h)^2 - d_h^2](4\sqrt{f_c'}) \\ &= \pi\, l_e(l_e + d_h)(4\sqrt{f_c'}) \end{aligned} \tag{2-2}$$

Two other references, the TRW-Nelson Studs (43) and the PCI Handbook (73), compute the capacity as the resultant of the tensile stresses equal to the maximum concrete tensile strength acting on the surface area of the truncated cone, but directed parallel to the applied load. This produces an equation which is the same as eq. (2-2), but has an extra $\sqrt{2}$ term.

$$P_c = \pi\sqrt{2}\, l_e(l_e + d_h)(4\sqrt{f_c'}) \tag{2-3}$$

Klingner and Mendonca (56) clearly show that eq. (2-3) is unconservative due to the extra $\sqrt{2}$ term. The use of eq. (2-2) appears to produce the best results for the prediction of the nominal tensile capacity (56).

For the case where the edge distance controls such that a full failure stress cone cannot be developed, all of the above references use their formula for P_c times a ratio to compute a new pullout strength, P_c'. The ACI 349-85 Code Appendix B (3) and the TVA (47) methods define the ratio to be equal to the projected area of the partial cone divided by the projected area of the full cone. In addition to the above criteria, the ACI 349-85 Code Appendix B (3) includes a minimum edge distance below which lateral bursting of the concrete around the anchor head will occur. For a single embedment, this distance, m, may be determined from the formula found in the Commentary to the ACI 349-85 Code Appendix B (3),

$$\beta P_t = (4\phi \sqrt{f_c'})(\pi m^2) \qquad (2\text{-}4)$$

where β is the lateral force coefficient (approximately equal to Poisson's ratio for the concrete), and P_t is the minimum tensile strength of the steel.

III. SHEAR CAPACITY OF SINGLE EMBEDMENTS

The capacity of steel embedments loaded in pure shear is governed by either a shear failure of the steel member or failure of the concrete. Similar to the tensile failure case, the embedment fails in the steel shear failure mode when the depth of the embedment is sufficiently large that the tensile pullout strength of the concrete exceeds the shear strength of the anchor, and edge distance is not critical. A concrete failure mode occurs when either partial embedment or a small edge distance exists.

The determination of the shear failure capacity of the steel embedment is relatively straightforward to calculate. There are three methods discussed in the literature. TRW (43), McMackin (62), and PCI (73) calculate the shear capacity as the anchor's cross-sectional area

times the steel minimum ultimate tensile strength, $V_s = A_s f_{ut}$, while Klingner et al. (54) suggests using an estimate of the ultimate shear strength as $0.75f_{ut}$, resulting in $V_s = A_s(0.75)f_{ut}$. The ACI 349-85 Code (3), Cannon et al. (34), and TVA (47) use the shear friction concept based on the yield strength of the steel anchor (though Cannon uses the lesser of f_y or $0.8f_{ut}$). TVA computes the shear capacity as $V_s = (A_s f_y)/R$, where R is a friction factor. Both the ACI 349-85 Code and Cannon use the equation $V_s = A_s \mu f_y$, where the coefficient of friction, μ, varies between 0.55 and 0.9. Klingner and Mendonca (55) have indicated, based on a limited number of data points, that the approach of using $V_s = A_s f_{ut}$ appears to be unconservative, and that the procedures that use either a shear strength estimate or the shear friction concept produce conservative results.

There exist numerous published methods for determining the concrete failure case. Klingner et al. (54), TVA (47), ACI 349-85 (3), and Cannon et al. (33,34) assume that concrete failure does not control if full tensile embedment and sufficient edge distance are provided. PCI (73) computes the concrete strength as the lesser of $V_c = 800A_b\sqrt{f'_c}$ or $2\pi(d_e)^2\sqrt{f'}$. In the event that the edge distance is limited, the above procedures (3,33,34,47,54) idealize the concrete failure surface as a semi-cone, whose height is equal to the edge distance and whose sides are inclined at an angle α with respect to the face of the block. One procedure (33) uses a variable value for the angle α, while the others assume the angle to be 45°. The formula for the concrete pullout capacity based on a 45° failure surface slope is given by

$$V_c = 2\pi(d_e^2)\sqrt{f_c'} \qquad (2\text{-}5)$$

The other procedures (43,62), developed for studs, calculate the concrete capacity for partial embedment using empirical formulas obtained from experimental testing. McMackin (62) presents the following equation:

$$V_c = 1.106 A_s (f_c')^{0.3} (E_c)^{0.44} \quad (2\text{-}6)$$

where f_c' and E_c are in ksi units. All of these methods produce shear capacity values that are very much greater than the test results obtained from the embedded socket tests described later. The main reason for this lies in the fact that the embedded socket tests have a very low l/d value and are not fully embedded.

IV. EMBEDMENT OF STEEL SECTIONS IN CONCRETE

Mattock and Gaafar (61) reported on the behavior of embedded steel sections acting as brackets. Their study is of interest in the discussion of the strength of the sockets in concrete since the applied loading was very similar to that applied to the embedded concrete sockets, i.e., an eccentric shear load producing both a shear load and a moment. The remainder of this section discusses the Mattock and Gaafar paper.

Formulas for the nominal applied shear load and the maximum moment in the steel member were derived assuming a linear strain distribution along the embedment length and curvilinear compressive forces acting opposite to the applied shear load (near the surface) and in the direction of the load below the neutral axis of the embedment. The actual nonlinear force distribution acting immediately below the bracket was replaced with the ACI 318 (2) equivalent rectangular stress distribution.

In order to check the accuracy of their analytical solution, an experimental test program was performed where various steel shapes were embedded in concrete columns and loaded

to failure. The nominal shear strength, maximum moment occurring in the steel member, and the concrete bearing stress, f_b, at the failure level, were measured or determined. The concrete bearing stress at failure, in terms of the concrete 28-day strength, f'_c, is given by the equation

$$f_b = 54\left(\frac{t}{b}\right)^{0.66}\sqrt{f_c'} \tag{2-7}$$

where the term t/b is the ratio of the column width to the width of the embedded section (a measure of the degree of confinement). It is suggested by the authors that the ratio t/b not be taken larger than 12 when applying the above equation. It is shown later herein that eq. (2-7) produces values of K, where $K = f_b/f'_c$, that agree very well with the values obtained in the socket tests (31).

CHAPTER III

ANALYSIS OF THE GCEP CENTRIFUGE FLOOR MODULE

I. INTRODUCTION

The analysis of the structural load carrying capacity of a floor module centers around three basic issues:

1. How is the load transferred from a centrifuge machine to the floor module?,
2. How is the load then transferred from the floor module to the surrounding concrete slab?, and
3. What is the strength of the concrete in bearing?

Each of these issues is discussed in the following sections.

II. TRANSMISSION OF LOADS FROM MACHINE TO FLOOR MODULE

As a centrifuge machine wrecks it transfers the rotational energy of the rotor to the casing through the action (simplistically described) of shear and torque forces (Figure 3) and of heat energy. A machine is supported at five points - the four corner mount lugs/sockets and the central pivot point. Analysis normally assumes that the torque force is transmitted equally to each of the floor module corner sockets as a horizontal force acting tangential to a circle which passes through the centerline of each socket. The magnitude of this force remains constant from corner to corner. The assumption of equal distribution is also used

for the shear force, except that the four corner loads due to the shear load all act in the same direction. Thus the combination of shear and torque forces produces an unequal vector force at each socket, differing not only in magnitude, but in direction. Because the torque load is considerably greater than the shear load, the vector direction of the resultant at any corner is found to be within ±20° of the tangential direction, as shown in Figure 3. The resultant force at each corner socket acts approximately 2.7-in. above the plane of the concrete surface. Figure 4 shows a floor module in plan and elevation with the applied lateral loads indicated. A comment is worth making about the nature of the machine wreck horizontal shear load (the V's in Figure 3). This load was assumed to act as a unidirectional static load, with the direction which produced the largest total lateral force on the socket being the one used in the analysis. The floor module designers were generally convinced that this was a "pseudo-realistic" load, because this shear load was continuously changing direction very rapidly, rotating around as the rotor disintegrated, and thus, while at one instant it produced a load which added to the load on a socket from the torque load, the next instant it had already disappeared, or even reduced the resultant load. Thus, its real effect was smaller than assumed. However, for purposes of the design, it was assumed to be a real sustained load and was taken into full consideration.

The assumption of equal distribution of forces at the four corner sockets is obviously only approximate; however, it would have been extremely difficult to use any other distribution, since the true distribution depends on the fabrication tolerances of the floor module, the machine casing and flange, and these tolerances will vary not only from machine to machine, but will also be different at each of the four corner sockets of a floor module.

A design overturning moment also existed in the criteria, which produces rocking of the machine on the pivot point. The rocking effects are resisted by the rubber vibration isola-

tors which are attached to both the machine flange and the mount lugs, producing tension and compression loads in the mount lugs. These vertical forces are transmitted to the socket through the capture nut and retaining ring (Figure 2). The vertical forces so created were on the order of 23 kips, smaller by an order of magnitude than the resultant horizontal forces, and for the purposes of the concrete socket tests were neglected.

III. TRANSMISSION OF LOADS FROM FLOOR MODULE TO CONCRETE SLAB

A floor module corner socket is subjected simultaneously to a tensile pullout load (or a compressive downward thrust), a horizontal shear load (resulting from the combination of the machine torque and shear loads), and a bending moment (due to the eccentricity of the shear type load).

The pullout loading is resisted by the concrete in tension (due to the friction between the socket and the concrete), the floor module lower beam flanges encased in concrete, and the anchor bar. The downward thrust loading is obviously no problem.

The shear, torque, and moment forces are resisted primarily through bearing of the socket on the concrete, but additional pullout resistance is provided by the anchor bar acting in tension. The floor module steel beams, used to accurately position and install the four embedded sockets, provide only a very small amount of lateral resistance because of their weakness in bending about the weak axis, and their contribution is neglected throughout all the analyses - a simplifying and conservative assumption.

IV. DETERMINATION OF CONCRETE BEARING CAPACITY

In order to determine the actual capacity of the floor module to resist loads, the bearing capacity of the concrete under the given conditions must be known. The method to

be used to obtain this quantity is not immediately obvious. The ACI 318 (2) and the ACI 349-85 (3) codes present procedures for determining the bearing strength of concrete. The ACI 318 states that the bearing strength on concrete shall not exceed $0.85f'_cA_1$ (omitting the ϕ-factor), where A_1 is the loaded area, but allows this value to be further increased by a factor $(A_2/A_1)^{1/2} \leq 2$ in the event that the supporting surface (A_2 is the area of the bearing surface) is wider on all sides than the loaded area. The increase provided for by the term A_2/A_1 is not strictly applicable in the case of the corner sockets because the bearing surface and the loaded area are flush at the top of the concrete slab; hence the maximum value of the concrete bearing stress allowed by the ACI 318 Code is $0.85f'_c$ (it might be argued, however, that the area in bearing that exists at the lower back side and bottom of the socket does satisfy the code increase). It should be recognized that the Code does not attempt to address the situation that exists here, i.e., bearing in the plane of 24-in. thick reinforced concrete slab.

Appendix B of the ACI 349-85 Code recognizes that extremely and undefinably large bearing stresses exist around the head of embedded anchor bolts due to the degree of confinement. Tests by Cannon et al. (33) and McMackin et al. (62) have demonstrated that the head of a standard anchor bolt or stud, without a plate or washer, is sufficient bearing area to fully develop the tensile strength of the anchor bolts without damaging the concrete, so long as adequate side cover is present to allow the development of the necessary confining pressure. Test data clearly show that bearing stresses higher than $10f'_c$ are not uncommon around the head of an anchor bolt (33).

The concrete in the vicinity of a corner socket is certainly more highly confined than that suggested by ACI 318; the lack of confinement at the top surface of the slab implies that it is not as well confined as the concrete around the head of an anchor bolt. Precisely where the bearing capacity of the concrete around a socket lies in the spectrum of values between

the two extremes is not clear. It was the need to obtain a better understanding of this bearing strength (the use of the ACI 318 values would have resulted in an extremely bulky and expensive floor module design; the use of the $f_b = 10f'_c$ was simply unwarranted and undefendable) that led to the concrete socket tests (31) discussed in detail in the next chapter.

The assumed force distribution used in analysis of the sockets is shown in the free body diagram of the socket in Figure 5. There exist four unknown quantities: f_1, f_2, f_b, and λ. f_1 is the maximum bearing stress at the bottom of the socket on the loaded side and the stress distribution is assumed to be linear, and f_2 is the maximum bearing stress against the bottom of the socket and again a linear stress distribution was assumed to exist. f_b is the maximum bearing stress directly in front of the socket and at the surface of the slab, and the ACI 318 rectangular stress block is assumed to exist here (the actual ultimate stress distribution is more parabolic in shape, but the ACI rectangular stress block produces similar results and simplifies the analysis). Mattock and Gaafar (61) used essentially the same stress distribution for the analysis of brackets in concrete columns, as was described in the last section of the previous chapter. λ is the distance from the top of the socket to the neutral axis measured along the length of the socket. Friction forces resulting from the three normal forces, C_1, C_2, and C_3, are not included in the analysis since their inclusion would have added considerable complexity to the analysis. Approximate calculations, performed to determine the effects of friction forces, indicate that the maximum effect on the bearing stress, f_b, is on the order of 10%.

There are four unknowns in the free body diagram, and only three statics equations ($\sum F_x$, $\sum F_y$, and $\sum M$) are available to solve for them. A separate effort, using data from the corner socket tests, was made to determine the neutral axis location (depth below slab

surface) using the concept of a beam on an elastic foundation. This study resulted in neutral axis depth values ranging from $4.6 \leq \lambda \leq 5.5$-in., depending on whether a uniformly or a linearly varying foundation modulus (i.e., the concrete under the "socket" beam) was assumed to exist. A value of $\lambda = 4.6$-in. was used since it was in somewhat better agreement with the results found during the testing. Knowing a value for λ made the solution of the remaining three unknowns a simple matter. The solution of the three equations for f_b results in the following equation (31):

$$f_b = \frac{P(\frac{2L}{3} + e + \frac{\lambda}{3}) - 400.3}{3.4\lambda L - 0.4675\lambda^2} \qquad (3\text{-}1)$$

The derivation of eq. (3-1) is given in Appendix 3.

The values for f_b determined from the socket tests varied from 9.71 to 13.77 ksi; and thus, the values of the ratio f_b/f'_c ranged from a 3.15 to 4.43. Using eq.(2-7) from the Mattock and Gaafar (61) paper ($f'_c = 3000$ psi) produces results for the ratio f_b/f'_c which range from 2.85 (for t/b = 5) to 5.08 (for t/b = 12). These are in very close agreement to the socket test results.

CHAPTER IV

FULL-SCALE SOCKET TESTING PROGRAM

I. REVIEW OF THE GCEP TESTING PROGRAM

In 1980 the GCEP Project approved a testing program whose purpose was to certify the design of the mount system for the centrifuge machines. The testing program was carried out in three stages:

1. Mount hardware testing
2. Socket/concrete tests
3. Floor module tests

Each of these is briefly described in the following paragraphs.

Mount Hardware Testing

Testing of the mount lugs, bushings, socket, and retaining rings with capture nut was performed. The mount lug tests (48) took place at the Oak Ridge Y-12 Plant in September and October 1980. The mount lugs were tested in shear and bending. The main reason for performing the mount lug tests was to certify that the heat treatment specified to obtain the high strengths (120 ksi to 190 ksi) for the mount lugs was adequate and to check for any brittleness resulting from the heat treat.

The remainder of the mount hardware was tested (49) in early 1981 at the Oak Ridge Gaseous Diffusion Plant (K-25). Figures 6 and 7 show the testing arrangement for the latter tests. The sockets were set in a specially machined steel plate. The objective of these tests

was to determine the behavior (load vs. deflection, strain of lugs) of the assembled socket and the associated hardware (mount lugs, bushing, retaining ring with capture nut) when subjected to the criteria loading. The system was tested initially up to the "yield estimate" load for the system (about 200 kips), and after the load was removed the test setup was dismantled and a dimensional inspection was made of the hardware. After the inspection was completed, the system was reassembled, all the gages rezeroed, and load was then applied to the operational limit of the hydraulic ram - about 330 kips - a load greater than the design ultimate load per socket. The results of these tests indicated that deformation of the mount lugs at the "yield" load level was negligible (in fact, measurements indicated that each lug was still within the machining tolerances as specified on the drawings) indicating reusability at this point. None of the tests reached ultimate strength levels for the system, though permanent deformation occurred, and some cracking of the softer bushings took place. The results of these tests indicated that the steel hardware components of the mount system were capable of transmitting the loads to the surrounding concrete. The next step was to determine the behavior characteristics of a socket in a concrete field.

Concrete/Socket Tests

These are the tests described in detail (and later analyzed with a finite element model) in this dissertation. Eight tests were performed between November 1981 and the end of January 1982 at the Oak Ridge Gaseous Diffusion Plant. Floor modules, rejected during the manufacturing process, were obtained from the vendor and the sockets removed for these tests. The main objective of these tests was to determine the bearing capacity of the surrounding concrete subjected to an eccentric load. The bearing capacity so determined would then be used in the design calculations to obtain the total structural capacity for the

centrifuge machine mounts. It was expected that the results would indicate a considerably larger bearing capacity than that allowed by the ACI 318 Specifications and also prove the adequacy of the floor module design. The testing confirmed the original concepts and resulted in bearing capacities four to five times the ACI Code allowables.

GCEP Floor Module Tests

The last phase of the testing program was to perform load tests on actual floor modules. Full-scale, nondestructive static load tests were performed on four in-place floor modules located at the GCEP facility near Portsmouth, Ohio (45). These tests had two major objectives: (1) determine the as-built load capacity defining the limit of reusability and (2) substantiate the adequacy of the design analysis.

A combination of shear and torque loads were applied to a floor module with a 300-ton capacity hydraulic ram through a 2-in. thick steel torque plate sitting on rollers on the floor. The geometry of the plate was such that the loads to the floor module produced the same ratio of shear to torque as produced by a centrifuge machine upon wrecking. The torque plate had four holes that slipped over the four corner mount lugs of the test module, and shims were used to assure that the four lugs were being loaded simultaneously. The two lugs directly in front of the jack were loosely connected (zero load transfer) in order to provide additional protection against an unexpected failure. Figure 8 shows a photograph of the test setup with the large torque plate in place. In the photograph the floor module being load tested is on the right under the torque plate. Also visible are the reaction plates attached to three floor modules directly behind the ram.

Strain gages were placed on the floor module steel beams, the concrete floor slab in the vicinity of the sockets, the loading plate, and the mount lugs. Strain gages were placed

on the mount lugs to directly indicate shear loads. Deflections of the sockets were measured using two orthogonal displacement transducers (string pots). Dial-gages were placed at various locations in order to provide supplemental deflection data. Each test was run to either a predetermined ram load or a maximum displacement of 0.050-in. at any socket. The displacement of the four sockets was being monitored graphically during each test.

A test achieving a ram load in excess of 325 kips, while still meeting the reusability criteria, would serve to verify the pretest analysis of a floor module. Table 1 shows the results of the four tests. From the table it can be seen that the 325 kip load was reached by two tests. Test No. 1 was stopped at the lower load because of problems during the testing and the possibility of permanently damaging the floor module (these tests were under a GCEP management requirement that floor modules being tested remain fully reusable).

The four tests had one major, very frustrating problem: the measured system forces (ram and four lugs) were not in static equilibrium, not even approximately close - an obvious anomaly. The amount of horizontal force transferred in friction from the plate to the floor through the rollers supporting the loading plate was assumed to be small. The ram load measurements were verified to be accurate, indicating that the shear bridges on the mount lugs (some or all) were obviously giving erroneous readings. The problem was never satisfactorily resolved. Since knowing the horizontal forces in the lugs was not a test requirement, the tests were continued. For purposes of analyzing the load-displacement behavior at a socket the theoretical loads at the sockets were used. Other than for some spalling of the concrete around the sockets, none of the tests caused any permanent damage to the modules and the slab. This series of tests provided a good check on the analysis techniques on which the design of the GCEP floor mounts were based and substantiated the

predictions that had been made for the behavior of the mount system subjected to loads supposedly approaching a yield threshold.

II. DESCRIPTION OF THE SOCKET TEST SETUP

Introduction

The mount hardware tests tested the socket and mount lug behavior and not the surrounding medium. It was decided that similar tests should be performed with the sockets embedded in a concrete slab similar to the actual GCEP floor slab. Since the overall stiffness of the socket/mount lug assembly is much greater than that of the surrounding concrete, this type of test would provide a good test to measure the concrete bearing strength for the given configuration and loads. The objective of the tests was to measure the actual concrete bearing capacity in order to obtain a relationship between the concrete ultimate strength as determined from the cylinder break tests, and the bearing capacity obtained from the tests. The testing was located in the basement of Building K-1401 at the K-25 Site. The test area was about 25-ft square, which made the testing arrangement a bit cramped. It was very poorly accessible for placing the concrete, causing problems during that phase.

Concrete Slab

Six floor modules, that had been rejected during the manufacturing process, were obtained from the vendor and shipped to Oak Ridge. The reasons for the rejections included incorrect taper dimensions inside the sockets, grooves in the taper areas of the sockets, bad welds, and cuts into the side steel beams. Eight sockets were selected from these floor modules for the tests. In a floor module the sockets are supported by the floor module steel beams, and some additional stability is provided by an anchor bar (ASTM A441 steel having

F_y = 66 ksi) attached to the outside of the socket. The floor modules were sent to the machine shop at K-25 where the sockets with the anchor bar attached were carefully removed; then any remaining machining (a couple required some minor additional work on the tapped holes for the taper lock bushing) was performed. No part of the steel beams was retained since these beams provide very little additional load capacity to the system.

The concrete test block was designed to be large enough to hold all eight of the sockets, allowing sufficient distance between the sockets such that one test would not affect the integrity of the adjacent socket locations prior to their being tested. The concrete block was 12-ft square and 2-ft thick (the same thickness as the floor slab in the GCEP facility). Figure 9 shows the slab details. The sockets were arranged in two rows of four, spaced at 31-in. intervals along each row; the two rows were spaced 6-ft back-to-back. Down the middle of the slab, in between the two rows of sockets, was a 31-in. wide by 6-in. deep cutout in which were placed four 2-in. thick steel plates, measuring 30-in. x 30-in., used to support the thrust bracket assembly. Each plate was supported on a one-inch layer of grout used for leveling purposes, and was anchored to the slab with 28 3/4-in. diameter anchor bolts having a 9.5-in. embedment length. The reinforcing steel in the vicinity of the sockets, #7 bars (conforming to ASTM A615 Grade 60) continuous in both directions at three elevations, was representative of the amount and size of steel that existed parallel to and in between the floor modules in the GCEP floor slab. There was extra steel embedded in the central portion of the block under the loading plates in the direction of the applied loads in order to resist the tension in the concrete developed by the loads. The photograph in Figure 10 shows the slab during the construction phase.

The sockets were embedded in the slab such that the top surface was at the same elevation as the concrete surface and positioned so that the attached anchor bars were

aligned with the applied load and facing towards the center of the slab. Channel beams (seen in Figure 10) were used to provide a means of holding the sockets in place until the concrete was placed. Four sockets were hung underneath the channel web using the tapped holes in the sockets; the channel spanned the 12-ft wide forms. Once the concrete hardened, the channels were removed.

The concrete was made with shrinkage-compensating cement (as in GCEP) and was non air-entrained with a specified 28-day compressive strength of $f'_c = 4000$ psi. A data sheet was prepared giving the mix design including the materials, sieve analysis, and the mix proportions. The supplier was required to provide sufficient concrete for the slab plus an additional 58 standard test cylinders - about 12 cu. ft. of concrete. The guidelines set forth in ACI 223-77 (1) were followed in establishing procedures for placing the concrete.

Construction Problems

The placement of the concrete for the concrete block proved to be very difficult and frustrating. Three major problems arose during the process: (1) fast setting of the concrete, (2) the chute being used to direct the concrete from the basement window to the concrete form broke in two, dumping much of the concrete mix on the floor, and (3) good consolidation of the concrete was difficult to obtain underneath the steel channels which were supporting the sockets.

Even though precautions were taken to ensure the adequacy of the concrete mix, the supplier apparently had little experience with the use of shrinkage-compensating concrete, which imposes some constraints during the placement. With shrinkage-compensating concrete timing is of the essence, and this was simply not properly maintained, despite the efforts of the engineers to communicate this to the supplier. The concrete-mix trucks had been delayed

and the concrete had begun to harden. The mix simply would not flow from the first truck. The addition of large quantities of water was approved, even though this would substantially reduce the strength of the concrete. Since the second truck arrived while the concrete from the first truck was still being placed, it was required to wait, compounding the problems with its concrete. Probably more water was added to the second truck than to the first.

The option was to send the trucks back to the batch plant, but at the time this was not desirable from a scheduling standpoint. Even though the concrete would have a lower strength than specified, it was decided that the test cylinders would provide good supporting data on which to base the tests.

The second problem encountered was a consequence of the poor accessibility of the basement from the road. The building itself is set back about twelve feet from the edge of the road and there is a "moat" in between. The basement is about twelve feet below the road level. The chute for the concrete had to cross the moat and drop at about a 45° angle, go in through a window and span another eight feet to the slab. During placing, the portion of the chute inside the room where the slab was located broke in two at a joint, spilling the concrete onto the floor and causing a temporary halt in the proceedings. Since there was not time to get the carpenters (this was a union atmosphere) to repair the chute because of the condition of the concrete, the rest of the concrete was carried in buckets from the window until a quick fix was performed to the chute to allow it to be used carefully. This accident added to the time required for placing the concrete, which led to the poor condition of the final concrete. It proved difficult to adequately consolidate the concrete underneath the channels being used to support the eight sockets and resulted in badly pocked areas around the sockets. This may have been less a situation where the channel prevented the proper vibrating than a case of concrete that was already setting. In addition the concrete was

setting quite rapidly towards the end of the vibration phase which certainly added to the problem. Typical pocked areas are shown in Figure 11. The pocked areas were later filled in with high strength grout, though this was more for cosmetic purposes than for strength.

Loading Assembly

The loading assembly consisted of four items: (1) the embedded load plates in the slab, (2) a large, very stiff steel thrust bracket which held the two hydraulic rams rigidly and transferred the reaction forces to the embedded plates, (3) two 100 ton hydraulic rams, and (4) a load plate which transferred the load from the two rams to the mount lug. The first was discussed previously.

The thrust bracket, seen in Figure 12, attaches to the embedded load plates with sixteen 1-in. diameter bolts. It has locations to hold three hydraulic rams (spaced at 18-in.) though only two were used per test, and has a large stiffener bracket directly behind each ram location. Since the bracket was large and bulky (1480 lb without the rams), it was necessary to devise a means to move it from one test location to another with relative ease. The arrangement of the test sockets required that the thrust bracket be completely turned around to test the sockets on the back row. Since this required the use of a small portable crane, it was decided to test all the sockets in one row, then rotate the thrust bracket assembly once and test the backside sockets. The thrust bracket was designed so that two tests could be performed without having to move it. In order to perform the second test, the outside ram was moved to the unused location, and the eight outer bolts were moved to the adjoining plate holes. In order to ensure that the two rams were producing an equal load they were driven from a common hydraulic source. The applied load was determined by measuring the

fluid pressure. The rams were 100-ton single-acting hydraulic cylinders manufactured by Enerpac and had a stroke of 6-5/8-in.

The load was transmitted from the rams to the mount lug and then into the socket through the use of a loading plate. The plate was 1.5-in. thick, and had 1.25-in. stiffener bars welded on both the top and the bottom along the edges and in a X-pattern on the top. The plate is shown clearly in the photographs in Figures 7 and 12. It has two locations where the rams fit into and push on it. There is a stiffened hole, 3.71-in. diameter (same diameter hole that exists in the centrifuge machine flange), through which a mount lug fits. A special nut was attached loosely to the top threads of the mount lug preventing the loading plate from lifting vertically. The plate was supported on six 1-in. diameter cylindrical rollers which sat on teflon sheets on the concrete block. The rollers allowed the plate to translate easily, and also served to produce the desired eccentricity of the load above the slab. For a centrifuge machine the center of the machine flange (which delivers the load to the mount lugs) is located nominally 2.6-in. above the surface of the concrete slab. In these tests the eccentricity distance was calculated from the top of the socket to the center of the contact length between the plate and the mount lugs. Measurements were taken of the actual geometry prior to the start of a test. Excluding the first test, the eccentricity was fairly constant, ranging from 2.62-in. to 2.75-in. (average 2.68-in.). The socket used for Test No.1 was shorter than the others by 3/8-in. and the eccentricity of the load was greater by the same amount.

Instrumentation

Numerous measurements were obtained during the tests. The most important (and useful) of these were the load-displacement data for both the mount lugs and the embedded sockets. For the first two tests, deflection measurements were taken at a point on the top

of the mount lug using an optical arrangement; no data were taken at the concrete surface level. Readings were made at 5 kip increments. In order to obtain these readings the load had to be held for a few seconds at each load level, an increasingly difficult task at the higher loads due to creep of the concrete. Because of this phenomenon and also the desire to obtain deflections at the top of the embedded socket, the displacement measurements for the remaining six tests were made using position transducers (linear potentiometers with a flexible cable) which permitted continuous monitoring using an XY-plotter, a much more satisfactory solution. As a consequence, the load-displacement data from the last six tests are more readily interpretable.

In addition to the load-displacement data, the other instrumentation used during the socket tests included (1) strain gages on the anchor bars, (2) four Carlson strain meters embedded in the concrete along the length of each socket, and (3) six one-inch concrete surface gages located two per line in front of the sockets and oriented at 0°, 45°, and at 90° to the line of loading. The purpose of the Carlson strain meters was to obtain a profile of the deflection along the embedded length of the sockets in order to try to obtain the center of rotation. The location of the center of rotation of the socket is a variable needed in the calculation of the concrete capacity. Additional readings were taken on the later tests to try to determine the plumbness of the sockets before and after a test (due to the manner in which the sockets were supported prior to and until the concrete had been placed and hardened there was no assurance that the sockets would end up perpendicular to the surface of the concrete).

The most useful and by far the most reliable results obtained were the load-displacement curves. The Carlson strain meters did not perform as expected; many of them were not able to be balanced at the time of a test (probably the embedded wires were

damaged during the consolidation process). The strain gages on the anchor bars were arranged in a bridge so that the bending strains were eliminated from the results, thus providing the axial strains in the bar. The strain gages indicated that the anchor bar yielded during the tests. These data were useful in deriving eq. (3-1). The concrete surface gages performed acceptably, but the data were not used in the analysis of the system.

Concrete Cylinder Tests

A total of 71 cylinders were prepared from the concrete that was placed; twelve cylinders were made from the first mix truck (this concrete went into the lower portion of the concrete block) and 59 were taken from the second mix truck. In all cases where cylinders from the two mix trucks were tested on the same day, the mix-1 breaks resulted in a higher breaking strength due to the fact that less water was added. The bulk of the data was taken from the second mix truck; these data are used in obtaining the results for the tests since it was the concrete placed in the upper portion of the block and thus was more directly involved with the tests. The cylinder break tests were performed in accordance with ASTM C-469-83 (9). One mix-2 cylinder was broken at 7-days and 26 more at 28-days. The 28-day breaks resulted in a mean strength of f'_c= 2,754 psi with a standard deviation of 129 psi. An additional four mix-2 cylinders were broken on or very near the day of a test providing reliable concrete data for each specific test. The concrete increased in strength from 2,754 psi at 28-days to 2,890 psi (up 5%) at the time of the first test (49 days), and to 3,110 psi (up 12%) for the last test (120 days).

In addition to obtaining the ultimate failure levels from the cylinder tests, load-displacement curves were obtained in both the longitudinal and transverse directions for each cylinder using a mechanical compressometer-extensometer test fixture. The transverse data

provided the Poisson's ratio for the concrete. Table 2 provides a summary of the cylinder test results for all the breaks. A typical load-displacement curve for a concrete cylinder break test is shown in Figure 13.

Test Procedure

Prior to the start of a test the condition of the concrete in the vicinity of the embedded socket was noted and monitored for hairline cracks that may have developed since the time of the concrete placement and also to note the condition of the filled in pocked areas. The latter was required to determine the behavior of the pocked areas that had been "repaired" during a test. Initially a small load of about 10 to 20 kips was applied to the system to check the strain gages and position transducers and to check the polarity settings for the XY-plots. The load was removed and the entire system rezeroed.

The load was applied by manually pumping the hydraulic system. As such it was not possible to maintain an accurate constant rate of load application throughout a test since at the higher loads more pumping was required to maintain a given load level due to creep in the concrete. This did not appear to pose serious problems. The procedure in the first two tests differed from that in the last six in that the applied load (usually at 5 or 10 kip intervals) was held at various load levels in order to obtain the deflection readings for the top of the mount lug. Determining the behavior of the concrete surface was done by monitoring the XY-plots and by listening for audible sounds emanating from the concrete itself as it was not possible to visually monitor the concrete surface in the immediate vicinity of the socket since the edge of the loading plate extended beyond the front of the lug. None of the area behind the socket was visible as it was totally covered by the loading plate.

In the early tests loading was applied to a predetermined level, usually about 100 kips, the load was removed in 10 to 20 kip decrements, and the permanent set recorded. The test setup was then dismantled and the concrete inspected for damage. In the second phase of these tests the load was continuously increased to a failure level - failure being defined as the point where increasing the load became very difficult due to the creep of the system. In no test did the load-displacement actually reach a peak value and start to fall, but in all cases the behavior was very nonlinear. In some of the tests the load was applied as fast as possible until failure was reached in an attempt to measure the effect of loading rate on the strength of the system (the results of this parametric test were inconclusive simply due to the fact that the fastest loading rate was still a static load test - about one minute to failure - as far as the concrete was concerned). Once the system had been loaded to failure and then unloaded, the test setup was dismantled and the concrete area was photographed and measurements were taken of the failure zone.

III. SUMMARY OF THE SOCKET TESTS

This section presents a very brief description of each of the eight concrete/socket tests. Highlights and problems encountered during any individual test are mentioned. During some of the tests, the researchers made an audio recording of events as they transpired, which was later transcribed to paper. These were very useful in preparing this section.

Test No.1

In this test the deflection of the top of the mount lug was read optically. The deflection of the top of the socket was not monitored. All of the strain gage data were sampled at 5 kip intervals, and the data were recorded with data acquisition equipment. This

process required holding the applied load constant for a few seconds in order to sample the necessary channels of data. At the end of the test the data were printed out. Plotting of the load-displacement data for the top of the mount lug was done manually in order to monitor the progress during the test. At a load of 81 kips the curve showed some small nonlinearity. The load was run up to 100.5 kips, then reduced in 10 kip increments until the load was completely removed; the permanent set measured 0.043-in. During the first 10 kip decrement of the load the deflection increased due to creep of the concrete. At this point the loading plate was removed and the concrete was inspected to determine the effects of the 100 kip load. Some minor spalling of the concrete in front of the socket was noted. The affected area, which was not present prior to the start of the test, was 1/30-in. deep by 1-in. long and 1/4-in. wide. In the second phase of the test the load was applied constantly until a failure level was reached. The reloading portion of the curve was linear until the 100 kip load level was reached. Based on the load-displacement curve, failure was taken to be 164.5 kips (with a deflection of 0.574-in.). Again, during the unloading, creep was taking place. The final permanent set was 0.45-in. The concrete had spalled around the socket and the horizontal deflection of the top of the socket was about 0.2-in. There was also some rotation of the socket.

Test No.2

This test, which was taken to failure of the concrete, included two unloading cycles, though the test apparatus was not disassembled to inspect the condition of the concrete or the socket after the unloading steps. As in the previous test, the only deflection measured was that at the top of the mount lug using the optical instrumentation. The first loading cycle was taken to a load of 56.6 kips. The resulting permanent set, upon unloading, was 0.020-in.

After eight minutes the set had not changed. The second loading sequence was taken up to 81 kips before unloading. The permanent set had increased to 0.030-in. The final sequence reached a load of 185 kips, by which point the concrete surface had visibly ruptured, accompanied by a large deflection. Figure 14 shows a photograph of the concrete after the test was terminated. The concrete that popped up on the back side is from the anchor bar attached to that side raising up with the rotation of the socket. Note that the concrete on the front edge spalled far beyond the area which had been refilled after the concrete consolidation problems. The concrete immediately in front of the socket was crushed. The damage pattern shown in Figure 14 is fairly typical of all the tests.

Test No.3

This was the first test in which position transducers were used to measure the deflection data. Load-displacement data were obtained for the top of the mount lug and also for the top of the socket. The maximum load measured in this test was 152 kips, but accurate deflection data were not obtained at load levels above 120 kips due to a problem in the recording instrumentation. The socket deflection at the upper load is only an approximation. The use of an XY-plotter would have been very useful in obtaining better data, and this was recommended for future tests.

Test No.4

In this test simultaneous recording of the load-displacement data for the top of the socket was obtained using an XY-plotter. All the data were still fed into the data acquisition equipment. The plateaus seen in the XY-plot of the socket deflection (Figure 15) were caused by holding the load constant for the few seconds required to take readings. The

relative displacement between the top of the mount lug and the socket was nearly 3/8-in., comprised of bending of the lug and rotation of the socket. The maximum load was 164 kips and the final permanent set of the top of the socket was about 0.25-in.

Test No.5

Three attempts were required to perform this test. Problems in both XY-plotters forced a rescheduling the first time. The second try was made three weeks later, and this time the epoxy holding down the string pot on the socket would not set properly. In addition, the loading transducer appeared to be behaving erratically, so once again the test was postponed. The third try proved successful. After a very short load sequence to only 20 kips (to test the data and equipment), the load was quickly run up to 120 kips (the run was supposed to go only to 80 kips, but due to the fast loading rate this level was overshot), then removed. The final loading sequence was made to a level of 163 kips with more than 0.3-in. lateral deflection of the socket, but the test was terminated because the XY-plots pegged out around 155 kips, due to the large deflection. The maximum load obtained for this test was the lowest of the eight tests, which might be at least partially explained by the fact that this socket location (No. 8) was the last one where concrete was placed around, and as a result probably had the worst concrete of the lot surrounding it.

Test No.6

An error in the pressure transducer readings was encountered during this test. The problem was noted during the last loading sequence when the XY-plotter pegged out at what was thought to be 200 kips, but the load continued to increase easily. Since it was too late to stop this test and determine the cause of the error, the test was continued to failure.

Fortunately, the data were being stored separately in the data acquisition system, and the ram pressure and socket deflections for the test were able to be retrieved. After the test, the pressure transducer was recalibrated and corrected load-displacement curves were obtained. The adjusted loads were found to be approximately 33 percent lower than the original values. After a quick loading and unloading cycle up to about 13.5 kips, the load was run up to 54 kips, removed and a permanent set of 0.003-in. was measured. The last loading sequence eventually reached a load of 173 kips and showed a total socket deflection of 0.138-in.

Test No.7

This test was the only one of the eight that reached a load level of 200 kips, at which point the test was terminated. Four load-unload cycles were performed. The first one, to 20 kips, was the data check run. The next two load cycles were taken to 80 and 100 kips respectively. The permanent set after the 80 kips cycle was 0.005-in., and after the 100 kips cycle it had doubled to 0.01-in. The last load sequence was stopped at the 200 kips plateau. The deflection of the top of the socket at this level was 0.266-in. The loading curve still had a noticeably positive slope at the time of termination, indicating that the socket could continue to resist a higher load. The final permanent set upon unloading was not obtained.

Test No.8

This test was also a very successful one. It reached a maximum load of 193.7 kips. The XY-plotter pegged at a deflection of 0.295-in. and a load of about 188 kips. With a load of 185 kips the measured deflection was 0.260-in., so it can be seen that the concrete was highly inelastic at this stage. Loading cycles to 20, 80, and 100 kips were performed as in the previous test. The permanent sets measured after the latter two cycles were 0.006-in. and

0.012-in., respectively. Figures 16 and 17 show the XY-plotter load-displacement curves for both the top-of-socket and the top-of-lug displacements. The measured displacement of the top-of-lug at a load of 185 kips was 0.655-in.

Summary of Tests

Table 3 presents a brief summary of the tests along with the analysis results of the actual bearing strength using eq. (3-1). The initial slope values are based on the load-displacement data for the top of the socket which were available only for the last six tests.

Figure 18 presents the load-displacement curves at the top of the socket for Tests 3 through 8. The graph shows that there was a substantial variation from test to test in the maximum loads, the maximum deflections, and the initial "linear" slopes. It is difficult to make any conclusive statements concerning either the maximum loads or the amount of deflection observed in these tests, except to state the tests clearly indicate that a large margin over the Code allowable concrete bearing values, about three to four times, is available for these embedments.

CHAPTER V

FINITE ELEMENT ANALYSIS OF CONCRETE - A DISCUSSION

I. INTRODUCTION

The advent of high speed computers and the development of finite element technique formulations have presented the structural engineer and the engineering researcher with very powerful tools to study quite complex structural configurations. While concrete structures, on a large scale, have been analyzed and designed quite adequately using linear theory for many years, the analysis of highly complex concrete configurations requiring the use of more sophisticated mathematical models describing the behavior of concrete as a nonlinear material is more recent. However, the use of nonlinear finite element methods for analyzing concrete and concrete structures is still rare because, as pointed out by Bedard and Kotsovos (29), of the unpredictability of the results.

Literature Search

The current engineering data bases contain a wealth of literature in the areas of (1) constitutive modeling of concrete and (2) finite element analysis, both linear and nonlinear, of concrete structures. New articles appear almost on a monthly basis in numerous journals. Two literature searches were conducted for this study, both using the DIALOG Information Services available through the library system at the DOE facilities in Oak Ridge. The first, in late 1985, spanning ten years between 1975 and 1985, listed close to 8000 articles whose abstract (or key words) included the term "concrete" along with "finite element or model or

stress/strain or constitutive or endochronic or nonlinear or inelastic or plastic or elastic-plastic" - and which were written in English. Narrowing the search by appending only the terms "finite element or constitutive or endochronic" reduced the number of articles considerably down to 950. The second literature search, conducted in January 1989 and using the same search pattern, continued from where the first ended and went through the end of 1988 (however, many articles which appeared in the engineering journals in 1988 may not have yet been entered into the data base). This second search produced an additional 815 articles, giving a total over the last 15 years of nearly 1800 articles dealing with the topic being discussed herein. The abstracts for these were printed out and reviewed for possible usefulness to this study. Of these, about 200 articles could be considered to more-or-less apply to the study at hand, and only a small number of these were actually used. The ASCE journals of the Structural and Engineering Mechanics Divisions were invaluable sources of information and additional references.

II. CONSTITUTIVE MODELING OF CONCRETE

Although the finite element method of analysis has been around for many years, its application and usefulness to concrete structures for anything but the simplest configurations has been generally limited due to the lack of adequate mathematical material models. Even though, in recent years, a considerable amount of research has been done in studying the behavior of concrete, the constitutive modeling of concrete remains an extremely active research area, and will certainly continue to remain so for many more years.

Constitutive modeling of concrete can be classified into the following general categories: (1) mathematical curve fitting methods of the stress-strain curves, (2) linear and nonlinear elasticity models, (3) perfect and work hardening plasticity models, (4) fracture

(damage) type models, and (5) the endochronic theory of plasticity. The current trend in research is towards the last four categories. A number of papers (32,39,42) and conference proceedings (27,40,41,64) dealing with the general issues of constitutive modeling of concrete and reinforced concrete are included in the references. The ASCE report (81) on finite element analysis of reinforced concrete was an early (1982) review of the subject. The textbook by Chen (36) presents a good, if slightly dated (1982), discussion of the subject of plasticity of reinforced concrete. Bangash (14) presents a later treatise on concrete modeling, while the two textbooks by Chen et al. (37, 38) are more recent references on the subject of plasticity and nonlinear analysis in structural engineering and soil mechanics.

Linear and Nonlinear Elastic Theory Methods

The linear-elastic approach has been widely used in modeling plain and reinforced concrete because of its ease of application. Incrementally linear constitutive models characterized by an orthotropic tangential stiffness have been used with good results by Balakrishnan et al. (11-13) recently, although Bazant and Bhat (24) critique the use of orthotropic models as being restricted to loading histories in which the principal stress directions do not rotate. Also, when strain localization occurs, the standard tests do not accurately measure material properties.

The mathematical characterization of the concrete can be improved through the use of a nonlinear elastic stress-strain relationship where the material behavior is characterized by a variable secant-modulus. There are primarily two approaches commonly used in the formulation of nonlinear elastic models for concrete: (1) the hyperelastic formulation which is a path independent reversible process with no memory , i.e., the current response is a function of the current state of stress and not of the load history, and (2) the hypoelastic

formulation which is a path dependent, irreversible process with limited memory, where the instantaneous response is a function of the current state of strain and of the stress path followed to reach that strain. Numerous articles are found in the literature (7,8,22,23,46,57, 59,67,68,70,74) on the nonlinear-elastic formulation. The ADINA concrete model is based on the hypoelastic theory and is described in detail by Bathe and Ramaswamy (22). Gedling et al. (46) evaluated the ADINA-81 concrete model. The most recent modifications to the ADINA concrete model are described by Bathe et al. (23). There have been eight ADINA conferences (16-21). The ADINA concrete material model is discussed in more detail in Section III of this chapter.

Plasticity Theory Methods

Constitutive modeling of concrete based on the theories of perfect and work-hardening (44,50,58,65,77) plasticity have also been studied. Although the concept of perfect plasticity, in which the onset of yield is followed by a yield plateau, was originally developed for metals, it has been used to model the behavior of concrete. For concrete that is highly confined this assumption leads to a rather simple, but probably reasonable, first approximation for the behavior of concrete. A generalization of the elastic-perfectly plastic model is one that allows for work-hardening (or strain-hardening) to occur. In this method the material is initially linear-elastic up to some level, defined by an initial yield surface. The material behavior beyond this initial yield surface is characterized by an associated flow rule (so called because the plastic flow is associated with the current yield surface and is directed normal to the yield surface) which will apply until a fracture (cracking in tension or crushing in compression) load surface is reached. As the material is stressed beyond the initial yield surface, a subsequent yield surface, called the loading surface, is developed, which replaces the initial yield surface.

If the material is then unloaded, upon reloading to the new loading surface no additional permanent deformation occurs. Straining and stressing beyond this new yield surface continue to move the loading surface outward once again, until eventually the fracture surface is reached. Once the loading level has reached the fracture surface, the concrete starts to flow under constant stress (perfectly plastic) until it either cracks or crushes. The work-hardening plastic theory models accurately predict inelastic dilatancy (increase in volume in the plastic range) and hydrostatic loading conditions, but fracturing accumulation and stiffness degradation due to stress reversals may not be as acceptable (32).

The hypoelasticity and plasticity theories are equivalent during loading, but differ in defining the unloading paths (32). The critical elements in the work-hardening models are the definition of the associated flow rules, the concrete fracture levels, and the mathematical behavior at the fracture surface levels. The modeling of the stress-strain softening behavior beyond the point of peak stress is also very difficult to accurately represent.

Fracture and Endochronic Theory Methods

The combination of plasticity theories and fracture (damage) concepts to obtain the constitutive relations for concrete have been in use for a number of years and include the plastic-fracturing model (28), the endochronic model (25,53), the elastic progressive fracturing model, and the bounding surface model of the softening type. These models account for such behavioral characteristics as stiffness degradation as damage progresses, energy dissipation during cyclic loading, shear compaction-dilitancy phenomenon, hydrostatic pressure sensitivity, and strain softening. Bazant, at Northwestern University, has done substantial research (26) in the area of fracture mechanics in concrete and reinforced concrete, much of which is being applied towards developing material models for concrete.

The endochronic theory uses the concept of intrinsic time (or endochronic time) to measure the extent of damage of the internal structure of the concrete material as it is subject to deformation histories; it is able to characterize the behavior of concrete without having to rely on either the yield condition or the hardening rules. The endochronic and the plastic-fracturing material models are very powerful in simulating a broad range of concrete material behavior, but they have drawbacks in that they require a large number of material parameters which may be difficult to obtain without extensive testing, and secondly, that the incrementally nonlinear approach results in very costly numerical computations for the finite element calculations.

III. FINITE ELEMENT MODELING OF CONCRETE STRUCTURES

Even though the focus of the previous discussion has been on the importance of defining adequate material models in order to obtain more meaningful and accurate results in analyzing concrete structures by the finite element method, there exist other areas of equal importance that are pertinent to a successful analysis which must not be overlooked. These include such varied topics as numerical methods and modeling techniques, the effect of mesh size on the accuracy of the finite element results, the effects of loading type and load increment size, the appropriate convergence and equilibrium criteria, and the modeling of the interface contact between two solid surfaces. Bathe's textbook on finite element methods (15) is a thorough work on finite element methods, and covers much of the theoretical basis for the finite element procedures used in ADINA.

As expected, numerous references for any of these topics exist and may be found in a number of conference Proceedings (16-21,27,40,41,64) or engineering journals. Numerical aspects of modeling in the field of geomechanics is discussed by Zienkiewicz (82) and Bergan

(30). Sussman and Bathe (80) review the techniques used in obtaining an adequate finite element mesh for a typical linear-elastic static analysis. The problem of modeling an interface surface between two dissimilar contacting materials where friction exists and where slip, or potential slip, may occur is discussed by Herrmann (51) and Ruina (75). Other articles relevant to the constitutive modeling of friction and slip appear in the Proceedings for the two Constitutive Laws Conferences edited by Desai et al. (40,41).

Finally, the theories surrounding concrete as a material and the finite element analysis of concrete and reinforced concrete structures are eventually only meaningful to the practicing engineer if they can be related to solving problems in the real world. Again, there are many articles showing applications of nonlinear finite element techniques and their relationship to certain types of constitutive models for concrete. General discussions on the subject are presented by Bedard and Kotsovos (29), Leibengood et al. (60), and Meyer and Bathe (63). Mroz (66) gives a general discussion of the current state-of-the-art (1985 time frame) of inelastic analysis as it pertains to geomaterials (rocks, soils, and concrete) and presents future areas of possible research. Balakrishnan and Murray (11) develop a nonlinear elastic orthotropic constitutive model for concrete and then apply this relationship in a smeared cracking nonlinear finite element analysis of two-dimensional panels and beams (12,13). Chang et al. (35) present a complete time-independent plasticity model and incorporate it into a smeared cracking nonlinear analysis applied to four concrete panels and compare the results with experimental biaxial data. Ottosen performs a nonlinear axisymmetric finite element analysis of concrete cylinder tests (69) and studies the effects of varying the element size and h/d ratio.

Three papers, by James et al. (52), Ottosen (71), and Peier (72), are of particular interest to this study as they deal with analyzing the tensile pull-out strength of embedded

bolts and anchors in concrete using nonlinear techniques. Peier's study is of interest because it considers relatively short anchors (l/d = 3.2) and, furthermore, because it uses the ADINA program.

IV. GENERAL DESCRIPTION OF ADINA

Material Models

ADINA is a computer code, developed by Dr. K. J. Bathe of the Massachusetts Institute of Technology, that performs two and three-dimensional static and dynamic, linear and nonlinear, displacement, force, and stress analysis of structures. It includes a number of different element types. For each type of element a number of material models are available (twelve different material models including a user-supplied model), which can be grouped into three general categories: (1) linear elastic - where the displacements are small and the strains infinitesimal, (2) materially nonlinear only - where the displacements are small, the strains infinitesimal, and only the material stress-strain relationship is nonlinear (no geometric nonlinearities exist), and (3) large deformation - where large deformations may be exhibited by an element having large strains and both the material stress-strain relationship and geometric nonlinearities are permitted. The first two types were used in the analyses described herein. Table 4 presents a listing of the element and material models available in the ADINA program. In the present work the isotropic linear elastic (constant Young's modulus and Poisson's ratio), the nonlinear elastic (stress is specified as a piece-wise linear function of the strain), the concrete, and the elasto-plastic material models were used. The concrete model is characterized by a multi-axial stress-strain relation defined by using for the three principal stress directions a uniaxial stress-strain relation that is modified under biaxial and triaxial stress states. The concrete model implemented in ADINA is discussed in detail

later in this chapter. Complete details of the other elements and material models available in the ADINA program can be found in the ADINA manuals (4,5,6) and the textbook by Bathe (15).

Elements

As can be seen in Table 4, ADINA provides thirteen element types, including the general element which is a special user supplied element in which the stiffness, mass, and damping matrices are input parameters. For the analyses described in this work, four elements were used, these being the truss, the two-node beam (later the isoparametric beam), the shell element, and the three-dimensional solid.

Truss element: The truss element is a one-dimensional element containing 2- to 4-nodes which transmits only axial forces. Translation in the three global directions is permitted at each node. The reinforcing bars are modeled using the linear material model truss element.

The truss element is also used to model the interface between two surfaces, such as that of the steel socket and the concrete slab, where compression forces, but not tensile forces, are allowed. This is accomplished by using the concept of a gap element, which is a two-node, materially nonlinear, truss element. Gap elements are used to model contact situations when the bodies undergoing the contact experience only small displacements and rotations. The gap element provides resistance to compression but not to tension; its material stress-strain curve is sketched below. Even though there has to be a minute original length to the gap element (this is done by setting the vector distance between the two end nodes equal to a small number, in this case it was set to 0.001-in.) so that ADINA can calculate the strain in the element, the program is given an initial zero gap width indicating the two bodies

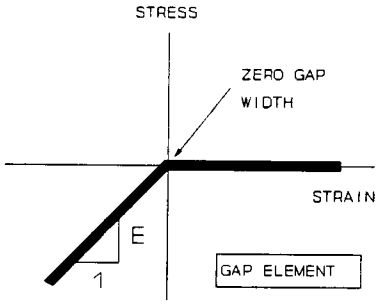

are initially in contact. If the use of the gap element is not desired at a given location, one of the two nodes is simply "frozen" out of the analysis (fixing all of its degrees of freedom and not connecting it to any active element) while the second one is used to connect the two elements in a rigid fashion at that point.

Shell Element: The shell element in ADINA is a 4- to 32-node isoparametric triangle or quadrilateral with the option of having the nodes at the mid-surface or on the top or bottom surfaces of the element. The shell elements used in this analysis are of the 4-node mid-surface (i.e., the nodes represent the four mid-surface corners of the shell) variety and are used to represent the steel plates anchoring the reaction/loading assembly located in the central portion of the slab. It has both membrane and bending behavior capabilities. The choice of using the shell element instead of the plate element was based solely on the fact that the plate element in ADINA is available only as a triangular shape and would require more elements to model the same geometry.

Beam and Isoparametric Beam Element: The beam element is a two node element, having six degrees of freedom per node, which transmits arbitrary forces and moments. This element was used to model the anchor bar that is welded to the backside of the socket and is embedded into the concrete slab providing some resistance against rotation and pullout. The iso/beam element is a 2- to 4-node element having the same general characteristics as

the beam element. In an isoparametric element the geometry and displacement of the element are described in terms of the same parameters and are of the same order. The most common use of the iso-beam elements is to model curved beams. The iso/beam element was used after an error was detected, and verified, in the computation of strains in the beam element, which appears to be an error with the ADINA code. This error was found in all three versions of ADINA that were used. On the first load step of a problem, ADINA correctly calculates the stresses and deflections, but the strains are double the correct value; thereafter, ADINA correctly determines strains, but the initial error is carried throughout. The nonlinear elastic material model formulation was used for the anchor bar. Near the conclusion of this work the iso/beam element was eliminated from the model because the anchor bar was eventually modeled using the 3-D solid element.

Three-Dimensional Solid Element: The three-dimensional solid element found in the ADINA code is an 8- to 27-node isoparametric element. The most commonly used 3-D solid element in the model was the 8-node rectangular solid element consisting of the eight corner nodes. Wedge shaped prisms are formed by degenerating the rectangular solid element by forming a zero length side (i.e, a surface is described by corner nodes X1, X2, X3, and X1 again). The concrete slab, the steel socket, and the steel mount lug were modeled using the three-dimensional elements. The large majority of the concrete elements and all of the steel socket elements used the basic rectangular solid element, while the steel mount lug elements used the wedge definition. A few concrete elements required that a ten node element be defined, for elements bordered on one side by two elements rather than one; the extra two nodes are added along the appropriate edges of the element. In general a 3 x 3 x 3 integration order was used (a total of 27 integration points) for these elements. A linear elastic material formulation was used for the elements representing the steel socket and

mount lug as it was assumed that these elements remained below the yield point of the material at all times.

The concrete elements used either the nonlinear concrete model or the linear elastic model to represent the material behavior. Limiting the number of nonlinear concrete elements was done in order to reduce the computation time and the storage space required to calculate and reformulate the stiffness matrix during the loading cycle and to reduce the complexity of calculating a state of equilibrium after each load step. About 20 percent of the concrete elements were modeled using the concrete material formulation. The intent was to initially assume a nonlinear region, and after reviewing the output results at higher loads modify the model as needed. The concrete in the vicinity of the loaded socket was modeled using the concrete material model, while the concrete further away was assumed to behave linearly. The nonlinear concrete region was 18-in. long (9-in. on either side of the center of the mount lug in the direction of the load) by 21-in. (10.5-in. due to the symmetry in the model) wide and 16-in. deep.

V. ADINA-84 CONCRETE MODEL

Introduction

The concrete model incorporated in the ADINA-81 code is described by Bathe and Ramaswamy (18) and also in the ADINA System Theory and Modeling Guide (6). The remainder of this section provides a brief review of the concrete model used in the -84 version; the -81 and -84 versions of the concrete model were identical, so the discussion below refers only to the -84 version. The characteristics of the early ADINA concrete model are as follows:

1. It is a hypoelastic model based on a uniaxial stress-strain relation that is generalized to take multiaxial stress states into account;
2. Tensile cracking and compression crushing are identified using either default or user defined failure surfaces;
3. Strain softening occurs from crushing (at ultimate stress) to ultimate strain, at which the material totally fails;

The model employs three basic features (22) to describe the material behavior. These are (1) a nonlinear stress-strain relation that includes strain-softening to allow for the material weakening under increasing compressive stress, (2) a set of failure envelopes that define cracking in tension and crushing in compression, and (3) a procedure to model the post-cracking and crushing behavior of the material. The following paragraphs discuss the uniaxial and multiaxial relations, the failure envelopes, and the post-cracking and crushing behavior.

Material Failure Criteria

The material models are separated into uniaxial and multiaxial loading conditions and also into pre- and post-failure modes. The general multiaxial stress-strain relations are derived from the uniaxial stress-strain relations. The remainder of this section describes the uniaxial and multiaxial stress-strain relations, the material failure envelopes, and the post-failure material behavior.

Uniaxial conditions: The ADINA uniaxial stress-strain curve is shown in Figure 19 (the uniaxial parameters are identified by the curl over them, and the superscript "t" refers to time "t" - in the case of a static analysis "t" should be considered as a load step number). It can be seen from this figure that the uniaxial stress-strain curve has three segments, namely (1) ${}^t\tilde{\varepsilon} \geq 0$, (2) $0 > {}^t\tilde{\varepsilon} \geq \tilde{\varepsilon}_c$, and (3) $\tilde{\varepsilon}_c > {}^t\tilde{\varepsilon} \geq \tilde{\varepsilon}_u$. If ${}^t\tilde{\varepsilon} \geq 0$, the material is in tension, the stress-

strain relation is linear, and a constant Young's modulus, $\tilde{E}_o$, is used. In this case the stress-strain relationship is expresses as ${}^t\tilde{\sigma} = \tilde{E}_o {}^t\tilde{e}$, or

$$\tilde{E}_o = \frac{d^t\tilde{\sigma}}{d^t\tilde{e}} \tag{5-1}$$

For the case of ${}^t\tilde{e} \leq 0$ then the following relationship (22) is used for the Young's modulus:

$${}^t\tilde{E} = \frac{\tilde{E}_o[1 - B({}^t\tilde{e}/\tilde{e}_c)^2 - 2C({}^t\tilde{e}/\tilde{e}_c)^3]}{[1 + A({}^t\tilde{e}/\tilde{e}_c) + B({}^t\tilde{e}/\tilde{e}_c)^2 + C({}^t\tilde{e}/\tilde{e}_c)^3]^2} \tag{5-2}$$

where

$$A = [\tilde{E}_o/\tilde{E}_u + (p^3 - 2p^2)(\tilde{E}_o/\tilde{E}_s) - (2p^3 - 3p^2 + 1)]/[p(p^2 - 2p + 1)]$$

$$B = [(2(\tilde{E}_o/\tilde{E}_s) - 3) - 2A]$$

$$C = [(2 - \tilde{E}_o/\tilde{E}_s) + A]$$

In the above equations, $\tilde{E}_o$ is the initial tangent modulus, $\tilde{\sigma}_c$ is the maximum compressive stress, $\tilde{e}_c$ is the strain corresponding to $\tilde{\sigma}_c$, $\tilde{E}_s = \tilde{\sigma}_c/\tilde{e}_c$ is the secant modulus corresponding to the maximum stress, $\tilde{\sigma}_u$ and $\tilde{e}_u$ are respectively the ultimate compressive stress and strain, $\tilde{E}_u = \tilde{\sigma}_u/\tilde{e}_u$ is the secant modulus corresponding to ultimate stress, and $p = \tilde{e}_u/\tilde{e}_c$. All these parameters are obtained from uniaxial tests. The stress-strain relation in eq. (5-1) assumes monotonic loading.

Multiaxial Conditions: The stress-strain relations are evaluated differently for multiaxial conditions depending on whether the material is loading or unloading. Poisson's ratio remains constant for all stress conditions. Loading and unloading of the material are measured by the loading function:

$$ {}^{t}f = {}^{t}s + 3\alpha\,{}^{t}\sigma_m \tag{5-3} $$

where

$$ {}^{t}\sigma_m = {}^{t}\sigma_{ii}/3 $$

$$ {}^{t}s = [(1/2)\,{}^{t}s_{ij}\,{}^{t}s_{ij}]^{1/2} $$

$$ {}^{t}s_{ij} = {}^{t}\sigma_{ij} - \delta_{ij}\,{}^{t}\sigma_m $$

and α is an input constant and δ_{ij} is the Kronecker delta ($\delta_{ij}=1$ when i=j and 0 otherwise). The material is loading if ${}^{t}f \geq f_{max}$ and unloading if ${}^{t}f < f_{max}$ where f_{max} is the maximum value of the loading function that has been reached during the analysis up to time "t".

During unloading the material is considered to be isotropic, and the initial Young's modulus, $\tilde{E}_o$, is used in forming the incremental stress-strain matrix for both stiffness and stress calculations.

In loading, ADINA uses a stepwise iteration where the stress and strain increments are determined using an equivalent multiaxial Young's modulus. The principal stresses ${}^{t}\sigma_{pi}$ (where ${}^{t}\sigma_{p1} \geq {}^{t}\sigma_{p2} \geq {}^{t}\sigma_{p3}$, tensile positive) are calculated, and for each principal stress direction, a tangent modulus, ${}^{t}\tilde{E}_{pi}$, corresponding to the strain state, ${}^{t}\tilde{e}_{pi}$, is evaluated using the uniaxial equations (5-1) and (5-2). In the latter, the strains ${}^{t}\tilde{e}_{pi}$ are used and the parameters $\tilde{\sigma}_c$, $\tilde{\sigma}_u$, $\tilde{e}_c$, and $\tilde{e}_u$ are replaced with the variables $\tilde{\sigma}'_c$, $\tilde{\sigma}'_u$, $\tilde{e}'_c$, and $\tilde{e}'_u$, which are described later in the section on material failure envelopes.

When the material is in tension or low compression, it is assumed to be isotropic, the stress state being defined by ${}^{t}\sigma_{p3} \geq \kappa\tilde{\sigma}'_c$ where κ is an input parameter typically between 0.4

and 0.7. For this condition, the multiaxial Young's modulus, ${}^{t}E$, is determined using the following equation:

$$ {}^{t}E = \frac{|{}^{t}\sigma_{p1}|{}^{t}\bar{E}_{p1} + |{}^{t}\sigma_{p2}|{}^{t}\bar{E}_{p2} + |{}^{t}\sigma_{p3}|{}^{t}\bar{E}_{p3}}{|{}^{t}\sigma_{p1}| + |{}^{t}\sigma_{p2}| + |{}^{t}\sigma_{p3}|} \tag{5-4} $$

The stress increment from time t to time $t+\Delta t$ is calculated from the relationship

$$ \sigma = \hat{C}e \tag{5-5} $$

where $\hat{C}$ is a matrix providing the relationship between the stresses and strains and can be described for either two-dimensional or three-dimensional stress conditions. For the case where the material is undergoing tension or low compression, the matrix $\hat{C}$ is given by:

$$ \frac{{}^{t}E}{(1+\nu)(1-2\nu)} \begin{bmatrix} 1-\nu & \nu & \nu & 0 & 0 & 0 \\ & 1-\nu & \nu & 0 & 0 & 0 \\ & & 1-\nu & 0 & 0 & 0 \\ & & & \frac{1}{2}-\nu & 0 & 0 \\ & sym. & & & \frac{1}{2}-\nu & 0 \\ & & & & & \frac{1}{2}-\nu \end{bmatrix} \tag{5-6} $$

If the material is subject to high compression, ${}^{t}\sigma_{p3} < \kappa\tilde{\sigma}'_{c}$, it is assumed to be orthotropic with the orthotropy directions defined by the three principal stress directions. The three-dimensional stress-strain matrix, $\hat{C}$, corresponding to the high compression case is given by:

$$\frac{1}{(1+\nu)(1-2\nu)}\begin{bmatrix} (1-\nu)^t\tilde{E}_{p1} & \nu^tE_{12} & \nu^tE_{13} & 0 & 0 & 0 \\ & (1-\nu)^t\tilde{E}_{p2} & \nu^tE_{23} & 0 & 0 & 0 \\ & & (1-\nu)^t\tilde{E}_{p3} & 0 & 0 & 0 \\ & sym. & & (\tfrac{1}{2}-\nu)^tE_{12} & 0 & 0 \\ & & & & (\tfrac{1}{2}-\nu)^tE_{13} & 0 \\ & & & & & (\tfrac{1}{2}-\nu)^tE_{23} \end{bmatrix} \tag{5-7}$$

where ν is Poisson's ratio (constant as mentioned previously) and the ${}^tE_{ij}$, with $i \neq j$, are evaluated using the relationship

$${}^tE_{ij} = \frac{|{}^t\sigma_{pi}|\,{}^t\tilde{E}_{pi} + |{}^t\sigma_{pj}|\,{}^t\tilde{E}_{pj}}{|{}^t\sigma_{pi}| + |{}^t\sigma_{pj}|} \tag{5-8}$$

The principal stresses, ${}^t\sigma_{pi}$, together with the three-dimensional tensile and triaxial compressive failure envelopes, shown in Figures 20 and 21 and discussed in the next paragraph, determine a pseudo-uniaxial stress-strain curve accounting for behavior of the concrete material during multiaxial stress conditions, and determine whether the material is undergoing a tensile or compressive (crushing) failure. For example, in the case of the material undergoing tension or low compression, the stress-strain matrix is given by eq. (5-6) and the multiaxial Young's modulus is given by eq. (5-4), where the ${}^t\tilde{E}_{pi}$, representing the uniaxial Young's modulus corresponding to the current strain increment e are evaluated from the uniaxial stress-strain relationship in Figure 19 as

$$ {}^{t}\bar{E}_{pi} = \frac{[\tilde{\sigma}|_{at}({}^{t}e_{pi} + e_{pi}) - \tilde{\sigma}|_{at}({}^{t}e_{pi}]}{e_{pi}} \tag{5-9} $$

where the ${}^{t}e_{pi}$ and e_{pi} are the strain and incremental strain components, respectively, at time t measured in the directions of the principal stresses ${}^{t}\sigma_{pi}$.

Material failure envelopes: ADINA uses failure envelopes to model the failure of the material in tension and compression and to account for multiaxial conditions in the uniaxial stress-strain law (Figure 19), and to determine the failure mode (tensile or crushing). The triaxial tensile failure envelope (Figure 20) and the triaxial compression failure envelope (Figure 21) have been implemented in the ADINA-81 and ADINA-84 versions of the program.

In the tensile failure diagram, the tensile failure stress (strength) decreases linearly as one (or both) of the other principal stresses, ${}^{t}\sigma_{pi}$, increases in compression. It is also to be noted that the tensile strength in a given direction is not affected when the stresses in the remaining two principal directions are in tension.

In Figure 21, the triaxial compression envelope, the magnitude of the maximum compressive stress, ${}^{t}\sigma_{p3}$, is plotted as a function of the other two principal stresses, ${}^{t}\sigma_{p1}$ and ${}^{t}\sigma_{p2}$, all normalized by dividing by the uniaxial compressive strength, $\tilde{\sigma}_c$. The failure surface is specified first by defining six values for the ratio ${}^{t}\sigma^{i}_{p1}/\ \tilde{\sigma}_c$ at which two-dimensional failure envelopes of ${}^{t}\sigma_{p2}$ and ${}^{t}\sigma_{p3}$ are defined using 18 input values for ${}^{t}\sigma^{i,j}_{p1}/\ \tilde{\sigma}_c$ (i=1,...,6; j=1,2,3) corresponding to the stress magnitudes ${}^{t}\sigma_{p2} = {}^{t}\sigma_{p1}$, ${}^{t}\sigma_{p2} = \beta\,{}^{t}\sigma_{p3}$ (where β is a constant), and ${}^{t}\sigma_{p2} = {}^{t}\sigma_{p3}$. The user has the option of inputing his known values for the triaxial compressive failure envelope parameters, or the ADINA set of default values (which are shown in Figure 21) may be used.

As indicated previously, the uniaxial stress-strain curve is modified in the case where multiaxial stress conditions exist through the use of the principal stresses, ${}^t\sigma_{pi}$, and the failure envelope curves. A modified uniaxial stress-strain curve (Figure 22) is obtained. One factor, γ, used to scale the strains $\tilde{\varepsilon}_c$ and $\tilde{\varepsilon}_u$, is an input parameter, and the other scaling factor, $\gamma_1 = \tilde{\sigma}'_c / \tilde{\sigma}_c$, is obtained from the triaxial failure envelope by holding ${}^t\sigma_{p1}$ and ${}^t\sigma_{p2}$ constant and reading the new value for the ultimate compression strength, $\tilde{\sigma}'_c$ on the ${}^t\sigma_{p3}/ \tilde{\sigma}_c$ axis. The new constants, $\tilde{\sigma}'_c$, $\tilde{\sigma}'_u$, $\tilde{\varepsilon}'_c$, and $\tilde{\varepsilon}'_u$, are now used in Eq. (5-2) in place of the corresponding unprimed terms, to establish the multiaxial stress-strain law. Tensile failure occurs if the tensile stress in a given principal stress direction exceeds the tensile failure stress as determined by the failure envelopes. ADINA assumes that failure on a plane perpendicular to the principal stress direction has occurred, which has the effect that the normal and shear stiffnesses across the plane are reduced, the corresponding normal stress is released, and a state of plane stress exists at the plane of failure. If the material is subject to a low compression state of stress, before tensile failure occurs the material stress-strain relation is given by eq. (5-6), but after tensile failure the new material stress-strain relation is given in eq. (5-10), where the η_n and the η_s are the stiffness and the shear reduction factors, respectively. The default values are η_n=0.001 and η_s=0.5, unless other values are input. The factor η_n is set to a small non-zero value in order to avoid a singular stiffness matrix.

If a tensile failure occurs while the material is undergoing high compression in the orthogonal directions, the same general procedure is followed, but the initial matrix $\hat{C}$ prior to the formation of the crack is given by eq. (5-7) instead of eq. (5-6).

ADINA uses the following scheme to determine if compressive failure has occurred: (1) the largest principal stress, ${}^t\sigma_{p1}$, establishes the proper biaxial failure envelope on ${}^t\sigma_{p2}$ and ${}^t\sigma_{p3}$ from the triaxial compression failure envelope, interpolating between curves as required,

$$\frac{{}^{t}E}{(1-\nu^2)}\begin{bmatrix} \eta_n & \nu\eta_n & \nu\eta_n & 0 & 0 & 0 \\ & 1 & \nu & 0 & 0 & 0 \\ & & 1 & 0 & 0 & 0 \\ & & & \eta_s\frac{(1-\nu)}{2} & 0 & 0 \\ & sym. & & & \eta_s\frac{(1-\nu)}{2} & 0 \\ & & & & & \frac{(1-\nu)}{2} \end{bmatrix} \tag{5-10}$$

and (2) if the stress state corresponding to the actual ${}^{t}\sigma_{p2}$ and ${}^{t}\sigma_{p3}$ lies on or outside the boundary of this biaxial envelope, then crushing has taken place.

Post Material Failure

ADINA handles the post-tension and post-crushing failures differently, as would be expected. A crack which has developed due to a tensile failure may, in a subsequent loading step, close, in which case the failure becomes inactive. The failure is considered to become inactive if the normal strain across the failure plane is both negative and smaller than the strain at which the original failure occurred. Hence, a tensile failure may be cycled between active and inactive during an analysis. However, any subsequent tensile failures are considered to act first in the initially failed plane, then in planes perpendicular to that plane, i.e., the stresses and strains at a given integration point are no longer calculated along the principal stress and corresponding directions as is done for the unfailed material, but the stresses in the directions defined by the material tensile failure plane are now used to obtain the new stress-strain matrix, corresponding to those directions. A second failure plane occurs perpendicular to the initial tensile failure plane when the stress normal to the first failure plane reaches a failure level.

In the case of a material that has crushed in compression, the material is assumed to strain-soften in all directions until the minimum principal strain, ${}^{t}e_{p3}$, reaches the ultimate failure strain, $\tilde{e}'$, at which time all the stresses are completely released and the crushed material has no further stiffness during the analysis. If the crushed material undergoes unloading, in the strain-softening region, the stress increments are defined to be zero. The strain-softening behavior and the corresponding algorithm is discussed in various references (4-6,22) and will not be covered in detail here.

VI. ADINA 5.0 CONCRETE MODEL

Discussion of Problems with Original Concrete Model

Gedling et al. (46) evaluated the -81 concrete material model, discussed a number of problems which the ADINA concrete model encountered in matching the compressive behavior of concrete, and suggested some modifications to the model. The problematic areas discussed were (1) the material failure envelopes, (2) the stress-strain relations, (3) the lack of a variable Poisson's ratio, (4) the lack of tension stiffening, and (5) shear transfer upon crack formation. Each of these is briefly discussed:

Material failure envelopes. The basic model used in the ADINA-81 version has been described previously. Two major concerns were expressed by Gedling et al. (46): (1) the three-dimensional tensile failure stress decreases linearly as either of the other principal stresses increase in compression in a manner which allows the concrete to decrease its tensile strength faster than observed under experimental conditions and (2) experimental studies by Schmidt-Goner et al. (78) show concrete to have a much greater triaxial strength than the ADINA default envelopes show.

Stress-strain relations. The uniaxial stress-strain curve is modified in the case where multiaxial stress conditions exist through the use of the principal stresses, ${}^t\sigma_{pi}$, and the failure envelope curves. A modified uniaxial stress-strain curve is obtained. A factor, γ, is used to scale the strains $\tilde{\varepsilon}_c$ and $\tilde{\varepsilon}_u$, and the other scaling factor, $\gamma_1 = \tilde{\sigma}'_c / \tilde{\sigma}_c$, is obtained from the triaxial failure envelope by holding ${}^t\sigma_{p1}$ and ${}^t\sigma_{p2}$ constant and reading the new value for the ultimate compression strength, $\tilde{\sigma}'_c$ on the ${}^t\sigma_{p3} / \tilde{\sigma}_c$ axis. The new constants are then used in Eq. (5-2) in place of the corresponding unprimed terms to establish the multiaxial stress-strain law. However the use of a fixed parameter, γ, produces unsatisfactory results since the amount of shift along the strain axis is highly stress dependent. The use of the relationship

$$\gamma = C_1\gamma_1 + C_2 \tag{5-11}$$

using $C_1 = 1.4$ and $C_2 = -0.4$ has been shown to produce better results.

Poisson's ratio varying with loading. Experimental tests have observed that the ratio of lateral strain to principal compressive strain remains essentially constant until approximately 80% of the maximum compressive stress is reached. Above this level, the apparent Poisson's ratio begins to increase. ADINA-84 uses this ratio as constant for all levels of stress. Gedling et al. (46) propose a modification by using a secant value formulation of Poisson's ratio which is a function of the stress state.

Tension stiffening. In the ADINA-81 and -84 codes a smeared crack model was used for tensile failure. Crack formation is considered to be brittle and instantaneous. When the maximum principal stress at any integration point equals or exceeds the tensile failure stress level (which is a user input), a failure plane is said to exist normal to this stress, the direction of the crack plane is now defined, and the normal and shear stresses across the crack are set to zero. Further cracking will take place in orthogonal directions. While the use of the

instantaneous drop to zero is commonly used, in fact the tensile strength decreases gradually as microcracking takes place and the concrete between the cracks can still carry some tensile load. This resistance continues to decrease as the bond between the concrete and the reinforcing steel breaks down.

Shear stiffness reduction. ADINA-84 uses a constant factor (user input), η_s, to produce a shear stiffness reduction once a crack has formed. Shear stiffness is dependent on a number of physical factors, such as aggregate shape and size, reinforcement ratio, and bar size. Thus, representing the shear stiffness reduction with a single factor is an oversimplifying assumption, and a better representation would be to use a variable reduction factor based on crack width.

ADINA 5.0 Concrete Model

The ADINA 5.0 version (5) became available in late 1987. The concrete model used in 5.0 is described in detail by Bathe et al. (23). It is worth noting that two of the authors of the paper discussing the limitations with the -84 model are also co-authors in this paper. The new concrete material model and the differences from the earlier version are described in the following paragraphs.

Multiaxial conditions. The stress-strain relations are evaluated differently for multiaxial conditions depending on whether the material is loading or unloading. Poisson's ratio remains constant for all stress conditions. Loading and unloading of the material are measured by the loading function:

$$t_f = t_s \tag{5-12}$$

where the variables are defined the same as for eq. (5-3). The material is loading except when ${}^{t}f < f_{max}$, where f_{max} is the maximum value of the loading function that has been reached during the analysis up to time "t". This formulation of the loading function is different from that used in the -84 version, and given by eq. (5-3). The second term has been dropped, effectively setting the value of α to zero.

Whereas previously eq. (5-4) and eq. (5-6) were used to define the multiaxial Young's modulus in either tension or low levels of compression (this stress state was defined by the condition ${}^{t}\sigma_{p3} \geq \kappa\tilde{\sigma}_c'$, where κ was an input parameter typically about 0.4), the multiaxial stress-strain formulation now use eq. (5-5) and eq. (5-7) at all times. These are used for determining the stiffness matrix at time t. If one is calculating the stress increment, σ, from time t to time $t + \Delta t$, the stress calculation is done using $\sigma = \hat{C}e$, where e is the strain increment. The stress-strain matrix, $\hat{C}$, is the same as eq. (5-7) except that the Young's modulii ${}^{t}\tilde{E}_{pi}$ are replaced by the modulii ${}^{\tau}\tilde{E}_{pi}$, which are evaluated using the uniaxial stress-strain relationship. Thus, when ${}^{t}\sigma_{pi} \geq 0$, ${}^{t}\tilde{E}_{pi} = \tilde{E}_o$, and when ${}^{t}\sigma_{pi} < 0$, the definition for the stress is:

$$t+\Delta t\sigma_{pi}' = \frac{\tilde{E}_o \, {}^{t+\Delta t}\tilde{e}_{pi}}{[1 + A({}^{t+\Delta t}\tilde{e}_{pi}/\tilde{e}_c') + B({}^{t+\Delta t}\tilde{e}_{pi}/\tilde{e}_c')^2 + C({}^{t+\Delta t}\tilde{e}_{pi}/\tilde{e}_c')^3]} \tag{5-13}$$

and then

$$\tau+\Delta\tau\tilde{E}_{pi} = \frac{t+\Delta t\sigma_{pi}' - t\sigma_{pi}}{t+\Delta te_{pi} - te_{pi}} \tag{5-14}$$

In the last equation, the e_{pi} are the strain components at the two times being considered in the direction of the principal stresses, and the primed terms refer to the multiaxial conditions.

Material failure envelopes and stress-strain relations. Most of the suggestions described by Gedlin et al. (46) were incorporated into the ADINA 5.0 concrete model. These included the following:

1. modification of the triaxial tensile failure envelope. The -84 model reduced the tensile strength to zero once either of the other two principal stresses reached the uniaxial compressive strength limit. The new model reduces the tensile strength to $0.25\sigma_t$ when one of the other principal stresses reaches σ_c.
2. The post-tensile cracking behavior has been modified to include the possibility of tension "stiffening" so called because this approach is stiffer than assuming a brittle, instantaneous reduction to zero. If the strain at tensile failure is e_t, then the tensile strength decreases linearly to zero between e_t and ξe_t, where $\xi = 8$ unless otherwise changed by the user. Young's modulus in this region varies and is equal to the ratio σ/e along this straight line, the value depending on the actual stress-strain state at time t. Thus, at the tensile strength of the original material the modulus is equal to $E_o = \sigma_t/e_t$ and this is reduced to zero at a strain equal to ξe_t. In this region the shear modulus is also not constant, but rather is given by:

$$G_{ij}^{f} = \eta_f \frac{\tilde{E}_0}{2(1 + \nu)} \tag{5-15}$$

where η_f is equal to unity for $e \le e_t$, varies linearly between 1.0 at $e = e_t$ and η_s (a user input value) at $e = \xi e_t$, and remains constant at η_s thereafter. This

differs from the -84 version in that G_{ij} immediately was reduced to $\eta_s G_{ij}$ upon reaching the tensile strength.

3. The formulation used to convert the uniaxial σ-e curve to a multiaxial σ-e curve was modified. The -84 version used two constants, shown in Fig. 22, γ and γ_1, where $\gamma_1 = \tilde{\sigma}'_c / \tilde{\sigma}_c$, and $\gamma = 1$ (unless changed by the user). The 5.0 model uses the same definition for γ_1, but $\gamma = C_1\gamma_1 + C_2$, where the constants are input parameters, normally set at $C_1 = 1.4$ and $C_2 = -0.4$. This change was also suggested in the Gedling et al. (46) paper.

Further discussion. Two other options to the -84 version were indicated to exist in the 5.0 version by Bathe et al. (23). These are (1) a variable Poisson's ratio and (2) a post-compression crushing strain softening, i.e., a gradual stress unloading after the material has reached the ultimate stress, σ_u, instead of setting the stress to zero instantaneously. However, neither of these options were included with the version of the program available for this work. Note that the 5.0 version of ADINA available in Oak Ridge was dated from 1987, while the Bathe paper was published in 1989. Apparently, these changes will be included in a later version of the code.

CHAPTER VI

FINITE ELEMENT ANALYSES

I. INTRODUCTION

The feasibility of using a finite element analysis to help design the centrifuge mount system arose during the design phase of the project. However, it was felt that the analysis would prove very complex, and that too many unknown parameters existed to be able to have the necessary degree of confidence in the answers obtained. It was not desirable to base the final design on an analysis that would be at best questionable; the goal was always to perform testing in order to certify the design. Consequently, there was no attempt to perform a finite element analysis in order to develop the behavioral characteristics of the socket-concrete system.

Once the concrete-socket and full-scale tests had been performed and data were available, it was decided to perform a finite element analysis of the GCEP mount design, or some portion thereof, to complement the hand calculations and tests. An analysis of the mount-socket-slab configuration would explore the feasibility of using finite element techniques for complex situations involving concrete. Three questions needed to be resolved prior to proceeding with the analysis:

1. Which of the tests, the embedded socket tests or the full-scale floor module tests, would be modeled?

2. Since the response of the concrete in either test was clearly nonlinear, which finite element codes were commercially available that performed nonlinear analysis, and specifically which programs had built-in material models for concrete or concrete type materials? Maybe a more pertinent question was simply which programs were readily available? Were any available in the DOE Oak Ridge complex?
3. What literature existed on the subject of finite element analysis of concrete and concrete structures?

The third question has already been discussed at some length in Chapter V.

The embedded socket tests were selected to be used for the finite element modeling for two reasons. First, the socket tests were the main test in understanding the behavior and determining the strength capacity of the GCEP floor modules. Second, modeling of a single socket with the surrounding reinforced concrete slab was going to be complex enough without having to cope with the rest of the embedded floor module structure. Since the tests had verified that the overall strength of the floor module could be adequately modeled as the sum total strength provided by the four sockets, it was also a reasonable decision.

The selection of ADINA as the finite element code for the analysis was also a simple choice. Many commercially available finite element codes were available to the author, through the MMES computer systems, among them MSC-Nastran, SAPIV and SAPV, PAFEC, and ADINA, but the last named was the only one that was specifically suited to a nonlinear analysis. More importantly, ADINA included a concrete material model option for two and three-dimensional elements (which has already been discussed in Chapter V). ADINA-81 was available on the ORNL IBM-3033 machine, and the -84 version was on the

Cray computer located at K-25. ADINA 5.0 later replaced the -84 version in 1989. The -81 version was used initially to debug the model and perform a few runs, but that model was converted over to the -84 version because it was more efficient to run on the Cray, both with respect to cost and time. The conversion from the -81 to the -84 version required only minor modifications of the data files and was easily done. There were no analyses run in 1989 through 1991, but when the problem was restarted in early 1992, ADINA 5.0 was available on the Cray in Oak Ridge and the data deck was converted to run on that version; again, the conversion changes were minimal. However, the Cray was shut down at the end of September 1992 and ADINA will no longer be available on the Oak Ridge mainframe computers.

Three finite element analyses were performed as part of this work. The first was a very simplistic analysis of a standard concrete cylinder which was run for crushing loads; the main reason for this analysis was to run a simple problem using the ADINA code; however, some interesting findings were made. The second analysis was the finite element analysis of the concrete-socket test, which forms the bulk of the discussion in this chapter. Finally, because of problems encountered in obtaining a complete solution to the concrete-socket test problem, a pseudo-Cerruti's problem was devised and run in order to check the ADINA results. Cerruti's problem solves the case of a tangential force acting on the boundary of a semi-infinite solid. Each of these is discussed in detail in the following sections.

II. CONCRETE CYLINDER MODEL ANALYSIS

The concrete break cylinders used in the project were the standard 12-in. long and 6-in. in diameter. The finite element analysis model (using ADINA version 5.0) used the rotational symmetry of a cylinder to reduce the size of the model, which consisted of a one

degree wedge, 12-in. high, having nodal point layers every inch along the length. Node points were placed at one inch radial intervals, starting at the center of the cylinder and continuing in the sequence shown in the following sketch (the bottom layer of the model is sketched).

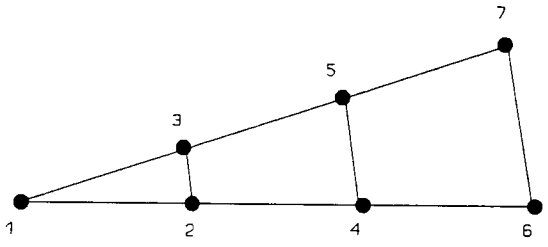

The elements were of the 3-D solid type and used the nonlinear ADINA concrete material model. The uniaxial material properties were based on the longitudinal and lateral load-displacement and stress-strain measurements determined from the laboratory cylinder breaks discussed in Chapter IV and summarized in Table 2. Test No. 2-17 was used (arbitrarily) for the material data. The load-displacement curves for No. 2-17 are shown in Figure 13. The following data were used: Young's modulus = 3.15×10^6 psi, Poisson's ratio = 0.18, and f_{ult} = 2890 psi at a strain = 0.002 in./in.

Symmetrical boundary conditions were used to represent the cylinder: the center point of each layer, no. 1 in the sketch, was constrained against any horizontal movement and the side nodes, nos. 2-7, were constrained from displacing in the hoop direction. All nodes, except those at the bottom layer, were free to move vertically. Radial displacement was permitted for all non-center nodes, except that two cases were considered for the edge nodes (nos. 6 and 7) on the top and bottom surfaces: (1) free (ADINA Run CYLIN1DF) and (2) constrained (ADINA Run CYLIN2DR). The second case (Run CYLIN2DR) represents the real boundary conditions more accurately since the top and bottom caps provide a degree of confinement at these surfaces.

A uniform element compressive pressure load was applied to the top surface of the model. The pressure load was applied in 100 psi increments.

The ADINA results depended on which case of top and bottom surface confinement was considered. Figure 23 compares the axial and transverse stress-strain curves obtained from Run CYLIN2DR (top and bottom edges radially restrained) with the stress-strain data from the cylinder break test. The longitudinal cylinder break test data were taken over the entire length of the cylinder and the transverse data were taken at the mid-height of the cylinder, so the ADINA plotted results are obtained in a similar manner (i.e., the axial strain is based on the vertical deflection of the top surface, and the transverse strains are derived from the radial displacement of node no. 48 located on the outside edge and at the mid-height of the model). The comparable curves from run CYLIN1DF were indistinguishable from those shown in Figure 23. It can be seen that ADINA produces reasonably good agreement with the test data in the axial direction, and also matches most of the transverse response. However, at approximately 80% of the ultimate level, ADINA deviates from the measured transverse response, and in fact, the ADINA results show a very small stiffening in that direction. The ratio of transverse to axial strains starts out equal to the input value of 0.18 and steadily decreases until at 2800 psi its value is 0.114. This behavior does not appear to be consistent with the statement in the ADINA manual that Poisson's ratio remains constant throughout the analysis. However, had ADINA implemented the variable Poisson's ratio above 80% of ultimate stress level as recommended by Gedlin et al. (46), the match for the lateral stress-strain curve might have agreed better. It is interesting to mention that the same model run on ADINA-84 produced a constant Poisson's ratio up to a stress of 2200 psi before it started decreasing.

The failure sequence, however, depends on the type of edge restraint provided for the upper and lower surfaces. In run CYLIN1DF all layers of elements were allowed to behave identically with respect to horizontal motion, and the analysis accordingly predicted that all the elements (for all layers) behaved identically and crushed simultaneously when the material uniaxial ultimate stress was exceeded. However, when the top and bottom surface edge nodes were restrained against radial displacement, a quite different failure pattern resulted, as shown in Figure 24. The confinement from the caps prevented tension cracking in the top and bottom layers along with most of the second layer. The crushed elements formed a v-shaped failure pattern, and most of the rest of the elements displayed some degree of crushing. As in the previous case, no cracking or crushing appeared until step 29 (2900 psi) at which point the pressure loading exceeded the ultimate strength of the concrete (2890 psi).

III. CERRUTI'S PROBLEM ANALYSIS

As is made clear in Section V of this chapter, many problems were encountered in trying to solve the concrete-socket test model problem. In order to provide a simple check of the general adequacy of the finite element model, it was decided to use the model to solve Cerruti's problem, in which a semi-infinite solid is loaded with a tangential force acting on the surface. The concrete-socket model crudely met these requirements, assuming that 30-in. away from the loading point approximates infinity. All non-essential elements were deleted from the model (rebars, reaction plates, and the protruding portion of the mount lug) and the remaining elements were modeled as linear elastic, isotropic, concrete. Thus, the model became a 6-ft long, 5-ft wide (because of symmetry), and 2-ft deep unreinforced concrete slab. Figure 25 presents two views of the model. The displacements for the problem were presented in the X1, X2, and X3 coordinate system shown in the figure, but the model

geometry was defined in terms of the XYZ coordinate system shown in the same figure in parenthesis. The boundary conditions were as follows (with respect to the original XYZ system): the nodes at Z = 0 (bottom surface) were restrained from motion in the z-direction, nodes on the X = 0 plane were constrained in the x-direction (due to symmetry), and the negative y-edge nodes (at Y = -36 and Y = -20 where that becomes an outer edge) were constrained in the y-direction. A 200 kip horizontal load in the X1-direction was applied at the center of the top surface of the slab. The material properties were given as E = 3.122 x 10^6 psi and G = 1.29 x 10^6.

Saada (76) gives the solution of the displacements and stresses to the problem as a function of coordinates from the loading point (X1, X2, and X3) within the solid. Table 5 presents the X1 displacement at various locations near the point of load application as determined by the analytical solution and ADINA, and gives the percent difference between them. The displacements in the X2 and X3 directions were smaller than those in the X1 direction by at least a factor of four and usually an order of magnitude, so they were not included in the comparison. The table shows the displacements for the same locations at two elevations. On the surface (X3 = 0) the ADINA results are reasonably acceptable, within ten percent of the theoretical values when the distance from the loading point is less than 14.50-in. However, at an elevation X3 = 7.0, the computer results are considerably less accurate, except along the line where X2 = 0.0. In the model the area of major interest, where the concrete was modeled using nonlinear properties, lies within 10-in. of the loading point. Considering that this model is, at best, a crude approximation of an infinite solid, the results roughly support the adequacy of the given modeling to be able represent the behavior of the concrete-socket system in the immediate vicinity of the loading point.

IV. CONCRETE-SOCKET TEST MODEL

Definition of Model

The finite element model represents a typical test location of the concrete-socket tests. The section being modeled, shown in Figure 26, is bounded by two vertical planes running through the sockets on either side of the test socket, a vertical plane representing the outer face of the concrete slab, a vertical plane running down the middle of the slab between the two rows of sockets, the top surface of the concrete slab, and the surface of the slab at an elevation of 1-in. above the floor where the bottom layer of reinforcement lies (therefore the model is only 23-in. thick instead of the actual 24-in. shown in the drawings). Symmetry about the vertical plane running through the center of the test socket was used to reduce the size of the model in half. Appropriate boundary conditions accounted for the other half (nodes located on the symmetry boundary do not displace normal to the plane, i.e., $\Delta x=0$). The vertical plane through the center of the slab and behind the socket was restrained from movement in the y-direction up to an elevation of 16.0-in. This indirectly models the side of the concrete slab that is not included in the model. The upper part of the model on the negative y-planes was not restrained because that portion of the slab is not continuous through to the other side. Even though the edges of the area being modeled include part of the adjacent steel sockets, this region was modeled as solid concrete, i.e., the effect of the embedded steel located 31-in. from the test socket was assumed to be negligible. Figure 27 shows the model in a full perspective view, while Figure 28 shows an enlarged view of the center area of the test slab where the socket and mount lug are located.

Finite Element Model

The finite element model of the concrete-socket test contains 1228 nodes and 857 elements (not including the optional gap elements). Table 6 summarizes the model including the number of elements used and the different material models.

The model included elements for the concrete slab, the reinforcing bars, the anchor bar, the embedded socket, the mount lug, and the load reaction plates. The load reaction plates were included to resist surface tension in the concrete elements and provide additional stiffness to the model. For the field tests, the loading plates were attached to the concrete with 28 anchor bolts each (Figure 9) and levelled with a 1-in. grout base. In the model the plates were simply connected to the concrete at the corners of the top surface of the concrete slab elements. In addition, the option to include gap elements between the steel socket and the adjacent concrete elements, as well as between the socket and the mount lug, was provided.

At the time that the initial model was assembled, there was no pre-processor available (in Oak Ridge) with ADINA-81 to help with the data input. The ADINA nodal input format is very similar to that used by the SAP type codes, so a preprocessor, MTAB, was used to create the node data and output it in a SAP format. MTAB had an interactive graphics capability allowing the model geometry to be shown simultaneously on the screen as the nodes were being defined, which provided an excellent check on the accuracy of the node data input. MTAB also allowed the nodal point constraints to be input. Even though the bottom layers include the outline of the socket and mount lug, the bottom surface of the steel socket is at an elevation of Z=16.0, and there is only concrete below this layer. This was done strictly to simplify the nodal point input of succeeding layers, since, as much as possible, layers were created by copying an entire lower layer and renumbering the nodes.

The input of the element data was more complex. Since the data input for elements in ADINA is unlike any other program used by the author, a BASIC program was written by the author to create the data input for the three-dimensional solid element (accounting for 90 percent of the elements). Where repetitive input was possible, with the node numbers from one element to the next varying by constant increments, the program automatically created the next element. Once a layer was created, the one above was created with relative ease using another program. The rest of the data deck (master control cards, time and load step data, initial conditions) was created using a simple program editor on a personal computer. The final data deck was approximately 3850 lines long.

Figures 29 through 45 show the horizontal cross-section layers of the model starting with the bottom layer; node numbers are shown at the corners of elements and element numbers are shown inside circles for linear elements, hexagons for nonlinear elements, and triangles for the anchor bar. The element number is indicated in the layer where the top face of the element lies (the bottom face of the same element lies in the layer immediately below). Each layer, except for the top of the mount lug, is shown in two figures. For example, the layer at Z = 21.5 is shown in Figures 41 and 42. Figure 41 shows the entire layer including the central portion surrounding the socket (which is left without nodes and element numbers) and Figure 42 is an enlarged view of the socket area. In Figure 41, elements 463 through 514 represent concrete modeled as a linear elastic material having the initial modulus of the concrete uniaxial stress-strain curve. In Figure 42, four elements of the socket test are shown: (1) elements 71 through 105 are concrete modeled using the ADINA nonlinear concrete material model, (2) element 5 (in the rectangle) is the steel anchor bar, modeled with a nonlinear elastic-plastic bilinear material model, (3) elements 583 through 590 represent the steel socket, modeled as linear elastic, and (4) elements 607 through 614 represent the steel

mount lug, also modeled as linear elastic. Note that two nodes exist at the interfaces between the socket and the concrete and the socket and the mount lug at layers $Z \geq 16.0$. These double-nodes were included in the model to be able to use gap elements as desired at these locations.

All the elements in layers $Z = 0$ to $Z = 16.0$, including the central socket area are concrete (except for one element per layer down to $Z = 5.0$ representing the anchor bar), modeled as a linear material. The nonlinear concrete elements and the steel socket start at elevation $Z = 16.0$ (Figure 36), and the mount lug starts at $Z = 17.5$. The top of the mount lug, which protrudes above the concrete surface, is shown in Figure 45. The lateral ram load was applied to the model at node 1219, the top center node of the mount lug, acting in the positive y-direction.

In the ADINA-84 runs, the anchor bar was modeled with two beam elements, capable of resisting bending, the first going from node 192 (at $Z = 5.0$, Figure 32) to node 345 (at $Z = 10.5$, Figure 34), and the second from node 345 to node 501 ($Z = 16.0$, Figure 36). These nodes were corner nodes of concrete elements, and 501 was also part of the socket.

Reinforcing steel elements were located in layers $Z = 16.0$ (Figure 46) and $Z = 21.5$ (Figure 47). This is fairly representative of the actual distribution of reinforcing steel as shown in Figure 9. The 2-in. thick steel embedded loading plate elements were connected on top of concrete elements 240 to 251 at layer $Z = 16.0$ (Figure 36). They sit in the cutout running down the center of the concrete slab (see Figure 12) in the x-direction.

One element in the test setup which was not included as part of the model in any of the computer runs was the heavy steel reaction block connected to the top of the loading plates (partially visible in Figure 12) which held the two hydraulic rams in place during the test. During loading, an equal and opposite load to that applied to the mount lug was

transmitted to the middle of the concrete slab through this arrangement. The omission of this structure from the model was the reason that the nodes on the Y = -36 plane (layers Z = 0.0 to Z = 16.0) were constrained against translation in the y-direction, in effect providing a reaction wall at this surface.

Boundary Conditions

Table 7 summarizes the different boundary conditions used for these analyses. Three sets of boundary conditions were used. The -81 and -84 version runs (run mostly in 1988) used Set 1 (except for one run that used Set 2), while all the later runs (1992) used Set 3. The three sets handled the boundary conditions on the plane of symmetry at X = 0 and on the plane at Y = -36 in the same way, restraining displacements normal to those planes at all elevations. Sets 1 and 3 constrained the bottom nodes against vertical displacement. This is correct in the case where the slab tries to displace in the negative z-direction (into the floor), but not quite accurate if the bottom of the slab tries to uplift. Thus, Set 2 permitted vertical displacement at all bottom nodes except those located on the edge of the slab at Y = +36, i.e. this condition modeled the slab as a simply supported beam with pinned ends, which resulted in a 0.012-in. uplift at the center of the slab at a 70 kip load. A very simple pinned beam model (shown below) having the cross-sectional properties of the slab (concrete only) and loaded as shown at the mid-depth of the slab thickness gave a 0.017-in. vertical deflection at the center node, which, considering the crudeness of the model, compares favorably with the full-size model solution.

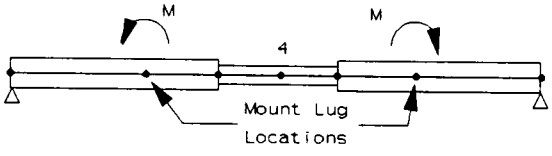

However, these models did not account for the dead load of the rest of the concrete slab, about 25 kips, which when applied to the small beam model, reduced the vertical displacement to only 0.003-in. (probably less in the large model, maybe even negative). This was considered insignificant, and thus, Set 3 used a vertical constraint at all bottom nodes. Also, Set 3 assumed that the mass of the rest of the slab and friction between the slab and the floor prevented displacement in the x- and y-directions at the free edges of the model on the bottom surface.

Material Properties

The material models used in the finite element analysis were presented in Table 6, but no discussion of the material properties was included. There are two types of materials in the concrete-socket test slab: steel and concrete. Both the steel and the concrete were modeled using a linear elastic formulation or some form of nonlinear formulation.

Mount lug and socket. These steel elements were modeled with 3-D solid elements using a linear-elastic material behavior with an elastic modulus $E = 29 \times 10^6$ psi and Poisson's ratio $\nu = 0.30$.

Reinforcing steel. The reinforcing steel #7 bars were modeled using the 3-D truss element having $A = 0.601$ in.^{2} and a modulus $E = 29 \times 10^6$ psi.

Load reaction plates. The steel plates were modeled using the shell element with a thickness $t = 2.0$-in., and a linear-elastic material model with an elastic modulus $E = 29 \times 10^6$ psi and Poisson's ratio $\nu = 0.30$.

Anchor bar. In the final set of computer runs, the steel anchor bar was modeled using 3-D solid elements. Early in the analysis, beam elements were used. In both cases a materially nonlinear formulation, elastic-plastic with isotropic hardening, was used. The

anchor bar was modeled as a nonlinear material because strain gages mounted on the bar indicated nonlinear behavior during the tests. A bilinear stress-strain curve was defined, with $E_{elastic} = 29 \times 10^6$ psi up to a yield stress of 36,000 psi, after which a hardening modulus, $E_{hard} = 3 \times 10^6$ psi, was used. No limit was placed on the ultimate strain level.

For purposes of this study the anchor bar, which was welded to the backside of the socket, was taken completely to the top surface of the concrete slab. In the real concrete slab a small square of concrete, about 1½-in. thick, existed between the top of the anchor bar and the concrete surface. During all the tests this piece of concrete (and a little bit more) popped off (Figure 14 shows this failed area to the left of the socket) as it was pushed upwards by the top of the anchor bar as the socket rotated. However, the manner, time, or load at which this piece broke off was never determined because the area was not visible as it was covered by the steel plate (seen in Figure 7) which transferred the ram load to the mount lug. The resistance provided by this chunk of concrete to the overall strength of the concrete and socket system was considered minimal, and it was felt that including it as a concrete element might produce an even earlier termination of the analyses, and for the wrong reasons, since the real intent of these studies was to obtain the bearing behavior of the concrete around, but primarily in front of the socket. However, to verify this assumption, two analyses were run which modeled the top element as very soft steel (nlin13) and nonlinear concrete (nlin15), and are discussed in a later section.

Gap elements. Gap elements should be used where separation between the socket and the concrete is expected, since they provide resistance to compression but not to tension (refer to Chapter V, Section IV). Based on the free-body diagram of the socket (Figure 5), gap elements could have been placed in three regions: (1) lower front of the socket (front and back define the face of the socket in and opposed to the direction of the load, respective-

ly), (2) upper back of the socket, and (3) underneath the socket near the anchor bar. However, when included in the analysis, gap elements were used only between the socket and the concrete on the backside of the socket at layers $Z \geq 17.5$ at locations shown below.

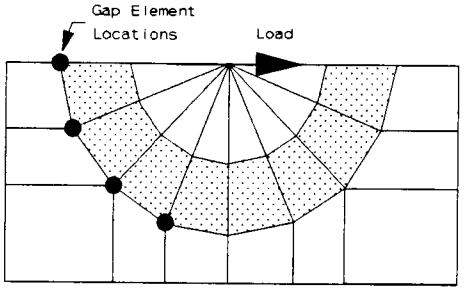

Thus, gap elements were used for the upper 5.5-in. of the socket (compared with the value of λ = 4.6-in. determined from the tests as discussed at the end of Chapter 3 and shown in Figure 5).

Gap elements are nonlinear truss elements, requiring the area and modulus in compression to define the compressive behavior (of course, $E_{tension} = 0$). In effect, each gap element acting in compression, should behave, as closely as possible, as if a concrete element existed. Thus, the area of a gap element at each node corresponded to the tributary area of the concrete that was replaced and $E_{compr} = 3.5 \times 10^6$ psi, the same as the replaced concrete.

Concrete (linear). A large number of the solid elements representing the concrete slab were modeled using a materially linear-elastic formulation, assuming that the major failure zone would be concentrated in the vicinity of the socket, i.e., beyond a certain distance from the load point, the stresses in the concrete were expected to remain small. It was felt that this was a reasonable first approximation, which if proved incorrect, could later be modified as needed. The value of the elastic modulus in the final group of runs was E = 3500 ksi and Poisson's ratio was $\nu = 0.21$ (some early runs used E = 3122 ksi and one run used $\nu = 0.15$).

The linear behavior assumption appears to be justified, based on computer runs up to about 85 kips, which indicated that the largest stresses in these elements were 102 psi in tension and 280 psi in compression. These low stress values (25% of the tensile strength and only 9% of the compressive strength of the concrete) - at half the expected load capacity - also eases the concern that using the linear material behavior model would increase the overall stiffness of the model.

Concrete (nonlinear). Two nonlinear material models were used to represent the nonlinear concrete in this work. The first, and by far the more important one, used the nonlinear concrete material model available in ADINA. The second method used an elastic-plastic formulation.

The material data required for the nonlinear concrete model in ADINA 5.0 includes the (a) uniaxial curve parameters (Figure 19), (b) triaxial failure envelope parameters (Figure 21), and (c) control parameters such as (i) the principal stress ratio, $\beta = \sigma_{p2}/\sigma_{p3}$, which is used in defining input to the triaxial data envelope, (ii) the normal and shear stiffness reduction factors, η_n and η_s respectively, (iii) the constants C_1 and C_2 used for definition of critical strains in eq. (5-11), and (iv) the constant ξ, the ratio of ultimate tensile strain to cracking tensile strain. The principal stress ratio, β, was always set to 0.75; the constants C_1 and C_2 were set to 1.4 and -0.4 as recommended by Gedling et al. (46) and the ADINA manual; the stiffness reduction factors, η_n and η_s were defaulted to 0.0001 and 0.5 respectively; and ξ was defaulted to 8.0. The -84 version input was a little different. In addition to using a, b, c(i) and c(ii), it had three other constants, λ, κ, and α. λ, described earlier in Chapter V, pg. 65, was used to determine the uniaxial critical strains (this method was replaced by the input described in c(iii) above) and it was allowed to be set to its default value of 1.0; κ is the control parameter which ADINA used to determine if it was in a state of tension or low

compression and was also set to its default value of 0.7; and α was the constant used in the loading function (eq. 5-3). α was set to -1.0 during the analysis (ADINA recommended α be set to a small negative number or even zero, but one run (not described in this work) where α was changed from -1.0 to -0.15 resulted in a termination at a smaller load, so all the remaining runs using the -84 version retained α = 1.0).

The uniaxial parameters used by the program are the tangent modulus at zero strain, $\tilde{E}_o$; Poisson's ratio, ν; the cutoff tensile stress, $\tilde{\sigma}_t$; the maximum compressive stress, $\tilde{\sigma}_c$; the compressive strain at $\tilde{\sigma}_c$, $\tilde{\epsilon}_c$; the ultimate compressive stress, $\tilde{\sigma}_u$; and the ultimate compressive strain, $\tilde{\epsilon}_u$. For all the nonlinear concrete runs, Poisson's ratio was set at 0.21, $\tilde{E}_o$ = 3500 ksi, $\tilde{\sigma}_t$ = +410 psi, $\tilde{\sigma}_c$ = -3100 psi, and $\tilde{\epsilon}_c$ = -0.002. For all of the -81/-84 runs, and for some of the 5.0 runs, $\tilde{\sigma}_u$ = -2500 psi and $\tilde{\epsilon}_u$ = -0.003. These last two parameters were varied in some of the later runs.

Finally, the triaxial envelope parameters were, for the most part, input using the default ADINA curves because no triaxial test data had been obtained for these tests. Six curves with three points each are required to be input (Figure 21). Each curve is anchored at a specific ratio of $\sigma_1/\tilde{\sigma}_c$. Table 8 lists the input data for the triaxial envelope used during this study. Three sets of data are shown in the table, the ADINA default data set and two modified data sets which are obtained by extrapolating additional values of the stress ratio $\sigma_1/\tilde{\sigma}_c$ curves from the default data.

V. CONCRETE-SOCKET MODEL ANALYSES

Introduction

This section presents the results of the finite element model computer runs of the concrete-socket tests and compares them with the field test results.

In order for the reader to properly understand the sequence of these analyses, a brief summary of the computer work sequence leading to the present writing is in order. Tables 9, 10, and 11 summarize the computer runs performed during this study. The ADINA-81 runs were performed at the very end of 1987, the -84 runs were done in 1988, and the 5.0 runs were performed in 1992 (the Cray computer was taken off line at the end of September, which terminated the use of ADINA at the Oak Ridge facilities, at least on a mainframe computer). The expense and space needed to run the analyses during 1988 required that runs be made only on weekends; this was no longer the case in 1992. By the Fall of 1988, the author, discouraged at the lack of any reasonable results with the computer analyses, stopped work. Then, in January 1992, another attempt was begun. The analytical results the second time through were certainly no better than the first, but a better understanding of the problems involved in the analyses were obtained because the 1992 work was performed in a more structured manner. By the time the work was restarted, a newer version of ADINA (5.0) with some enhancements to the concrete model was available, so the model was converted. Linear runs (Table 9) were then performed in order to gain an understanding of the effects on the load-displacement curve of various parameters, and eventually to determine the final configuration of the elements to be used in the model. Therefore, during the nonlinear analyses (Table 10), changes were made to the anchor bar, to the nonlinear concrete properties, and to the method used to increment the load. Finally, when all practical means to obtain a satisfactory solution using the ADINA concrete model failed (and with time constraints), a few runs were made in which the nonlinear concrete was modeled with an elastic-plastic material (Table 11). The elastic-plastic formulation did reach higher loads, but agreement with the test curves was very poor.

In Chapter I two goals were set out for this part of the project: (1) perform a nonlinear finite element analysis of the test and compare the resulting load-displacement curves, and (2) determine the feasibility of using such an analysis in order to predict the behavior of the embedded sockets (in lieu of performing the tests). Generally, the results of the finite element analysis were very poor. From Figure 18 it can be seen that the test curves remained "fairly elastic" through 40 kips, had a small amount of inelasticity from 40 kips up to about 120 kips (in some cases, maybe even 140 kips), and then flattened out. It should be recalled that it is the deflection at the top front edge of the socket (node 1161 in layer Z = 23.0, see Figure 44) that is plotted in these curves. The smallest load obtained by any of the eight socket tests was 142 kips (test 5). However, none of the ADINA runs using the nonlinear concrete material model were able to get past 90 kips. All stopped for one of two reasons: (1) inability to converge or reach equilibrium after some of the concrete elements reached the crushing stage, and (2) reaching the maximum allowable stress ratio ${}^{t}\sigma_{p1}/\tilde{\sigma}_{c}$ (see Figure 21) for the least negative of the compressive stresses (σ_1) in a triaxial state of stress.

In an attempt to resolve these problems, a number of significant modifications were made to the model during the course of the work. These included:

1. varying the load step size, including using the Automatic Time Step feature in the ADINA 5.0 version,
2. modifying the ADINA concrete triaxial envelope data (used in Figure 21),
3. varying the uniaxial concrete σ-e softening parameters: the ultimate compressive stress, σ_u, and the ultimate compressive strain, e_u, and
4. modeling the nonlinear concrete elements using the elastic-plastic material model instead of the nonlinear concrete material model.

The following modifications were also made, principally to improve the accuracy of the model and not to overcome the problems inherent with the solution: (1) three sets of boundary conditions were used, (2) loading plates were added to the model (as previously discussed in Section IV of this chapter) roughly about a third of the way through the work, (3) the anchor bar element type was changed from a beam (or iso-beam) to a 3-D solid, and (4) gap elements were added or removed from run to run (in the final runs they were completely left out).

The selection of the test curve to use as the base case for the computer runs was one of the first items to resolve. Figure 18 presented the complete load-displacement curves measured at the top of the steel socket for tests 3 to 8. Figure 48 presents the curves for the same six tests, but only up to 100 kips, which gives a better idea of the behavior of the tests at lower load levels. It is clear that Test No. 3 was quite soft in comparison with the other tests, but otherwise there is no distinct reason to select one of the other test curves as the "most representative" of the set. Test 8 was eventually used to compare with the ADINA runs because its overall behavior fell roughly in the middle of the test data, though it had a high initial stiffness. Test No. 4 was also used during the stiffness effect studies (of the linear runs), since it had the lowest stiffness of the tests (not including Test 3).

The remainder of this section is divided into subsections discussing the linear runs, the nonlinear runs, and the nonlinear concrete modeled as an elastic-plastic material.

Linear Analyses

A number of linear models were run to verify the general adequacy of the model prior to running a nonlinear model and also, significantly later in the project, to perform some parametric studies to improve the overall accuracy of the model. These are summarized in

Table 9. The table lists the version of ADINA that was used for each run, the boundary condition set number, the element type used for the anchor bar, the concrete linear properties E and ν, the applied load, the y-deflection at node 1161, the model stiffness based on the y-deflection at node 1161, and whether gap elements (really springs in the case of a linear run) and load plates were used in the run. Run lin04 was set up and run to compare the solutions between the -84 and 5.0 versions, and the results were identical.

The only difference between the linear and the nonlinear runs was that the material behavior was linear elastic for all elements, with the properties varying according to the material (steel or concrete) of each particular element. The anchor bar element type was changed depending on which element type was being used or proposed to be used in the nonlinear models at the time of the run. The first linear run (lin01), based on the ADINA-81 code, did not include either gap elements or load plate elements. The load reaction plates were added to the model about halfway through the 1988 analyses and run lin03 included them. Figure 49 shows that the stiffness (based on y-deflection at node 1161) increases a modest 10% due to adding the loading plates to the model (also see Table 9). Also shown in the figure are the load-displacement curves for tests 4 and 8 which bracket the stiffness range for the tests. The additional stiffness produced by adding the loading plates was fully expected, since the steel plates, attached to the surface of the concrete slab, are considerably stiffer than the surrounding concrete.

"Gap elements" in the linear analysis are linear truss elements (springs) used between elements, and allow tension resistance (as opposed to the nonlinear gap element which does not). This was done to study the stiffness of the system using the truss elements instead of using rigid node connections. The modulus and area values for each truss element used the corresponding values in the nonlinear analysis. Gap elements were included in the model

early in the work, and one linear run was made with them (lin02). Figure 50 clearly shows that the inclusion of gap elements produces a much softer response than measured by the tests. Removing the gap elements produces a stiffness that falls in between the tests. This result led to the decision not to use gap elements in the final set of nonlinear runs.

The effect of changing the anchor bar from a beam to an iso-beam element had absolutely no impact on the stiffness of the model, but changing it to a 3-D solid element increased the stiffness by about 20% as shown in Figure 51. Because it would have required a major revision to the model to accurately include the anchor bar bottom plate (see Figure 2), the plate was not included. In order to represent an increased resistance near the bottom of the bar, and also to represent the fact that the anchor bar leg is embedded at about a 15° angle from the vertical, the 3-D elements of the bar below the bottom of the socket were tapered outward in the negative y-direction. This can be seen in the socket area plan elevations of the model at Z = 5.0 and 10.5 (Figures 32 and 34). The anchor bar, as modeled, probably introduced a higher stiffness than actually existed in the field tests since in the computer model the bar and the lower slab concrete elements (which are modeled as linear elastic) are rigidly connected at all times, while in the tests the friction bond between the bar and the surrounding concrete broke at some load (unknown) and most of the pullout resistance provided by the anchor bar was due to the small plate at the bottom. This friction release was not properly accounted for in the model.

In Figure 51, the input elastic modulus for the concrete was 3500 ksi (see Table 9 for runs lin07 and lin08), which was about 12% higher than used in the runs plotted in the previous two figures. This was the value of the initial tangent modulus finally used for the nonlinear concrete model as it agreed with the value from Test 8 (based on the data in Table 2) rather than the value of 3122 ksi used in the earlier linear runs.

To summarize, the linear runs provided a means for experimenting in an efficient manner with some of the elements and material properties in order to help establish the final configuration of the nonlinear model. The final adjustments to the configuration of the nonlinear model used during the latter part of this project were based on the last linear run, lin09. Thus, the gap elements were removed, the anchor bar was modeled using 3-D elements, the load reaction plates were included, and the higher value of E was used. The total effect of incorporating these changes into the model was to increase the stiffness a little less than fourfold (lin02 vs. lin09 in Table 9).

Nonlinear Analyses

A summary of the nonlinear computer runs is given in Table 10. Most of the columns are self-explanatory, but a few need some explanation. The **Load Step Sequence** column presents the (step number,load) end points of straight line segments used to create the loading table (the first point is always 0,0). In Run nlin02, for example, the load table starts at zero, at step 1 the load is 40 kips, and at step 5 the load is 120 kips, the program providing linear interpolation between steps 1 and 5. Thus the load steps for Run nlin02 were 40, 60, 80, 100, and 120 kips. Note that the load step values listed in the data deck were half these values because the model represents one-half of the actual slab section, and the load point is on the symmetry plane; the displacements and stresses, however, were correct as calculated. The **Maximum Load** column represents the maximum true load value (double the value from the analysis) obtained in the analysis before the run terminated. Again, using Run nlin02 as an example, a value of 60 appears in the **Maximum Load** column, which means that ADINA obtained solutions to the first two load steps, 40 and 60 kips, before it stopped. For the remainder of this writeup, load value refers to the full load for each step. The **Comment**

column includes changes from one run to another. The comments include which type of triaxial concrete data set was used, the element type of the anchor bar, whether gap elements and load plate elements are included in the run, and modifications to the concrete uniaxial σ-e curve. An addition, deletion, modification, etc., once made, remains in effect until it is specifically changed again. For example, gap elements were added in nlin05 and removed in nlin07, which means that nlin06 still includes the gap elements.

As can be seen in Table 10, none of the nonlinear concrete material model runs exceeded a maximum load of 90 kips. Termination was for one of two reasons: (1) inability to converge or reach equilibrium at some stage in the analysis, and/or (2) a stress state was calculated where the current principal stress ratio ${}^{t}\sigma_1/\tilde{\sigma}_c$ exceeded the input value of sp1(6) (listed in the Table as p1 > sp1). Convergence problems were of two types: (1) the input limit on the number of iterations allowed was exceeded (shown as "iter > n" in Table 10), but the solution was still converging and (2) the out-of-balance loads were larger than the incremental loads which meant that the solution was diverging. The first case should have been solved by increasing the limit on the number of iterations allowed to obtain a solution, but doubling and tripling the iteration limit did not effect a solution. A brief discussion of each of the nonlinear runs follows.

Run nlin01. This was the first nonlinear run attempted. No gap elements nor load reaction plates were used. The run was set up to perform only two load steps in order to get a feel for the program and for the volume of printout that would result by printing out displacements at all nodes and stresses/strains at all elements. The run, using ADINA-81, terminated normally. The amount of printout was enormous, requiring almost 1000 pages per step for the requested printout. Obviously, the amount of printout had to be limited, at least until such time as a successful run was made, after which the run could be repeated with a

full printout. It was decided to print out displacements at the nodes that made up the anchor bar (at this time the bar was modeled with a beam element), those located at Y = -20.0" for the upper part of the slab, and all the nodes in the socket area of the slab at Z ≥ 16.0", plus the nodes at the top of the mount lug. In addition, stresses and strains would be printed out for the nonlinear concrete elements bordering the socket in the last two layers, the anchor bar, and all the socket elements. This reduced the number of elements having stress/strain output from 850+ to fewer than 50, which made the output considerably more manageable. The option to increase the output as needed was always present.

Run nlin02. The only changes to this run from nlin01 were the reduced printout requests and adding more load increments. A divide check error occurred in the middle of step 2 and only part of the second load printout was output. The divide check error appears to be a case of machine system error, though it may have been a fault with the ADINA-81 version. This was the last run using the -81 version of the code.

Run nlin03. This run was made about six weeks after the previous one, and was the first to use ADINA-84. Again, no load reaction plates or gap elements were included in the model, and the anchor bar was still being modeled using the beam type elements. The only difference between this run and nlin02 was the load step sequence. The first load step was still 40 kips, but the succeeding load increments were reduced to 5 kips. Six load steps, to 90 kips, were solved. The program terminated after it had performed fifteen iterations (the default number) without converging during step 7. The resulting load-displacement curve at node 1161 is given in Figure 52, which also shows the Test 8 curve for comparison. This is probably the best agreement with Test 8 that was obtained for this program.

ADINA prints out stresses at 27 integration points (IPT) for the 3-D solid element, located in a 3 x 3 x 3 pattern in the local r,s,t coordinate system (r and s form the local

horizontal axes and t forms the local vertical axis). Their exact location is not crucial to this discussion, but is described in the ADINA User Manuals (5). The stress output for each nonlinear element includes the six normal and shear stresses and the three principal stresses at each of the IPT, and a description of the current stress condition of the element (i.e, no crack, 1, 2, or 3 cracks, closed, or crushed). One crack implies that σ_1 has exceeded the allowable tensile stress and a crack has opened; 2 cracks imply that both σ_1 and σ_2 have exceeded the allowable tensile stress, etc. Closed means that all cracks have closed at that point. Crushing means that at a given stress level of ${}^t\sigma_{p1}$, the stress state corresponding to ${}^t\sigma_{p2}$ and ${}^t\sigma_{p3}$ lies outside the biaxial failure curve as obtained from the input triaxial data. Once this happens, the material strain softens in all directions until the minimum principal strain ${}^te_{p3}$ reaches $\tilde{e}_u$, at which point the stresses are released and the material has no further stiffness.

In the last completed load, 90 kips, for nlin03, fourteen of the nonlinear concrete elements were partially or fully crushed. These are shown in Figure 53, where the steel socket is shown cross-hatched, the partially crushed elements are lightly shaded, and the one fully crushed element (in layer Z = 23.0) is diagonally striped (darker shading). The elements in the Z = 19.0 had crushing at less than a third of the IPT and all still were strain softening; those in the next higher layer indicated crushing at approximately half of the IPT, some of them with the stresses fully released. In layer Z = 23.0, the three elements in front of the socket had the most crushing. In these, crushing occurred at two-thirds of the IPT, and one, element 131, was totally crushed with all its stresses released. It is not clear why this element and not the one directly in front of the socket (element 132) totally crushed, but element 132 was also almost gone. It is worth noting that in the preceding load step of 80 kips, these two elements were in almost the same state, except that strain softening was still taking place at

many of the IPT and both elements still had some stiffness (actually, element 132 had more crushing at 80 kips than element 131).

Run nlin04. The load step increment above the 90 kips level was reduced in this run from 10 kips to 5 kips. However, the results were the same as for Run nlin03, except that this run terminated because the current principal stress ratio ${}^t\sigma_1/\tilde{\sigma}_c$ = -3853 psi exceeded the input value of sp1(6) for element 62 (located directly in front of the socket at layer Z = 19.0 - see Figure 40) at IPT 18. From Table 8 the value for sp1(6) equals $1.2\tilde{\sigma}_c$ = 1.2(-3100 psi) = -3720 psi.

Run nlin05. This run and the next one incorporated gap elements. Load plates were still not included. Other than adding the gap elements, this run was identical in all respects with Run nlin04. This time the run terminated after reaching 70 kips, because the current principal stress ratio ${}^t\sigma_1/\tilde{\sigma}_c$ = -5934 psi exceeded the input value of sp1(6) = -3720 psi for element 97, located directly in front of the socket in layer Z = 21.5 (see Figure 42). Figure 54 plots the load-displacement curve for Runs nlin04 and nlin05 and Test 8. It is clear that the gap elements softened the system, especially in the load step between 60 and 70 kips. The reduced stiffness of the model meant that the displacement at the top of the socket at 70 kips load was about equal to the displacement at 90 kips when gap elements were not used, but the rotation of the socket was such that the crucial element (number 97) was now located only 1.5-in. below the surface instead of 4-in. (number 62) as in the previous run.

Run nlin06. In this run the triaxial concrete modified data set 1 was used. Since the value of the current principal stress ratio ${}^t\sigma_1/\tilde{\sigma}_c$ was exceeding the input value of sp1(6), the values of sp1(I) for the last three curves (I = 4, 5, and 6) were changed, which of course changed the corresponding values of sp2(I) and sp3(I) as shown in Table 8. The general shape and slopes of the curves were not changed, only the effective cap curves; and sp1(6)

was increased from 1.2 to 2.7. The load-displacement behavior at node 1161 was virtually identical to that obtained in nlin05, except that this run terminated at P = 60 kips after thirty iterations (increased from 15 used in earlier runs) were performed without reaching convergence during step 5.

Two additional runs (not listed in Table 10) used drastically modified shapes of the failure envelopes based on data in Gedling et al. (46). In the first run the six values of sp1(I) remained unchanged from the default curves, but the sp2 and sp3 values for each curve were substantially increased; in the second run the sp1 levels were increased along with using the higher sp2 and sp3 values. The results were no better than before: the first run stopped at 60 kips due to exceeding sp1(6) and the second due to the solution diverging after 70 kips.

Run nlin07. There were many changes made for this run: (1) load reaction plates were added and were used in all future runs; (2) gap elements were removed and were never added again, though they were used in the linear model analyses described in the previous subsection; (3) the anchor beam was modeled using the iso-beam elements; (4) in an attempt to overcome the termination problems, the load step sizes were changed; the first load step had been 40 kips for the previous runs, but in nlin07 the first 100 load steps were each 1 kip; (5) boundary condition set 2 was incorporated; and (6) the concrete triaxial data were changed back to the default data. The change of the anchor bar element type should have had no noticeable effect on the load-displacement curve, the addition of the load reaction plates and the removal of the gap elements stiffened the system as already shown, and the new boundary conditions (which removed the vertical constraints on almost all of the bottom nodes) probably reduced the overall stiffness by a small amount. This run stopped at a load of 70 kips for exactly the same reason as nlin06. It is difficult to make any firm conclusions with this run because so many changes had been made.

Run nlin08. The boundary conditions Set 1 were used, otherwise, there was no difference with Run nlin07. This run went to 60 kips, and this time stopped due to the stress ratio sp1(6) value being exceeded. Figure 55 shows a plot of Runs nlin07 and nlin08. As expected, nlin07, which uses the more flexible boundary conditions, produced a softer response. Neither run is very revealing. Based on the reasons given in Section IV of this chapter on boundary conditions, it was concluded that boundary condition Set 2 was not useful to the analysis.

Run nlin09. The load step increments were changed back to having the first load step 40 kips and each of the next five 10 kips, the same as used in runs nlin04 through nlin06. Figure 56 shows a comparison of this run with nlin08 where much smaller load step increments were used. A careful examination of the two curves shows that the stiffness of the first step for each is the same, as it should be since the first step is essentially a linear step. There is a small, but noticeable change in the slope of the curve in the second step of nlin08, but the slope between 5 kips and 50 kips is rather linear. Interestingly, the second step of run nlin09, between 40 kips and 50 kips, shows a marked change in slope, such that the displacement of the two curves intersect at 50 kips. The two curves then match up to 60 kips at which step nlin08 terminated (it actually got through 62 kips and failed in step no. 63, but the last printout step was no. 60) as already stated, while nlin09 continued up to 90 kips where it failed to converge. This behavior is very confusing, because it would seem that a program should be able to more easily reach a state of equilibrium if it has a smaller load increment to cope with. It did not seem reasonable that the large step run should get to the higher loads. It is not clear what influence, if any, the large first step has in this behavior. The reasoning behind using the large first step was that the early part of the load-displacement behavior of the concrete-socket system was expected to remain fairly linear; the

use of 40 kips, or about one-fifth to one-fourth of the expected capacity, was an estimate of this level. Based on Figure 56, it would appear that the 40 kips level was somewhat optimistic, and half that value would have been more appropriate.

Runs nlin10. This run was made using ADINA 5.0. The linear model parametric studies were complete and the final configuration for the model determined. This and all the rest of the analyses included the load reaction plates, used 3D solid elements for the anchor bar, used boundary condition set 3, and omitted the use of gap elements. For all these runs the load increments were 1 kip. Also, the output was entirely restricted to the displacements, at least until such time as a successful run was obtained or stresses and strains were required.

Figure 57 presents the load-displacement curve the run, which terminated after 84 kips due to the out-of-balance loads being larger than the incremental loads in step 85. At 80 kips, the displacement of Test 8 was about 2½ times larger than the displacement obtained by the finite element analysis.

Run nlin11. It was obvious that to be able to continue with the solution, the use of smaller load increments was going to be essential. At what load step to make the changes was not known before running an analyses, and also the size of the load step would require some trial-and-error procedure. ADINA has an option to run under Automatic Time Stepping (ATS) scheme whereby the program subdivides the time steps input by the user in order to obtain a converged solution for the given load levels. Under normal circumstances the program aborts when convergence is not reached after a specified number of iterations. Using the ATS routine, the program subdivides the failed load step into smaller increments (a maximum number is prescribed by the user) and tries to obtain a converged solution at these newer values of loads, until the entire original load step is completed. Then the program proceeds to the next load step as originally intended by the user.

Therefore, Run nlin11 (as did all the rest of the runs) incorporated the ATS method in the solution. The program succeeded in obtaining a solution only 0.5 kip higher before it also aborted for the same reason as nlin10. The ATS subroutine was only called into use by the run during the solution to step 85. The load-displacement curve was not affected.

Runs nlin12 and nlin14. It was stated that a concrete element that has crushed loses all stiffness only after the minimum principal strain ${}^{t}e_{p3}$ reaches $\tilde{e}_u$; at that point the element suddenly drops out of the problem. The value of $\tilde{e}_u$ which had been used for all the previous runs was -0.003 in./in. This may be a very conservative value for concrete under uniaxial compression, so the value was changed in run nlin12 to -0.100, or increased by 33 times. The resulting maximum load was increased 5 kips, up to 89.5 kips. The reason for failure was the same as for the past two runs, failure to converge. A restart run was performed, but the solution only succeeded in getting to 89.75 kips before the program stopped (with no possibility of a restart) because the current principal stress ratio ${}^{t}\sigma_1/\tilde{\sigma}_c$ exceeded the input value of sp1(6) for element 130 in layer Z = 23.0 (see Figure 44). Again, it was surprising that it was element 130 rather than 132 that produced the termination of the run.

Two changes were made in Run nlin14: (1) the value of $\tilde{e}_u$ was further increased from -0.100 (in nlin12) to -1.00, and (2) no softening of the σ-e curve was introduced beyond $\tilde{e}_c$; i.e., $\tilde{\sigma}_u$ was set equal to $\tilde{\sigma}_c$. This run terminated at 84 kips because the current principal stress ratio ${}^{t}\sigma_1/\tilde{\sigma}_c$ exceeded the input value of sp1(6) for element 135 in layer Z = 23.0 (see Figure 44). It is unusual that elements 131 and 132 were not the critical elements as they are both directly in front of the socket, and located between the socket and element 135.

Figure 58 compares the load-displacement curves for runs nlin10, nlin12, and nlin14. Run nlin10 which did include softening of the uniaxial σ-e curve for the nonlinear concrete elements is the softest of the three. No difference is discernable in the curves between runs

nlin12 and nlin14, except for the fact that the run having the higher ultimate strain value (nlin14) stopped at a smaller load (84 kips instead of 89.75 kips).

Up to this point only the load-displacement curves have been shown for runs using ADINA 5.0. A printout of the stresses and strains in the elements, concentrating on the nonlinear concrete elements, was obtained for Run nlin14. The stress/strain output for ADINA 5.0 is similar to that for ADINA-84 which was described under the discussion of Run nlin03. It was not easy to obtain a stress contour plot using the setup available in Oak Ridge, but from the printout it was an easy matter to determine the sequence of cracking and crushing in the nonlinear elements. Figures 59 through 63 show, for the area around the socket (shown cross-hatched), the sequence of cracking in elements, at all elevations, for loads of 20, 40, 60, 80, and 84 kips respectively. Thus, at P=20 kips, only one element at Z = 21.5 and three elements at Z = 23.0 (the surface of the slab) showed cracking. At P=40 kips, cracks had formed in at least one element in all four levels of nonlinear elements. At Z = 21.5, there were now six cracked elements (compared with one at 20 kips) and eleven at Z = 23.0. At a load of 84 kips (the last step for which a solution exists for nlin14) almost half of all the nonlinear elements and about two-thirds of the elements at the surface showed signs of cracking. Crushing of elements was first noted at a load of 80 kips, at elements 131 and 132, as shown in Figure 64. At 84 kips, these were still the only two elements that were partially crushed - element 132 was about 60% crushed and 131 about 30% crushed. This may be compared with Figure 53 (for Run nlin03), which shows that at a load of 90 kips, one element had fully crushed and thirteen others were partially crushed.

Run nlin13 and nlin15. These two runs studied the effect of changing the stiffness of the element at the very top of the anchor bar (element 6 in the square box in Figure 44). As mentioned earlier, this area was really concrete, but was modeled as steel in the model in

order to avoid an early termination of the runs due to failure of this one element because it was always pushed out of the way by the anchor bar and was not expected to add any strength to the system. However, the question arose as to what would result if this element were in fact modeled as being soft (i.e., not steel). In both cases $\tilde{e}_u$ was equal to -0.100.

Run nlin13 modeled it as very soft steel element having elastic-plastic behavior (it was still in the anchor bar group of elements) with E = 3.5 x 10^6 psi (same as concrete), σ_y = 1500 psi, and a hardening modulus E_{hard} = 30,000 psi. the run terminated at 83 kips because the current principal stress ratio ${}^t\sigma_1/\tilde{\sigma}_c$ exceeded the input value of sp1(6) for element 131 in layer Z = 23.0 (see Figure 44). The difference in the load-dispalcement curve between nlin13 and nlin12 is very small. At 80 kips, nlin12 had a displacement of 0.004106-in. and nlin13 0.004118-in.

In Run nlin15, this element was removed from the anchor bar group and put back into the nonlinear concrete group. This run stopped while solving load step 81 for lack of convergence. It reached 80.7 kips. Again the displacement at 80 kips was 0.00412-in., virtually identical to the displacement found in run nlin13.

It can be concluded from these two runs that modeling this element as steel rather than concrete has little effect on the analysis. Whether this conclusion would hold if the program had been able to reach load levels higher than 90 kips is unclear.

Runs nlin16 and nlin17. These two runs were identical except for the load step increments used in each. Both used the modified triaxial failure envelope set 2 (Table 8) which retained all but the last curve of the ADINA default curves. The last curve was set at a value of sp1(6) = $\sigma_1/\tilde{\sigma}_c$ = 10.0 instead of 1.2 as in the ADINA curves. The new curve was obtained by extrapolating from the default data set. As can be seen from the table, values of $\sigma_3/\tilde{\sigma}_c$ = sp3(6) as high as 16.9 are obtained with this data compared with only 3.2

using the default data. Run nlin16 retained the load step increments as in the previous runs. Run nlin17 had 1 kip increments up to 80 kips (same as nlin16), then 0.10 kip load increments thereafter. Both runs failed due to converge criteria, nlin16 after 85 kips, nlin17 after 84 kips, and both were restarted once. Run nlin16 actually decreased in deflection after the restart, going from a displacement of 0.00456-in.at 85 kips down to 0.00454-in. at 85.25 kips. Run nlin17 ran for 26 subdivided steps after the restart, and ended up at a load of 84.49 kips. Figure 65 shows a plot of nlin16 compared to Test 8.

These were the last runs performed that used the nonlinear concrete model. It was obvious that this approach was not producing an adequate solution to the concrete socket problem and, thus, the decision was made to change directions and model the nonlinear concrete using an elastic-plastic material model in order to study the effect this would produce.

Elastic-Plastic Analyses

A summary of these runs is presented in Table 11. The elastic-plastic model, for a given material property number, models the same behavior in tension as in compression, which for concrete is obviously not a good representation. The reason for performing these runs was simply to determine how well this approach would approximate the test data.

Runs nlinep01 and nlinep02. These two runs were similar, except that in nlinep02 the value of the hardening modulus was reduced by a factor of ten. Both runs used a bilinear model, which only required inputing the initial modulus, the yield point, and the hardening modulus. Linear behavior is then used in each segment. For these runs $E = 3.5 \times 10^6$ psi, $\sigma_y = 410$ psi (based on tension), and $e_u = 0.100$ (in the bilinear formulation, if a value of e_u is input, once that value is exceeded the element is assumed to have ruptured and the

stiffness of that element becomes zero). Run nlinep01 used E_{hard} = 35,000 psi and nlinep02 used E_{hard} = 3,500 psi. Figure 66 plots the load-displacement curves for these runs and also shows a portion of the Test 8 curve. Even though a low yield stress was used (410 psi), there apparently remains a substantial stiffness in the system as can be seen, as both are much stiffer in comparison with Test 8. Both analyses solved all the load steps that were requested.

Run nlinep03. In this run, instead of using a bilinear curve, a multilinear curve was input, i.e, different values of stress and strain are input to form the curve (more than two points are required). Again, the behavior in tension is the same as the behavior in compression. For this run, the σ-e curve that was entered approximated the actual uniaxial compression curve for concrete, including setting e_u = 0.003. The results were predictable: the run was stiff in comparison not only with Test 8, but also with runs nlinep01 and nlinep02. However, this run aborted at 157 kips because the plastic strain exceeded the value of e_u that was input. It turns out that the multilinear model does not assume rupture when e_u is exceeded; it simply prints out an error message and stops, which is just the opposite of the bilinear model.

Run nlinep04. A new tactic was used for this run, still using the multilinear model. For any given material, more than one material property is allowed. Thus, for those elements which were expected to go into tension, a stress-strain curve having concrete tension properties was used and for those elements which were expected to be in compression, the uniaxial compression curve was used. The ultimate strain for tension was set at 0.00015 in./in. After 10 kips, this value of e_u for tension was exceeded by some element and the run terminated.

Run nlinep05. The same approach as in the preceeding run was used for this run, except that a bilinear input was chosen in order to take advantage of the rupture mechanism.

Again, e_u in tension was as above, and e_u in compression was set to 0.100 in./in. This run failed to converge during step 34. The error message gave no further indications of where the problem lay.

Runs nlinep06 and nlinep07. These two runs were similar to nlinep05, with $e_u = 0.100$ in compression, but they allowed no limit to the maximum tension strain. Run nlinep06 used a hardening modulus equal to 3500 psi, and nlinep07 used a perfectly plastic curve ($E_{hard} = 0$). Both runs completed all the load steps requested. Their load-displacement curves are shown in Figure 67, along with those of runs nlinep02 and nlinep03 for purposes of comparison.

This run was the last run performed for the analysis of the concrete socket model. It had become obvious that a reasonable solution would not be achieved using the elastic-plastic modeling. It should theoretically be possible to obtain a solution using the elastic-plastic model as follows: perform a run and determine at which load an element has exceeded the tension (or compression) failure criteria, remove it from the model, and restart the analysis at that load. By repeating this cycle eventually a solution would be reached. Whether the results would compare favorably to test results is unknown. This is also a very lengthy and tedious procedure.

VI. DISCUSSION OF THE COMPUTER ANALYSES

It is clear that an adequate finite element solution is not obtainable by using the given approach. A discussion of the analyses and the problems encountered centers around two questions: (1) Was the finite element modeling adequate to solve the given problem?, and (2) Was the ADINA computer code capable of solving the problem? These two questions are also quite interrelated, since a good model cannot overcome a bad code, nor vice-versa.

The concrete socket test slab consisted of a highly non-isotropic assembly of substructures (the concrete slab, the reinforcing bars, the embedded socket with the attached anchor bar, the mount lug, and the load reaction plates which support the hydraulic ram reaction structure), having diverse material behavior and properties, and which, under load and deformation conditions interacted in a highly complex manner. Modeling and analyzing isotropic or orthotropic steel or concrete structures is a very common problem which generally lends itself readily to finite element solutions. Including nonlinear analyses with these problems is common, though a magnitude more complex. However, problems having a mixture of substructures and/or different materials, though not unusual, require understanding of the relationships that exist and careful modeling techniques in order to adequately predict the behavior of the system. The inclusion of nonlinear material behavior makes the problem that much more complicated.

There is no doubt that the analysis of the concrete-socket tests falls into the latter category. Two aspects of this problem require special attention: (1) modeling the behavior at the substructure interfaces and (2) using an adequate constitutive model for the concrete behavior.

Modeling of Interface Behavior

The areas where modeling the interface behavior between substructures should be carefully considered include the following:

1. the bond behavior (slip and friction) between the concrete and the reinforcing steel bars,

2. distribution of the forces transmitted from the hydraulic rams to the steel support structure to the load reaction plates which are anchored to the slab,
3. distribution of the forces between the socket and the mount lug,
4. the bond and friction behavior between the anchor bar and the surrounding concrete along the length of the bar from the base plate on the bottom of the bar to where it joins the socket,
5. the anchorage of the anchor bar after the bond along the length of the bar has broken, when the bulk of the pullout resistance is from the small footing plate at the bottom of the bar (see Figure 2), and
6. the bond, slip, and friction between the socket and the surrounding concrete.

In the model the reinforcing bars were connected to the concrete elements at corner nodes, which assumed that there was no loss of bond between the reinforcing steel and the concrete during the test. Since the maximum tensile stress in the reinforcing bars barely exceeded 2 ksi, the use of rigid connections had little effect on the overall behavior.

Distributing the reaction forces from the hydraulic rams to the middle of the slab was accomplished using boundary conditions that constrained the y-direction displacement on the Y = -36 plane. A more exact distribution of these forces would have been obtained by adding a very stiff steel block (representing the steel block supporting the rams) connected to the load reaction plates, and applying an equal but opposite load from that applied to the mount lug. The boundary conditions along the rear plane (Y = -36) would have remained the same. It is unclear just what difference this modification would have made to the overall solution of the problem.

The mount lug and the socket were rigidly connected along the length of the mount lug (note that the mount lug bottom was at Z = 17.5 because the capture nut on the bottom of the lug did not provide a full contact surface below that elevation). In reality, the mount lug segment between Z = 19.0" and Z = 21.5" had a slightly smaller diameter than the rest of the mount lug and did not contact the socket in this region. This deviation altered the load distribution to the socket from that existing in the real case, but probably not enough to have a significant effect on the behavior of the socket in the concrete.

Items 4 and 5 are part of the same issue. The anchor bar, as can be seen in Figure 2, extended 14-in. below the base of the socket almost to the bottom of the slab (the slab was 24-in. thick). In the finite element model the anchor bar was about 3-in. shorter. In the -84 runs the anchor bar was modeled with beam elements, and in the ADINA 5.0 runs the it was modeled using 3-D solid elements. Both configurations modeled the bar as a steel element connected to the surrounding concrete at three places along its length, which, because the concrete was modeled as a linear elastic material at all levels below the base of the socket, did not permit that interface connection to be broken. Thus the bond, slip, and friction between the anchor bar and the concrete was not adequately modeled. In the actual test, the bond (maybe very small depending on how well the concrete was placed around it) probably broke in small increments along the length of the outstanding leg, starting near the socket and progressing downwards until it reached the small plate welded to the bottom of the anchor bar. Once the bond broke, any friction along the bar and the bottom plate resisted the tension forces, the largest of these being due to the plate. A concrete failure cone would have developed in helping to resist the tension forces, somewhat different from those described in Chapter II since the anchor bar was inclined in the concrete. At the same time that the anchor bar was in tension, it was also subject to bending stress as the socket rotated

due to the lateral load. The bending was adequately modeled using the 3-D solid elements, but the way the anchor bar elements were connected to the concrete, at Z = 10.5" and higher, produced rigid connections that did not exist. As can be seen in Figure 14, there was a clear separation between the socket and the concrete near the surface, and which probably extended well into the concrete slab. Run nlin14 produced the following maximum effective stresses (in ksi) in the bar, starting with element one near the bottom of the slab and ending with the top of the bar at the surface of the concrete: 5.5, 9.5, 11.6, 11.2, 5.2, and 1.2. Strain gages attached to the bar during the test indicated that the anchor bars went nonlinear fairly early in the loading cycle, so this is very indicative that the interface between the anchor bar and concrete was not adequately handled in this analysis. Using 3-D solid elements is the correct way to model the anchor bar, but the use of rigid connections over the entire length of the anchor bar is inappropriate once the bond breaks.

However, properly modeling the socket and concrete interface behavior should have the most impact on the finite element solution among the items being discussed. Gap elements were tried and proved to be totally inadequate to model this behavior, producing a response that was too soft. The gap element is not adequate because it is a uniaxial type element (truss). True behavior requires a three-dimensional response in order to be able to model compression with no tension behavior (which the gap element does), and a capability to allow sliding with friction between the two surfaces (which it does not). In addition to these, the use of a gap element has another problem: a portion of the concrete may lose its capacity for resisting tension loads in one direction, but it is still able to resist forces in orthogonal directions, but the gap elements will change the load path that those forces must take to get into that piece of concrete.

The use of rigid connections is not very satisfactory either, because it provides a model that is too stiff beyond low load levels, though this was less evident for the -84 version runs than for the ADINA 5.0 runs (compare Figures 54 to 56 with Figures 57, 58, and 65). In the ADINA 5.0 runs, the stiffness of the test and the computer curves follow closely up through 15 kips, but thereafter the computer curve is much stiffer than the test curve. This is predictable since during the early part of the loading the socket and the concrete remain in contact, so the rigid connections are reasonable models. However, as the load continues to increase, there is separation between the socket and the concrete on the backside, and the rigid connections produce an additional resistance that does not exist. Even with this problem, however, the use of rigid connections produces a better model than using gap elements at this interface.

Concrete Constitutive Model

The constitutive model used for the concrete has the most influence on the response of the concrete-socket system. Using the ADINA 5.0 concrete model for the later part of the analysis was a decision prompted by the article by Gedlin et al. (46) which recommended many of the changes to the original concrete model that were incorporated in the later version.

However, there are a couple of major problems with ADINA that appear to be insurmountable as far as solving this problem is concerned, and they are directly related to the reasons why the program continued to terminate during the analyses. The first was the apparent inability to restore equilibrium (or converge to a solution) and continue with the solution after one of the elements had nearly or totally crushed, and the second is directly related to the concrete constitutive model parameters for the triaxial failure envelope.

Equilibrium Problems. After each load step (this was optional, it could have been after every second or higher step, but these analyses solved for equilibrium and a new stiffness matrix after each load step) the program would attempt to reestablish equilibrium. Once the new equilibrium condition had been established, the new stiffness matrix was obtained. Then the next load would be applied to the model. However, reaching equilibrium proved to be a difficult calculation after a certain stage in the solution had been reached, a stage which appears to occur almost immediately after any of the concrete elements had either been fully crushed or had come very near to being in that condition. Cracking did not appear to present problems of the same nature, but within a very short time (or load) after an element started seeing major portions of it being crushed, the program seemingly became unable to reestablish equilibrium. Convergence problems were of two types: (1) the program reached an input iteration limit without converging, but the solution appeared to be heading towards convergence, in which case increasing the number of iterations allowed might resolve the problem, and/or (2) after some step in the equilibrium calculations, the out-of-balance loads were larger than the incremental loads which indicated a divergent solution. Increasing the iteration limit was tried without any significant success.

ADINA provides a number of iteration techniques to obtain equilibrium. For this work the BFGS matrix update method with line search was utilized. The BFGS method was recommended in the ADINA modeling guide (5) in the case where the analyst is unfamiliar with the nonlinear response to be expected and when significant nonlinearities are to be analyzed. Another option, which was not used, would have been to use the full Newton iteration method with line search, which is the most powerful of the techniques available to use in the case of high nonlinearities, but it also would have been the most costly. The user is also able to select the criteria used by the program to determine convergence of the

equilibrium solution. For these analyses the energy convergence criteria was used, which was the default method used by the program.

In order to try to get past the equilibrium/convergence problems, the ATS routine (see paragraph under Run nlin11 for a description of ATS) was implemented as was decreasing the load step size. Using the ATS routine made a difference of maybe 1 or 2 kips in the maximum load obtained. In nlin17, the load steps beyond 80 kips were reduced to 100 lb increments. The result was that the maximum load went down (compare runs nlin16 and nlin17).

Triaxial Failure Envelope. The other reason for termination of the analyses runs was that a stress state was calculated where the current, at time t, principal stress ratio ${}^{t}\sigma_1/\tilde{\sigma}_c$ exceeded the input value of sp1(6), which is the maximum allowable value for the stress ratio for the maximum principal stress (the least negative one). Two modifications to the default triaxial failure envelope data were tried during these analyses where the maximum cap value for sp1(6) was doubled (run nlin06) and then increased almost tenfold (nlin16 and nlin17), but neither produced better results. Run nlin14 stopped after 84 kips because of exceeding the input value of sp1(6), but when sp1(6) was increased significantly in run nlin16 the load increased a mere 1.2 kips. Gedlin et al. (46) pointed out that experimental studies have showed that concrete has a much greater triaxial strength than the ADINA failure envelopes give credit for; thus using the ADINA default failure envelope data will lead to a conservative prediction of the actual strength of concrete structures under compressive loads. A partial set of data curves were included with the Gedlin et al. paper (46) showing that the entire set of failure envelope curves not only shift upwards (for a given value of sp1(I) the sp2 and sp3 values are larger than given in the ADINA data), but the slope of the line along the left edge where $\sigma_1 = \sigma_2$ is therefore steeper. Two runs using some of these data were run (see

discussion under Run nlin06) and both runs stopped, after 60 and 70 kips, for the same reasons as all the others. This serves to reinforce the conclusion that ADINA has problems establishing equilibrium once crushing has started, regardless of the data actually used for the failure envelopes.

Conclusions

The two questions raised at the beginning of this section can now be answered:

Was the finite element modeling adequate to solve the given problem? The model lacked some fine tuning, but the final version of the model should have been able to produce a reasonable solution. The changes discussed in the previous paragraphs could have been incorporated and would have provided a more realistic representation of the concrete-socket test. However, these modifications would not have prevented the equilibrium and convergence problems that were encountered.

Was the ADINA computer code capable of solving the problem? The answer to this question is that ADINA was not necessarily the best choice as the computer code to use in solving the concrete-socket modeling problem. However, the author is unable to offer suggestions as to which computer codes might be more appropriate. Selecting ADINA as the computer code for this problem was a reasonable choice at the time, as was continuing with it after the three year hiatus in spite of the difficulties experienced. The biggest problem encountered in running the analysis was the inability of the program to establish equilibrium after the apparent failure of a single element. In the tests the load continued to increase well beyond the point at which the concrete at the surface in front of the socket crushed. The analysis was never able to model this behavior. Had the problem been related entirely to the constitutive model parameters of the concrete, then there is a reasonable probability that, by

modifying the failure envelopes, a solution would have been obtained that produced better agreement.

CHAPTER VII

SUMMARY AND CONCLUSIONS

I. SUMMARY

The objective of this dissertation was to develop an understanding of the behavior of large inserts embedded in concrete and loaded in eccentric shear. This problem originated from the need to design the concrete floor slab which encased the GCEP centrifuge machine support structures (floor modules). The major design unknown was the bearing stress capacity the concrete could withstand at the corner of the floor modules, given the design failure loads. A standard design using ACI Code allowable bearing values was not desirable because it resulted in a very heavy and large design for the floor modules and floor slab which unacceptably increased the overall cost of the project. Preliminary calculations (based on the code, but taking credit for everything that seemed reasonable) showed that the bearing capacity could be increased at least two to three times the code allowable, but it was felt that this ratio could be even larger. Thus, the main goal for this project was to determine an allowable, yet safe, bearing capacity that would permit the design of the GCEP facility to remain within a reasonable cost.

A series of tests were planned, prepared, and performed to determine the strength and to study the behavior of individual components, the large corner socket embedments in concrete, and the final floor module/floor slab design. This dissertation focuses principally on the embedded socket tests and the finite element analysis that followed attempting to duplicate the test results.

A simple formula (eq. 3-1) was developed based on the configuration of the socket tests, and bearing capacity values were obtained for each of the socket tests. The results of this calculation were comparable with the test results of steel brackets embedded in a concrete column and loaded in eccentric shear. Eight socket tests were performed which resulted in bearing capacity ratios between 3 and 4½ times the concrete strength - a little larger than were obtained using the simple preliminary hand calculations. The GCEP floor slab and floor module design had been completed, based on the simple hand calculations, and a large portion of the facility was constructed. Thus, following the socket tests, load tests on four floor mount positions were performed to verify the adequacy of the design. The results of these tests generally supported the adequacy of the final design to withstand the design loads.

The last part of the dissertation work was to develop a finite element model of a typical corner socket test location in order to study the behavior of the large inserts in concrete, and to determine the feasibility of using such an analysis in lieu of testing. The analysis code selected for this study was ADINA because it contained in its materials library a nonlinear material model for three-dimensional concrete. It was also readily available to the author.

The basic finite element model was put together and first run in late 1987. Problems were encountered with the analysis, almost from the very beginning, due to the fact that the computer runs were unable to reach a solution for loads greater than about half the maximum loads observed in the tests. At loads between 70 and 90 kips, the runs always terminated due either to problems with the convergence of the solution or the material failure envelope for the concrete elements. In trying to obtain a higher load solution, a number of modifications were made to the geometry and physical characteristics of the model, to the concrete material data, to the load step increment size, and to some of the equilibrium parameters. None

succeeded. Successful solutions were obtained to two related problems using ADINA: (1) the standard concrete cylinder test and (2) Cerruti's problem of a semi-infinite solid loaded with a tangential force acting on the surface. A later version of ADINA, having a new concrete material model, was tried, but again, the same problems were encountered. After making another series of changes without any success, the finite element analysis effort was finally terminated.

II. CONCLUSIONS

The original goal of the GCEP design project was satisfactorily met: proving that the bearing capacity developed in the case of these large inserts embedded in concrete and loaded in eccentric shear was considerably higher than standard building code values would provide. The simplified hand solution initially produced a conservative, but higher than code allowable, estimate which was used to develop a preliminary design, and the corner socket tests which followed resulted in still higher values, which were implemented in the final design. The socket tests also provided data on the behavior of these inserts during a load test. Tests on actual floor module/floor slab structures installed in the GCEP facility proved that the socket tests produced an acceptable design.

Finally, the goal of obtaining a nonlinear finite element analysis of these socket tests was not satisfactory. Only a partial solution was obtained. There were a host of problems which arose during the many runs that were made during the better part of two years. The model did predict the general area where cracking and crushing would occur and provided information about the sequence of probable failure. However, whether due to inaccuracies in the actual model or deficiencies in the ADINA code, or both, the analysis did not produce an accurate representation of the load-displacement curve in the highly nonlinear behavior

regions of the test. Whereas the tests resulted in peak loads between 140 and 200 kips, no computer run was able to predict loads higher than 90 kips. Since first crushing of an element takes place at about 90 kips, it was concluded that ADINA has problems reestablishing a state of equilibrium once this first element has crushed and lost all stiffness. In the real test, it was clear that the concrete/socket system still retained a capacity to resist load well beyond the level of first crushing of the concrete located directly in front of the socket. ADINA was never able to produce the same behavior. The conclusion, based on these experiences, is that, while performing the nonlinear analysis was a good academic problem, the tests were essential to developing the design. The use of a nonlinear finite element analysis as the sole predictor of this theory is not recommended.

LIST OF REFERENCES

LIST OF REFERENCES

1. ACI Committee 223, "Recommended Practice for the Use of Shrinkage-Compensating Concrete (ACI 223-77)," American Concrete Institute, 1977.

2. ACI Committee 318, "Building Code Requirements for Reinforced Concrete (ACI 318-77)," and "Commentary on Building Code Requirements for Reinforced Concrete (ACI 318-88)," American Concrete Institute, 1977.

3. ACI Committee 349, "Code Requirements for Nuclear Safety Related Concrete Structures (ACI 349-85): Appendix B-Steel Embedments," and "Commentary on Code Requirements for Nuclear Safety Related Concrete Structures (ACI 349-85): Appendix B-Steel Embedments," American Concrete Institute, 1985.

4. "ADINA - A Finite Element Program for Automatic Dynamic Incremental Nonlinear Analysis: User's Manual," Report AE 84-1, ADINA Engineering, Inc., December 1984.

5. "ADINA - A Finite Element Program for Automatic Dynamic Incremental Nonlinear Analysis: User's Manual," Report ARD 87-1, ADINA R&D, Inc., December 1987.

6. "ADINA: System Theory and Modeling Guide," Report AE 83-4, ADINA Engineering, Inc., September 1983.

7. Ahmad, S. H. and Shah, S. P., "Complete Triaxial Stress-Strain Curves for Concrete," Journal of the Structural Division, ASCE, Vol. 108, No. ST4, April, 1982, pp. 728-742.

8. Ahmad, S. H. and Shah, S. P., "Orthotropic Model for Complete Stress-Strain Curves of Concrete under Multiaxial Stresses," in Proceedings of the Second International Conference on Constitutive Laws for Engineering Materials: Theory and Applications," Vol. II, Desai, C. S., Krempl, E., Kiousis, P. D., and Kundu, T. (Eds.), Elsevier Science Publishing Co., New York, 1987, pp.1421-1433.

9. "ASTM Standard Test Method for Static Modulus of Elasticity and Poisson's Ratio of Concrete in Compression (C 469-81)," 1983 Annual Book of ASTM Standards, American Society for Testing and Materials, Philadelphia, PA, 1983.

10. Bailey, J. W. and Burdette, E. G., "Edge Effects on Anchorage to Concrete," Civil Engineering Research Series No.31, The University of Tennessee, Knoxville, August, 1977.

11. Balakrishnan, S. and Murray, D. W., "Concrete Constitutive Model for NLFE Analysis of Structures," Journal of Structural Engineering, ASCE, Vol. 114, No. 7, July, 1988, pp.1449-1466.

12. Balakrishnan, S., Elwi, A. E., and Murray, D. W., "Effect of Modeling on NLFE Analysis of Concrete Structures," Journal of Structural Engineering, ASCE, Vol. 114, No. 7, July, 1988, pp.1467-1487.

13. Balakrishnan, S. and Murray, D. W., "Prediction of R/C Panel and Deep Beam Behavior by NLFEA," Journal of Structural Engineering, ASCE, Vol. 114, No. 10, October, 1988, pp.2323-2342.

14. Bangash, M. Y. H., Concrete and Concrete Structures: Numerical Modelling and Applications, Elsevier Applied Science, London, 1989.

15. Bathe, K. J., Finite Element Procedures in Engineering Analysis, Prentice-Hall, Inc., Englewood Cliffs, New Jersey, 1982.

16. Bathe, K. J. (Ed.), Proceedings of the 3rd ADINA Conference, in Computers and Structures, Vol. 13, Nos. 5/6, 1981.

17. Bathe, K. J. (Ed.), Proceedings of the 4th ADINA Conference, in Computers and Structures, Vol. 17, Nos. 5/6, 1983.

18. Bathe, K. J. (Ed.), Proceedings of the 5th ADINA Conference, in Computers and Structures, Vol. 21, Nos. 1/2, 1985.

19. Bathe, K. J. (Ed.), Proceedings of the 6th ADINA Conference, in Computers and Structures, Vol. 26, Nos. 1/2, 1987.

20. Bathe, K. J. (Ed.), Proceedings of the 7th ADINA Conference, in Computers and Structures, Vol. 32, Nos. 3/4, 1989.

21. Bathe, K. J. (Ed.), Proceedings of the 8th ADINA Conference, in Computers and Structures, Vol. 40, No. 2, 1991.

22. Bathe, K. J. and Ramaswamy, S., "On Three-Dimensional Nonlinear Analysis of Concrete Structures," Nuclear Engineering and Design, Vol. 52, 1979, pp. 385-409.

23. Bathe, K. J., Walczak, J., Welch, A., and Mistry, N., "Nonlinear Analysis of Concrete Structures," Computers and Structures, Vol. 32 Nos. 3/4, 1989, pp. 563-590.

24. Bazant, Z. P., "Comment on Orthotropic Models for Concrete and Geomaterials," Journal of Engineering Mechanics, ASCE, Vol. 109, No. 3, June, 1983, pp. 849-865.

25. Bazant, Z. P. and Bhat, P. D., "Endochronic Theory of Inelasticity and Failure of Concrete," Journal of the Engineering Mechanics Division, ASCE, Vol. 102, No. EM4, August, 1976, pp. 701-722.

26. Bazant, Z. P., "Fracture in Concrete and Reinforced Concrete," in Mechanics of Geomaterials: Rocks, Concretes, Soils, Z. P. Bazant, Ed., John Wiley & Sons, Chichester, England, 1985, pp. 259-303.

27. Bazant, Z. P. (Ed.), Mechanics of Geomaterials: Rocks, Concretes, Soils, John Wiley & Sons, Chichester, England, 1985.

28. Bazant, Z. P. and Kim, S. S., "Plastic-Fracturing Theory for Concrete," Journal of the Engineering Mechanics Division, ASCE, Vol. 105, No. EM3, June, 1979, pp. 407-428.

29. Bedard, C. and Kotsovos, M. D., "Application of NLFEA to Concrete Structures," Journal of Structural Engineering," ASCE, Vol. 111, No. 12, December, 1985, pp. 2691-2707

30. Bergan, P. G., "Numerical Aspects in Modelling of Inelastic Materials: Discusser's Report," in Mechanics of Geomaterials: Rocks, Concretes, Soils, Z. P. Bazant, Ed., John Wiley & Sons, Chichester, England, 1985, pp.527-536.

31. Burdette, E. G., Jones, W. D., and Fricke, K. E., "Concrete Bearing Capacity around Large Inserts," Journal of Structural Engineering, ASCE, Vol. 109, No. 6, June 1983, pp. 1375-1386.

32. Buyukozturk, O. and Shareef, S. S., "Constitutive Modeling of Concrete in Finite Element Analysis," Computers and Structures, Vol. 21, No. 3, 1985, pp. 581-610.

33. Cannon, R. W., Burdette, E. G., and Funk, R. R., "Anchorage to Concrete," Report No. CEB 75-32, Tennessee Valley Authority, Knoxville, December, 1975.

34. Cannon, R. W., Godfrey, D. A., and Moreadith, F. L., "Guide to the Design of Anchor Bolts and Other Steel Embedments," Concrete International, American Concrete Institute, July 1981, pp. 28-41.

35. Chang, T. Y., Taniguchi, H., and Chen, W. F., "Nonlinear Finite Element Analysis of Reinforced Concrete Panels," Journal of Structural Engineering, ASCE, Vol. 113, No. 1, January, 1987, pp.122-140.

36. Chen, W. F. Plasticity in Reinforced Concrete, McGraw-Hill Book Company, New York, 1982.

37. Chen, W. F. and Han, D. J., Plasticity for Structural Engineers, Springer-Verlag, New York, New York, 1988.

38. Chen, W. F. and Mizuno, E., Nonlinear Analysis in Soil Mechanics, Elsevier Science Publishers B. V., Amsterdam, 1990.

39. Chen, W. F. and Ting, E. C., "Constitutive Models for Concrete Structures," Journal of the Engineering Mechanics Division, ASCE, Vol. 106, No. EM1, February, 1980, pp. 1-19.

40. Desai, C. S. and Gallagher, R. H. (Eds.), Proceedings of the International Conference on Constitutive Laws for Engineering Materials: Theory and Application," University of Arizona, Tucson, Arizona, January 10-14, 1983.

41. Desai, C. S., Krempl, E., Kiousis, P. D., and Kundu, T. (Eds.), Proceedings of the Second International Conference on Constitutive Laws for Engineering Materials: Theory and Applications," Vols. I and II, Elsevier Science Publishing Co., New York, 1987.

42. Dougill, J. W., "Constitutive Relations for Concrete and Rock: Applications and Extensions of Elasticity and Plasticity Theory," in Mechanics of Geomaterials: Rocks, Concretes, Soils, Z. P. Bazant, Ed., John Wiley & Sons, Chichester, England, 1985, pp. 21-46.

43. "Embedment Properties of Headed Studs," Design Data 10, TRW Nelson Division, Lorain, Ohio, 1974.

44. Faruque, M. O., "A Cap Type Constitutive Model for Plain Concrete," in Proceedings of the Second International Conference on Constitutive Laws for Engineering Materials: Theory and Applications," Vol. I, Desai, C. S., Krempl, E., Kiousis, P. D., and Kundu, T. (Eds.), Elsevier Science Publishing Co., New York, 1987, pp. 395-402.

45. Fricke, K. E., Jones, W. D., and Burdette, E. G., "Full-Scale Shear Tests of Embedded Floor Modules," Proceedings of the Fifth Engineering Mechanics Division Specialty Conference: Engineering Mechanics in Civil Engineering, ASCE, Laramie, Wyoming, August 1-3, 1984, pp. 599-602.

46. Gedling, J. S., Mistry, N. S., and Welch, A. K., "Evaluation of Material Models for Reinforced Concrete Structures," Computers and Structures, Vol. 24, No.2, 1986, pp. 225-232.

47. "General Anchorage to Concrete," Civil Design Standard No. DS-C-1.7.1, Tennessee Valley Authority, Knoxville, TN, 1984.

48. Goodpasture D. W. and Fricke, K. E., "Mount Lug Tests - Part 1: Laboratory Bend Tests," Report K/D-5199 Part 1, Rev. 1, Union Carbide Corporation Nuclear Division, Oak Ridge, Tennessee, July, 1981.

49. Goodpasture D. W. and Fricke, K. E., "Mount Lug Tests - Part 2: Field Tests," Report K/D-5199 Part 2, Union Carbide Corporation Nuclear Division, Oak Ridge, Tennessee, June 1981.

50. Han, D. J. and Chen, W. F., "Constitutive Modeling in Analysis of Concrete Structures," Journal of Engineering Mechanics, ASCE, Vol. 113, No. 4, April, 1987, pp. 577-593.

51. Herrmann, L. R., "Finite Element Analysis of Contact Problems," Journal of the Engineering Mechanics Division, ASCE, Vol. 104, No. EM5, October 1978, pp. 1043-1057.

52. James, R. W., De la Guardia, C., and McCreary, C. R., "Strength of Epoxy-Grouted Anchor Bolts in Concrete," Journal of Structural Engineering, ASCE, Vol. 113, No. 12, December. 1987, pp. 2365-2381.

53. Jeter, J. W., "Path/History Dependent Behavior of the Endochronic Concrete Model," Proceedings of the International Conference on Constitutive Laws for Engineering Materials: Theory and Applications," C. S. Desai and R. H. Gallagher (Eds.), University of Arizona, Tucson, Arizona, January, 1983, pp. 457-462.

54. Klingner, R. E., Mendonca, J. A., and Malik, J. B., "Effect of Reinforcing Details on the Shear Resistance of Short Anchor Bolts Under Reversed Cyclic Loading," Journal of the American Concrete Institute, Proceedings Vol. 79, No.1, January-February, 1982, pp. 3-12.

55. Klingner, R. E. and Mendonca, J. A., "Shear Capacity of Short Anchor Bolts and Welded Studs: A Literature Review," Journal of the American Concrete Institute, Proceedings Vol. 79, No.5, September-October, 1982, pp. 339-349.

56. Klingner, R. E. and Mendonca, J. A., "Tensile Capacity of Short Anchor Bolts and Welded Studs: A Literature Review," Journal of the American Concrete Institute, Proceedings Vol. 79, No.4, July-August, 1982, pp. 270-279

57. Krajcinovic, D. and Selvaraj, S., "Constitutive Equations for Concrete," in Proceedings of the International Conference on Constitutive Laws for Engineering Materials: Theory and Applications," C. S. Desai and R. H. Gallagher (Eds.), University of Arizona, Tucson, Arizona, January, 1983, pp. 399-406.

58. Lacy, S. J. and Prevost, J. H., "Constitutive Model for Geomaterials," in Proceedings of the Second International Conference on Constitutive Laws for Engineering Materials: Theory and Applications," Vol. I, Desai, C. S., Krempl, E., Kiousis, P. D., and Kundu, T. (Eds.), Elsevier Science Publishing Co., New York, 1987, pp. 149-160.

59. Lade, P. V., "Three-Parameter Failure Criterion for Concrete," Journal of the Engineering Mechanics Division, ASCE, Vol. 108, No. EM5, October, 1982, pp. 850-863.

60. Leibengood, L. D., Darwin, D., and Dodds, R. H., "Parameters Affecting FE Analysis of Concrete Structures," Journal of Structural Engineering, ASCE, Vol. 112, No. 2, February, 1986, pp. 326-341.

61. Mattock, A. H. and Gaafar, G. H., "Strength of Embedded Steel Sections as Brackets," Journal of the American Concrete Institute, Proceedings Vol. 79, No.2, March-April, 1982, pp. 83-93.

62. McMackin, P. J., Slutter, R. G., and Fisher, J. W., "Headed Steel Anchors Under Combined Loading," Engineering Journal, AISC, 2nd Quarter, 1973, pp. 43-52.

63. Meyer, C. and Bathe, K. J., "Nonlinear Analysis of R/C Structures in Practice," Journal of the Structural Division, ASCE, Vol. 108, No. ST7, July, 1982, pp. 1605-1622.

64. Meyer, C. and Okamura, H. (Eds.), Proceedings of the Seminar: Finite Element Analysis of Reinforced Concrete Structures, held in Tokyo, Japan, May 21-24, 1985, ASCE, New York, NY, 1986.

65. Mould, J. C., Jr., and Levine, H., "A Three-Invariant Viscoplastic Concrete Model," in Proceedings of the Second International Conference on Constitutive Laws for Engineering Materials: Theory and Applications," Vol. I, Desai, C. S., Krempl, E., Kiousis, P. D., and Kundu, T. (Eds.), Elsevier Science Publishing Co., New York, 1987, pp.707-716.

66. Mroz, Z., "Current Problems and New Directions in Mechanics of Geomaterials," in Mechanics of Geomaterials: Rocks, Concretes, Soils, Z. P. Bazant, Ed., John Wiley & Sons, Chichester, England, 1985, 539-566.

67. Ohtani, Y. C. and Chen, W. F., "Hypoelastic-Perfectly Plastic Model for Concrete Materials," Journal of Engineering Mechanics, ASCE, Vol. 113, No. 12, December, 1987, pp. 1840-1860.

68. Ottosen, N. S., "Constitutive Model for Short-Time Loading of Concrete," Journal of the Engineering Mechanics Division, ASCE, Vol. 105, No. EM1, February, 1979, pp. 127-141.

69. Ottosen, N. S., "Evaluation of Concrete Cylinder Tests Using Finite Elements," Journal of Engineering Mechanics, ASCE, Vol. 110, No. 3, March, 1984, pp. 465-481.

70. Ottosen, N. S., "A Failure Criterion for Concrete," Journal of the Engineering Mechanics Division, ASCE, Vol. 103, No. EM4, August, 1977 pp. 527-535.

71. Ottosen, N. S., "Nonlinear Finite Element Analysis of Pull-Out Test," Journal of the Structural Division, ASCE, Vol. 107, No. ST4, April 1981, pp. 591-603

72. Peier, W. H., "Model for Pull-Out Strength of Anchors in Concrete," Journal of Structural Engineering, ASCE, Vol. 109, No. 5, May, 1983, pp.1155-1173.

73. PCI Design Handbook - Precast and Prestressed Concrete, 3rd Edition, Prestressed Concrete Institute, Chicago, 1985.

74. Robinet, J. C. and Torrenti, J. M., "Prediction of Concrete Behavior Using a Non Linear Incremental Model," in Proceedings of the International Conference on Constitutive Laws for Engineering Materials: Theory and Applications," C. S. Desai and R. H. Gallagher (Eds.), University of Arizona, Tucson, Arizona, January, 1983, pp. 411-420.

75. Ruina, A. L., "Constitutive Relations for Frictional Slip," in Mechanics of Geomaterials: Rocks, Concretes, Soils, Z. P. Bazant, Ed., John Wiley & Sons, Chichester, England, 1985, pp. 169-188.

76. Saada, A. S., Elasticity - Theory and Applications, Robert E. Krieger Publishing Company, Malabar, Florida, 1983.

77. Salami, M. R. and Desai, C. S., "A Constitutive Model for Plain Concrete," in Proceedings of the Second International Conference on Constitutive Laws for Engineering Materials: Theory and Applications," Vol. I, Desai, C. S., Krempl, E., Kiousis, P. D., and Kundu, T. (Eds.), Elsevier Science Publishing Co., New York, 1987, pp.447-455.

78. Schmidt-Goner, G., Gerstle, K., and Mehlhorn, G., "A Comparison Between ADINA and Concrete Strength," Proceedings ADINA Conference (1979), Massachusetts Institute of Technology Report No. 8448-9, August 1979, pp. 671-680

79. Shipp, J. G. and Haninger, E. R., "Design of Headed Anchor Bolts," Engineering Journal, American Institute of Steel Construction, 2nd Quarter, 1983, pp. 58-69.

80. Sussman, T., and Bathe, K. J., "Studies of Finite Element Procedures - on Mesh Selection," Proceedings of the 5th ADINA Conference, K. J. Bathe (Ed.), published in Computers and Structures, Vol. 21, No. 1/2, 1985, pp.257-264.

81. Task Committee on Finite Element Analysis of Reinforced Concrete Structures, State-of-the-Art Report on Finite Element Analysis of Reinforced Concrete, ASCE, New York, NY, 1982.

82. Zienkiewicz, O. C., "Numerical Modelling and Geomechanics (Soil-Rock-Concrete)," in Mechanics of Geomaterials: Rocks, Concretes, Soils, Z. P. Bazant, Ed., John Wiley & Sons, Chichester, England, 1985, pp. 471-499.

APPENDICES

APPENDIX A

TABLES

Table 1: Summary Results of the Floor Module Tests

	Maximum Ram Load (kips)	Maximum Socket Deflection (in.)
1	224	0.0166
2	327	0.0417
3	250	0.0292
4	337	0.0544

Table 2: Summary of Cylinder Break Tests

Specimen No.	Socket Test No.	Concrete Age (days)	f'_c (psi)	Modulus of Elasticity (psi)	Poisson's Ratio
2 tests	mix #1	28	3265	----	---
26 tests	mix #2	28	2754	3125[1]	0.20[1]
2-15	1	49	2820	3300	0.22
2-17	1	49	2890	3150	0.18
2-51	1	49	2860	3150	0.21
2-52	1	49	2880	3000	0.20
1-7	2	55	3690	3800	0.20
1-6	2	55	3400	3550	0.20
2-26	2	55	2980	3200	0.20
2-35	2	55	2890	3100	0.20
2-54	2	55	2890	3250	0.21
2-57	2	55	2920	3200	0.22
2-22	3	63	2880	3250	0.20
2-38	3	63	2940	3250	0.19
2-42	3	63	2960	3250	0.21
2-49	3	63	2950	3150	0.21
1-5	4	66	3500	3650	0.22
1-10	4	66	3470	3650	0.21
2-39	4	66	3010	3300	0.21
2-41	4	66	3010	3250	0.20
2-50	4	66	2990	3200	0.21
2-53	4	66	2990	3200	0.20

[1] Based on six cylinder break tests only

Table 2 (cont.)

Specimen No.	Socket Test No.	Concrete Age (days)	f'_c (psi)	Modulus of Elasticity (psi)	Poisson's Ratio
2-29	5	77	3060	3400	0.21
2-30	5	77	3040	3250	0.20
2-31	5	77	3080	3300	0.21
2-32	5	77	3060	3200	0.20
1-11	6	114	3540	3900	0.23
1-12	6	114	3600	3750	0.22
2-33	6	114	3130	3500	0.22
2-34	6	114	3110	3400	0.20
2-47	6	114	3180	3350	0.21
2-48	6	114	3080	3600	0.21
1-8	7 & 8	120	3750	4100	0.22
1-9	7 & 8	120	3890	4050	0.22
2-36	7 & 8	120	3110	3450	0.20
2-37	7 & 8	120	3060	3550	0.21
2-40	7 & 8	120	2970	3300	0.19
2-43	7 & 8	120	3060	3400	0.20
2-44	7 & 8	120	3060	3400	0.21
2-45	7 & 8	120	2940	3500	0.23
2-46	7 & 8	120	3010	3500	0.22
2-59	7 & 8	120	3100	3500	0.21

Table 3: Parameters and Results of Socket Tests

Test No.	Initial Slope (kips/in.)	P_{max} (kips)	f'_c (ksi)	e (in.)	f_b (ksi)	$K = f_b/f'_c$
1	na	164	2.89	3.05	11.21	3.9
2	na	185	2.91	2.71	12.53	4.3
3	12,500	162	2.95	2.70	10.46	3.5
4	20,000	164	2.96	2.75	10.72	3.6
5	40,000	155	3.08	2.62	9.71	3.2
6	25,000	173	3.10	2.63	11.32	3.6
7	25,000	200	3.11	2.66	13.77	4.4
8	40,000	185	3.11	2.70	12.51	4.0

Table 4: ADINA Element and Material Model Summary

Element Type	Analysis Methods	Material Models
Truss	1,2,3	1,3,4,7,9,13,15
2-D Solid	1,2,3,4	1,2,3,5,6,8,10,11,14,16,17,18
3-D Solid	1,2,3,4	1,2,3,5,6,8,10,11,14,16,18
Beam	1,2,3	1,7
Isoparametric Beam	1,2,4	1,7,9
Plate/Shell	1,2,3	1,2,19
Shell	1,2,4	1,2,3,8
General	1	1
Pipe	1,2,4	1,7
2-D Fluid/3-D Fluid	1,3	20
2-D/3-D Contact Surfaces		

KEY TO NUMBERS IN TABLE

Analysis Methods

1. Linear elastic
2. Materially nonlinear only
3. Updated Lagrangian
4. Total Lagrangian

Material Models

1. Isotropic linear elastic
2. Orthotropic linear elastic
3. Isotropic thermo-elastic
4. Nonlinear elastic
5. Curve description nonlinear
6. Concrete model (with cracking and crushing)
7. Elastic-Plastic (isotropic hardening)
8. Elastic-Plastic (von Mises, isotropic hardening)
9. Elastic-Plastic (kinematic hardening)
10. Elastic-Plastic (von Mises, kinematic hardening)
11. Elastic-Plastic (Drucker-Prager Cap)
12. Isothermal plasticity (isotropic hardening)
13. Thermo-elastic-plastic & creep (isotropic hardening)
14. Thermo-elastic-plastic & creep (von Mises, isotropic hardening)
15. Thermo-elastic-plastic & creep (kinematic hardening)
16. Thermo-elastic-plastic & creep (von Mises, kinematic hardening)
17. Nonlinear elastic (Mooney-Rivlin model)
18. User supplied
19. Elastic-Plastic (Ilyushin, isotropic hardening)
20. Inviscid, compressible fluid with constant bulk modulus

Table 5: Cerruti Problem Summary

Point Coordinates		X1 Displacement (in.)		Percent Difference
X1	X2	Theory	ADINA	
X3 = 0.00				
3.00	0.00	0.00822	0.00840	2.2
6.00		0.00411	0.00407	-1.0
9.00		0.00274	0.00283	3.3
14.50		0.00170	0.00193	13.5
26.50		0.00093	0.00150	61.3
0.00	5.50	0.00354	0.00319	-9.9
6.00		0.00274	0.00275	0.4
9.00		0.00221	0.00233	5.4
14.50		0.00155	0.00182	17.4
6.00	10.50	0.00171	0.00170	-0.6
9.00		0.00157	0.00167	6.4
14.50		0.00128	0.00153	19.5
X3 = 7.00				
3.00	0.00	0.00232	0.00225	-3.0
6.00		0.00224	0.00228	1.8
9.00		0.00199	0.00215	8.0
14.50		0.00152	0.00185	21.7
26.50		0.00092	0.00150	63.0
0.00	5.50	0.00184	0.00233	26.6
6.00		0.00185	0.00239	29.2
9.00		0.00171	0.00219	28.1
14.50		0.00140	0.00177	26.4
6.00	10.50	0.00134	0.00148	10.4
9.00		0.00131	0.00153	16.8
14.50		0.00117	0.00149	27.4

Table 6: Summary of the Finite Element Model Configuration

Substructure	Modeling Element	Material Model	Number
Concrete	3-D Solid	Isotropic Linear Elastic	566
Concrete	3-D Solid	Nonlinear Concrete	140
Anchor Bar[1]	3-D Solid	Nonlinear	6
Steel Socket	3-D Solid	Isotropic Linear Elastic	32
Steel Mount Lug	3-D Solid	Isotropic linear Elastic	32
Loading Plates	Shell	Isotropic Linear Elastic	12
Reinforcing Bars	Truss	Linear Elastic	69
Gap Elements	Truss	Nonlinear Elastic-Plastic	varies

[1] Initially the anchor bar was modeled using the 2-D beam element and later the iso-beam element. However, the final version of the model used the 3-D solid element.

Table 7. Boundary Condition Sets Used in Analyses

Bondary Condition Case	nodes @ Z=0: $\Delta z=0$	nodes @ Y=-36: $\Delta y=0$	symmetry bc's at x=0: $\Delta x=0$	nodes at (x,36,0): restrained $\Delta z=0$	nodes @ (31,y,0) & (x,±36,0): restrained $\Delta x=0$ and $\Delta y=0$
1	x	x	x		
2		x	x	x	
3	x	x	x		x

Table 8. Nonlinear Concrete Triaxial Data Curves Used in Analyses

Principal Stress Ratios[1]	CURVE NUMBER[2]					
	I=1	I=2	I=3	I=4	I=5	I=6
ADINA DEFAULT TRIAXIAL DATA						
sp1(I)	0.000	0.250	0.500	0.750	1.000	1.200
sp3(I,1) (at σp2=σp1)	1.000	1.400	1.700	2.200	2.500	2.800
sp3(I,2) (at σp2=β*σp3)	1.300	1.500	2.000	2.300	2.700	3.200
sp3(I,3) (at σp2=σp3)	1.250	1.450	1.950	2.250	2.650	3.150
MODIFIED TRIAXIAL DATA SET #1						
sp1(I)	0.000	0.500	1.000	1.500	2.100	2.700
sp3(I,1) (at σp2=σp1)	1.000	1.700	2.500	3.250	4.170	5.050
sp3(I,2) (at σp2=β*σp3)	1.300	2.000	2.700	3.570	4.450	5.430
sp3(I,3) (at σp2=σp3)	1.250	1.950	2.650	3.550	4.550	5.470
MODIFIED TRIAXIAL DATA SET #2						
sp1(I)	0.000	0.250	0.500	0.750	1.000	10.000
sp3(I,1) (at σp2=σp1)	1.000	1.400	1.700	2.200	2.500	16.06
sp3(I,2) (at σp2=β*σp3)	1.300	1.500	2.000	2.300	2.700	16.91
sp3(I,3) (at σp2=σp3)	1.250	1.450	1.950	2.250	2.650	16.86

Notes: (1) spi = σ_i/σ_c, where $\sigma_1 \geq \sigma_2 \geq \sigma_3$ (algebraic value)
(2) refer to Figure 21

Table 9. Summary of ADINA Linear Runs

Run Number	ADINA Version	BC Set No.	Anchor Bar	Concrete Data	Load (kips)	Δy_{1161} (in.)	Stiffness (kips/in.) (x 10^4)	Comments
lin01	-81	1	beam	E = 3122 ksi ν = 0.15	200	0.01054	1.90	no gap elem. no load plates
lin02	-84	1	isobeam	E = 3122 ksi ν = 0.21	100	0.0128	0.78	gap elements no load plates
lin03	-84	1	isobeam	E = 3122 ksi ν = 0.21	100	0.0094	1.06	gap elements load plates
lin04 (same as lin03)	5.0	1	isobeam	E = 3122 ksi ν = 0.21	100	0.0094	1.06	gap elements load plates
lin05	5.0	1	isobeam	E = 3122 ksi ν = 0.21	10	0.000479	2.09	no gap elements load plates
lin06	5.0	1	isobeam	E = 3500 ksi ν = 0.21	10	0.000432	2.32	no gap elements load plates
lin07	5.0	3	isobeam	E = 3500 ksi ν = 0.21	10	0.000410	2.44	no gap elements load plates
lin08	5.0	3	3-D	E = 3500 ksi ν = 0.21	20	0.000687	2.91	no gap elements load plates

Table 10. Summary of ADINA Nonlinear Runs

Run Number	ADINA Vers.	BC Set	Load Step Sequence $(t_1,P_1)...(t_1,P_1)$	Max. Load	Reason Stopped	Comments
nlin01	-81	1	1,40 2,60	60k	finished	default conc data; anch bar = beam elem. no gap or plate elem. included
nlin02	-81	1	1,40 5,120	60k	div. chk	
nlin03	-84	1	1,40 17,200	90k	iter > n	
nlin04	-84	1	1,40 6,90 26,190	90k	p1 > sp1	
nlin05	-84	1	1,40 6,90 26,190	70k	p1 > sp1	gap elements added
nlin06	-84	1	1,40 6,90 26,190	60k	iter > n	concrete modified data set #1
nlin07	-84	2	100,100 300,200	70k	iter > n	add load plates; removed gap el; anchor bar = isobeam elem; default conc. data
nlin08	-84	1	100,100 300,200	60k	p1 > sp1	
nlin09	-84	1	1,40 6,90 26,190	90k	iter > n	
nlin10	5.0	3	250,250	84k	converge	anchor bar using 3d elements
nlin11	5.0	3	250,250	84.5k	converge	used Automatic Time Step option
nlin12	5.0	3	250,250	89.75k	converge	concrete e_u=-0.1 (instead of -0.003)
nlin13	5.0	3	250,250	83k	p1 > sp1	anchor bar top element has low E
nlin14	5.0	3	250,250	84k	p1 > sp1	conc. e_u=-1.0; no softening of σ-e curve
nlin15	5.0	3	250,250	80.7k	iter > n	anc bar top elem. = nlin. con; e_u=-0.1
nlin16	5.0	3	250,250	85.2k	iter > n	e_u=-1.0; concrete modified data set 2
nlin17	5.0	3	80,80 1280,200	84.5k	iter > n	

Table 11. Summary of ADINA Runs Modeling Concrete as an Elastic-Plastic Material

Run Number	Concrete Material Model	Max Load	Reason Stopped	Comments
nlinep01	bilinear elastic-plastic	200k	complete	tension properties = compression properties; E_{hard} = 35,000 psi
nlinep02	bilinear elastic-plastic	180k	complete	same as nlinep01, except reduced E_{hard} to 3,500 psi
nlinep03	multilinear elastic-plastic	157k	$e_{pl} > e_u$	tension prop. equal compression prop.; σ-e curve approximates concrete uniaxial compression
nlinep04	multilinear elastic-plastic	10k	$e_{pl} > e_u$	defined tension elements and compression elememts and used different σ-e curve for each type set e_{max} = 0.00015
nlinep05	bilinear elastic-plastic	33.7k	converge	defined tension elements and compression elememts and used different σ-e curve for each type set tension e_{max} = 0.00015 "/"
nlinep06	bilinear elastic-plastic	180k	complete	same as nlinep05, but set no limit on e_{max}; E_{hard} = 3500 psi
nlinep07	bilinear elastic-plastic	180k	complete	same as nlinep06, but tension elements perfectly plastic

Notes:
(1) all runs done with ADINA 5.0
(2) all runs used bc = 3
(3) all runs, anchor bar modeled using 3-D elements
(4) all runs load sequence is in 1 kip (total) increments

APPENDIX B

FIGURES

Figure 1. GCEP Floor Module with Mount Lugs

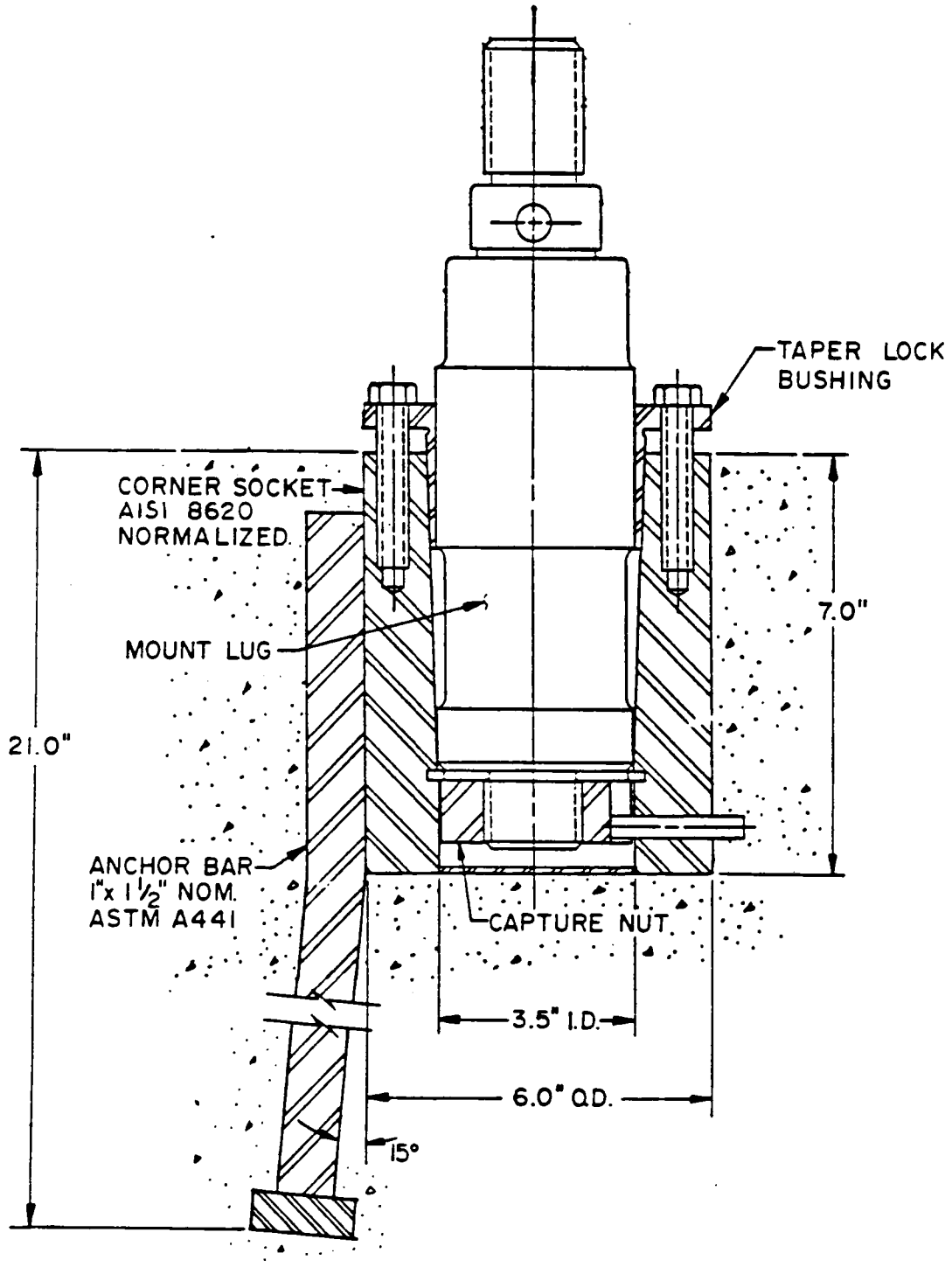

Figure 2. Detail of a Corner Socket with Mount Lug

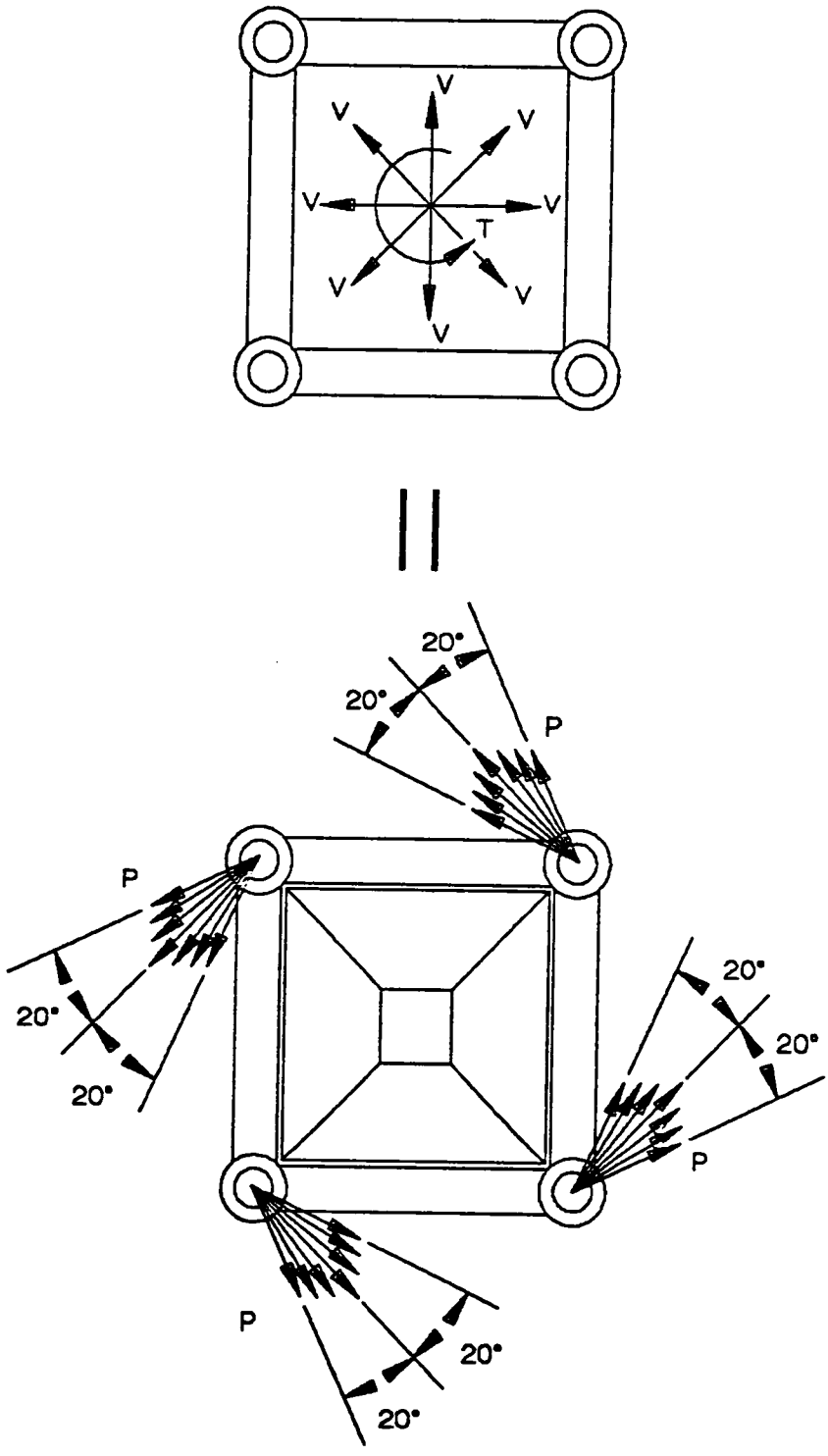

Figure 3. Typical Loading Pattern Analysis

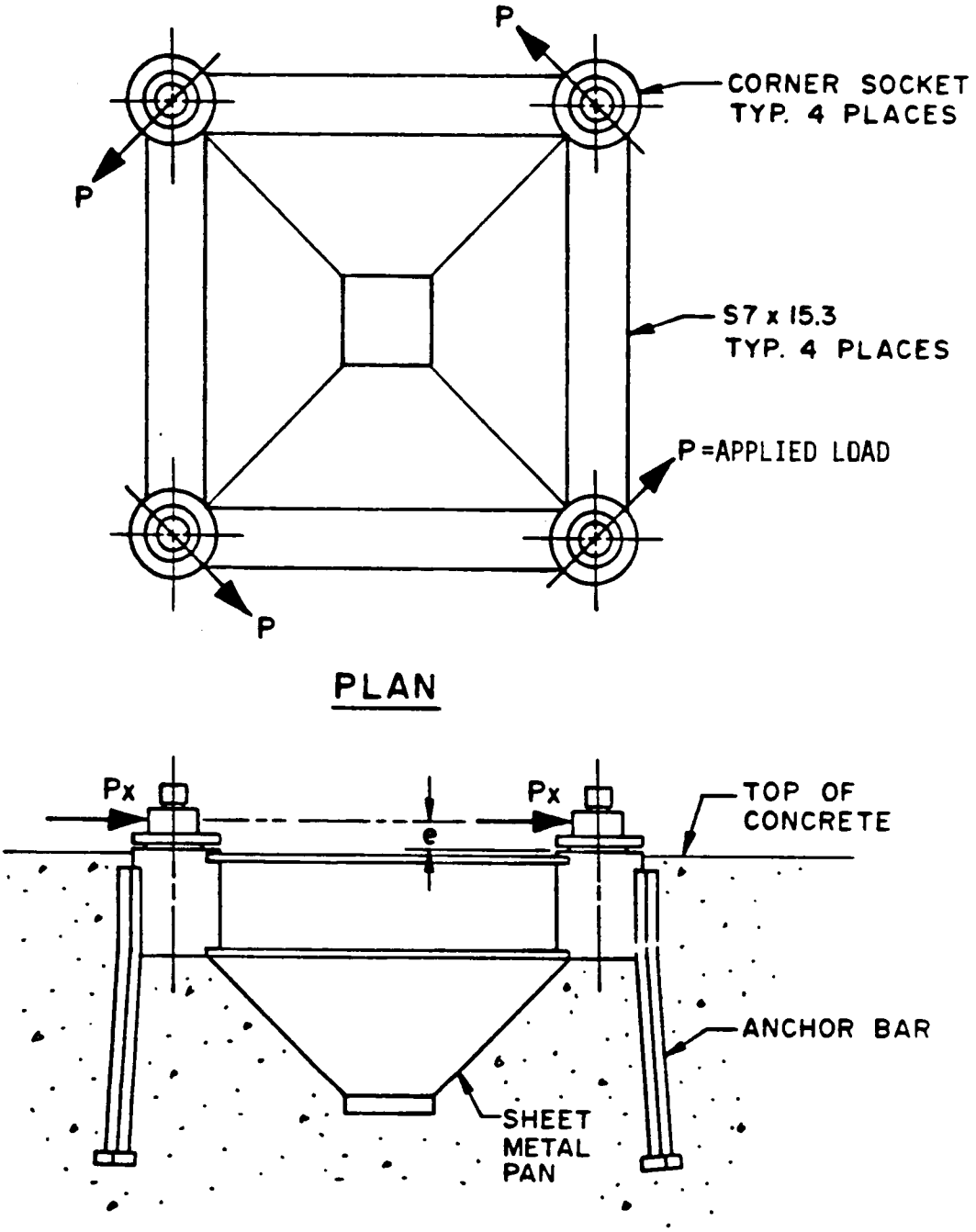

Figure 4. Floor Module Details

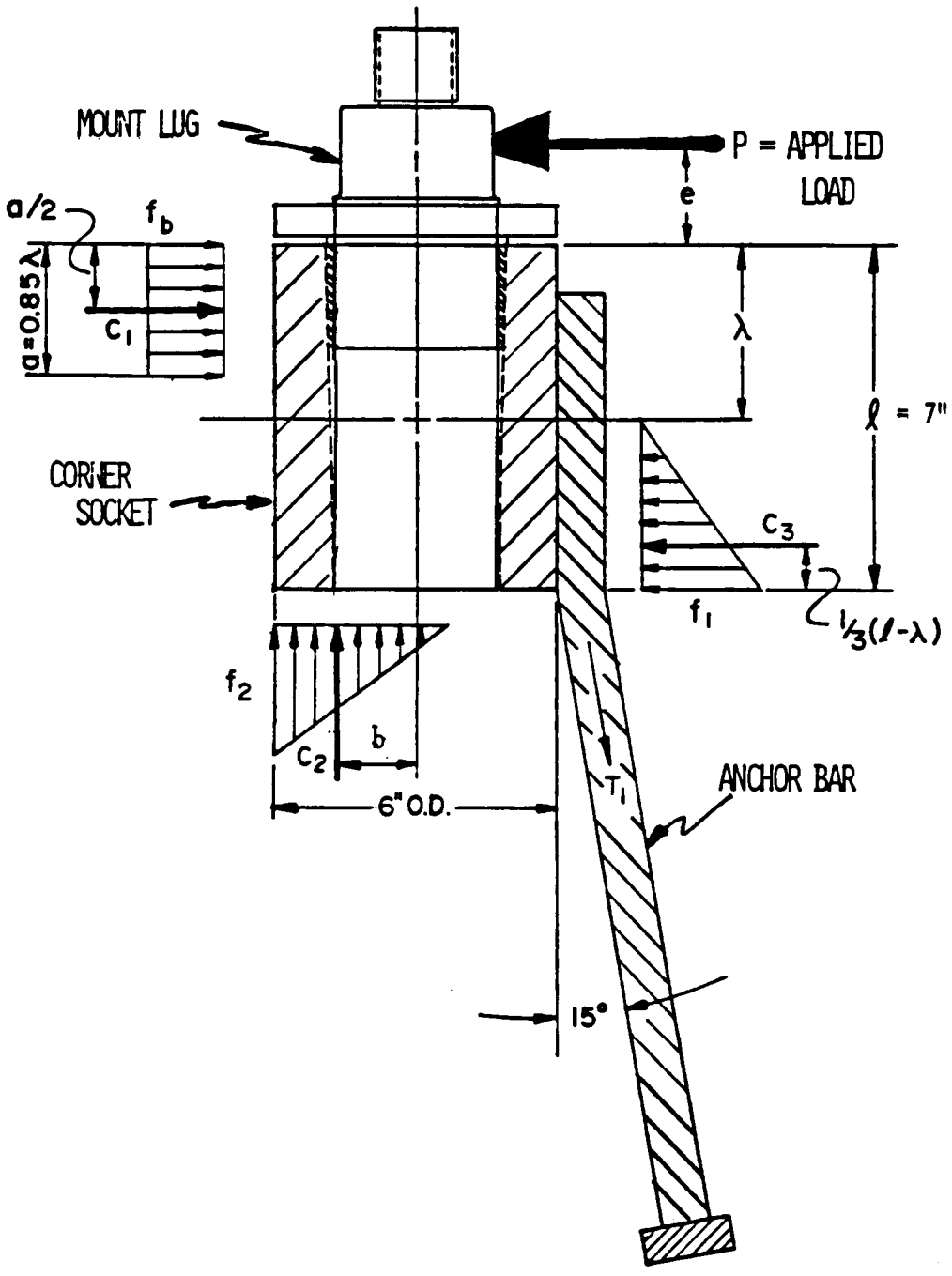

Figure 5. Free Body Diagram of Socket Test

Figure 6. Bushing and Mount Lug Installation

Figure 7. Typical Arrangement for a Socket Test

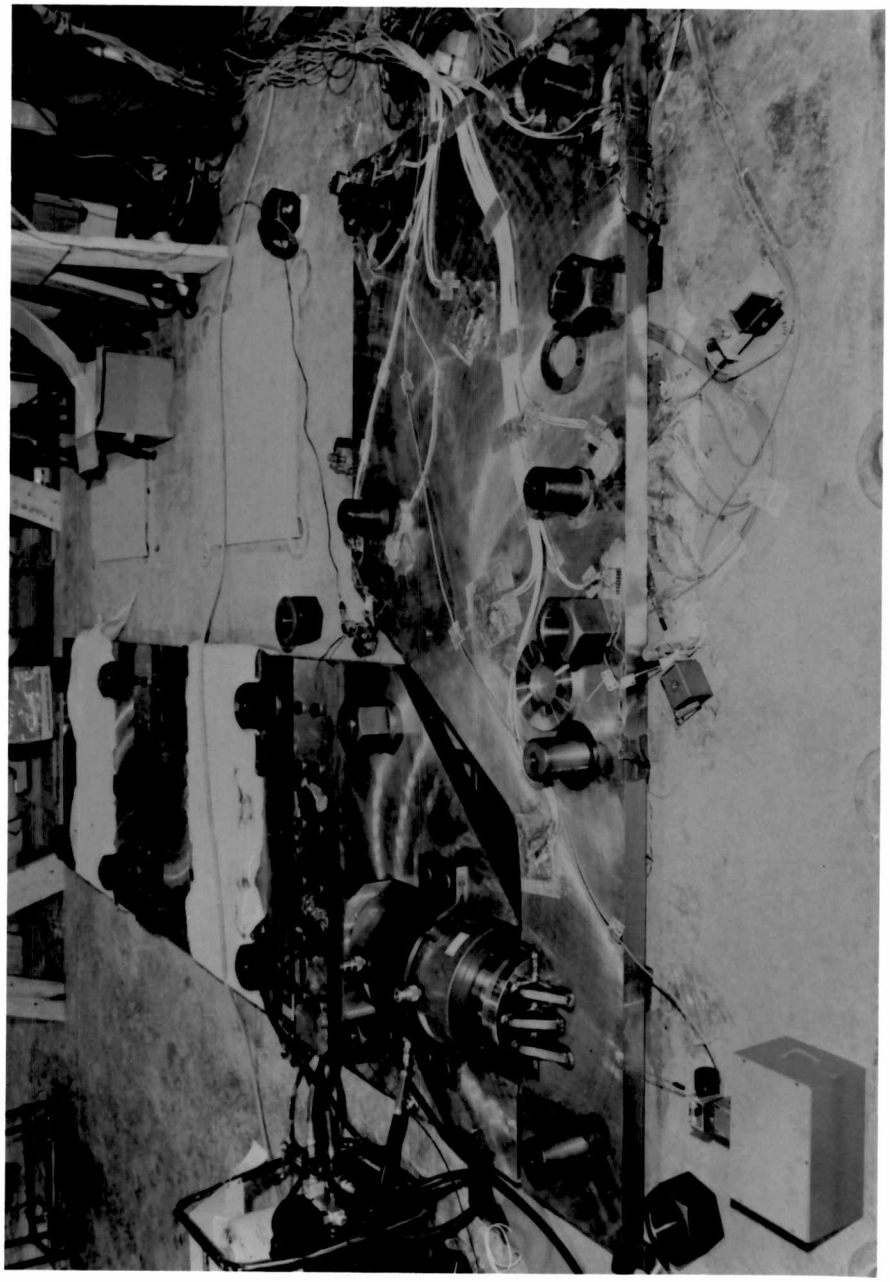

Figure 8. GCEP Full-Scale Floor Module Test Arrangement

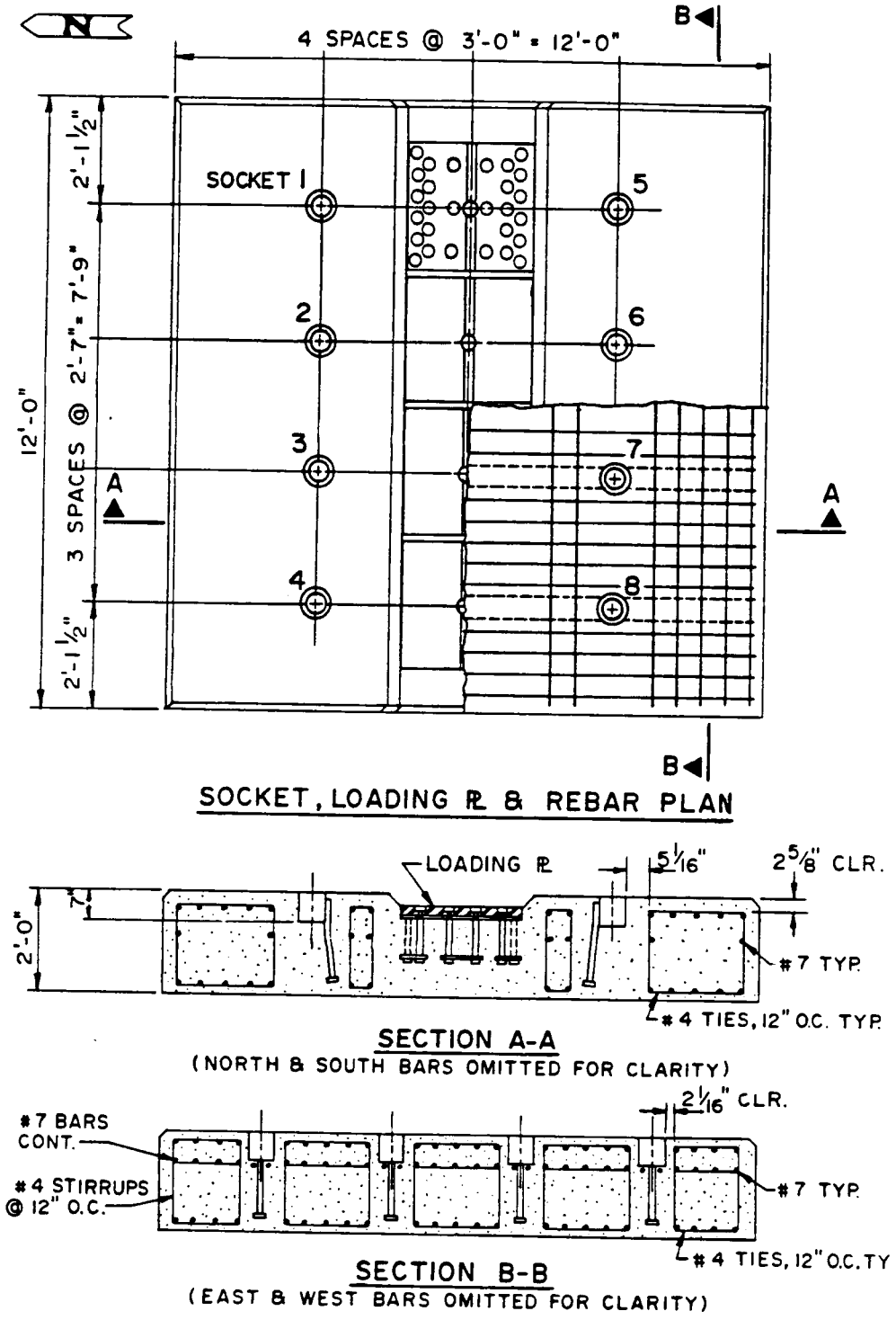

Figure 9. Socket Test Slab Details

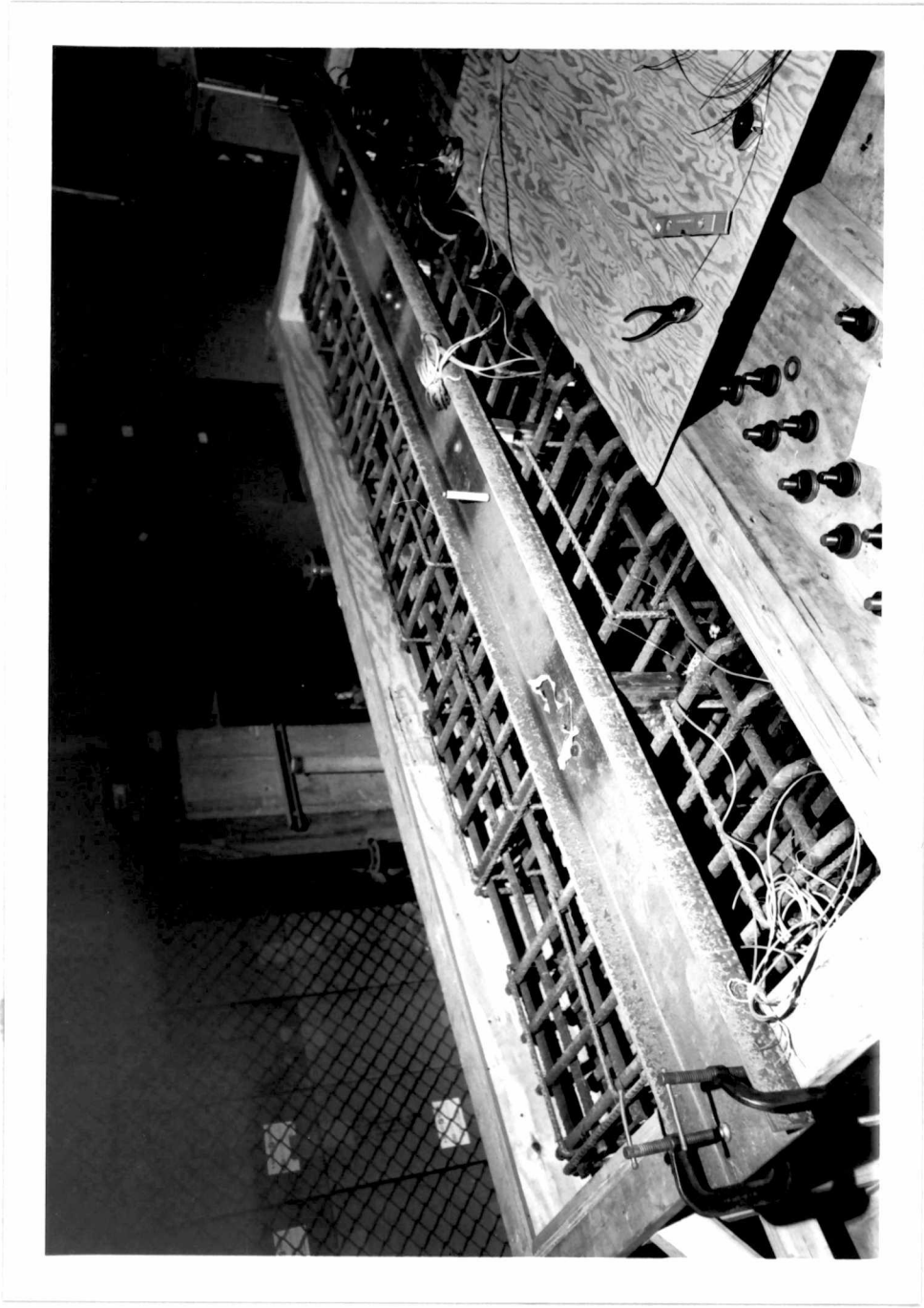

Figure 10. Socket Test Slab During Construction

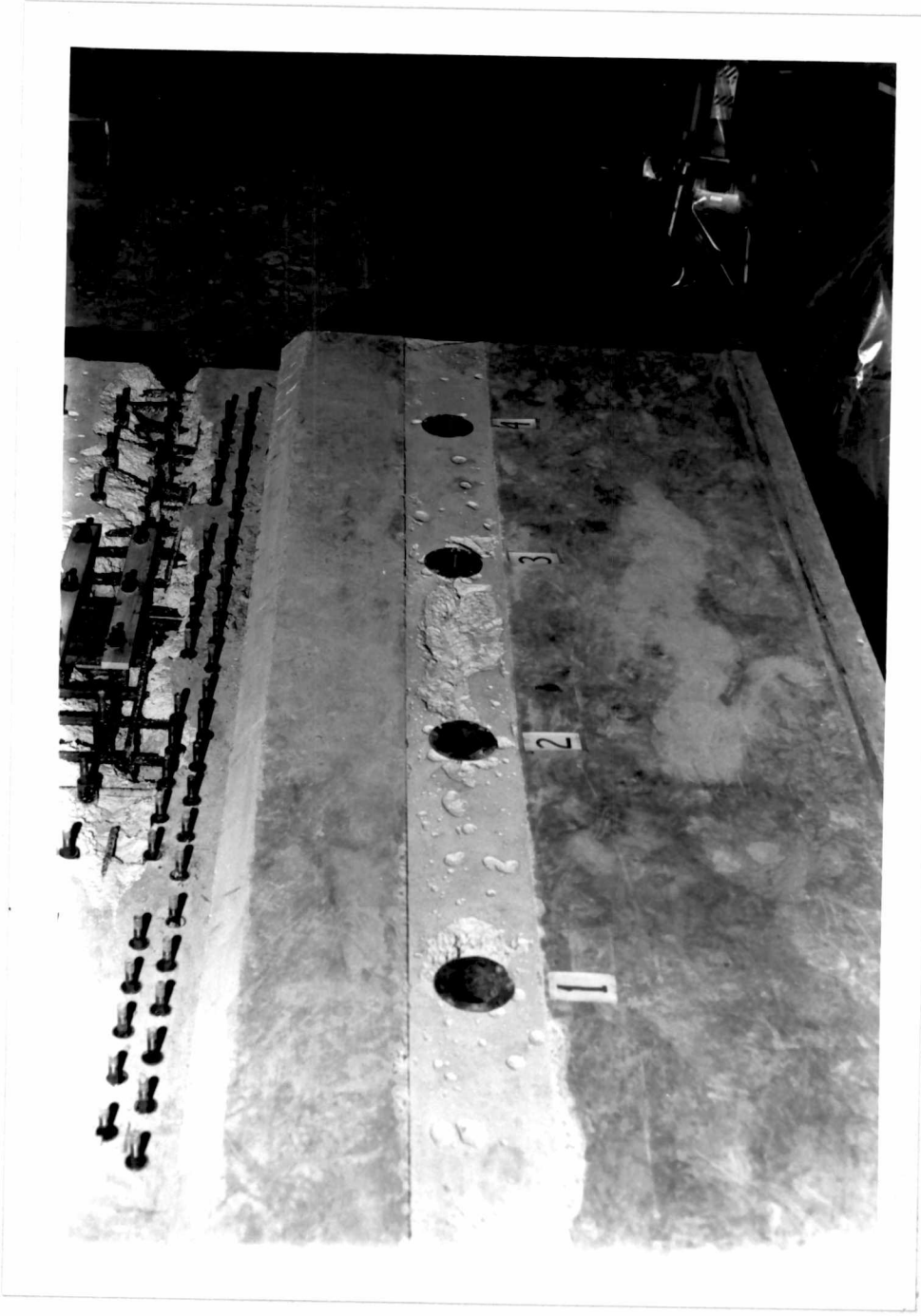

Figure 11. Pocked Area of Test Slab

Figure 12. View of Thrust Bracket Assembly with Hydraulic Rams

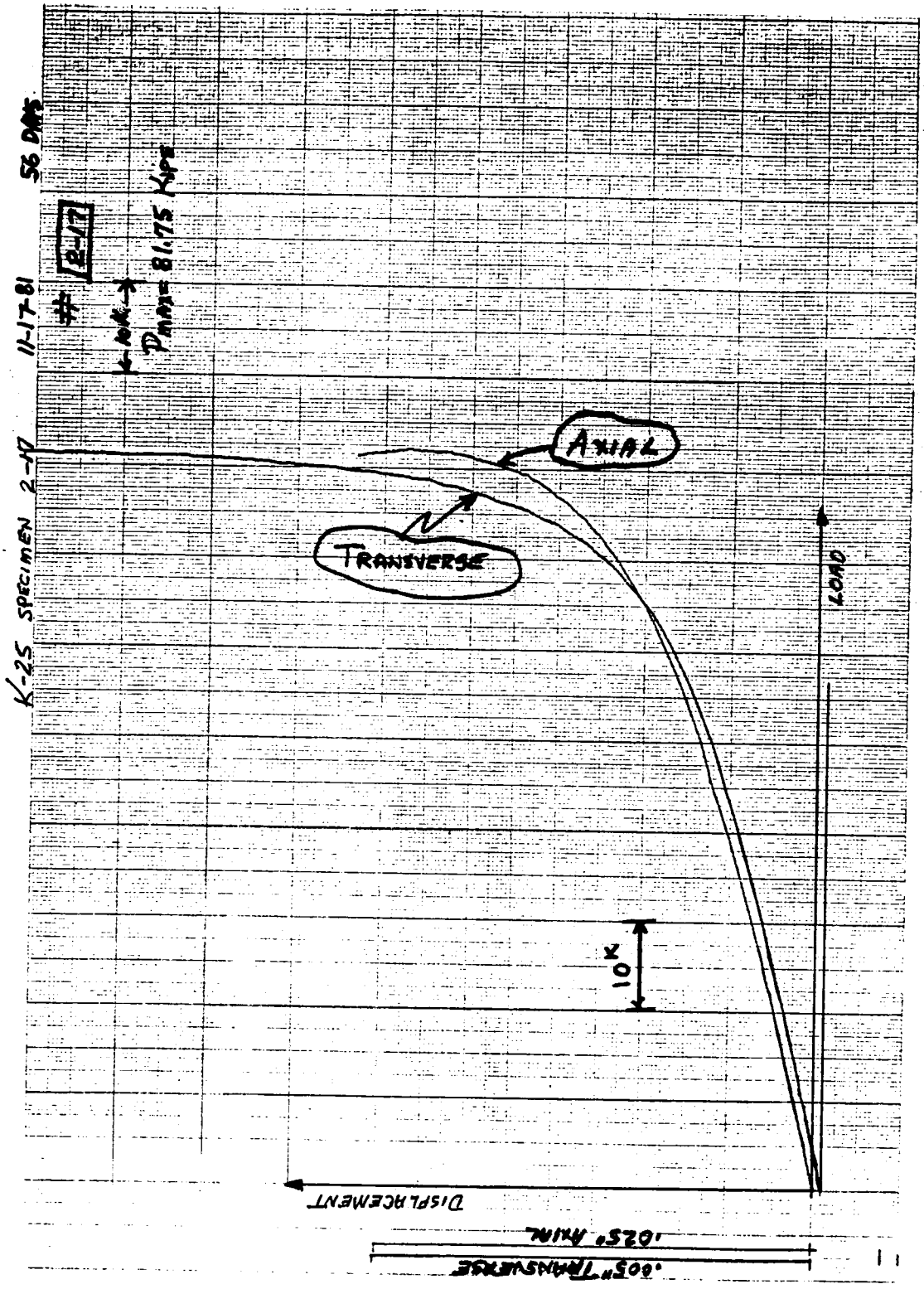

Figure 13. Cylinder Break Test 2-17 Load-Displacement Curves

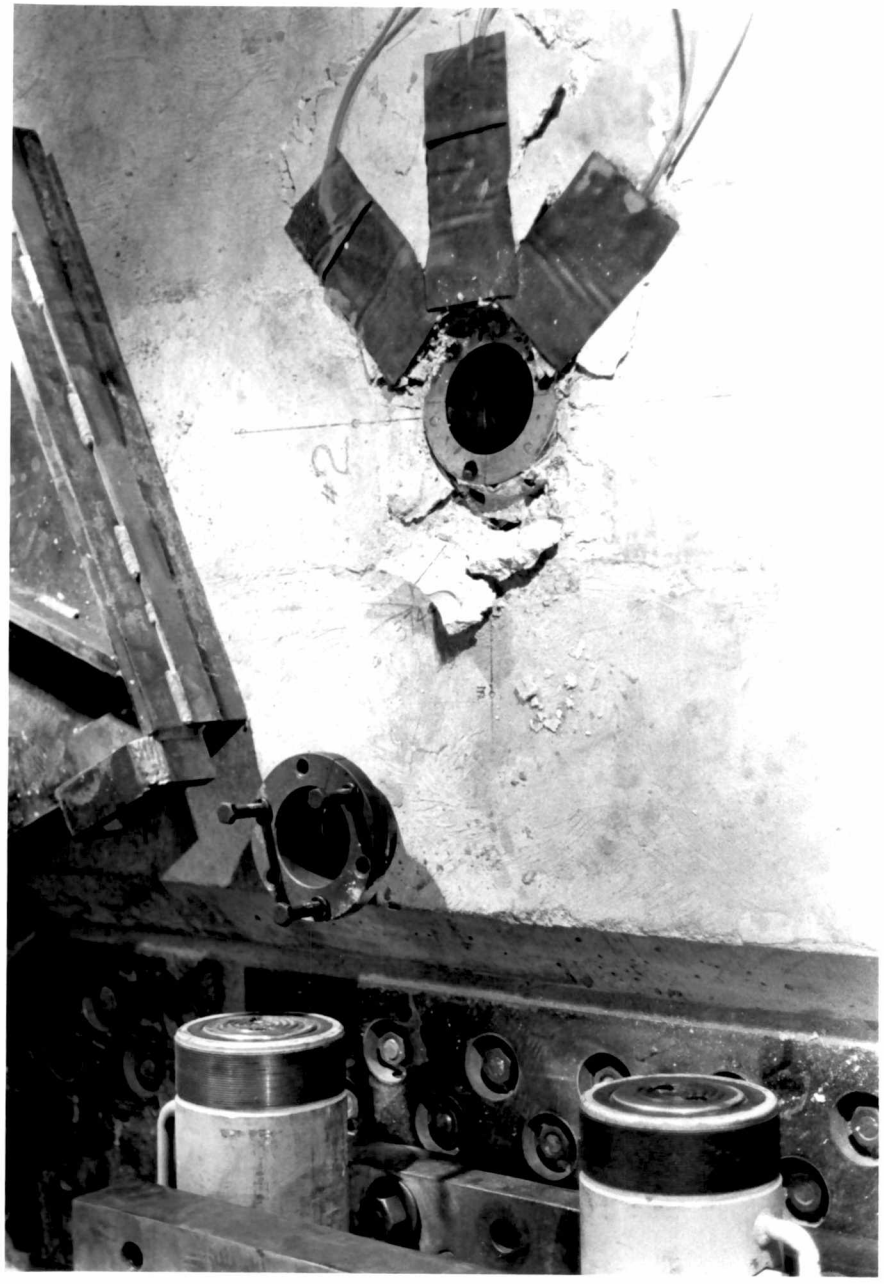

Figure 14. Condition of Concrete After Test No. 2

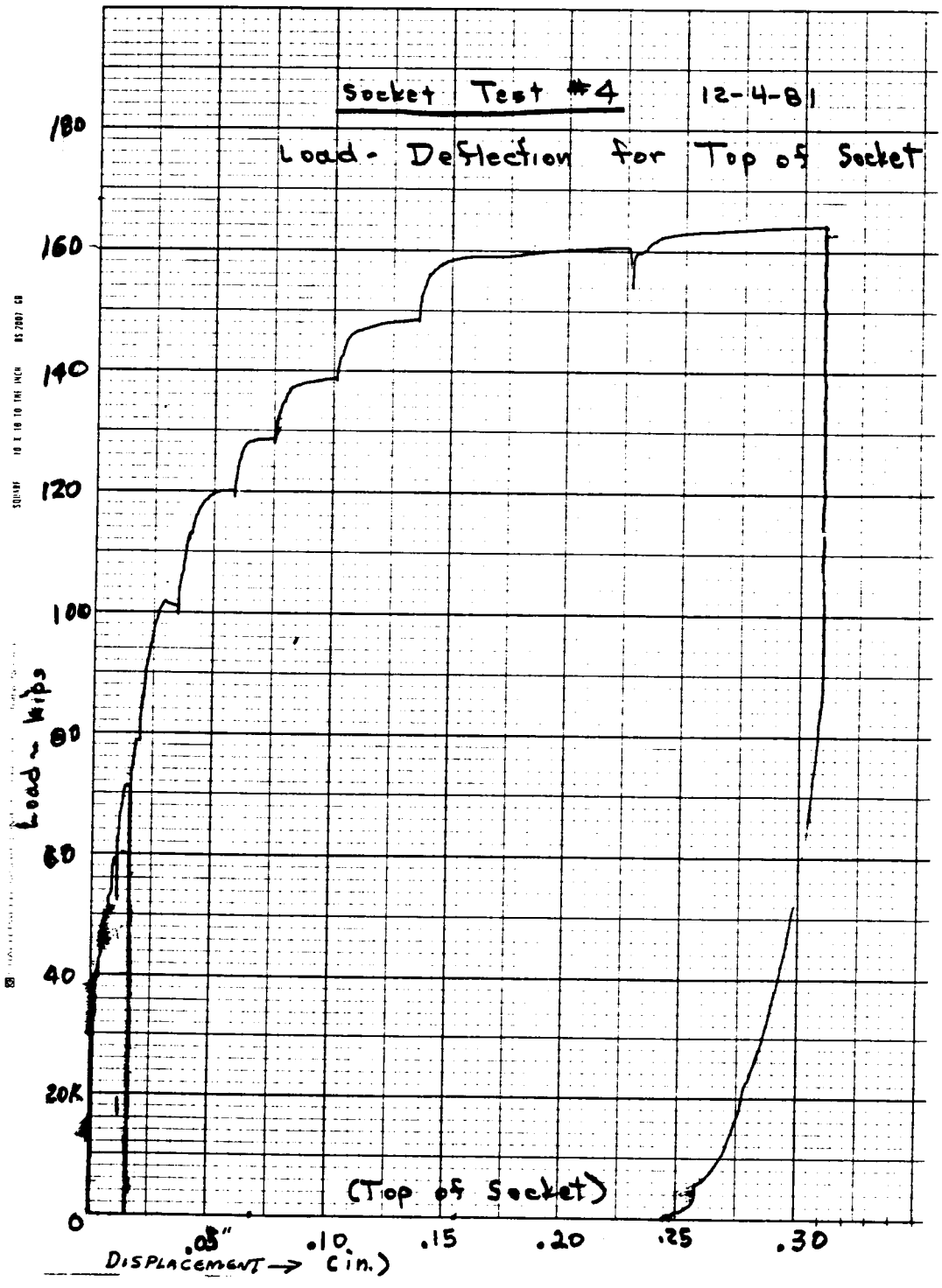

Figure 15. Test No. 4 Load-Displacement Curve at Top-of-Socket

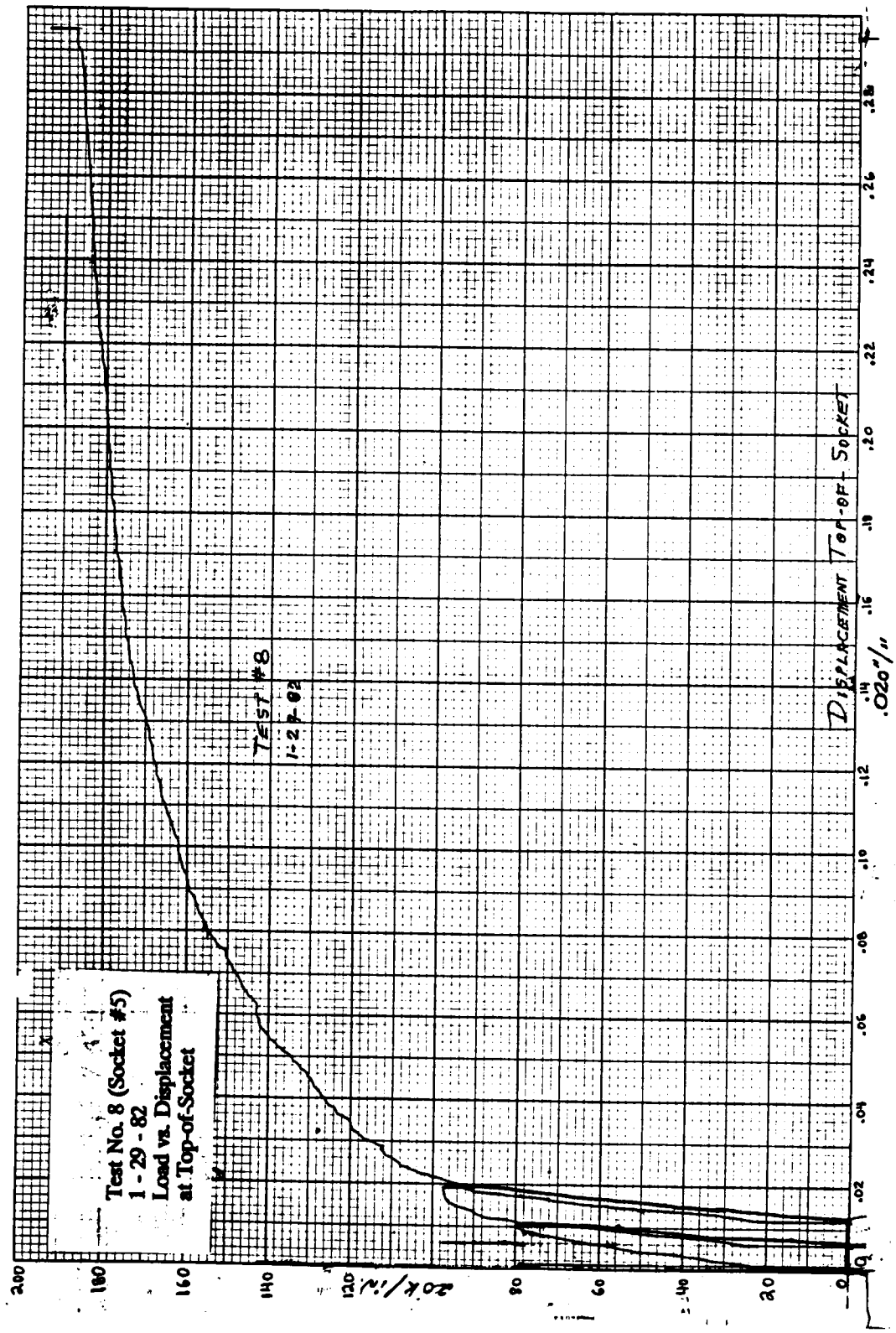

Figure 16. Test No. 8 Load-Displacement Curve at Top-of-Socket

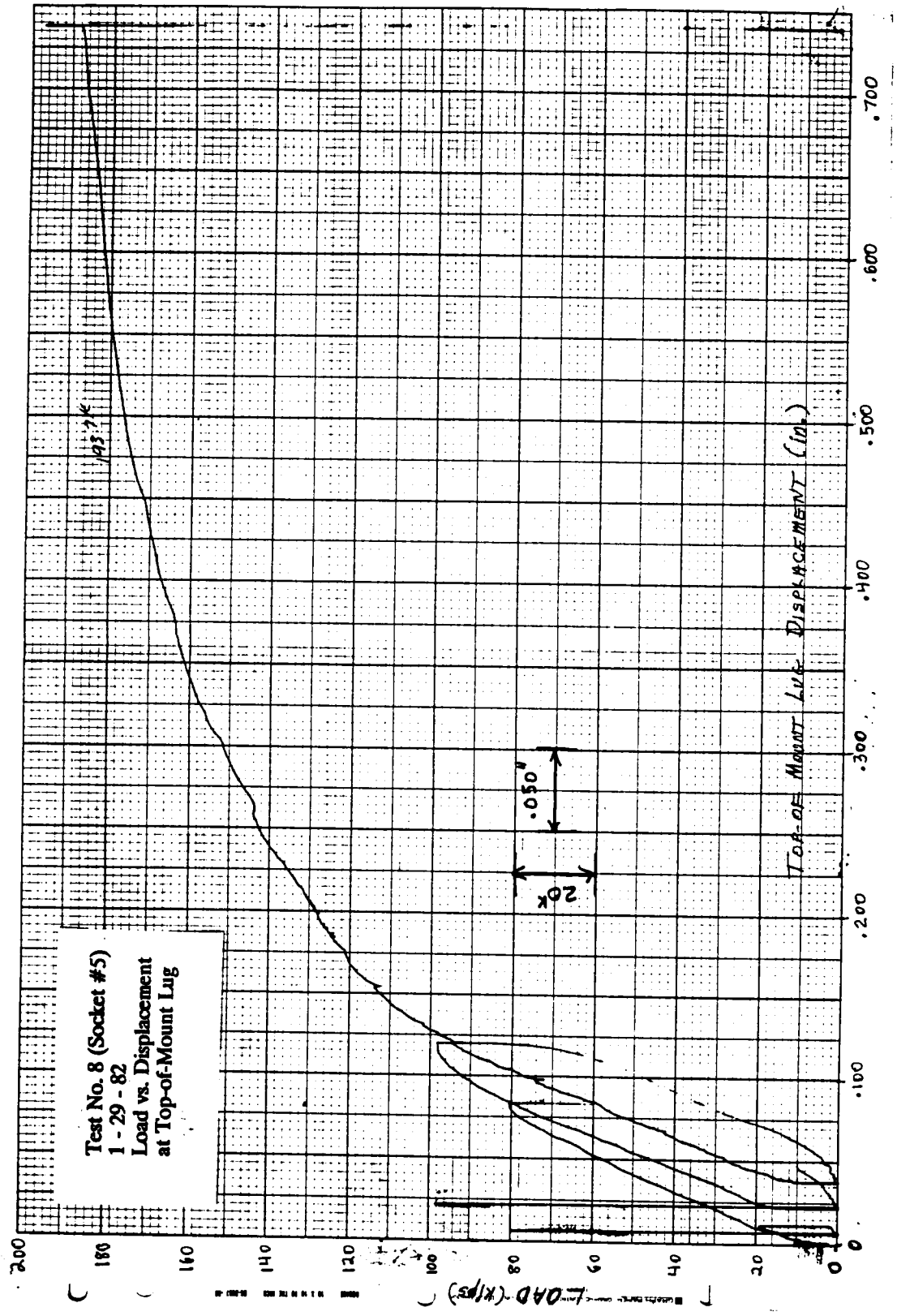

Figure 17. Test No. 8 Load-Displacement Curve at Top-of-Mount Lug

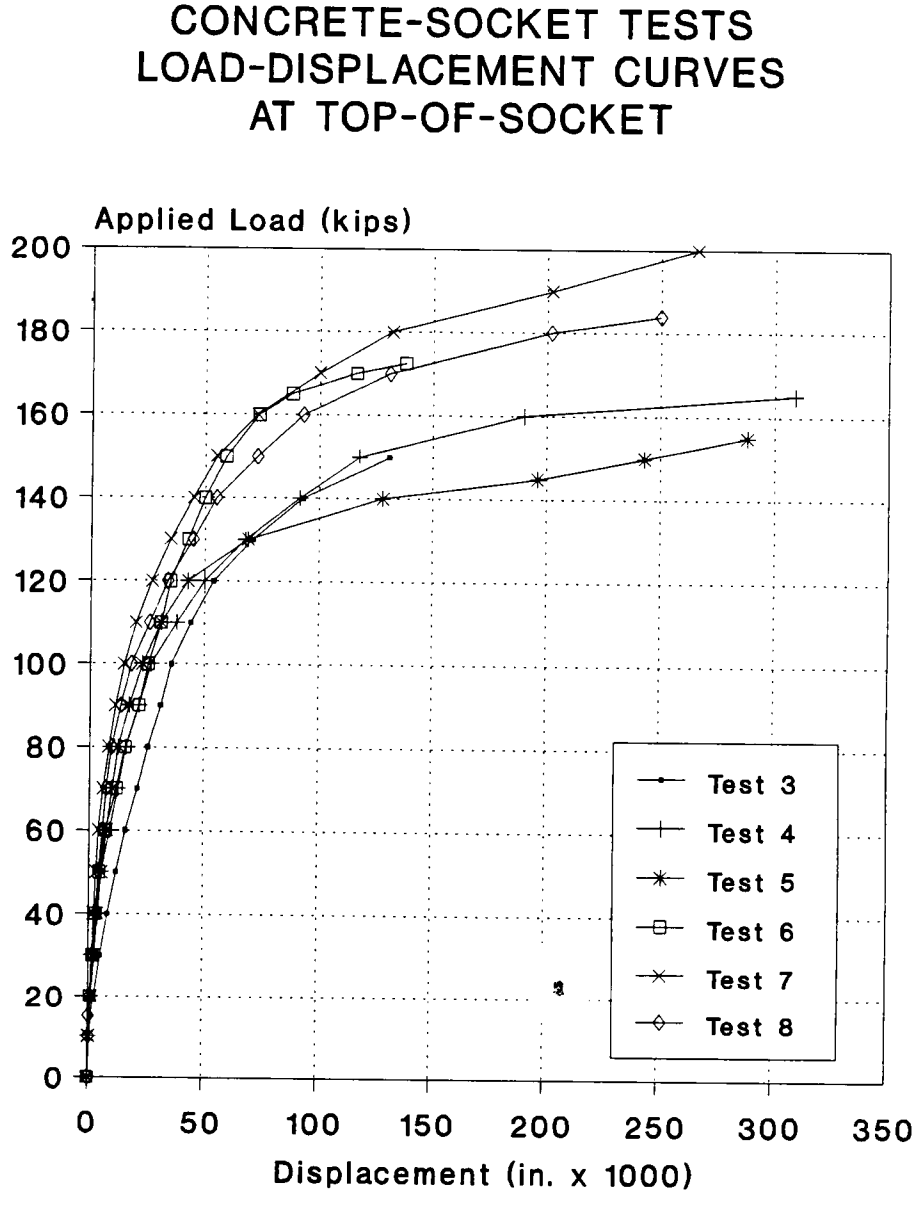

Figure 18. Load-Displacement Curves for Socket Tests

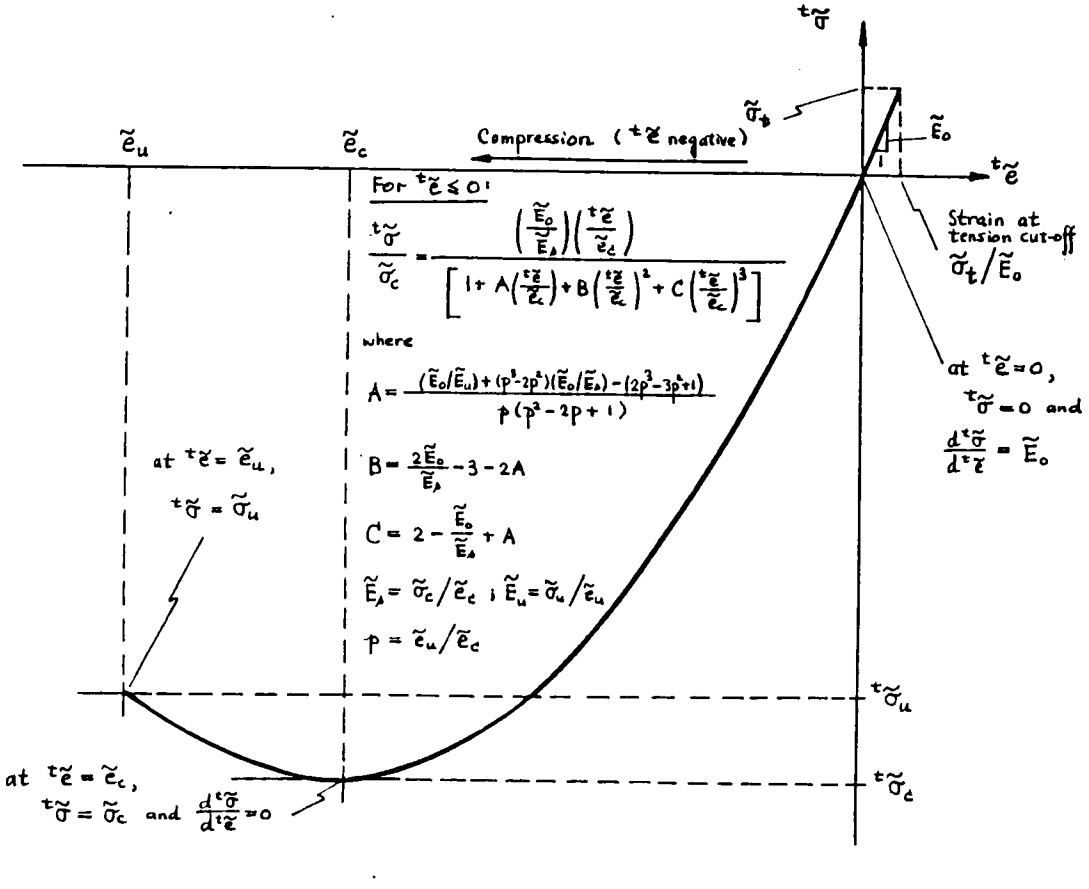

Figure 19. ADINA Uniaxial Stress-Strain Curve in Concrete Model

Taken from ADINA: System Theory and Modeling Guide, with permission from ADINA R & D, Watertown, MA.

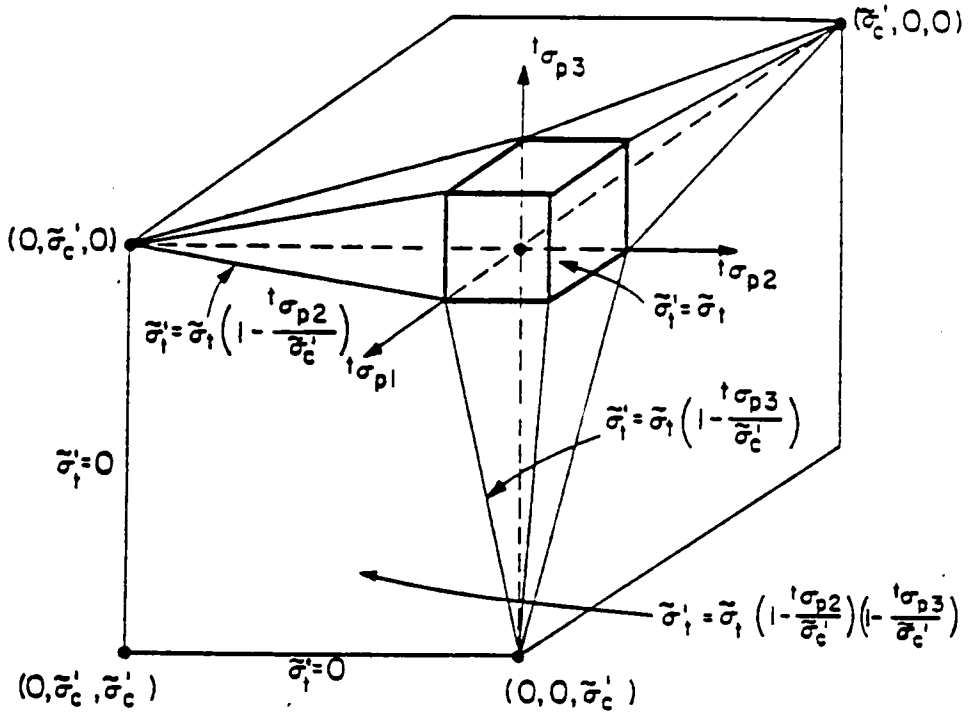

Figure 20. ADINA-84 Three-Dimensional Tensile Failure Envelope

Taken from ADINA: System Theory and Modeling Guide, with permission from ADINA R & D, Watertown, MA.

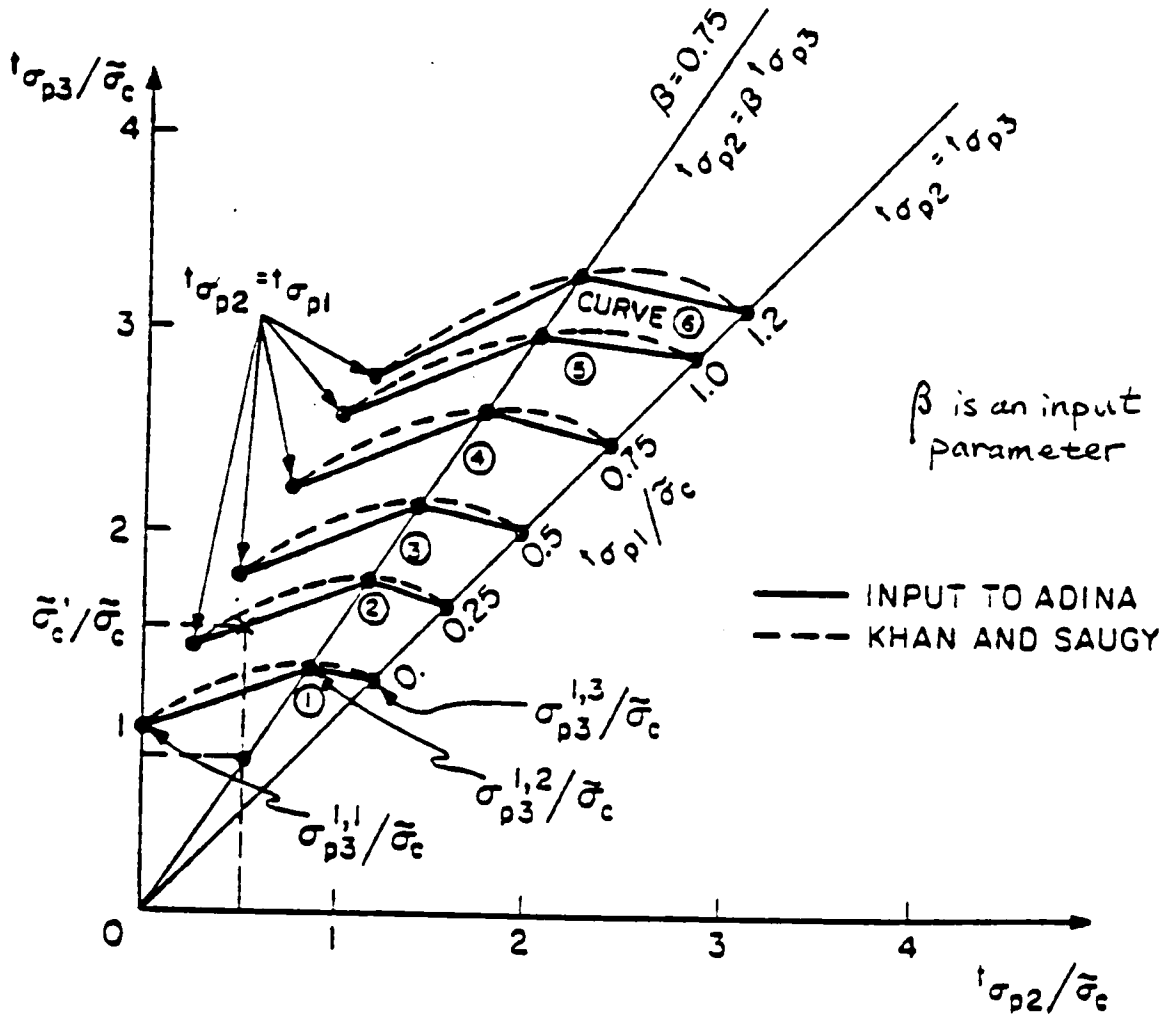

Figure 21. ADINA Triaxial Compressive Failure Envelope

Taken from ADINA: System Theory and Modeling Guide, with permission from ADINA R & D, Watertown, MA.

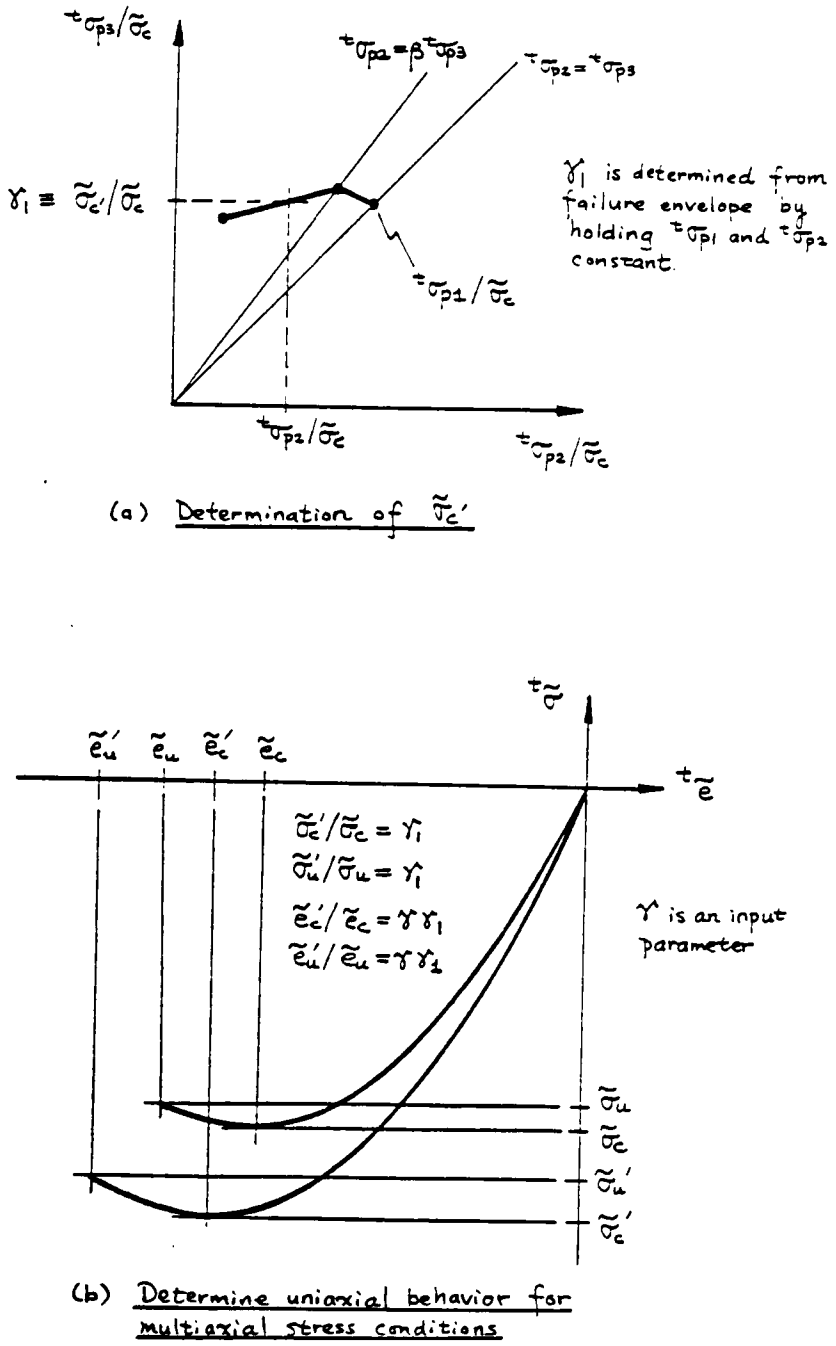

Figure 22. ADINA Uniaxial Stress-Strain Curve Modified for Multiaxial Stress Conditions

Taken from ADINA: System Theory and Modeling Guide, with permission from ADINA R & D, Watertown, MA.

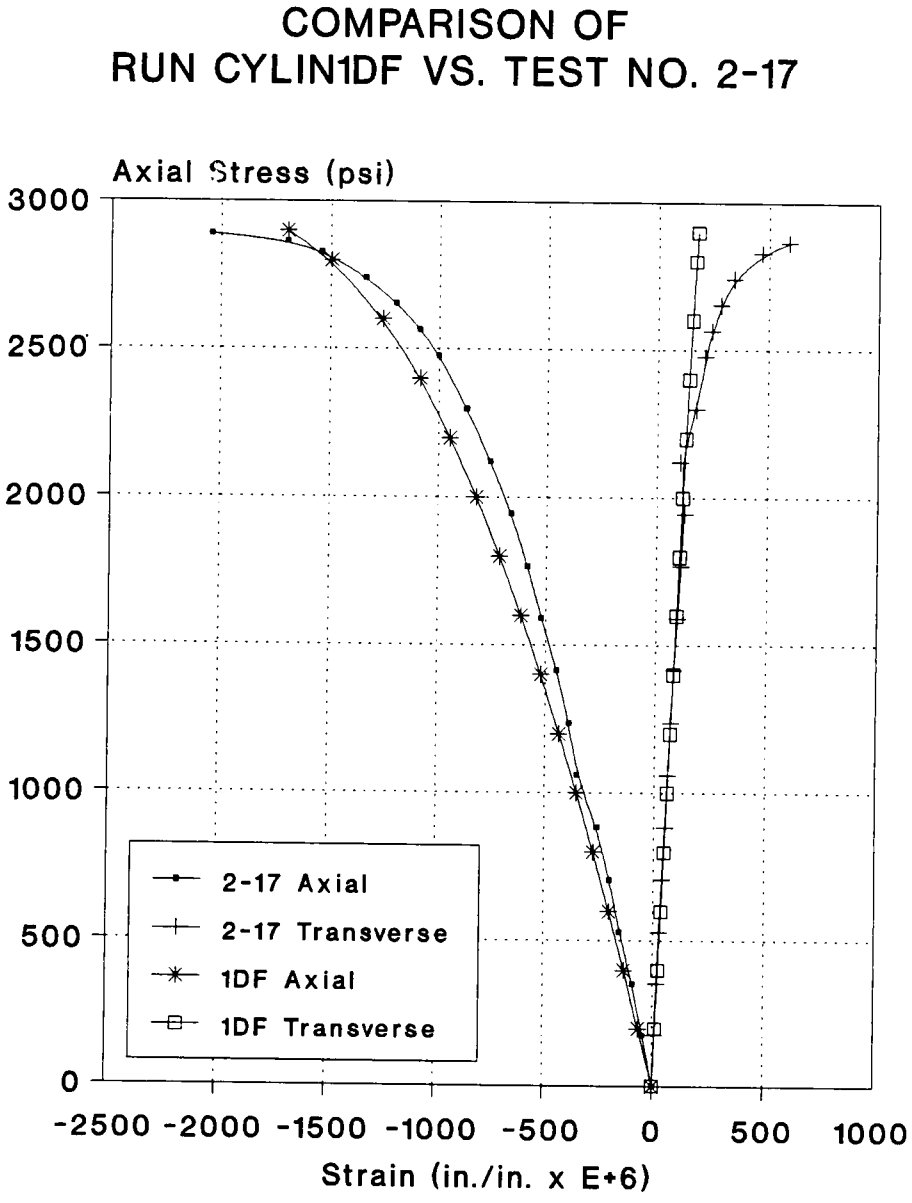

Figure 23. Comparison of ADINA Concrete Cylinder Model Results vs. Cylinder Test No. 2-17

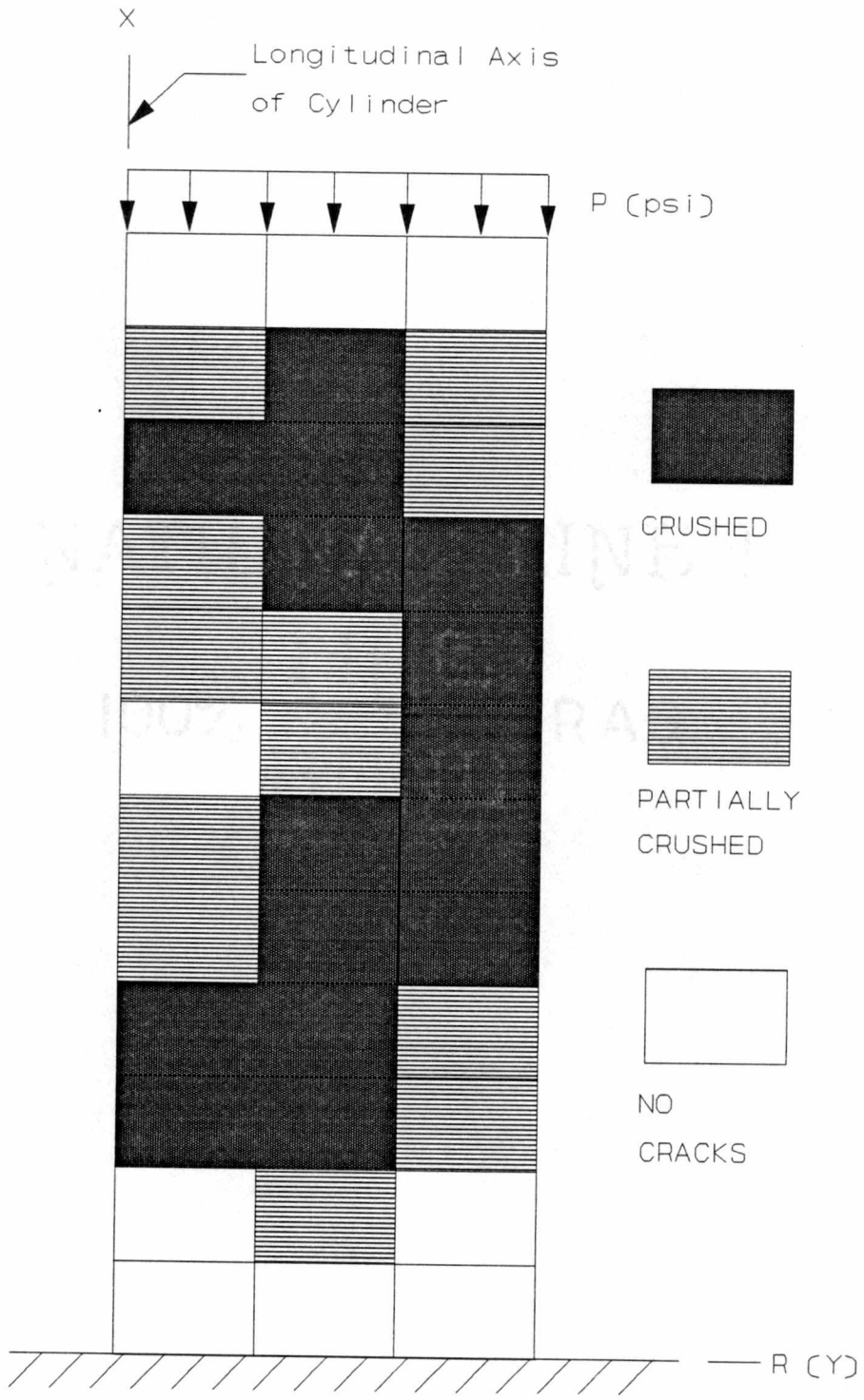

Figure 24. Cracking and Crushing Pattern for Run CYLIN2DR.

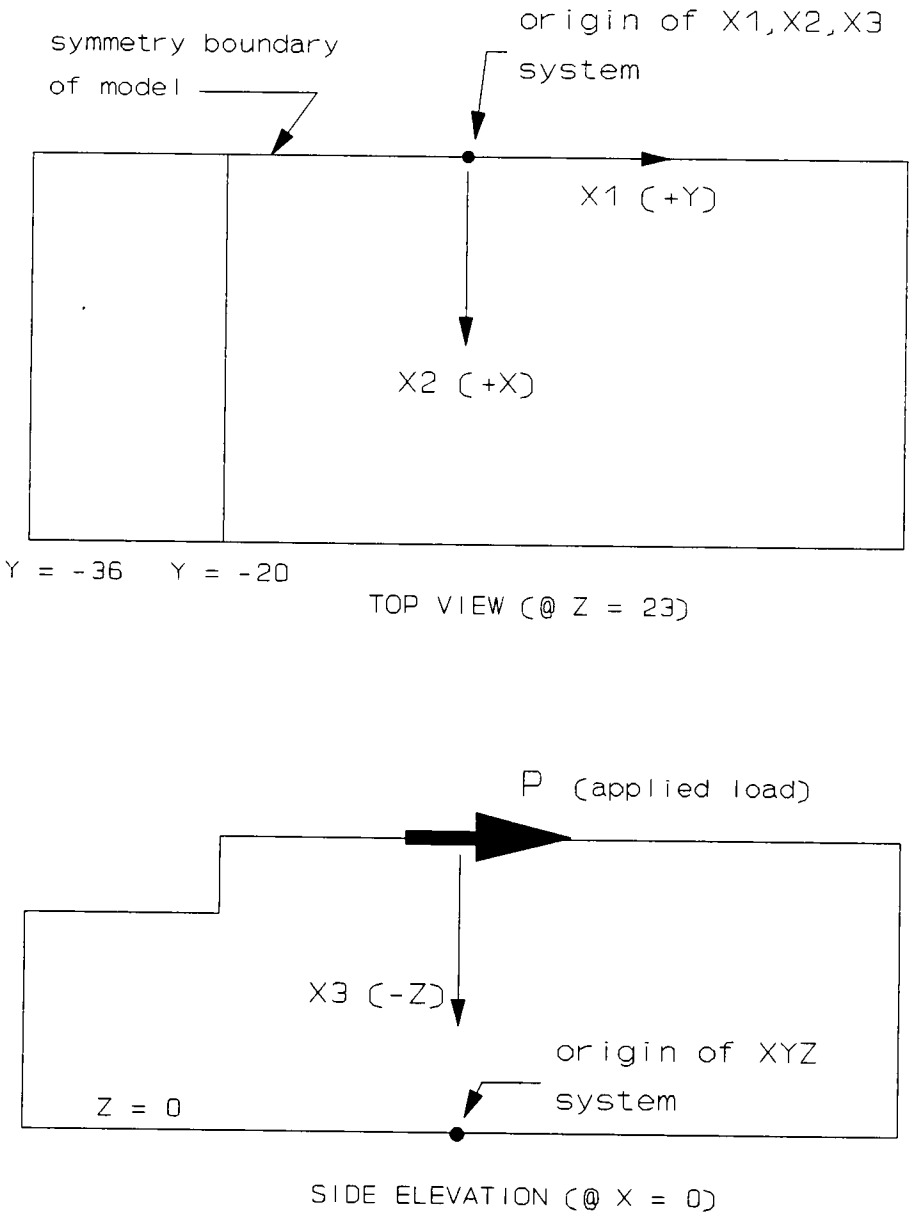

Figure 25. Model Used for Cerruti's Problem

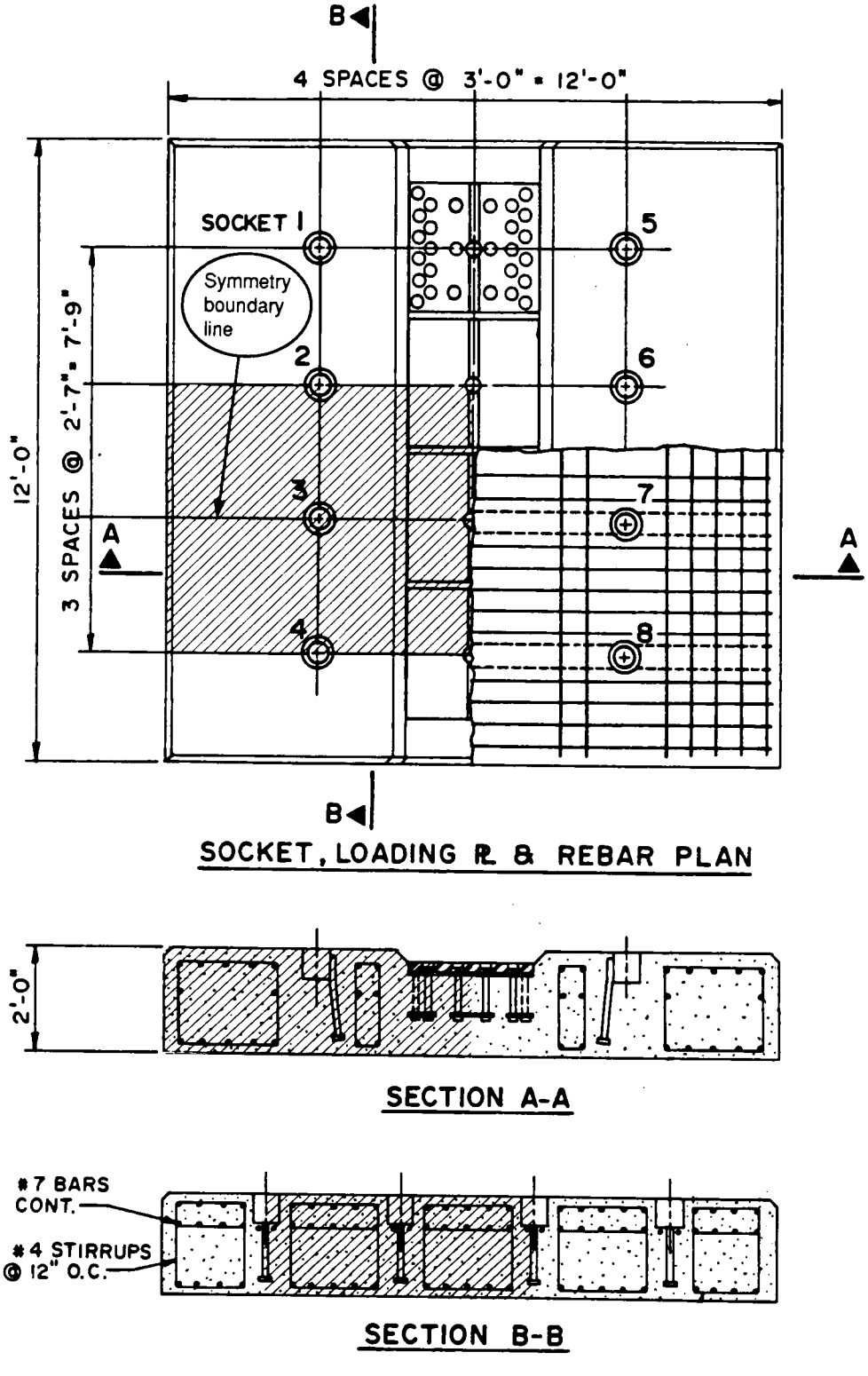

Figure 26. Portion of Socket Test in Finite Element Model

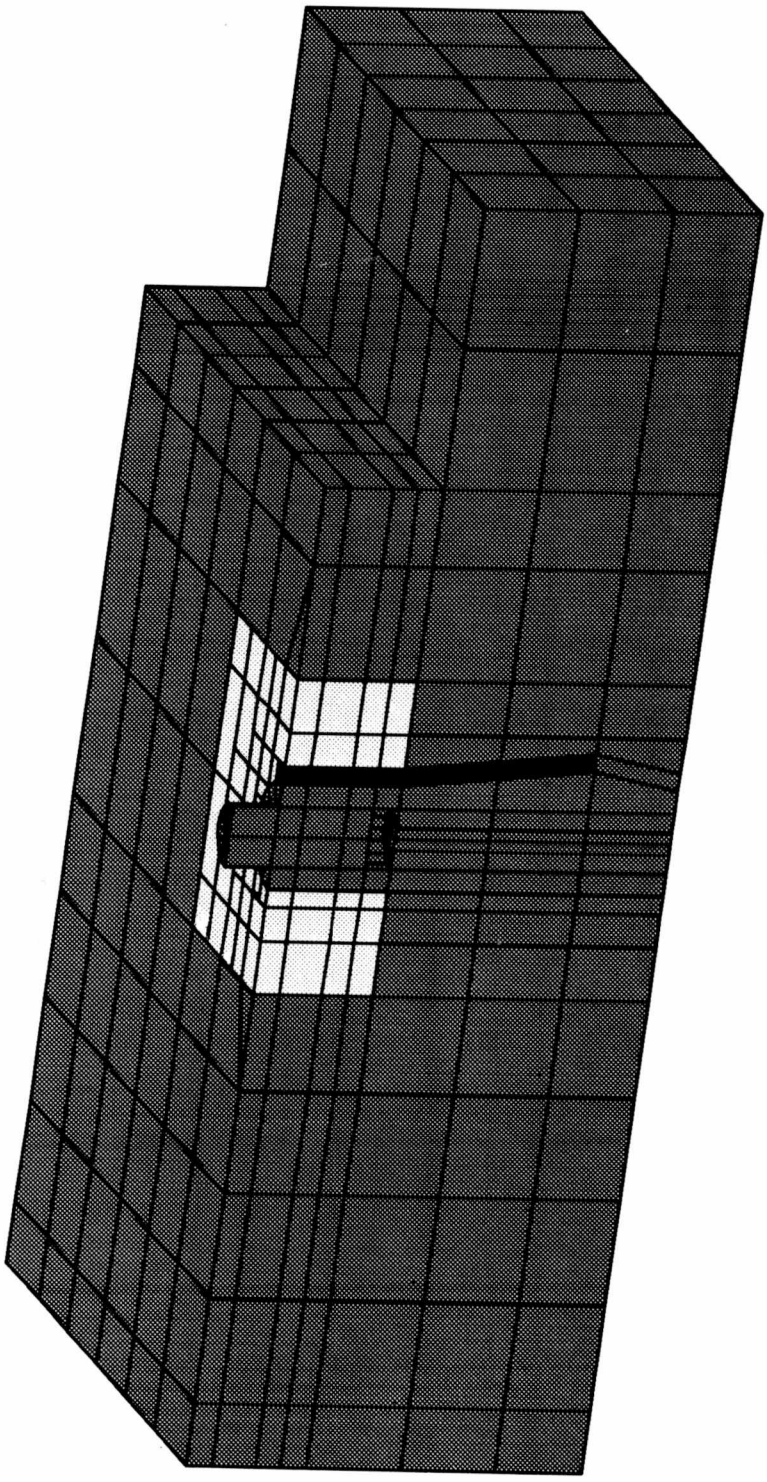

Figure 27. View of Model

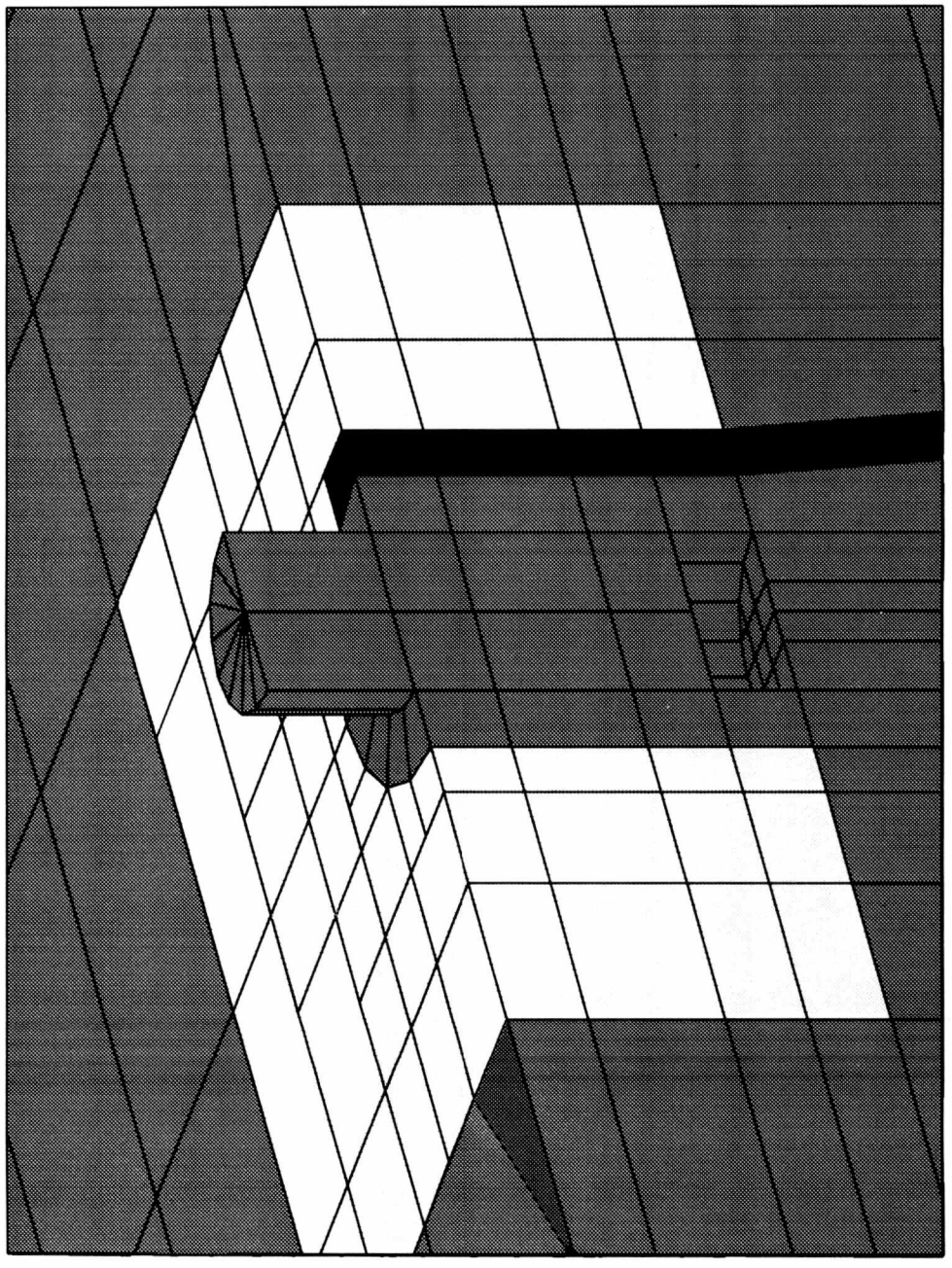

Figure 28. View of Socket Area of Model

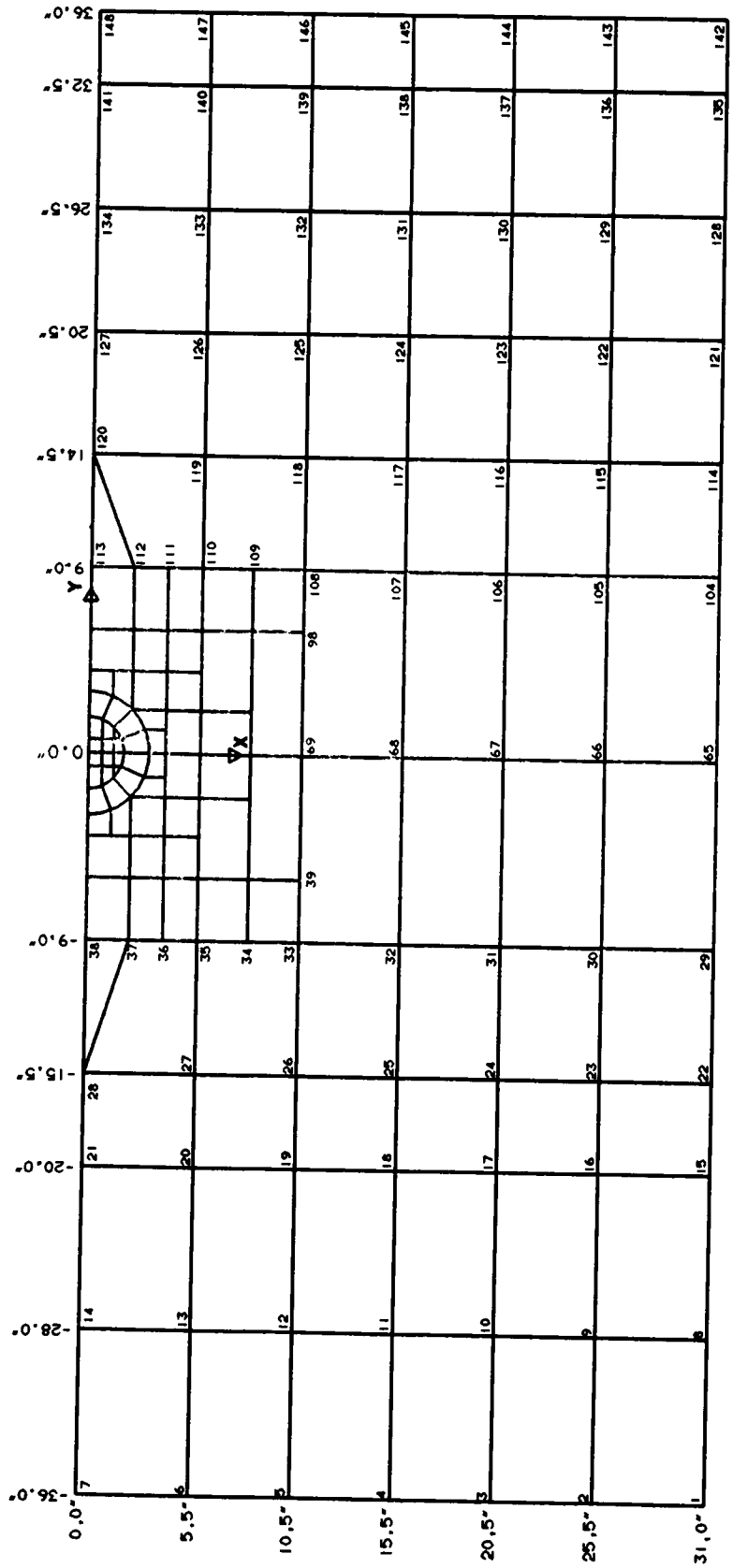

Figure 29. Plan of Model at Layer Z = 0.0

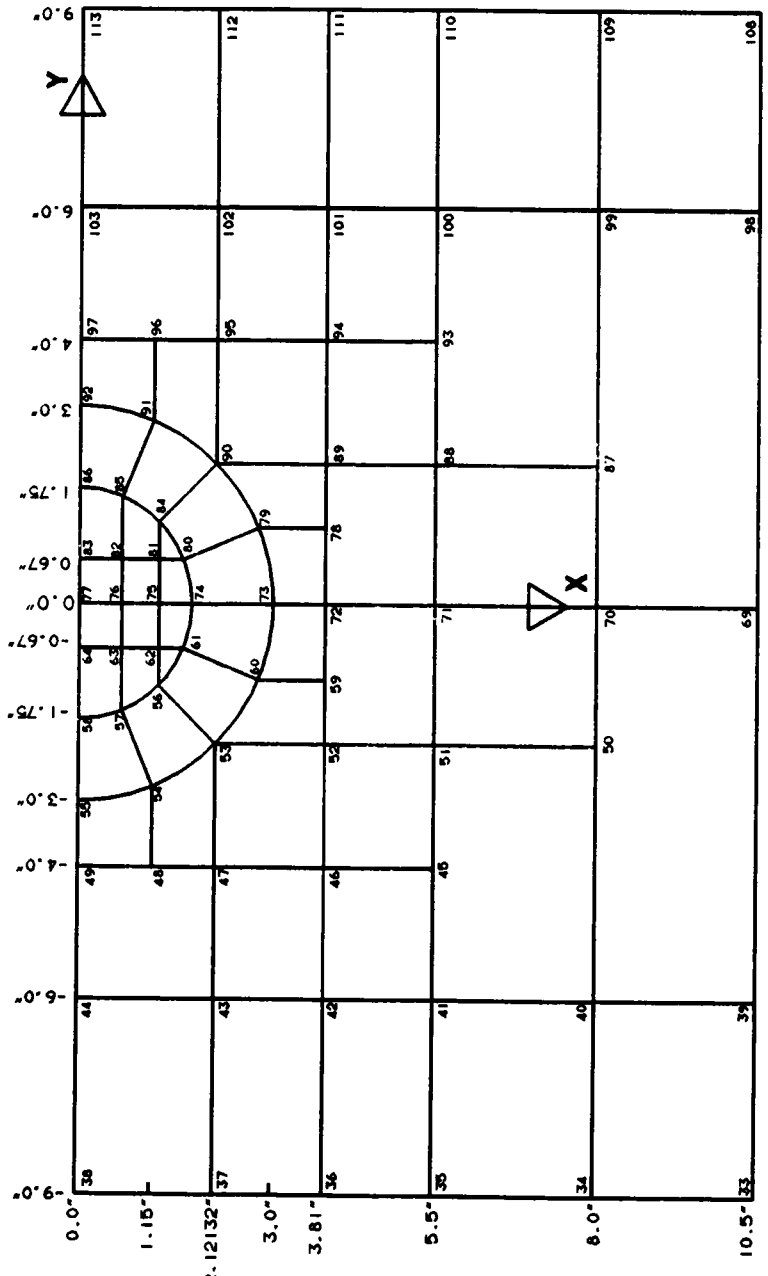

Figure 30. Plan of Model Socket Area at Layer Z = 0.0

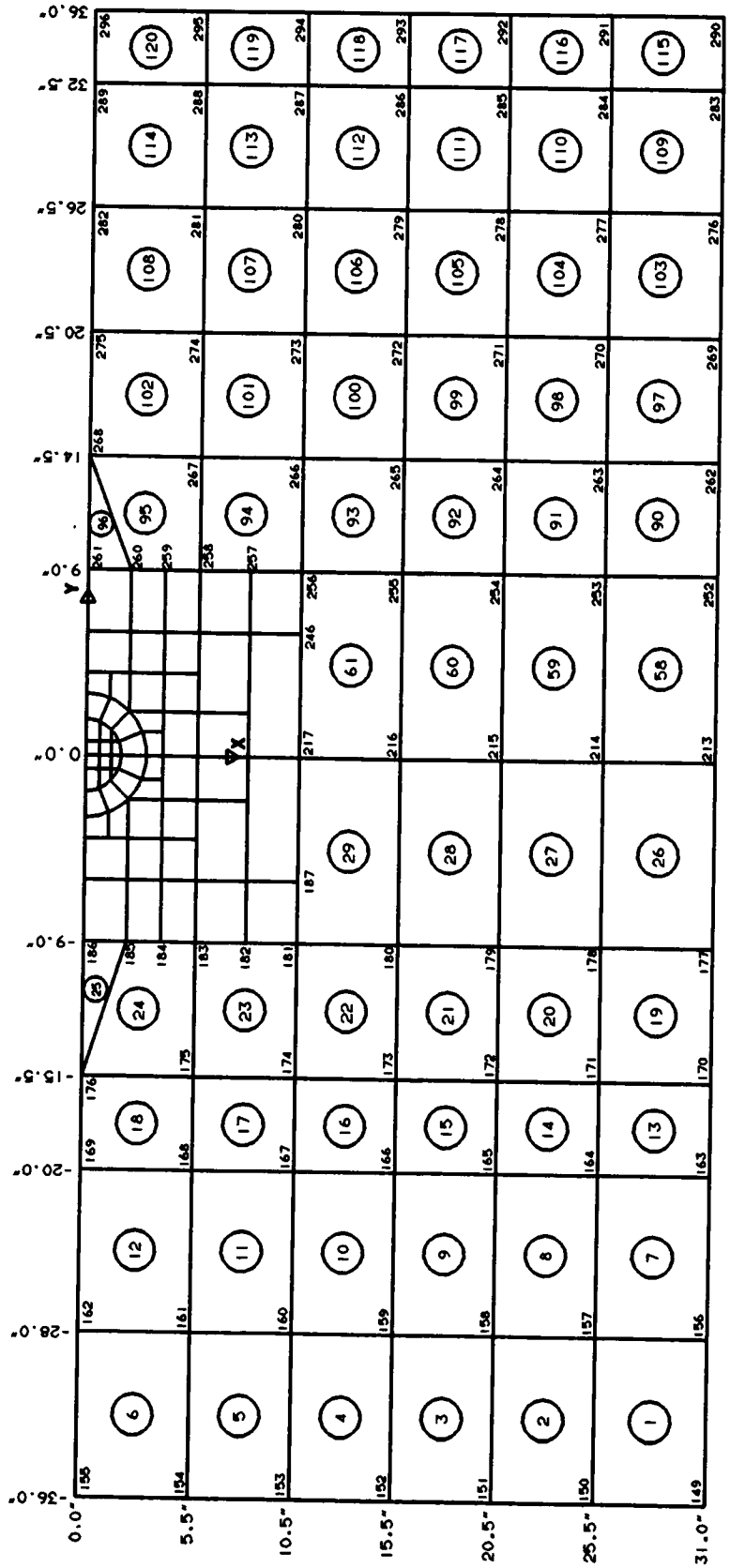

Figure 31. Plan of Model at Layer Z = 5.0

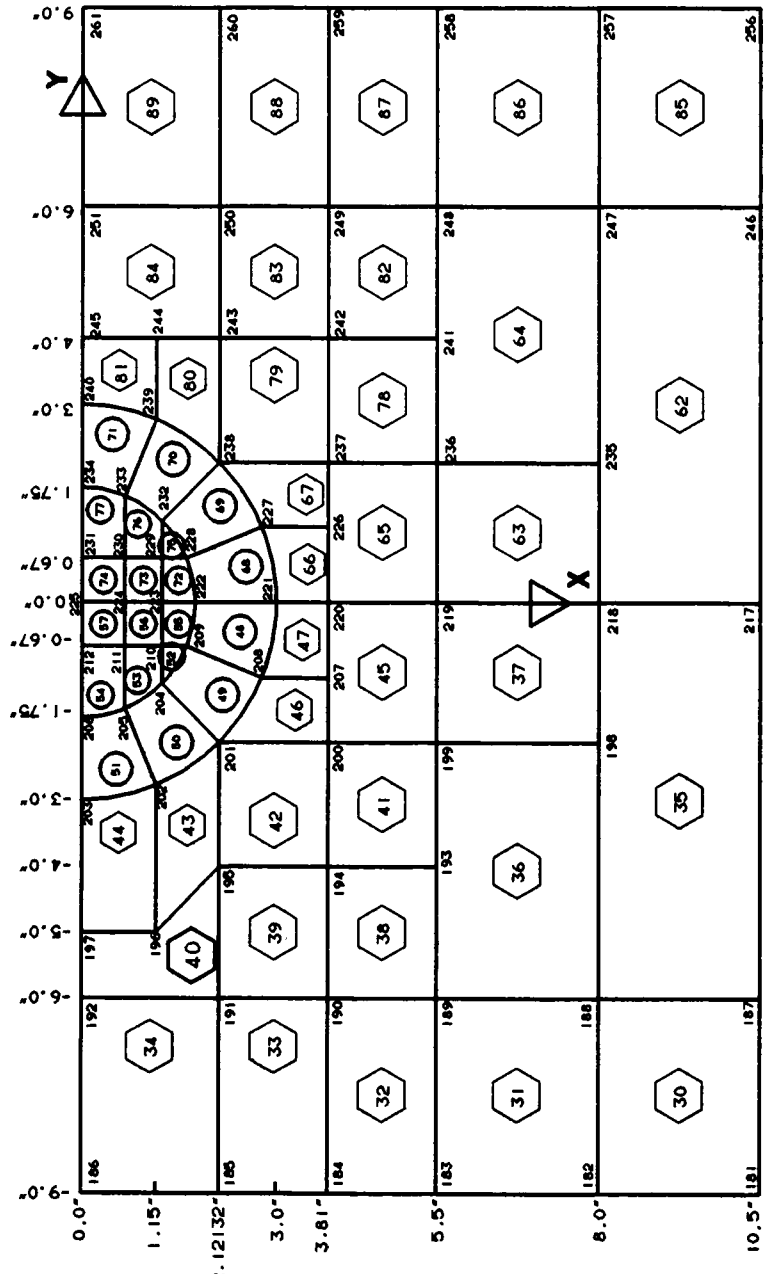

Figure 32. Plan of Model Socket Area at Layer Z = 5.0

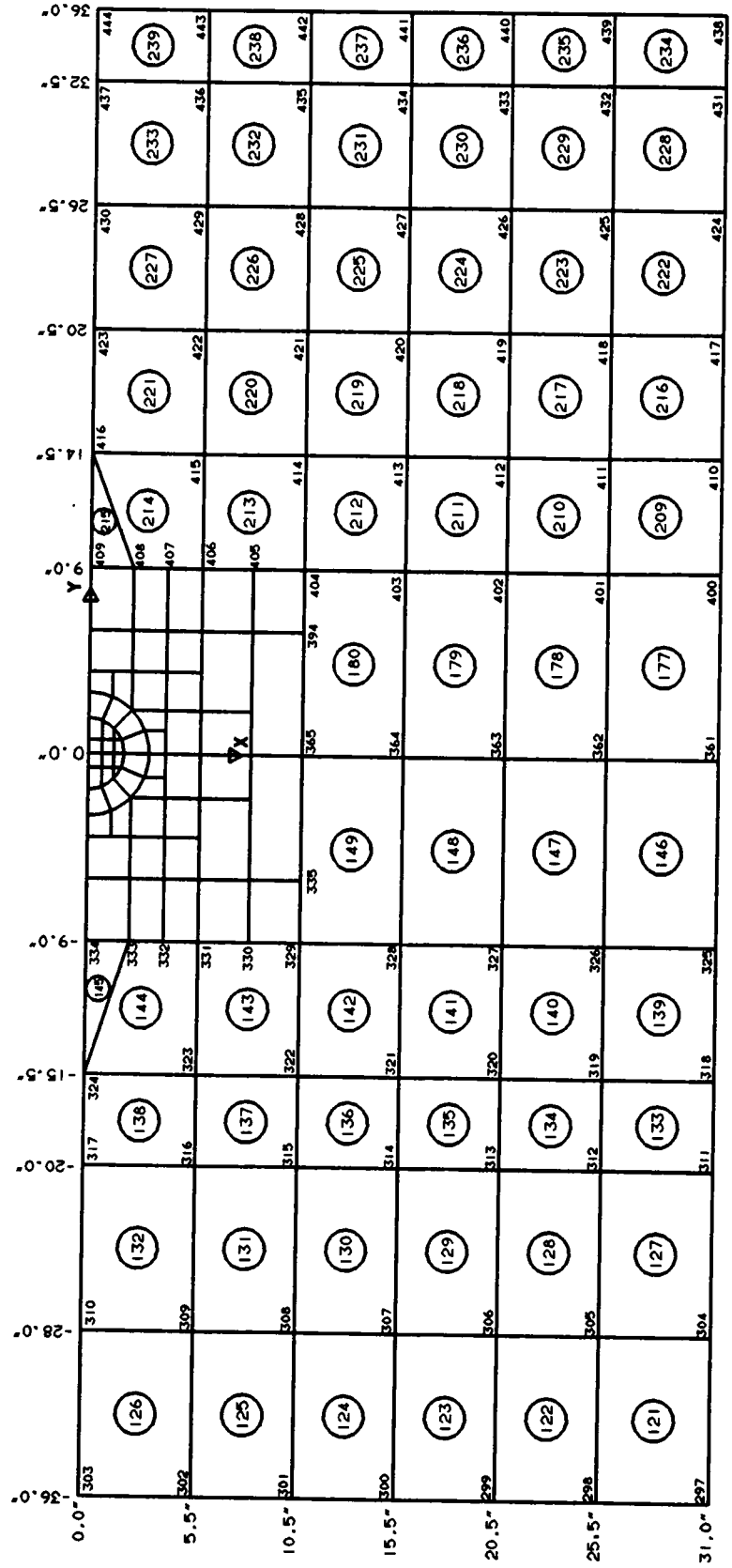

Figure 33. Plan of Model at Layer Z = 10.5

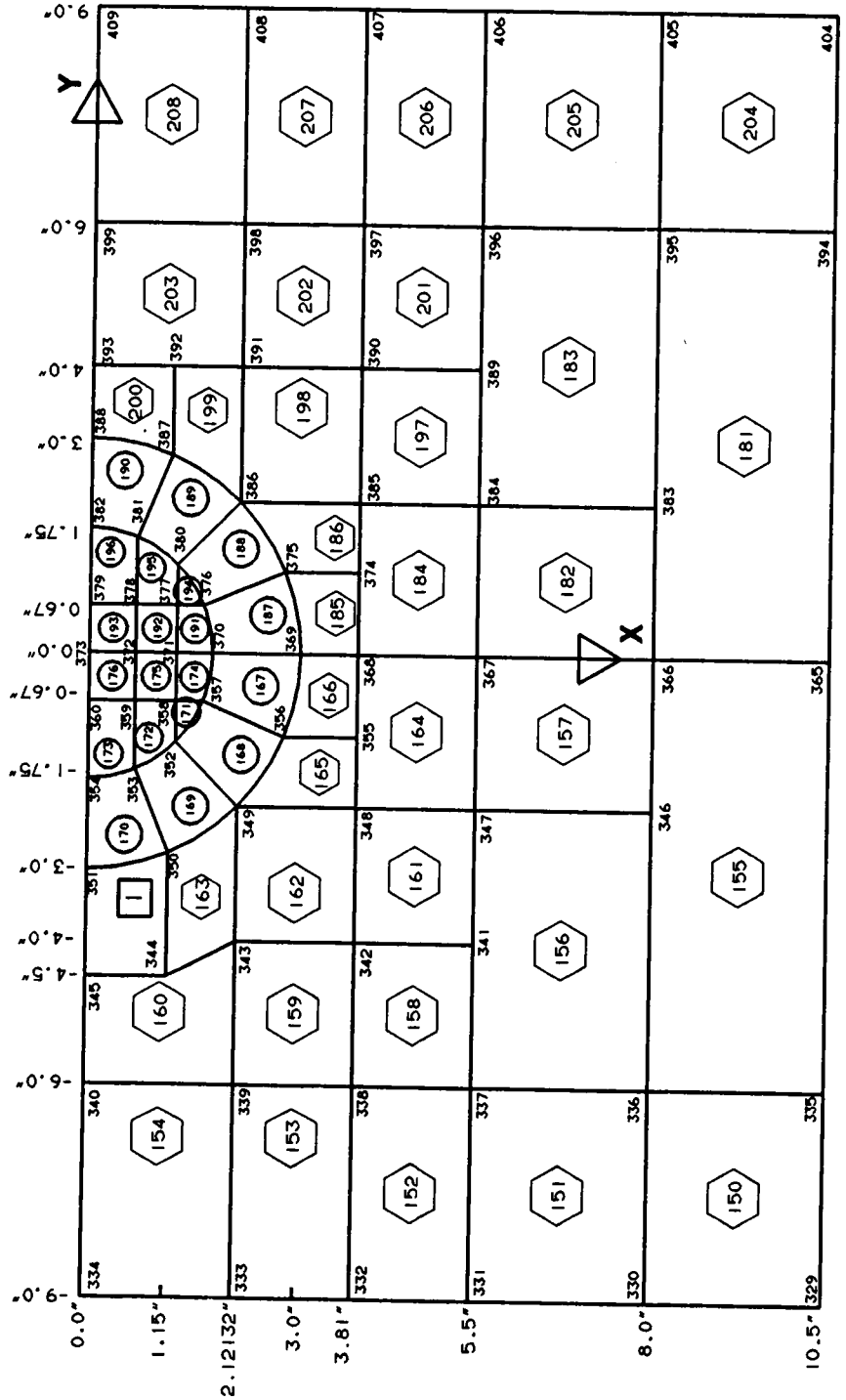

Figure 34. Plan of Model Socket Area at Layer Z = 10.5

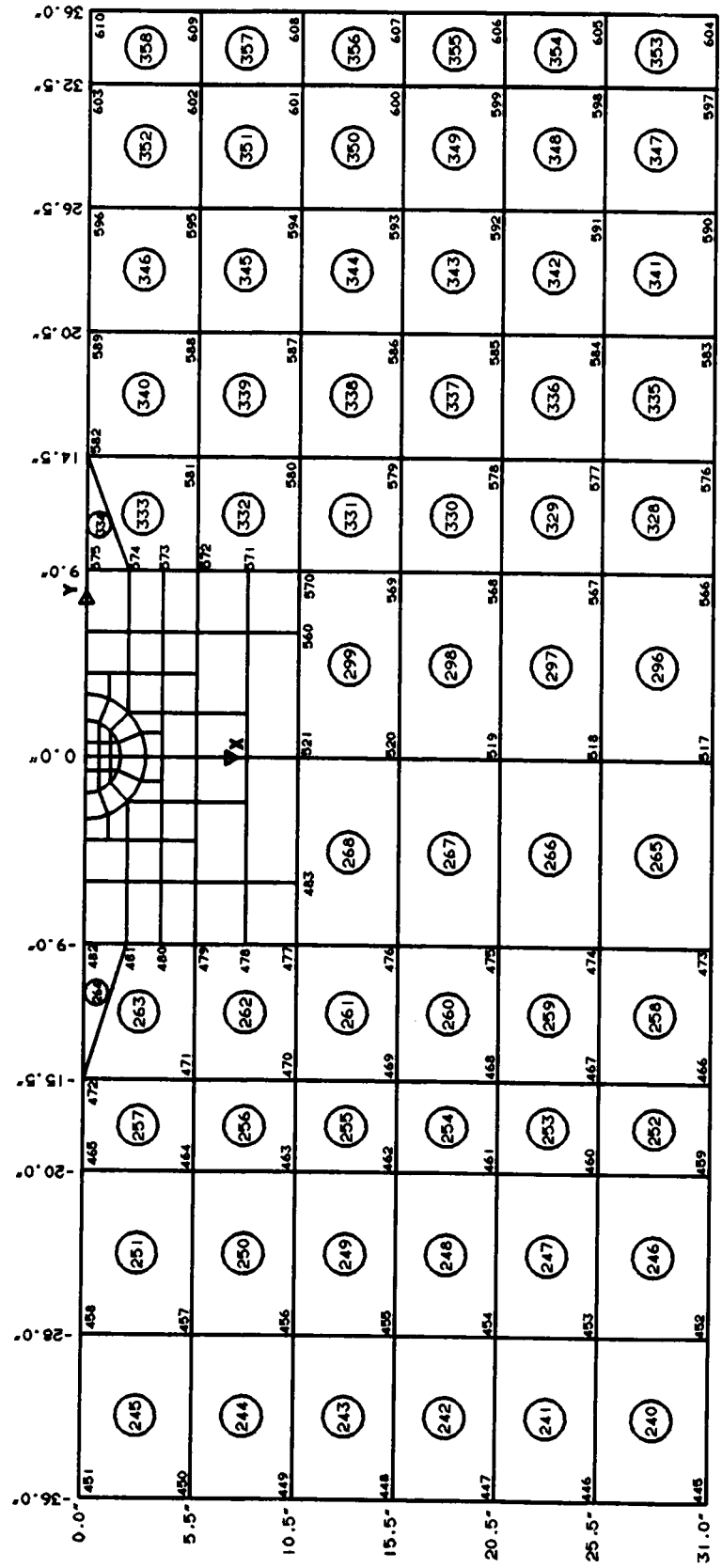

Figure 35. Plan of Model at Layer Z = 16.0

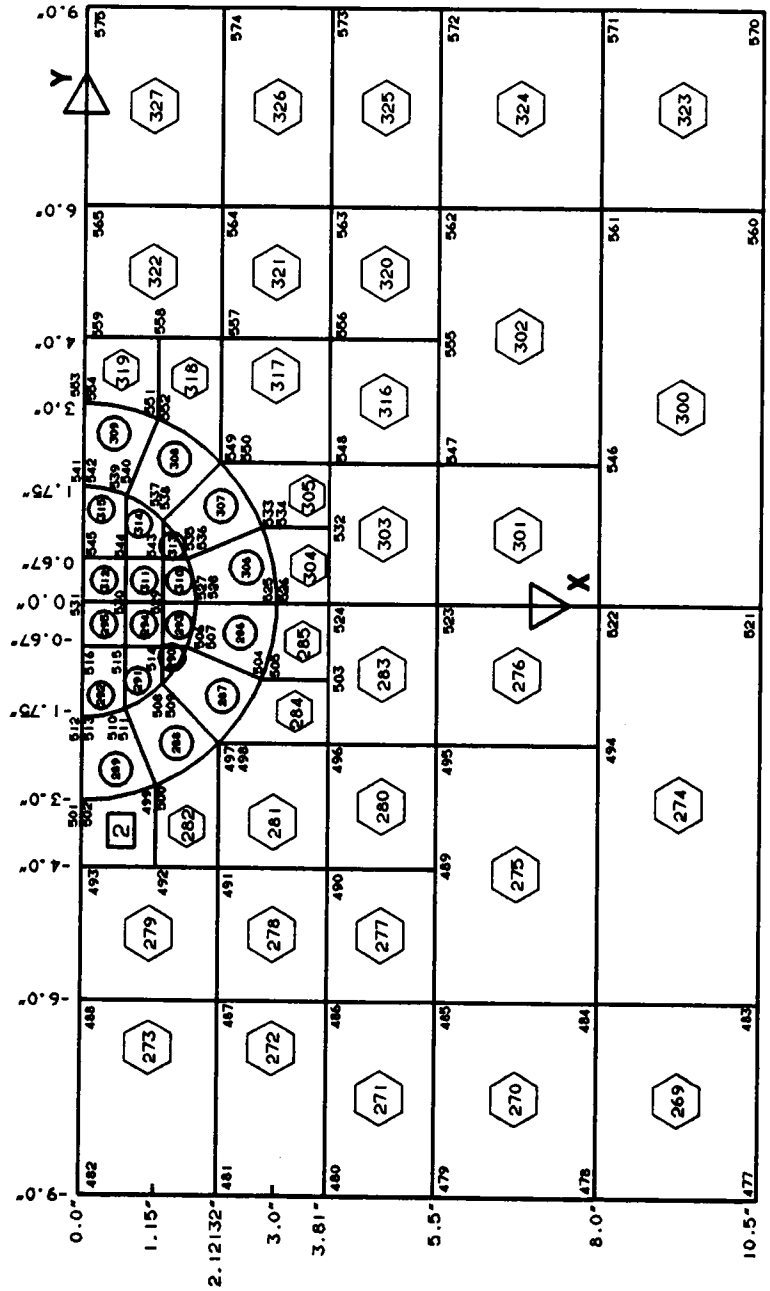

Figure 36. Plan of Model Socket Area at Layer Z = 16.0

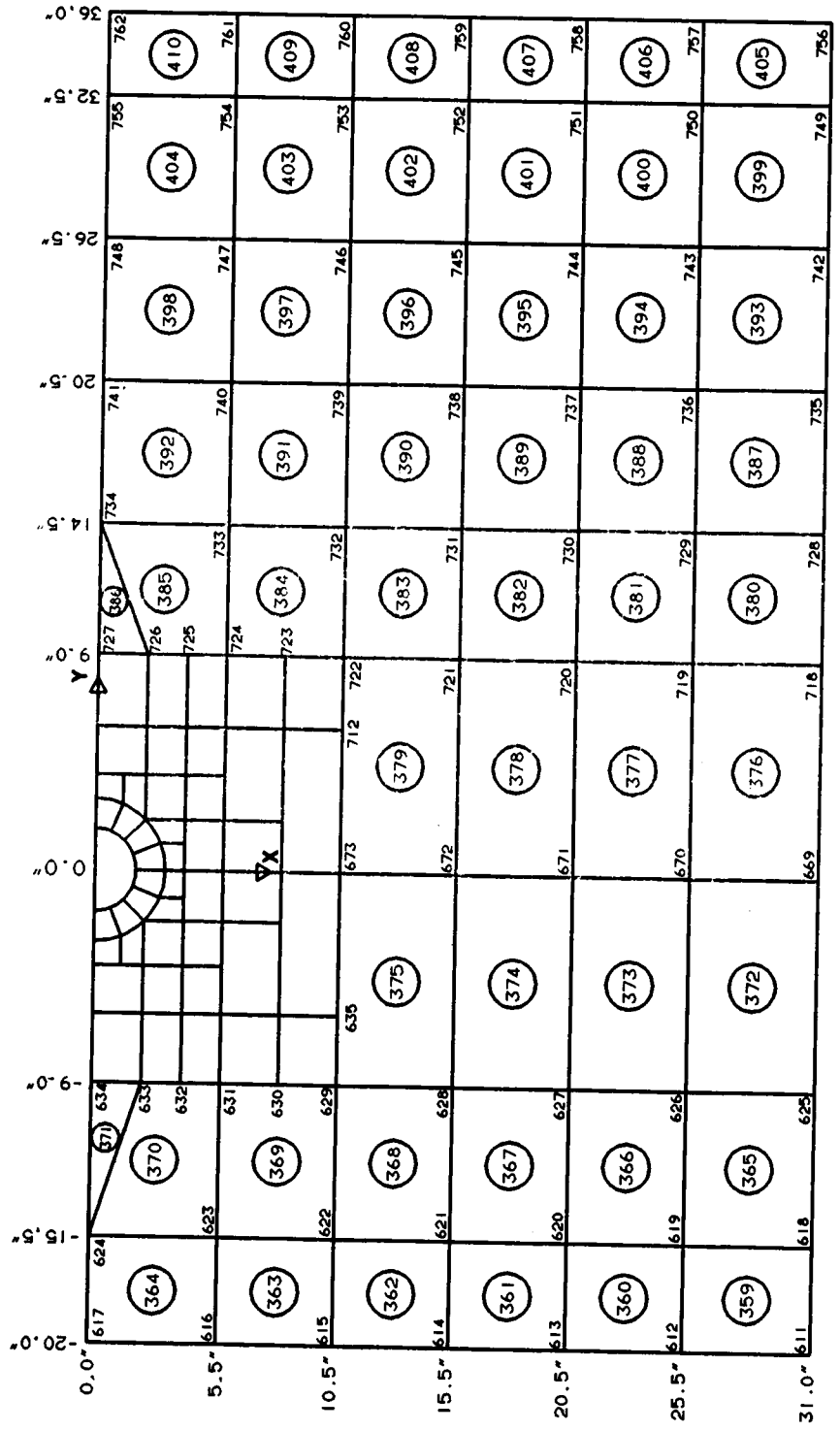

Figure 37. Plan of Model at Layer Z = 17.5

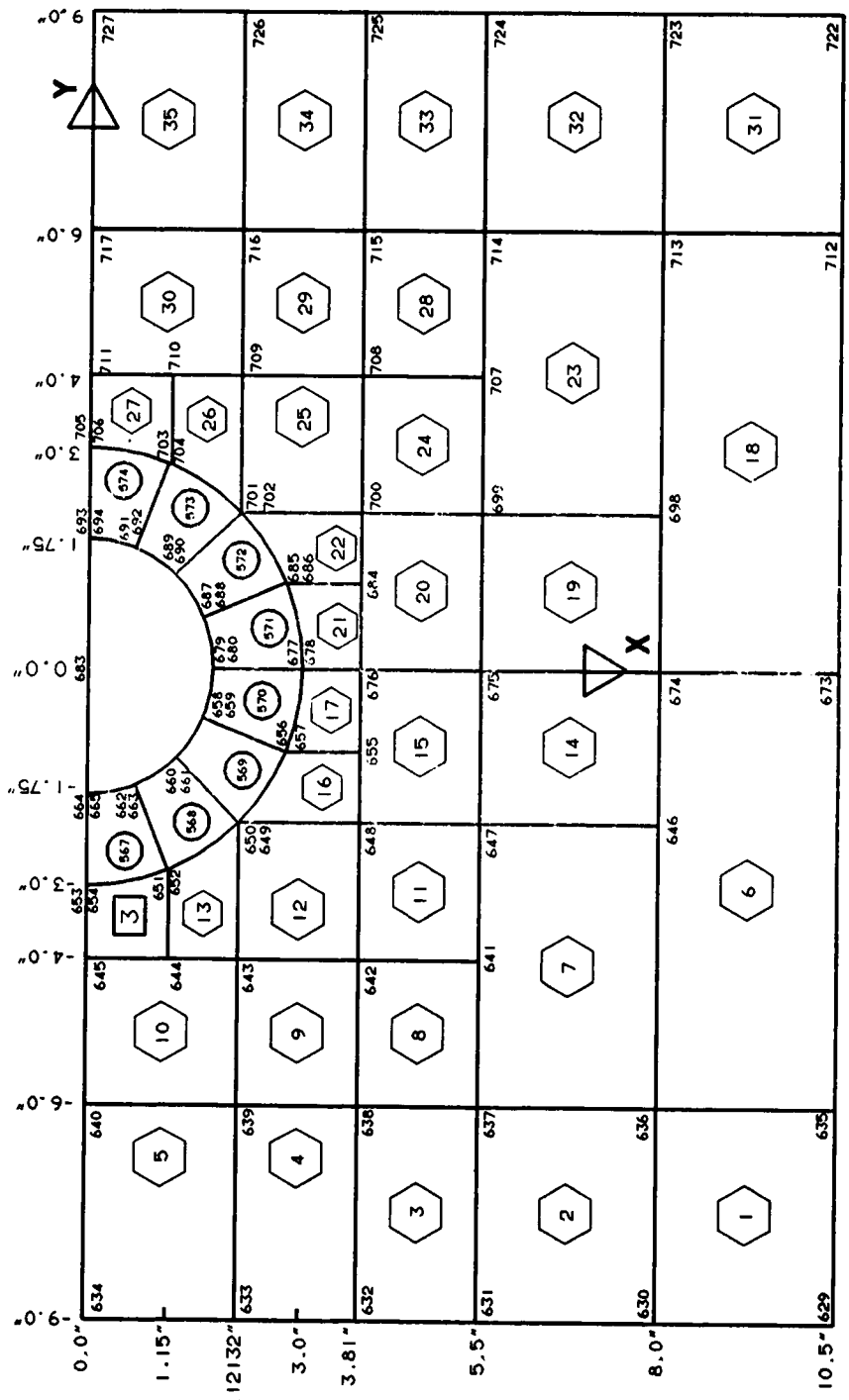

Figure 38. Plan of Model Socket Area at Layer Z = 17.5

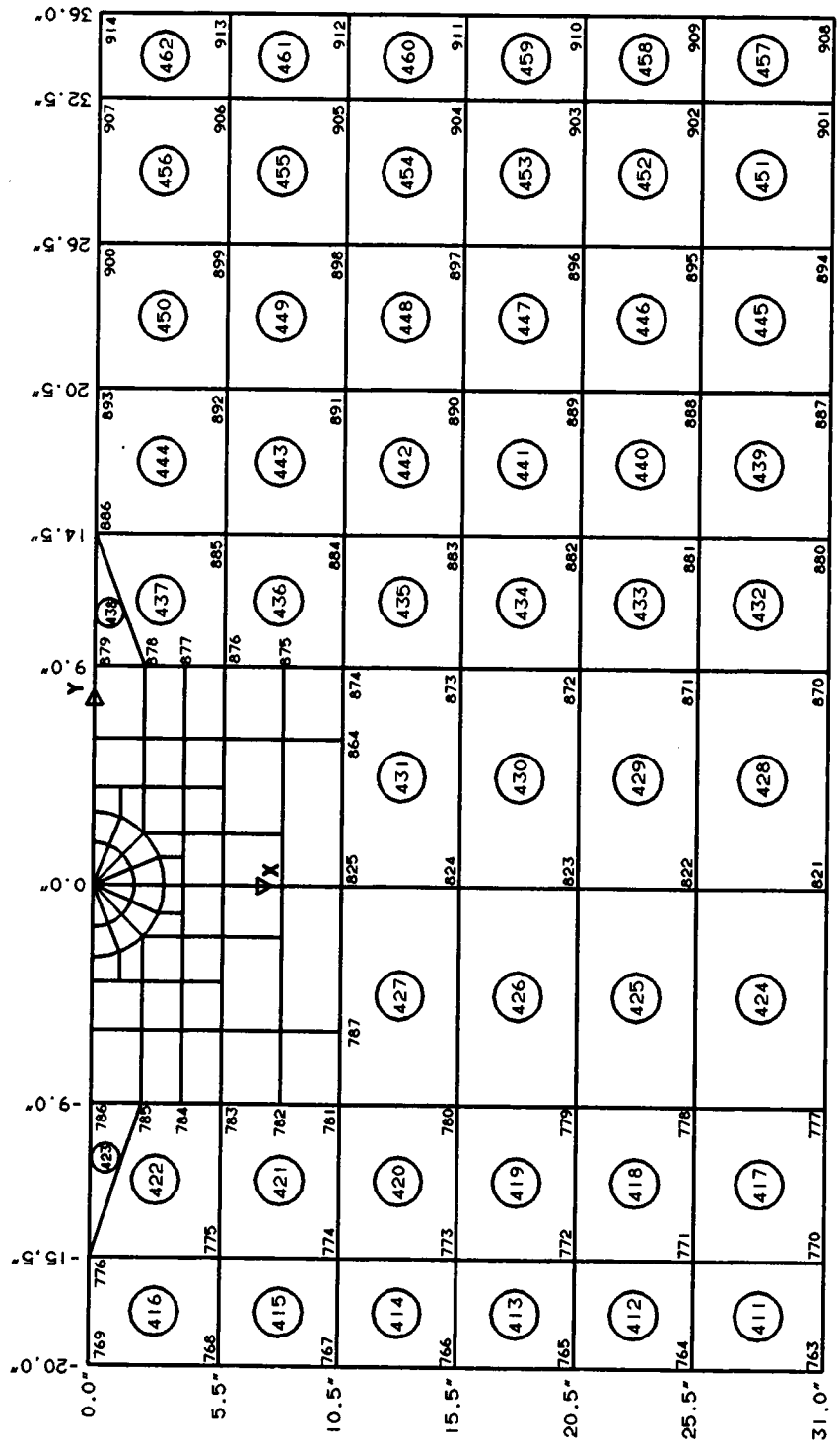

Figure 39. Plan of Model at Layer Z = 19.0

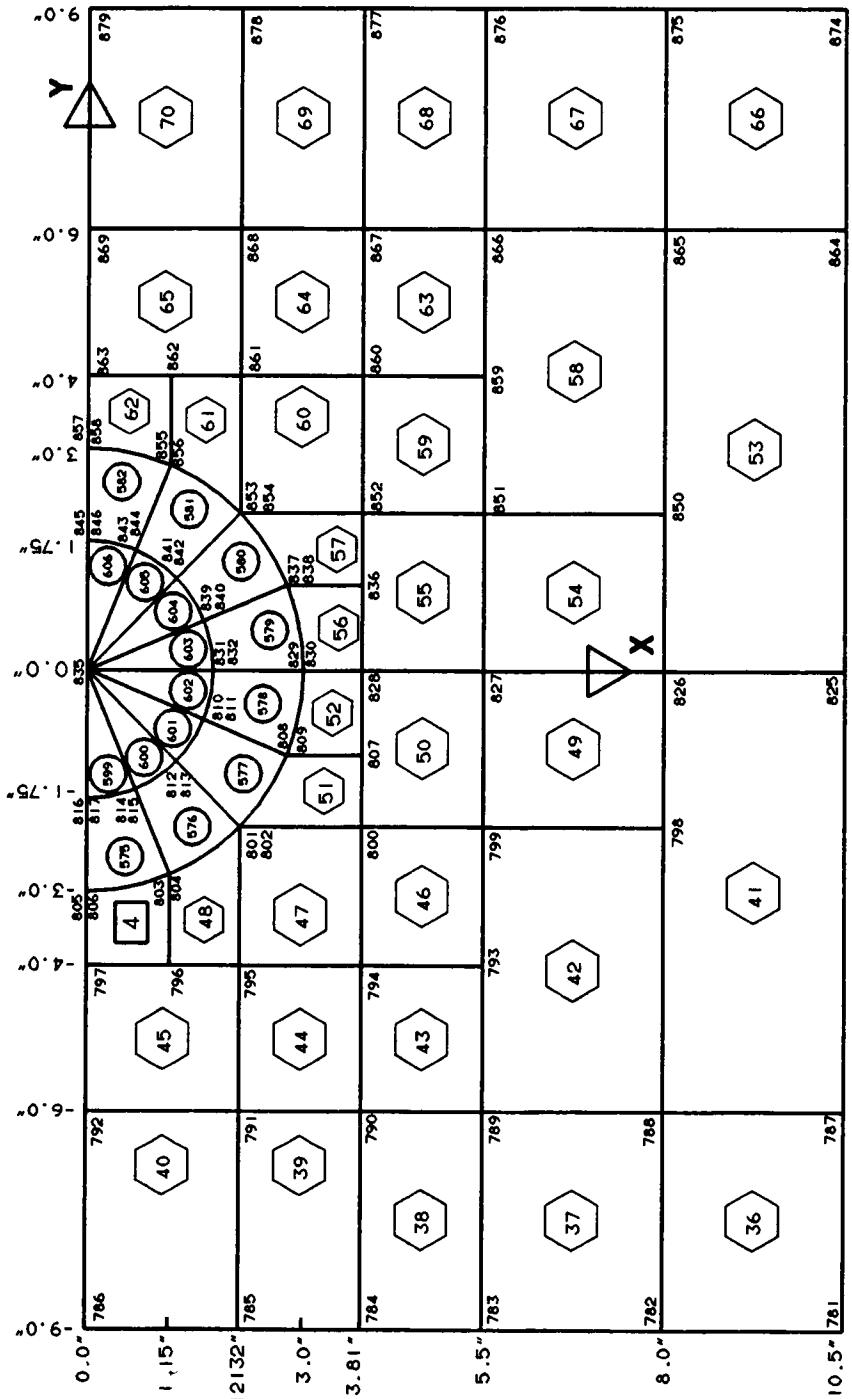

Figure 40. Plan of Model Socket Area at Layer Z = 19.0

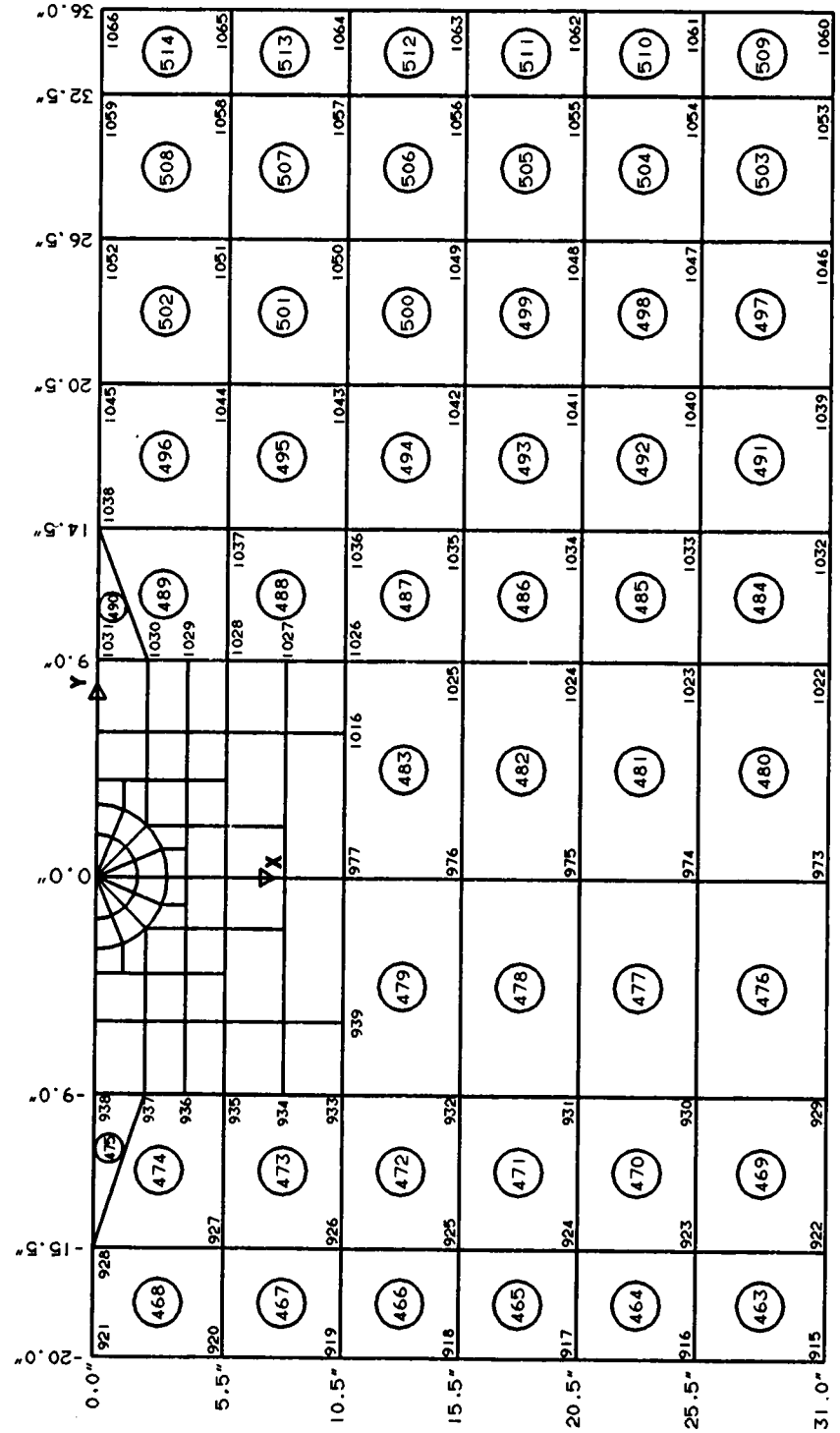

Figure 41. Plan of Model at Layer Z = 21.5

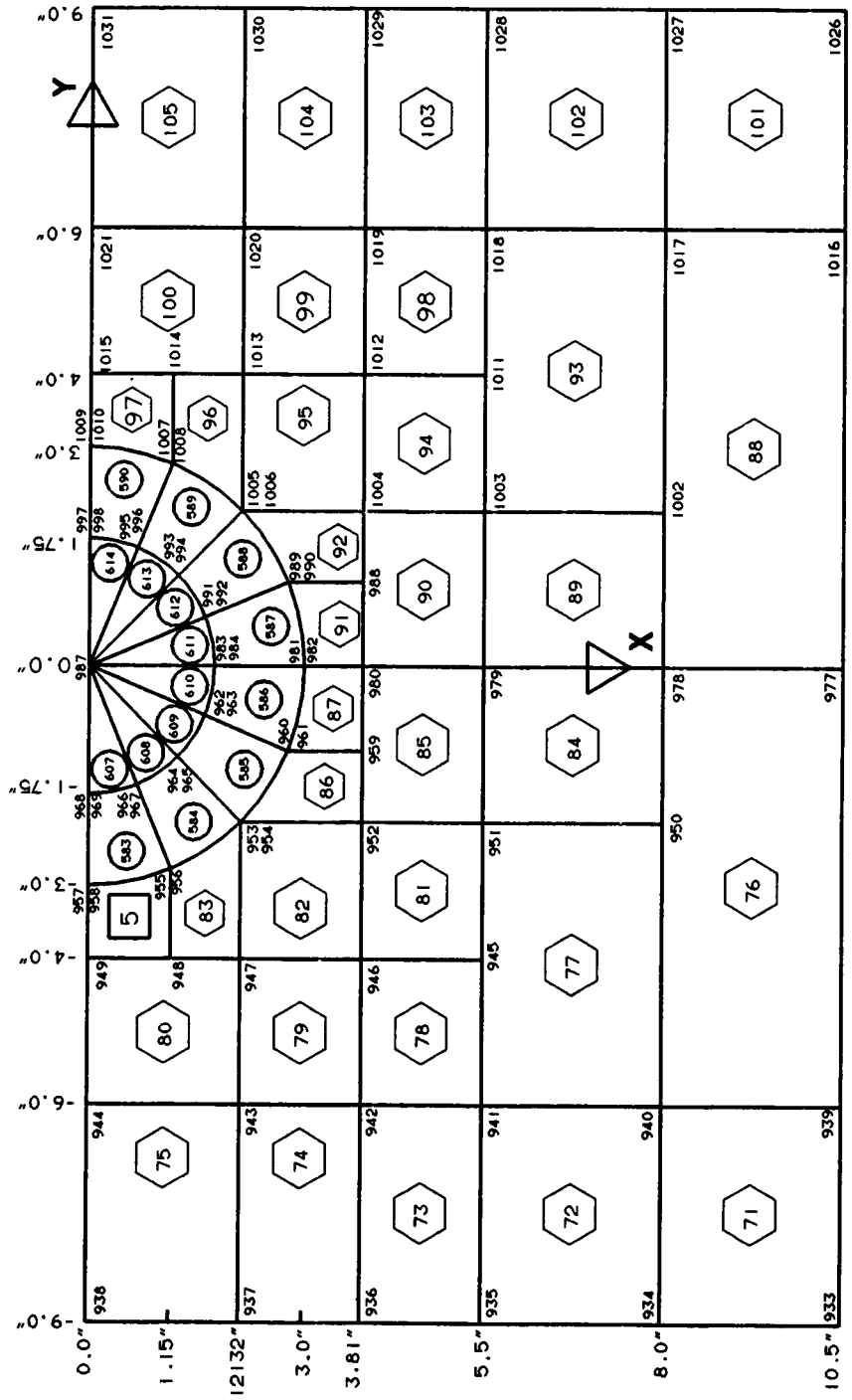

Figure 42. Plan of Model Socket Area at Layer Z = 21.5

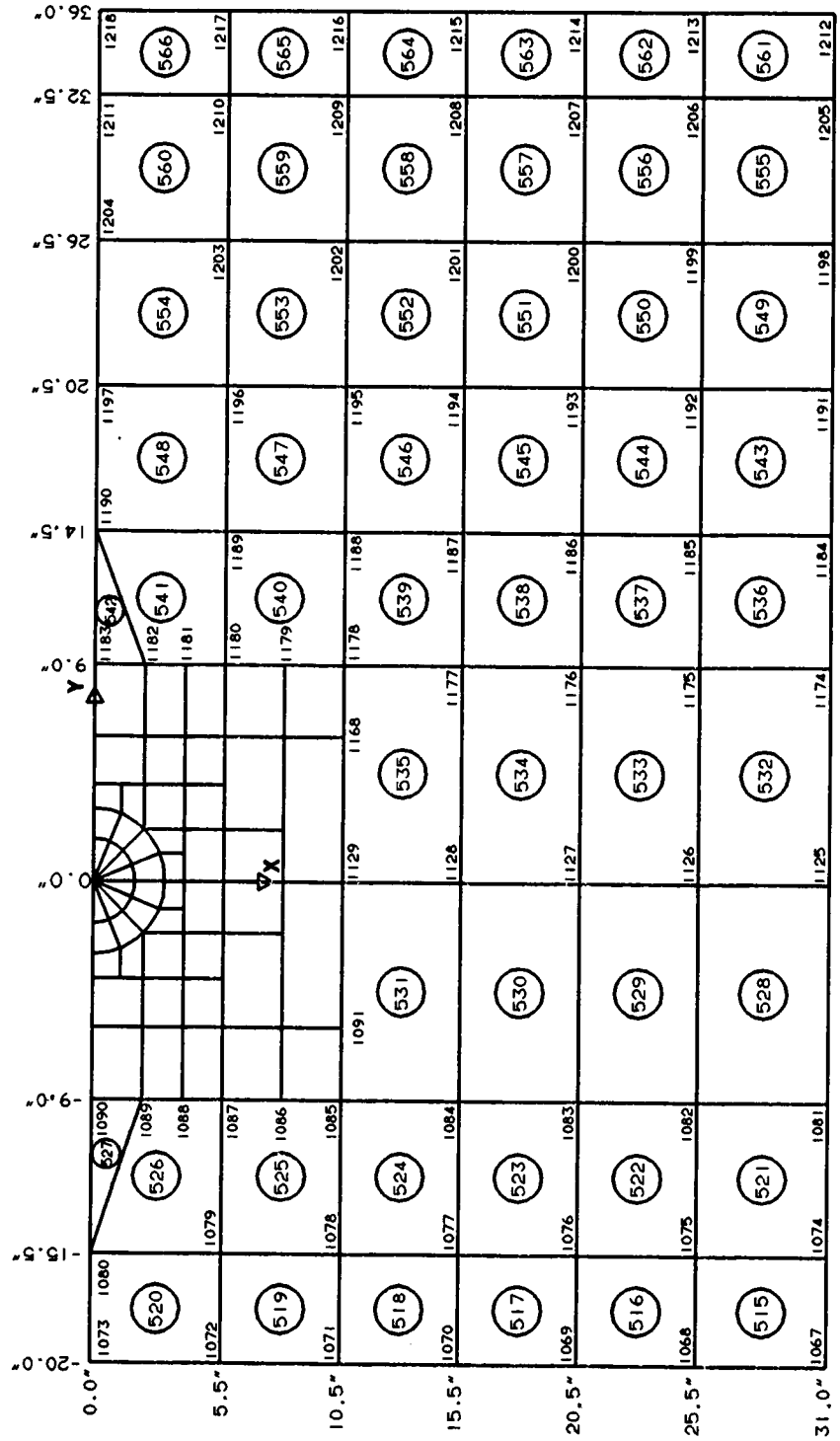

Figure 43. Plan of Model at Layer Z = 23.0

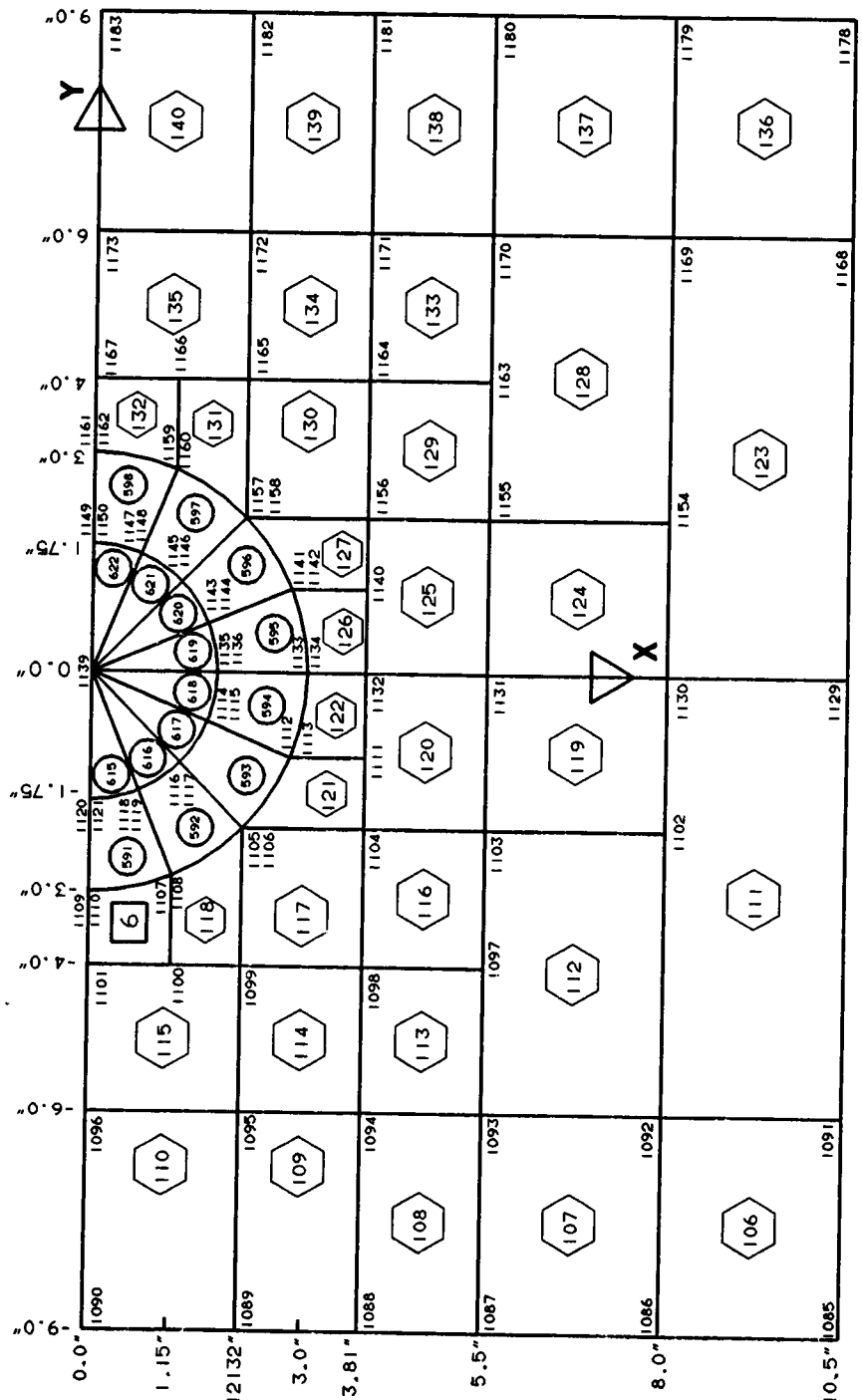

Figure 44. Plan of Model Socket Area at Layer Z = 23.0

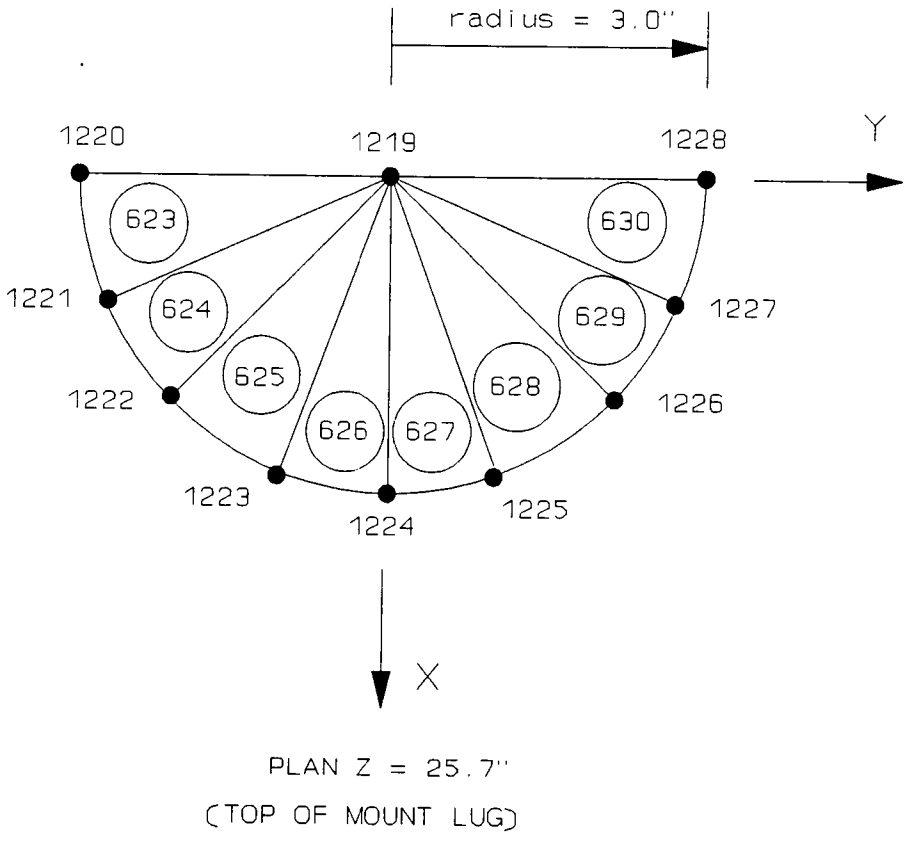

Figure 45. Plan of Model at Top of Mount Lug, Z = 25.7

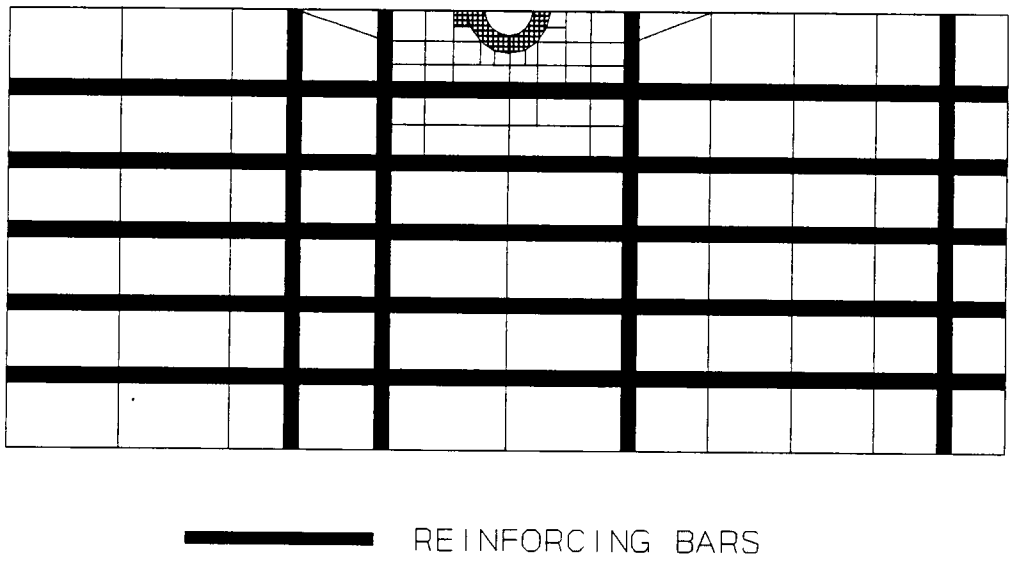

Figure 46. Reinforcing Bar Layout in Model at Elevation Z = 16.0

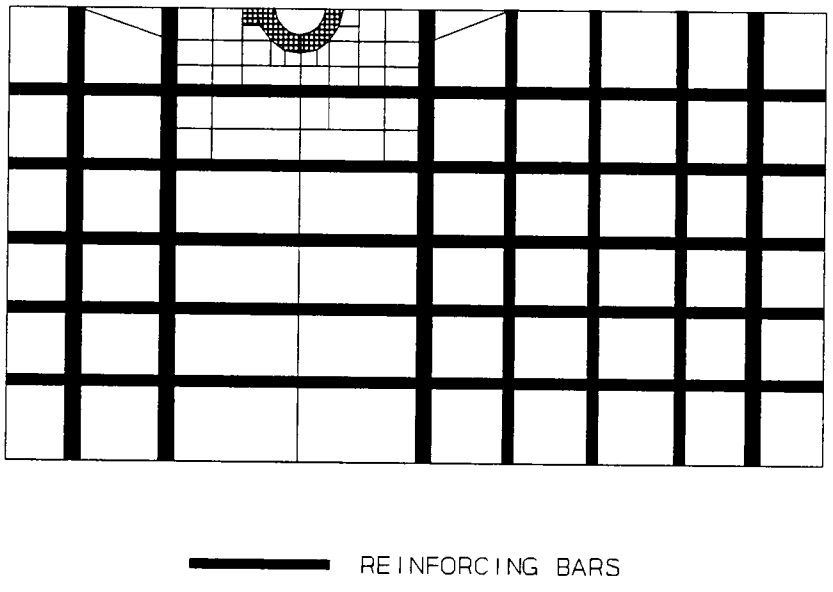

Figure 47. Reinforcing Bar Layout in Model at Elevation Z= 21.5

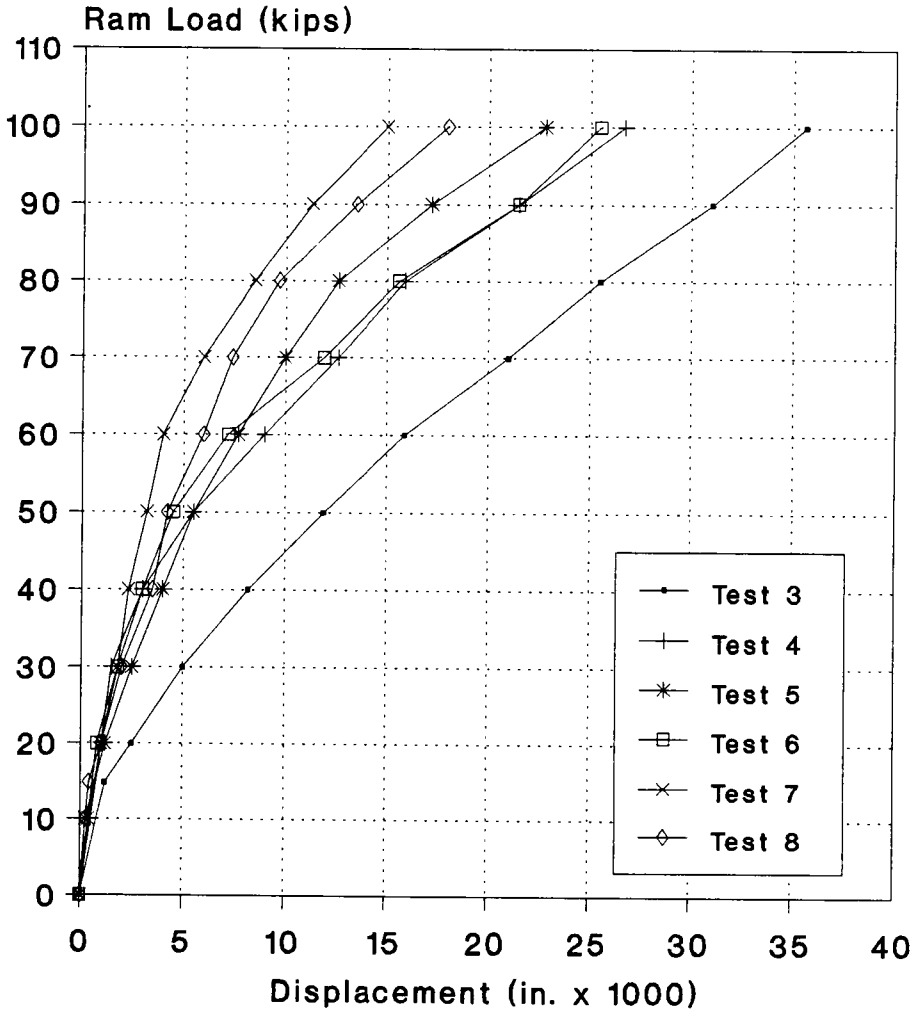

Figure 48. Load-Displacement Curves for Socket Tests, to 100 kips

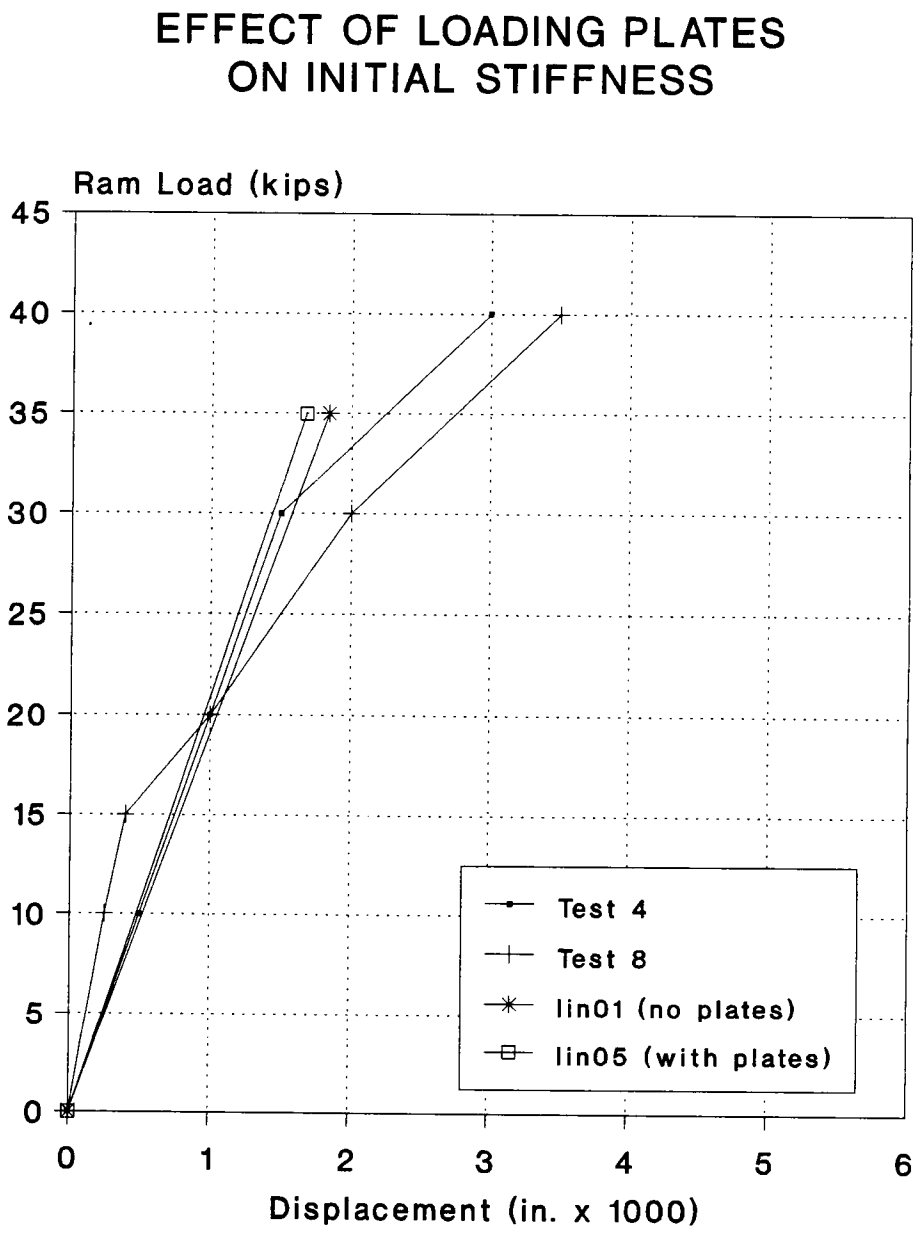

Figure 49. Effect of Loading Plates on Initial Stiffness

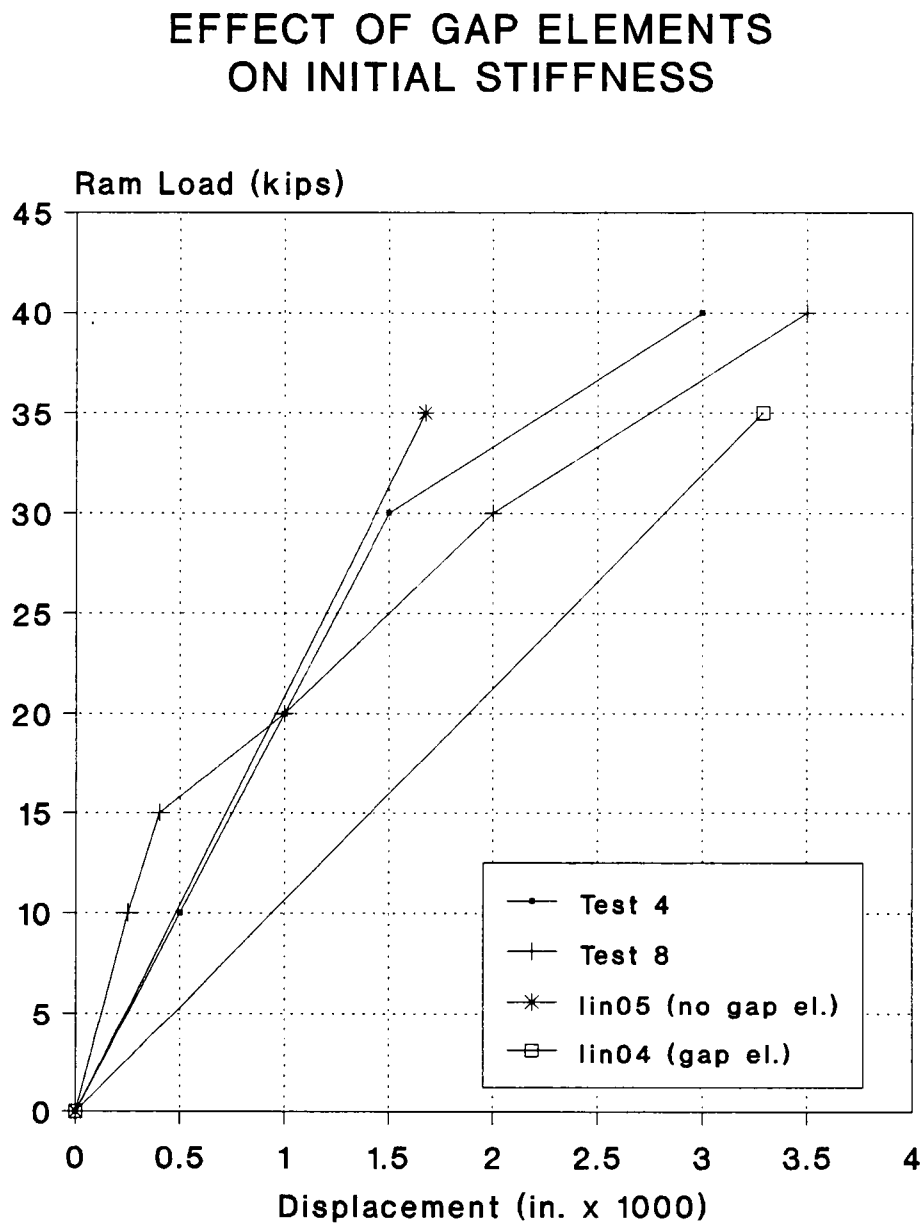

Figure 50. Effect of Gap Elements on Initial Stiffness

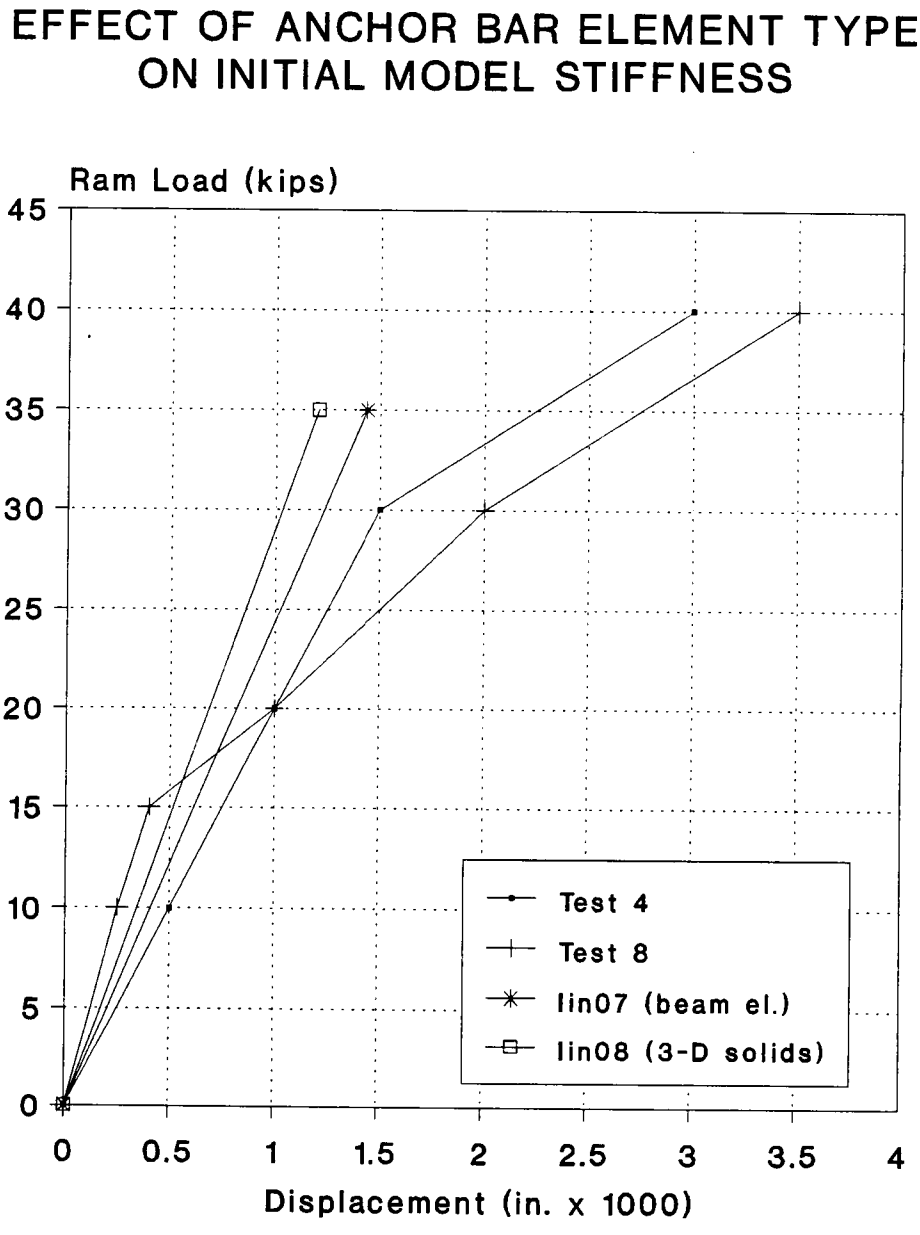

Figure 51. Effect of Anchor Bar Element Type on Initial Stiffness

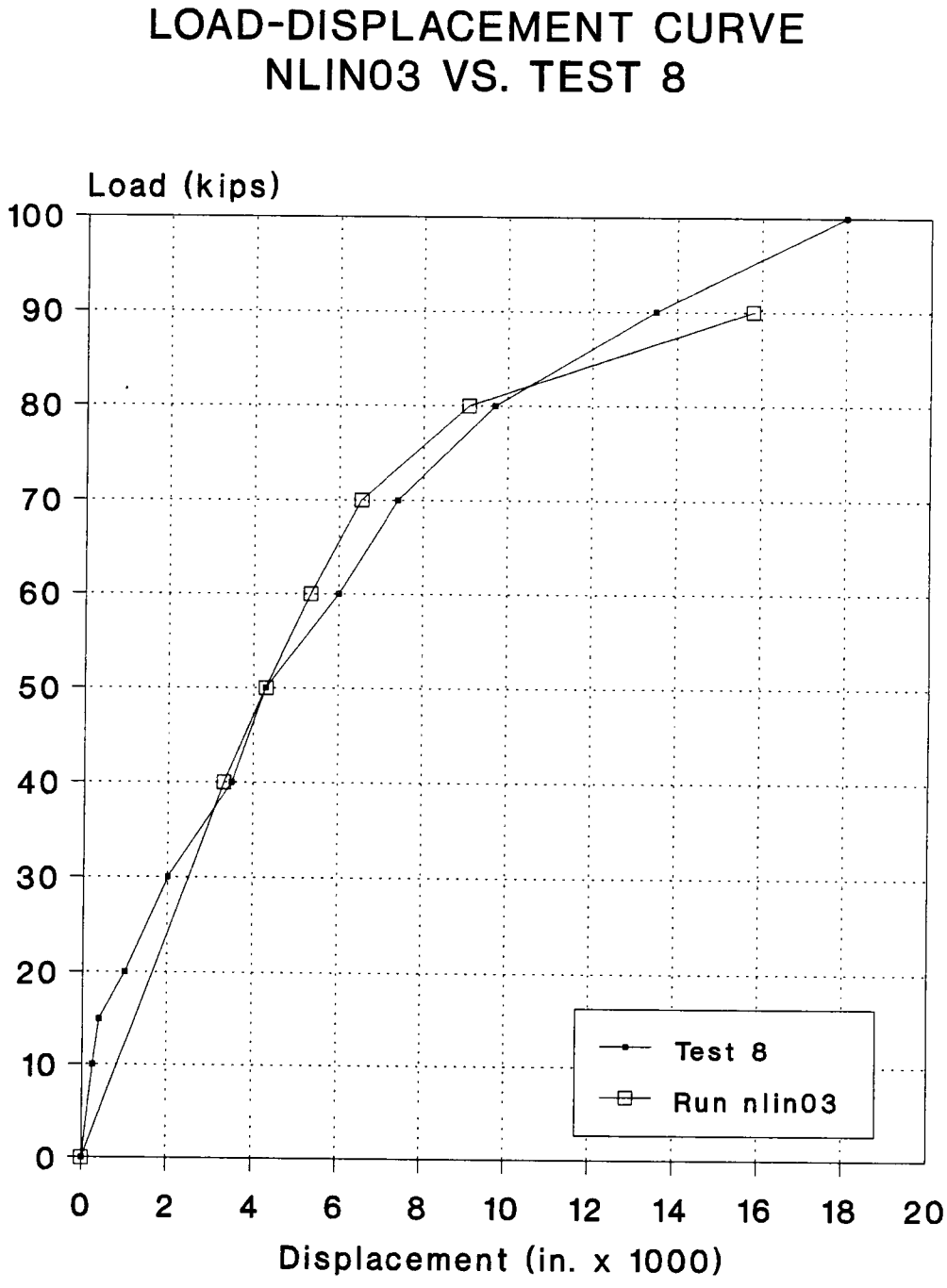

Figure 52. Load-Displacement Curve for Run nlin03

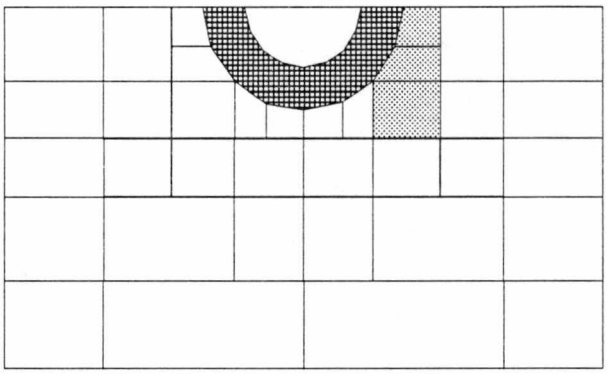

(a) Z = 19.0

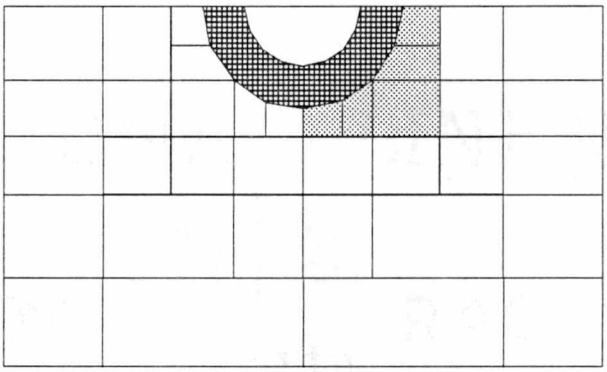

(b) Z = 21.5"

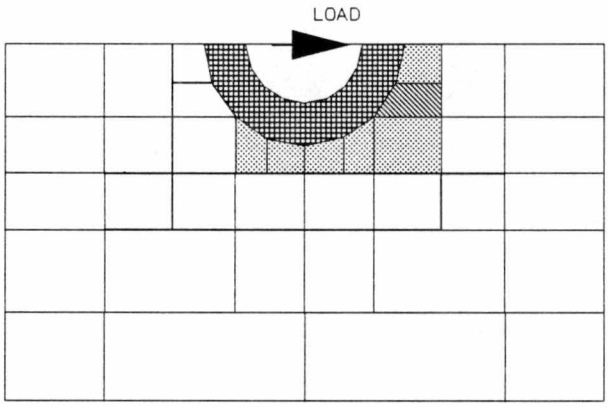

(c) Z = 23.0"

Figure 53. Crushed Elements, Run nlin03, at P=90 kips

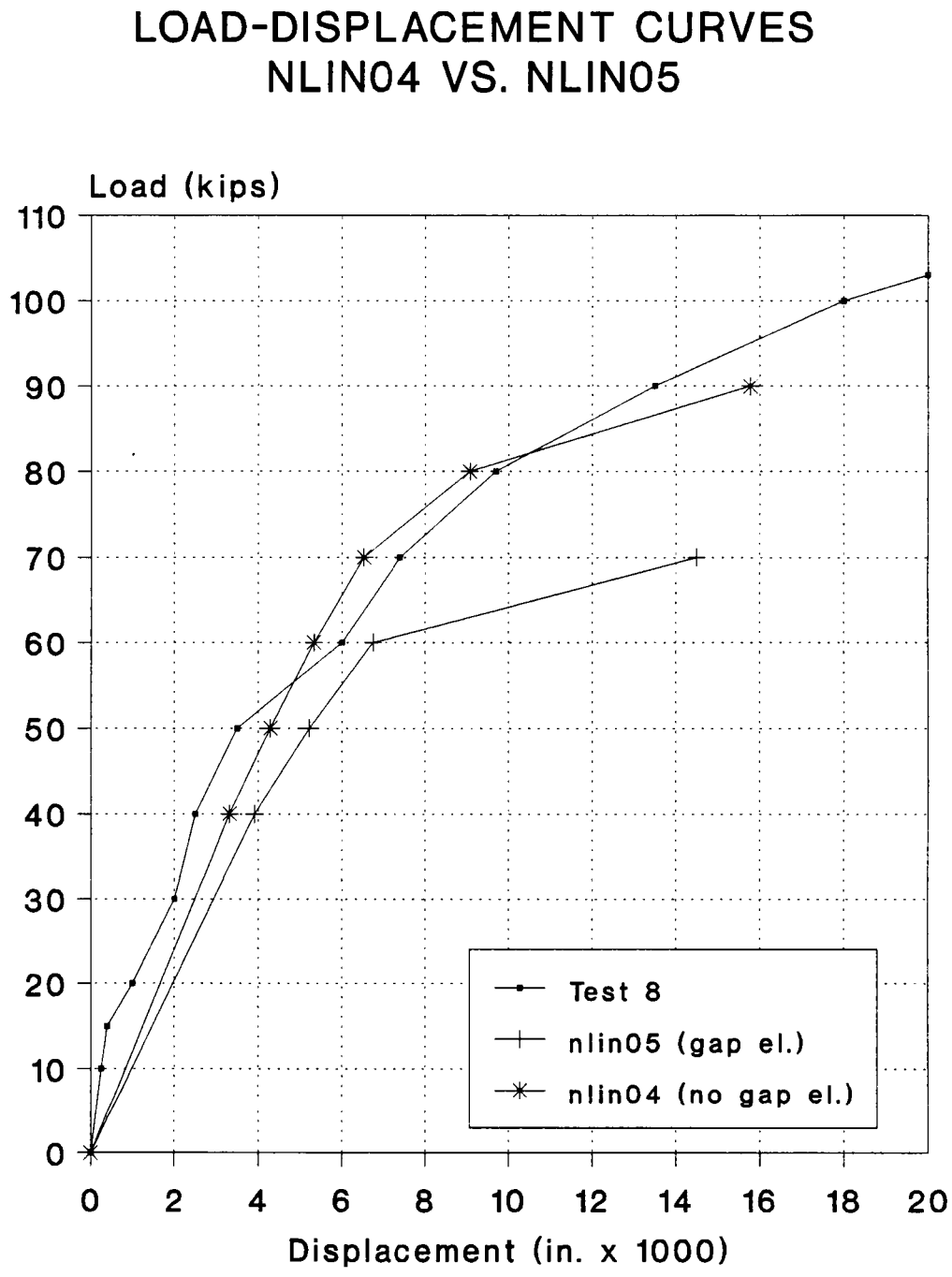

Figure 54. Load-Displacement Curves for Runs nlin04 and nlin05 Compared to Test 8, Showing the Effect of Gap Elements in Nonlinear Analyses.

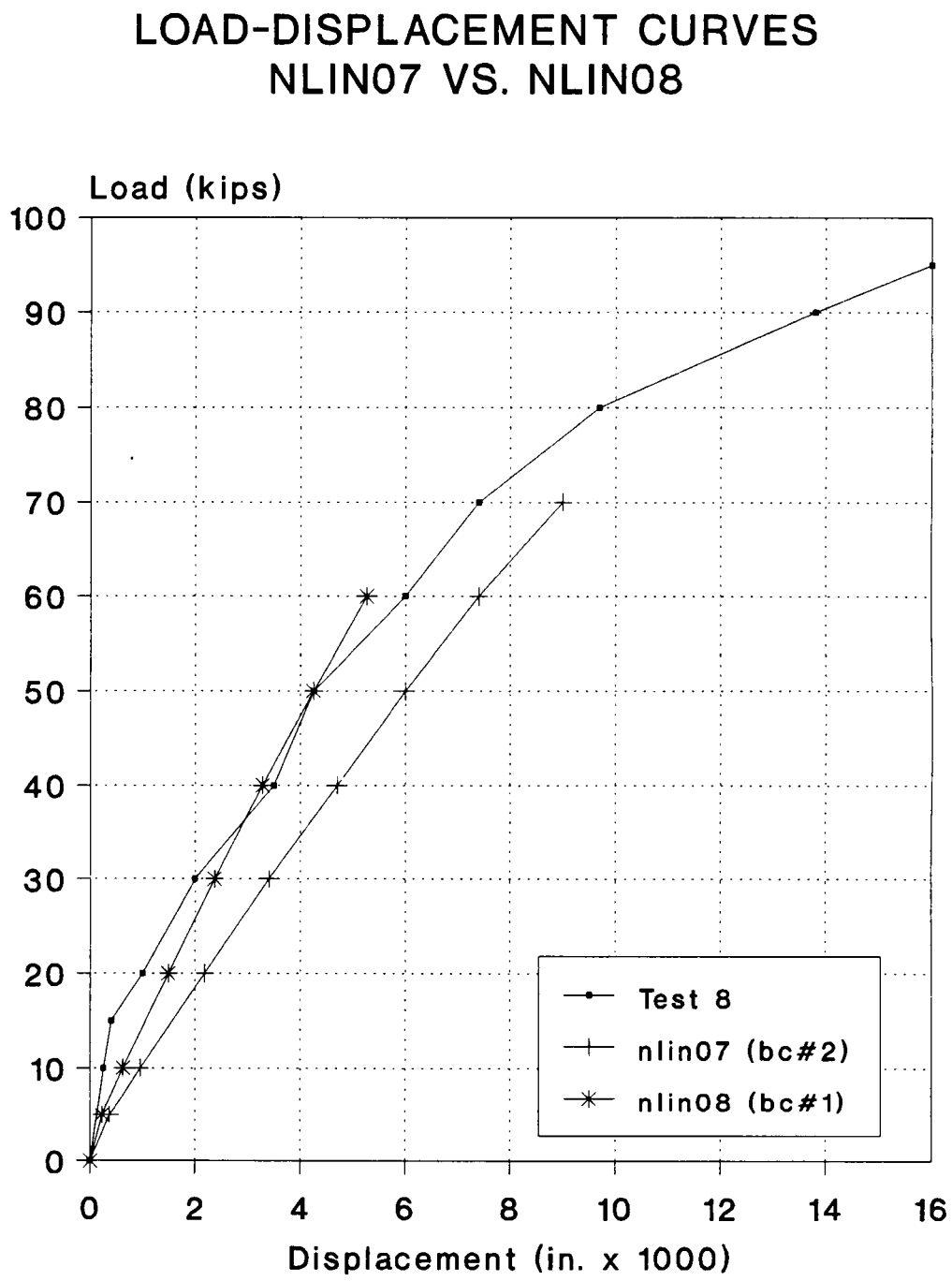

Figure 55. Load-Displacement Curves for Runs nlin07 and nlin08 Compared to Test 8, Showing the Effect of Boundary Condition Set 1 vs. Set 2.

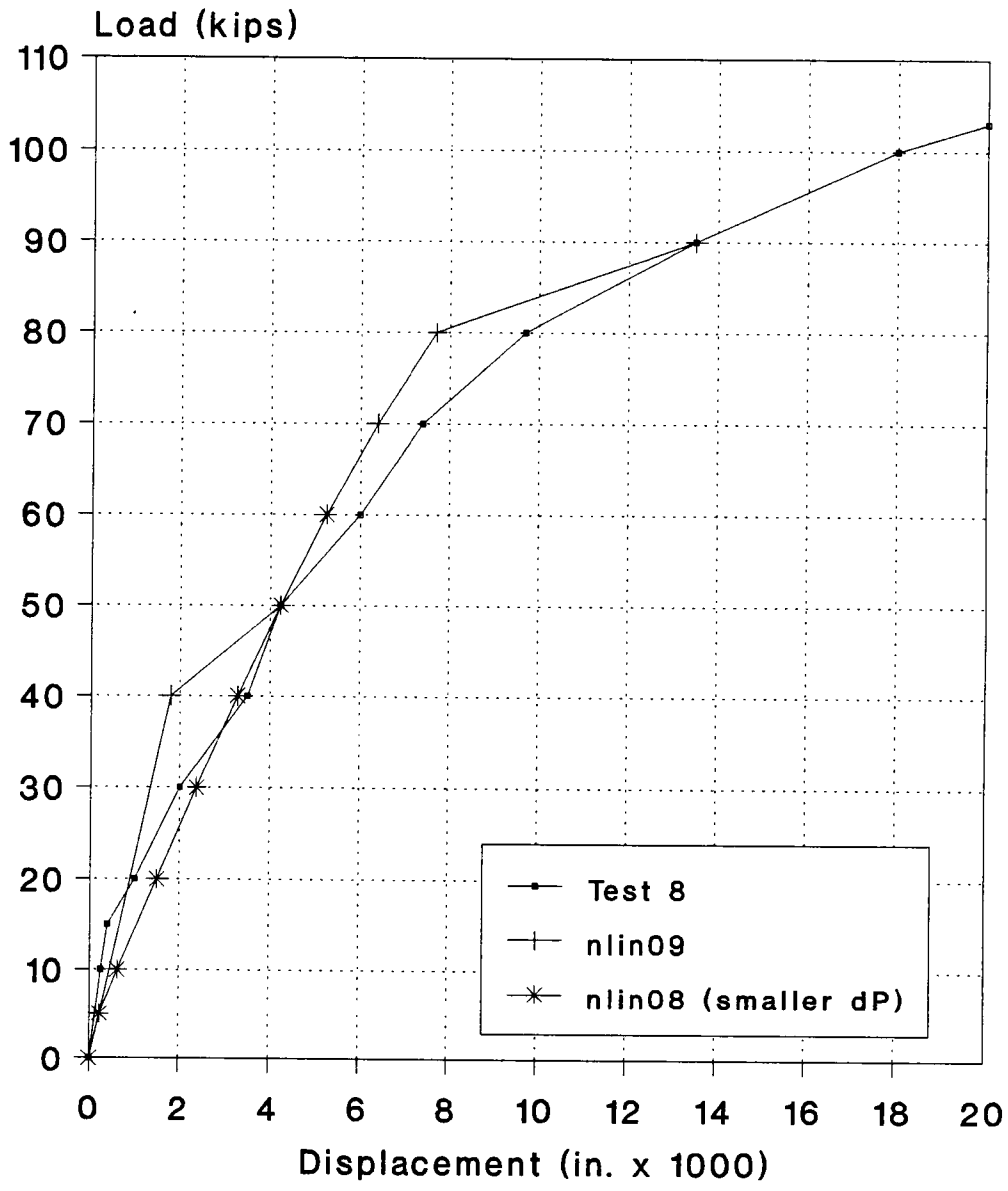

Figure 56. Load-Displacement Curves for Runs nlin08 and nlin09 Compared to Test 8, Showing the Effect of Load Step Increment

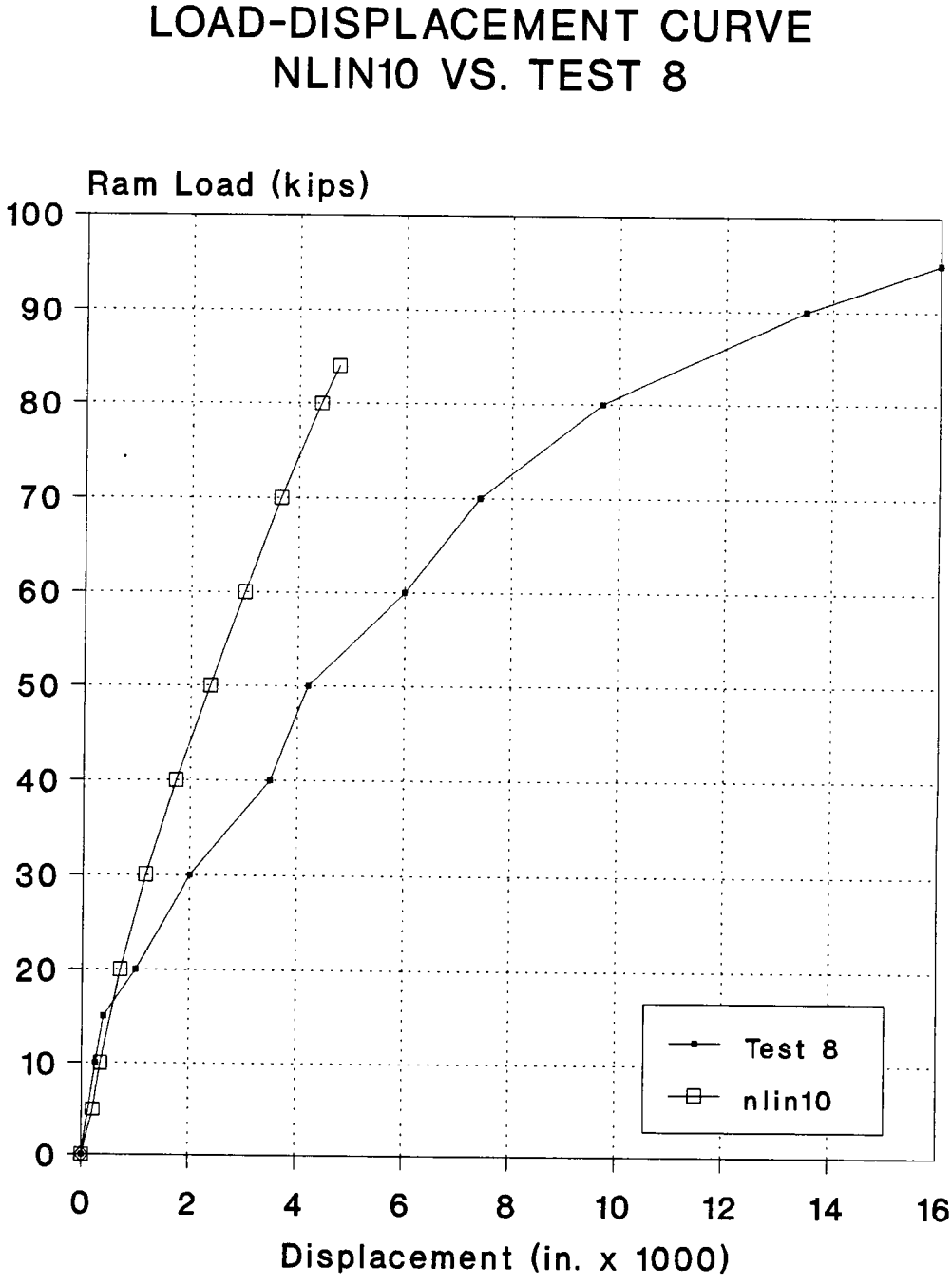

Figure 57. Load-Displacement Curve for Run nlin10

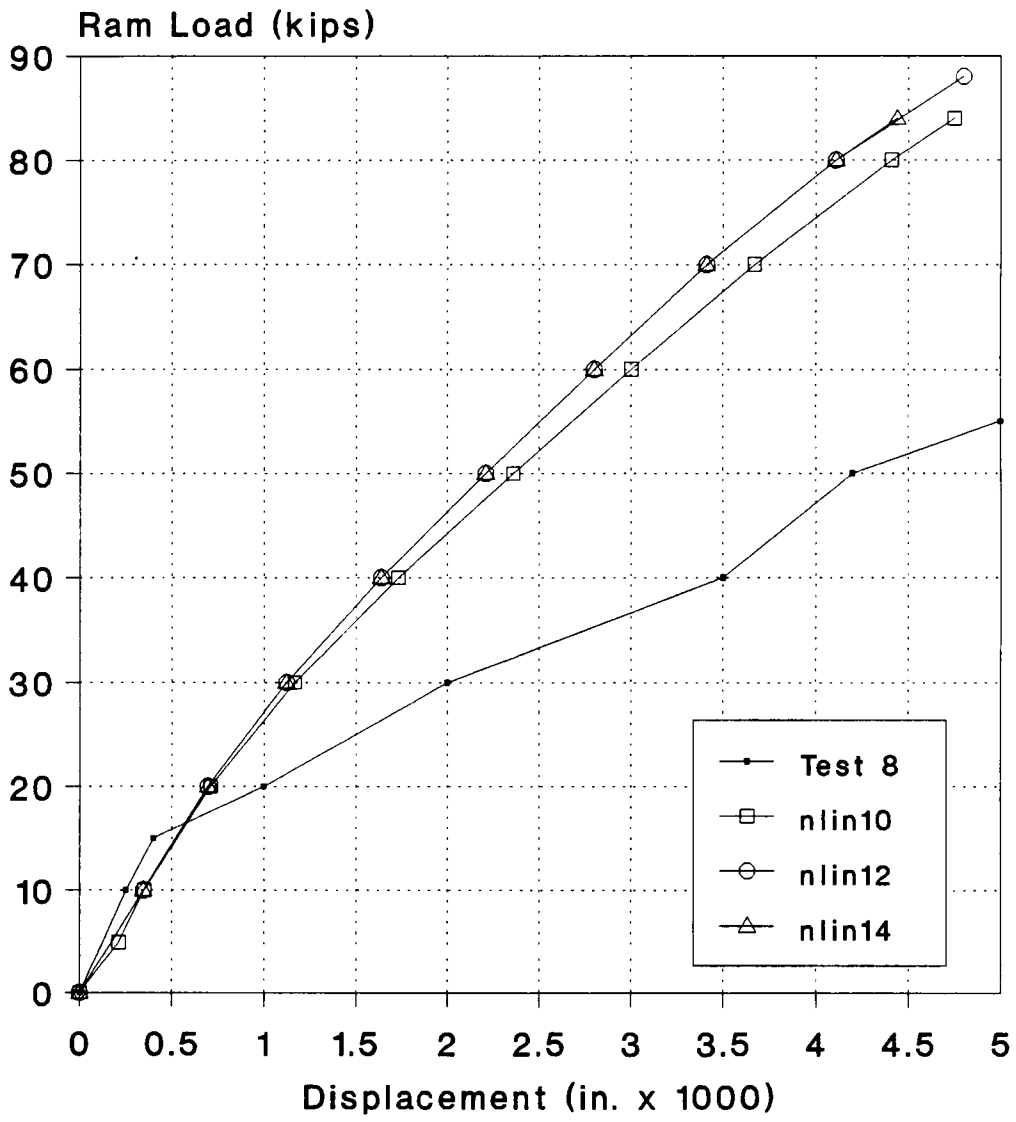

Figure 58. Comparison of Load-Displacement Curves for Runs nlin10, nlin12, and nlin14

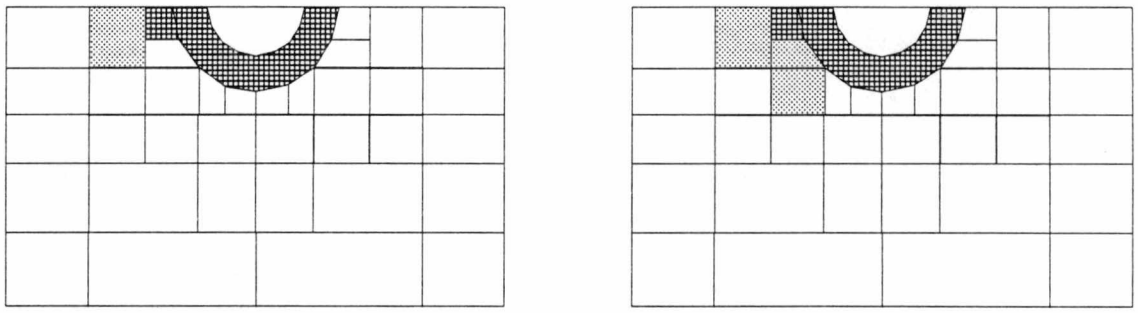

(a) Z = 21.5" (b) Z = 23.0"

Figure 59. Cracked Elements at Load P = 20 kips

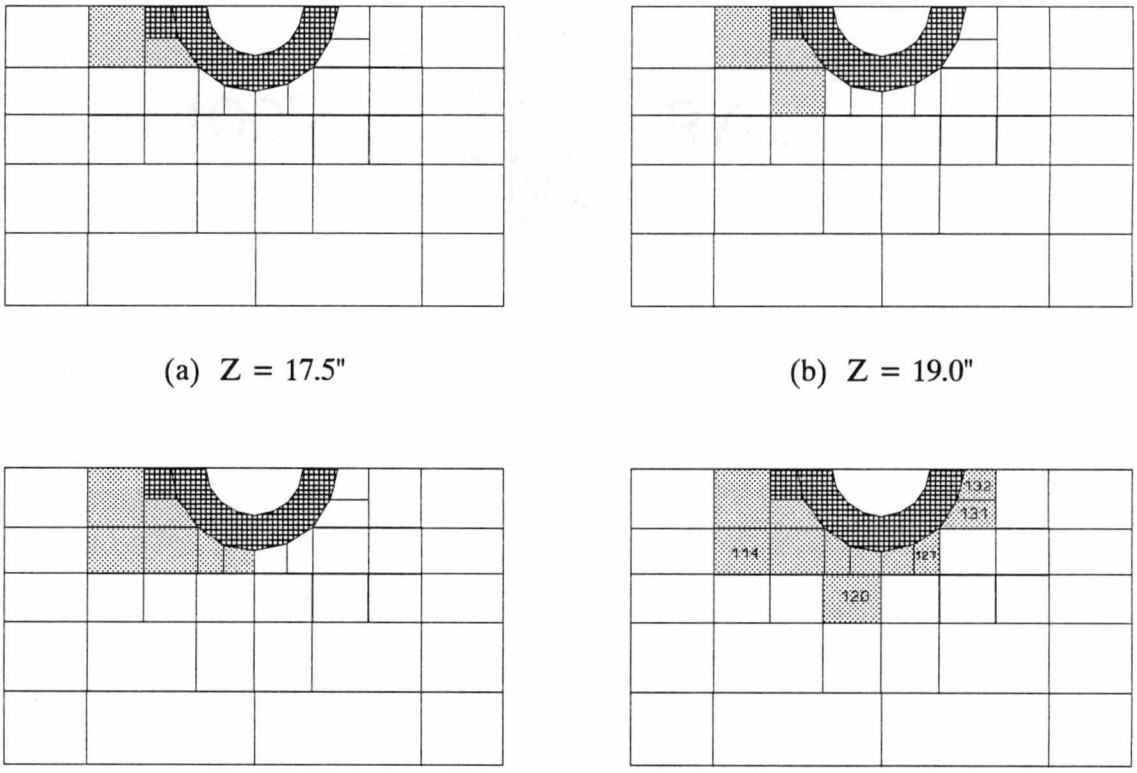

(a) Z = 17.5" (b) Z = 19.0"

(c) Z = 21.5" (d) Z = 23.0"

Figure 60. Cracked Elements at Load P = 40 kips

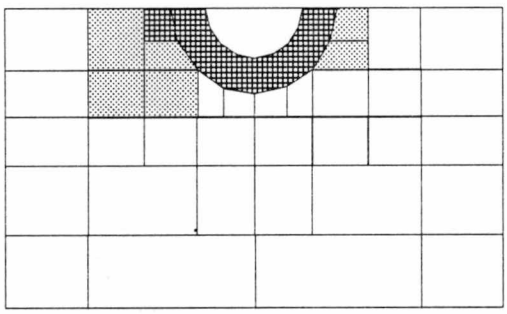

(a) Z = 17.5"

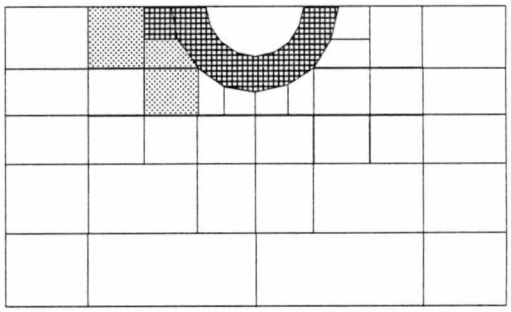

(b) Z = 19.0"

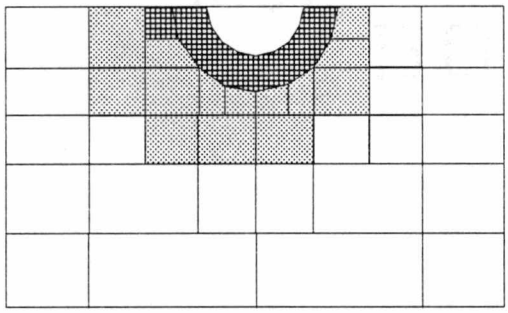

(c) Z = 21.5"

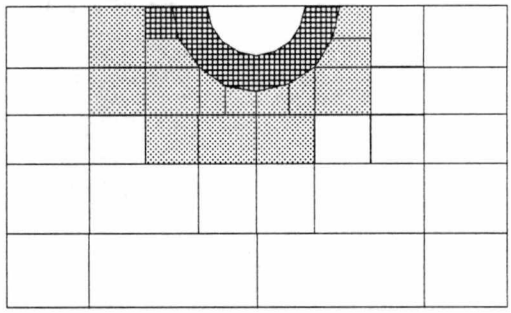

(d) Z = 23.0"

Figure 61. Cracked Elements at Load P = 60 kips

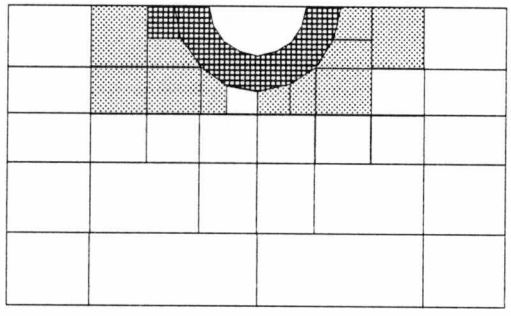

(a) Z = 17.5"

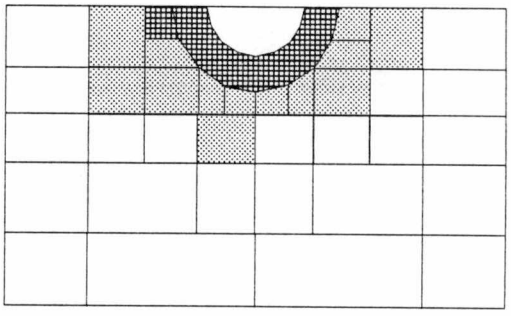

(b) Z = 19.0"

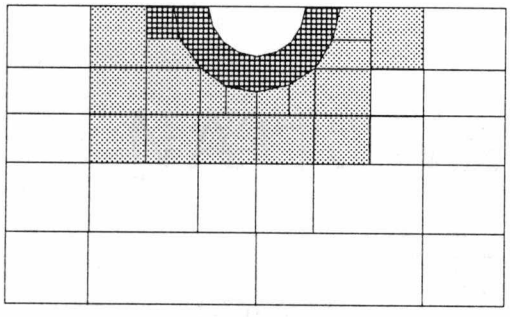

(c) Z = 21.5"

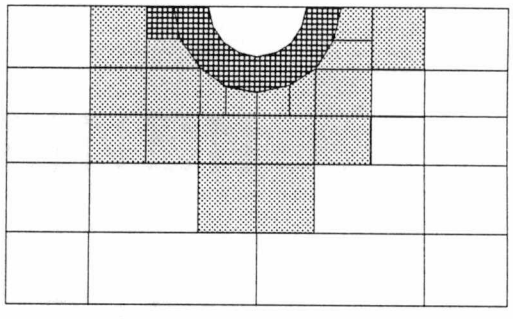

(d) Z = 23.0"

Figure 62. Cracked Elements at Load P = 80 kips

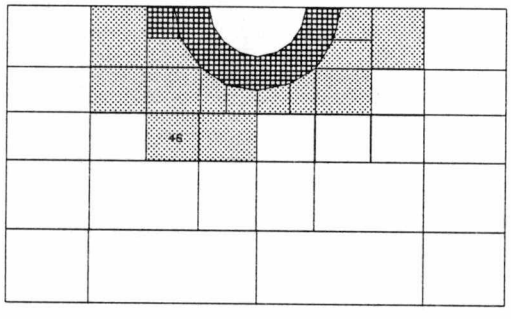

(a) Z = 19.0"

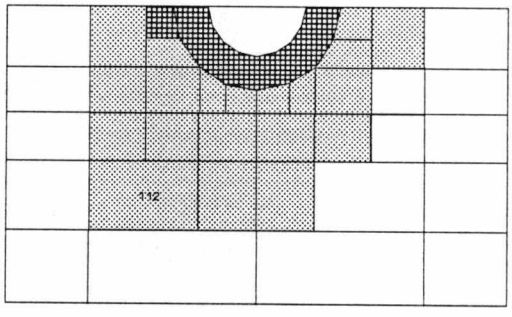

(b) Z = 23.0"

Figure 63. Cracked Elements at Load P = 84 kips

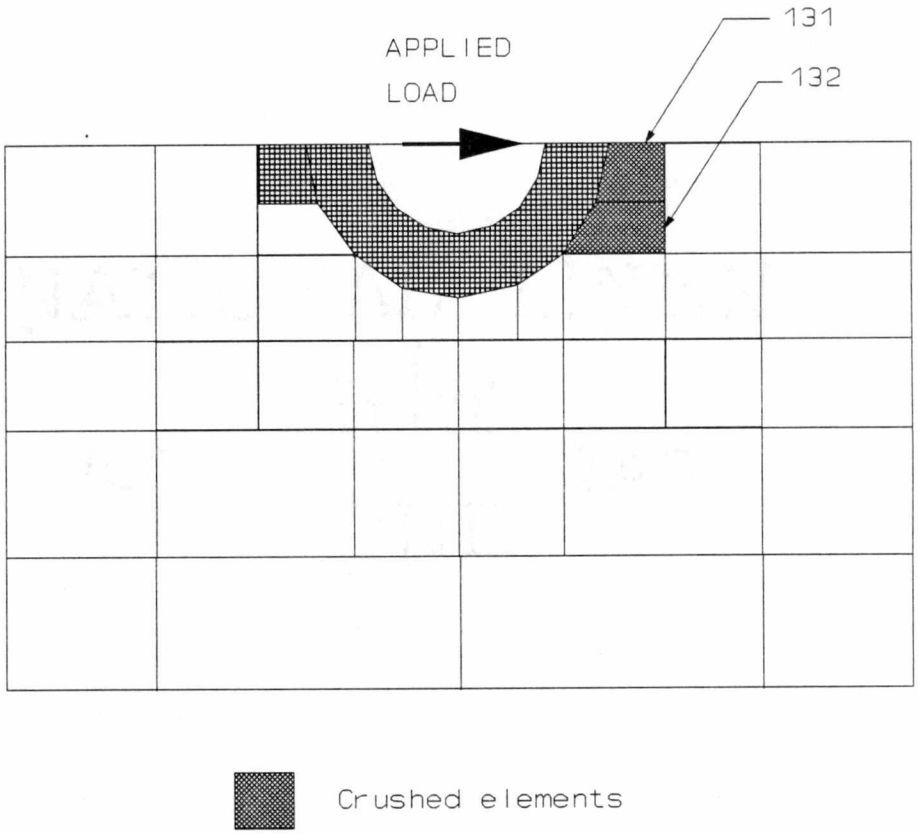

Figure 64. Location of Crushed Elements at Z = 23.0

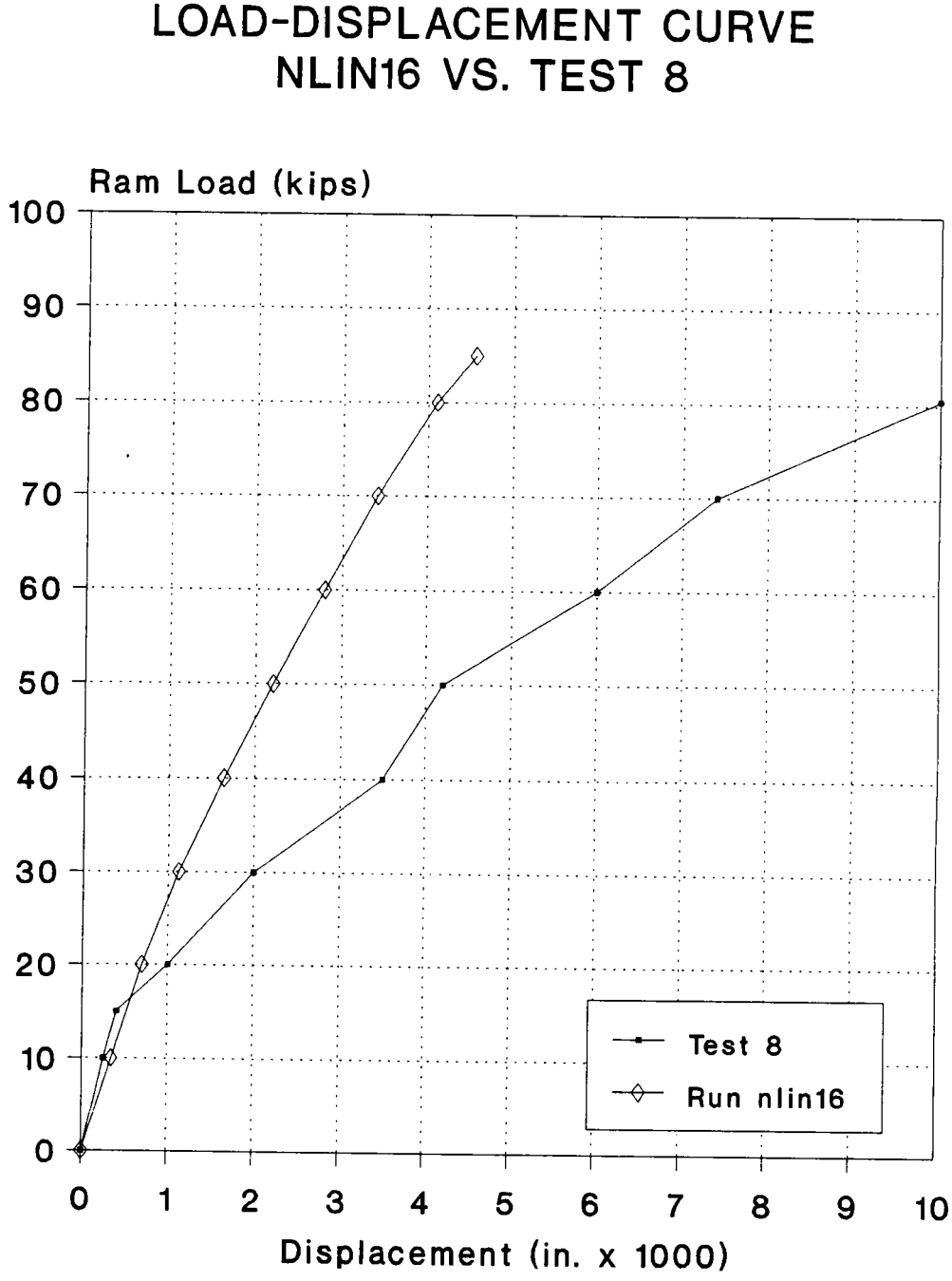

Figure 65. Comparison of Load-Displacement Curves for Run nlin16 and Test 8.

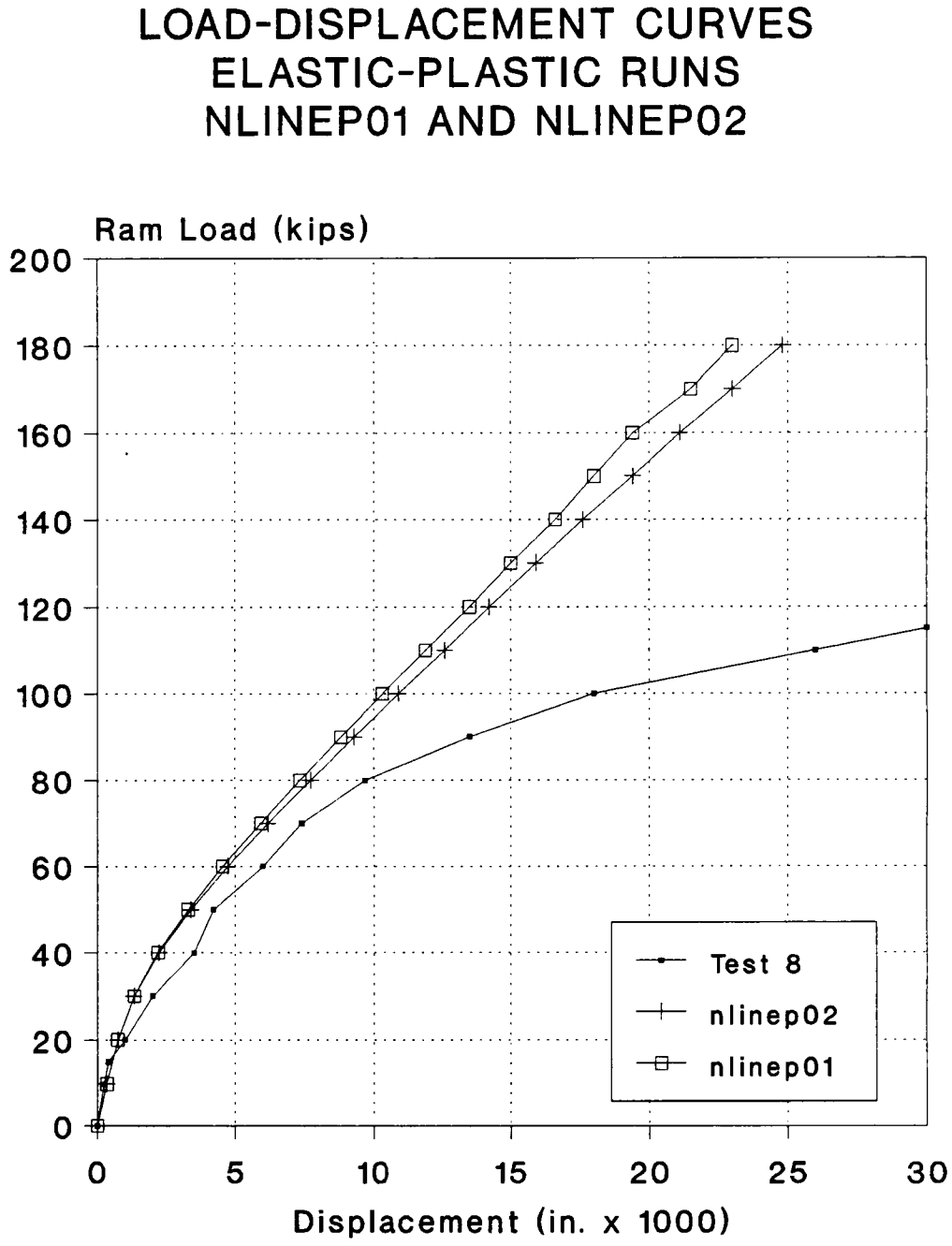

Figure 66. Load-Displacement Curves for Elastic-Plastic Runs nlinep01 and nlinep02.

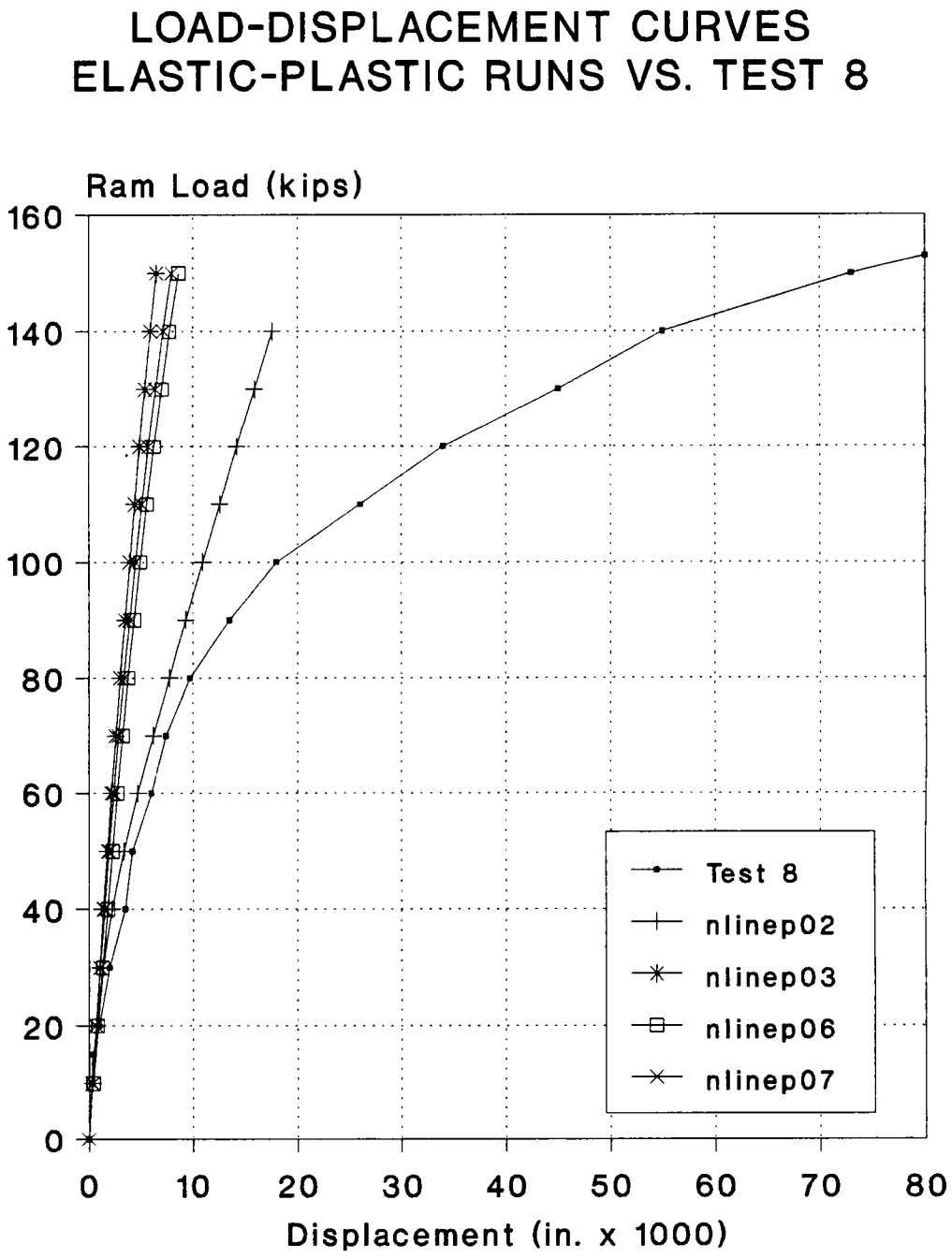

Figure 67. Load-Displacement Curves for Elastic-Plastic Runs nlinep02, nlinep03, nlinep06, and nlinep07, Compared with Test 8.

APPENDIX C

DERIVATION OF EQUATION (3-1)

DERIVATION OF EQUATION (3-1)

The derivation of eq. (3-1) is based on solving the equilibrium equations for the concrete bearing capacity in front of the socket, f_b, based on the free-body diagram of the concrete and socket system shown in Figure 5. In that figure there are five unknowns: f_1, f_2, f_b, λ, and b. f_1 is the maximum concrete bearing stress at the bottom of socket on the back side; f_2 is the maximum bearing stress against the bottom of the socket; "b" is the distance from the concrete bearing resultant force, C_2, at the bottom of the socket to the neutral axis of that surface; and λ is the distance from the top of the socket to the vertical stress neutral axis.

"b" is determined assuming a cracked-transformed section of the concrete and anchor bar system. The cracked-transformed section equates the area of the concrete compression region times the moment arm to the neutral axis to the transformed steel area (nA_s, where n is the ratio of the steel modulus of elasticity to the concrete elasticity, assumed to be 9 for this calculation) times its moment arm to the neutral axis. A preliminary calculation indicated that kd > R, the radius of the socket. The sketch on the right shows the geometry used to calculate the distance from the edge of the socket to the neutral axis, kd. The area of area 1 is $(\pi/2)R^2$ = 14.137, and its moment arm to the neutral axis is given by (0.4244R + X) = (1.273 + X).

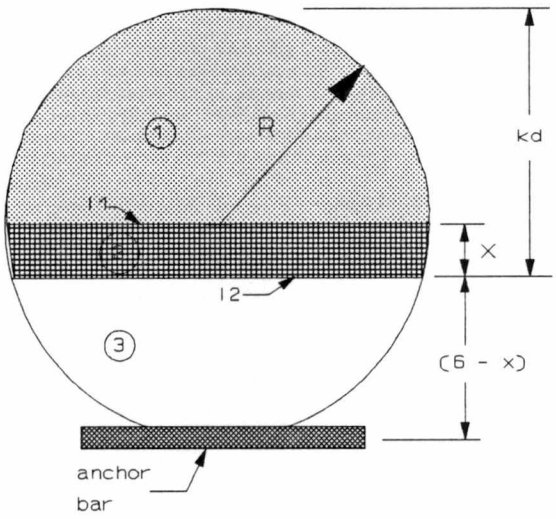

The area of area 2 is approximately given by (l1 + l2)X/2 and its moment arm is X/2 (if X is not very large with respect to R, this is a good assumption). l1 is the diameter of the socket, 2R = 6, and l2 is the base length of the segment (area 3) of the circle, $2\sqrt{(R^2 - X^2)}$ = $(2\sqrt{(9 - X^2)}$. The transformed steel area is $nA_s = 9(1.5) = 13.5$ and its moment arm to the neutral axis is (6 - X). Thus, the equation to solve for X becomes:

$$14.137(1.273 + X) + \frac{X^2}{4}[6 + 2\sqrt{(9 - X^2)}] - 13.5(3 - X) = 0$$

which has a root at X = 0.7534" (used 0.75"), and, finally, kd = R + X = 3.75". The resultant force, C_2, is located at kd/3 = 1.25" from the edge of the socket, and therefore

$$b = R - \frac{kd}{3} = 6 - 1.25 = 1.75$$

The value for the vertical distance to the neutral axis, λ, was determined from testing data, so eq. (3-1) obtained f_b as a function of λ. The resultant forces C_1 and C_3 are given in terms of the unknowns by the following expressions:

$$C_1 = 0.85\lambda f_b(2R) = 0.85(6)\lambda f_b = 5.1\lambda f_b$$

$$C_3 = \frac{1}{2}f_1(l-\lambda)(2R) = 3.0f_1(l-\lambda)$$

The term C_2 is obtained from the equation summing forces in the vertical direction. In this equation, the force due to the anchor bar, T_1, is assumed to act vertically (and not at 15°):

$$C_2 = T_1 = A_sF_y = 1.525(50) = 76.25$$

Summing forces in the horizontal direction ($\Sigma F_{horiz} = 0$)

$$P + C_3 = C_1$$

$$P + 3.0(l - \lambda)f_b = 5.1\lambda f_b$$

and solving for f_1:

$$f_1 = \frac{5.1\lambda f_b - P}{3.0(l - \lambda)}$$

The last equation is the summation of moments about the bottom front corner of the socket ($\Sigma M = 0$):

$$P(e + l) + C_3(\frac{l - \lambda}{3}) - 76.25(1.75 + 3.0 + 0.5) - C_1(l - 0.425\lambda) = 0$$

Substituting the expressions for C_1, C_3, and f_1 into the above equation:

$$P(e + \lambda) + 1.7\lambda(l - \lambda)f_b - \frac{P}{3}(l - \lambda) = 400.3 + 5.1\lambda f_b l - 2.1675\lambda^2 f_b$$

Combining all terms with f_b on one side of the equation:

$$P(\frac{2l}{3} + e + \frac{\lambda}{3}) - 400.3 = (3.4\lambda l - 0.4675\lambda^2)f_b$$

and solving for f_b:

$$f_b = \frac{P(\frac{2l}{3} + e + \frac{\lambda}{3}) - 400.3}{(3.4\lambda l - 0.4675\lambda^2)}$$

which is eq. (3-1).

VITA

Kenneth Eduardo Fricke was born on October 31, 1948 in Caracas, Venezuela. He attended elementary schools in Venezuela through the eighth grade, then attended Cascia Hall Preparatory School in Tulsa, Oklahoma from where he graduated in June 1966. He entered Case Institute of Technology (now part of Case Western Reserve University) in Cleveland, Ohio and received a Bachelor of Science degree in Engineering in May 1970. After working for one year at Pratt & Whitney Aircraft in Florida, he re-entered Case as a Graduate Assistant, graduating in June 1974 with a Master of Science degree in Civil Engineering.

After spending two more years at Case working on a PhD in the Engineering Mechanics Department, he left Case and joined the Civil Engineering Department at Union Carbide Corporation - Nuclear Division in Oak Ridge, Tennessee, in October 1976. In 1978 he started taking graduate classes at The University of Tennessee at Knoxville and received the Doctor of Philosophy degree in Civil Engineering in December of 1992.

He is currently employed by Martin Marietta Energy Systems, Inc. in Oak Ridge (the successor to Union Carbide) as an Engineering Specialist working in the areas of natural phenomena analysis and masonry wall strength testing. He has published a number of papers in recent years on masonry wall testing. He is a member of the American Society of Civil Engineers, The Masonry Society, and the Earthquake Engineering Research Institute.